

NASA TECHNICAL  
MEMORANDUM

NASA TM X- 64632

THE SMITHSONIAN EARTH PHYSICS SATELLITE (SEPS)  
DEFINITION STUDY  
VOLUMES I through III

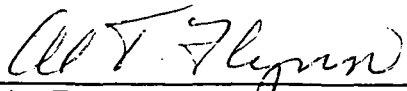
Coordinated By Program Development

September 1971

CASE FILE  
COPY

NASA

*George C. Marshall Space Flight Center  
Marshall Space Flight Center, Alabama*

1. REPORT NO. TM X-64632	2. GOVERNMENT ACCESSION NO.	3. RECIPIENT'S CATALOG NO.	
4. TITLE AND SUBTITLE The Smithsonian Earth Physics Satellite (SEPS) Definition Study (Volumes I through IV)		5. REPORT DATE September 1971	6. PERFORMING ORGANIZATION CODE PD-MP-P
		8. PERFORMING ORGANIZATION REPORT #	
7. AUTHOR(S) Coordinated By Program Development		10. WORK UNIT NO.	
9. PERFORMING ORGANIZATION NAME AND ADDRESS Mission and Payload Planning Office Program Development Marshall Space Flight Center, Alabama 35812		11. CONTRACT OR GRANT NO.	
		13. TYPE OF REPORT & PERIOD COVERED Technical Memorandum	
12. SPONSORING AGENCY NAME AND ADDRESS		14. SPONSORING AGENCY CODE	
15. SUPPLEMENTARY NOTES Volume I - Executive Summary; Volume II - Preliminary Design and Trade Studies Summary; Volume III - Project Planning Data; Volume IV - Cost Estimates.			
16. ABSTRACT <p>As a result of the mutual interest within OMSF and OSSA in the identification of beneficial missions utilizing unassigned space hardware, a limited Phase B study was undertaken at MSFC to determine the merit and feasibility of launching a proposed Earth Physics Satellite with Apollo-type hardware. The study revealed that it would be feasible to launch this Satellite using a S-IB stage, a S-IVB with restart capability, an Instrument Unit, a SLA for the Satellite shroud, and a nose cone (AS-204 configuration). All of this hardware exists in storage.</p> <p>Simultaneously, the Smithsonian Astrophysical Observatory (SAO) accomplished a Phase B definition of the proposed Satellite, which was specifically designed to satisfy the fundamental requirement of providing an orbiting benchmark of maximum accuracy. The Satellite is a completely passive, solid 3628-kg (8000-pound) sphere of 38.1-cm radius (30.0-inch diameter) and very high mass-to-area ratio (7980 kg/m<sup>2</sup>). In the suggested orbit of 55 degrees inclination, 3720 km (2010- n.mi.) altitude, and low eccentricity (<math>e \sim 0.01</math>), the orbital lifetime is extremely long, so many decades of operation can be expected.</p> <p>The results of this study are reported in four volumes: Volume I, Executive Summary; Volume II, Preliminary Design and Trade Studies Summary; Volume III, Project Planning Data; and Volume IV, Cost Estimates (bound separately).</p>			
17. KEY WORDS Unassigned Apollo Hardware; Earth Physics Program; Corner-cube Reflectors; Laser Ranging; Rotation of Earth; Polar Motion; Tidal Loading; Tectonic Motions; Terrestrial Coordinate System; Depleted Uranium.		18. DISTRIBUTION STATEMENT STAR Announcement  JAMES T. MURPHY Acting Director, Program Development	
19. SECURITY CLASSIF. (of this report) Unclassified	20. SECURITY CLASSIF. (of this page) Unclassified	21. NO. OF PAGES	22. PRICE \$3.00

## ACKNOWLEDGEMENTS

In response to a request from the Office of Space Science and Applications, NASA Headquarters, the George C. Marshall Space Flight Center undertook a limited Phase B definition study of a launch vehicle to orbit the proposed Earth Physics Program Satellite. Phase B project coordination was assigned to the Planetology Group in the Mission and Payload Planning Office of MSFC's Program Development.

Program Development's Preliminary Design Office was assigned the responsibility to conceive and design the Satellite shroud, support structure, ejection mechanism, and to accomplish the Satellite mission analysis.

Program Management's Saturn Program Office was assigned the responsibility of defining the launch vehicle and accomplishing the vehicle mission analysis. This effort was accomplished through the utilization of Saturn Program prime contractor off-peak manpower.

Science and Engineering's Central Systems Engineering (CSE) coordinated all launch vehicle activities within S&E. Contractor organizations, Chrysler Corporation, General Electric Corporation, International Business Machine, McDonnell Douglas Corporation, and Rocketdyne Division of North American Rockwell Corporation, performed studies on the SEPS mission and published reports showing their results. These results were summarized by Chrysler Corporation under the Saturn IB Systems Integration contract in Volume II (Preliminary Design and Trade Studies Summary).

Program Development's Program Planning Office, with direct support from the Advanced Program Support Office, was assigned the responsibility of preparing and publishing Volume III (Project Planning Data) and Volume IV (Cost Estimates).

The Products Office of Science and Engineering coordinated all payload activities within S&E.

All material relative to the Satellite itself was generated by the Smithsonian Astrophysical Observatory, Cambridge, Massachusetts, assisted by Arthur D. Little Corporation.

VOLUME I  
EXECUTIVE SUMMARY



## TABLE OF CONTENTS

	Page
1.0 PROGRAMMATIC SUMMARY	1-1
1.1 BACKGROUND	1-1
1.2 INTRODUCTION	1-1
1.3 EARTH PHYSICS PROGRAM (EPP) BACKGROUND	1-2
1.3.1 SCIENTIFIC	1-2
1.3.2 SCIENTIFIC OBJECTIVES	1-3
1.3.3 EARTH PHYSICS SATELLITE REQUIREMENTS	1-5
1.4 APPROACH AND LIMITED PHASE B STUDY OBJECTIVES	1-6
1.5 STUDY ASSUMPTIONS	1-6
1.6 RELATIONSHIP TO OTHER NASA EFFORTS	1-9
1.7 PHASE C/D SCHEDULE	1-9
1.8 ESTIMATED COSTS	1-9
1.9 CONCLUSIONS	1-11
2.0 TECHNICAL SUMMARY	2-1
2.1 LAUNCH VEHICLE CONFIGURATION DEFINITION	2-1
2.1.1 CONFIGURATION SUMMARY	2-1
2.1.2 STUDY GROUND RULES	2-1
2.1.3 S-IB STAGE SELECTION	2-3
2.1.4 S-IVB STAGE SELECTION	2-3
2.1.5 INSTRUMENT UNIT (IU) SELECTION	2-4
2.1.6 SATELLITE SHROUD SELECTION	2-6

## TABLE OF CONTENTS (CONCLUDED)

	Page
2.0 TECHNICAL SUMMARY (Concluded)	
2.2 SATELLITE SUPPORT STRUCTURE	2-7
2.3 SATELLITE EJECTION SYSTEM	2-7
2.4 SATELLITE ASSEMBLY DESCRIPTION	2-10
2.5 MISSION ANALYSIS	2-15

## LIST OF FIGURES

<u>Figure</u>	<u>Title</u>	<u>Page</u>
1-1	Management Relationships . . . . .	1-7
1-2	MSFC Working Group . . . . .	1-8
1-3	SEPS Development and Production Schedule . . . . .	1-10
2-1	Launch Vehicle Configuration . . . . .	2-2
2-2	Satellite Support Structure . . . . .	2-8
2-3	Satellite Support and Separation Mechanism . . . . .	2-9
2-4	Assembly Configuration of Cube Core . . . . .	2-11
2-5	Cross Section of Retroreflector Mounted in Cavity .	2-12
2-6	Satellite and Launch Vehicle Configurations and Parameters . . . . .	2-14
2-7	Flight Profile . . . . .	2-16
2-8	Orbital Flight Profile . . . . .	2-17

## LIST OF TABLES

<u>Table</u>	<u>Title</u>	<u>Page</u>
2-1	Saturn V S-IVB Stage Modifications . . . . .	2-5
2-2	Retroreflector Parameters . . . . .	2-13

# TECHNICAL MEMORANDUM X - 64632

## THE SMITHSONIAN EARTH PHYSICS SATELLITE (SEPS) DEFINITION STUDY

### VOLUME I - EXECUTIVE SUMMARY

#### SECTION 1. PROGRAMMATIC SUMMARY

##### 1.1 BACKGROUND

MSFC involvement in the Earth Physics Satellite Program resulted from the OMSF interest, during the fall of 1970, in launching an unmanned Saturn IB in order to verify Launch Complex 39 prior to the initial Skylab-A manned flight. Several suggestions for possible payloads were considered; and the proposal from the Earth Resources Office of OSSA (Code SR) for a low-drag, high-mass Earth Physics Satellite was selected as being a candidate.

As the idea of launching an unmanned Saturn IB to verify Launch Complex 39 was considered in more depth, it became apparent that this verification was not required and the plan was discarded; however, the interest in identifying viable programs for unassigned Apollo hardware remained. MSFC indicated to OSSA-SR that the Smithsonian Earth Physics Satellite was an attractive candidate for use of unassigned Apollo hardware should it become available subsequent to the flight of Skylab. OSSA-SR awarded a grant to the Smithsonian Astrophysical Observatory for the Satellite preliminary design.

In a memorandum to Mr. Meyers (dated January 27, 1971), Dr. Naugle requested support from MSFC to define the launch vehicle and payload adapter. Mr. Myers responded by letter to Dr. Naugle's request on February 16, 1971, indicating that the project warranted further consideration and that a limited Phase B study, to be undertaken at MSFC, would be desirable.

##### 1.2 INTRODUCTION

As a result of interest within OMSF in identifying beneficial missions utilizing surplus Apollo hardware and of OSSA's suggestion to

orbit an unmanned satellite, the Smithsonian Earth Physics Satellite seemed to be one possibility that warranted further consideration. Based on the mutual interest of OMSF and OSSA, a limited Phase B study was undertaken at MSFC to determine the merit and feasibility of a project which would utilize Apollo launch vehicle hardware. Simultaneously, the Smithsonian Astrophysical Observatory was awarded a six-month grant by OSSA to undertake the engineering definition of the proposed Earth Physics Satellite.

The results of these investigations are documented in this report, which is comprised of the following Volumes:

- Volume I - Executive Summary
- Volume II - Preliminary Design and Trade Studies Summary
- Volume III - Project Planning Data
- Volume IV - Cost Estimates

### 1.3 EARTH PHYSICS PROGRAM (EPP) BACKGROUND

#### 1.3.1 SCIENTIFIC

One of the principal recommendations of the Williamstown study on solid-earth and ocean physics (Kaula, 1969) was that NASA develop techniques for ranging to satellites to an accuracy of  $\pm 2$  cm. Range measurements at this level of accuracy will be necessary to accomplish many objectives of the Earth Physics Program (EPP), such as the determination of plate tectonic motions (continental drift), rotation variations and wobble of the earth, earth body tides, etc. These objectives must be attained by measuring the temporal variations of the following: the geometry of a global matrix of fiducial points on the earth's surface; the fiducial points with respect to the earth's center of mass; and the matrix with respect to an inertial reference. These geometric variations are known to have time scales ranging from a day (e.g., body tides) to millenia (continental drift).

What is needed is a means for making exceedingly accurate measurements on a global basis in such a way that, first, each position on the globe can be related to all others; second, complete sets of observations can be obtained in less than a day; and, third, continuity of observations is maintained over the longest possible time span. The

first two considerations clearly suggest the use of a satellite in a high-inclination orbit; the third suggests that the satellite be passive. It is concluded that a high-density satellite fitted with laser retroreflectors is an appropriate choice.

The Smithsonian Astrophysical Observatory (SAO) proposes to design and fabricate a compact, spherical, and completely passive laser-retroreflector Satellite of very high density. The Satellite is to be placed in a 3720-km-altitude, 55-degree-inclination circular orbit. Such a Satellite will allow very accurate range measurements from the earth's surface to an object in an extremely stable orbit, thus permitting global measurements of groundstation positions to accuracies of 10 cm or better, which satisfies one of the basic needs of NASA's Earth Physics Program.

This Satellite will make available, for the foreseeable future, an in-orbit capability for laser ranging of maximum accuracy. The high mass/area ratio and the precise, stable (attitude independent) geometry of the spacecraft in concert with the proposed orbit will make this Satellite the most precise position reference available. Because it will be visible to all parts of the world and will have an extended operating life in orbit, the SAO Satellite can serve as a fundamental global standard for decades. It would constitute an important first step in the NASA Earth Physics Program.

### 1.3.2 SCIENTIFIC OBJECTIVES

This Satellite was conceived for a single purpose: to measure positions anywhere on earth to an accuracy of at least 10 cm. This is basic to NASA's Earth Physics Program since many of the program's objectives will not be met without this capability. Some of these objectives are to measure or establish the following:

- a. Rotation of the earth
- b. Polar motion
- c. Earth body tides and tidal loading
- d. Tectonic motions
- e. A 10-cm terrestrial coordinate system

#### 1.3.2.1 ROTATION OF THE EARTH

The rate of rotation of the earth is equivalent to UT-1\* . The EPP objectives are to measure rotation to a relative accuracy of 0.002 arc second (130  $\mu$  sec, UT-1) for averaging times less than one day, to an absolute accuracy of 0.01 arc second (650  $\mu$  sec, UT-1) for averaging times of one day, and to an absolute accuracy of 0.01 arc second relative to an inertial coordinate system over decades. The periods of some components of rotational variations are known, namely, tidal and seasonal. The remaining components have been classified as irregular with a spectrum that encompasses the entire frequency range now observable with available instruments.

#### 1.3.2.2 POLAR MOTION

The accuracy requirements for the measurement of polar motion are the same as those for measuring the rotation rate. Two aspects of polar motion must be distinguished: motion of the spin axis with respect to inertial coordinates, and motion of the earth with respect to its spin axis. The periods of several components of polar motion have been identified or suggested, namely, diurnal, tidal, seasonal, 1.2-year, 18.6-year, 24-year, and secular.

#### 1.3.2.3 EARTH BODY TIDES AND TIDAL LOADING

These effects are vertical motions of the earth's surface, with maximum amplitude of the order of 50 cm and with a spectrum of discrete and very accurately known frequencies. The pertinent observational data should provide an accuracy of at least  $\pm 10$  cm (in the vertical) for averaging times of several hours or less.

#### 1.3.2.4 TECTONIC MOTIONS

Tectonic motions are of very great scientific interest but are extremely difficult to measure. It is desirable to attain an accuracy of at least 10 cm (1 cm would be much better) both horizontally and vertically in determining the relative positions of the major tectonic plates. It would also be of considerable interest to determine the stability or rigidity within each plate.

---

\* Universal Time corrected for the earth's polar variations.

#### 1.3.2.5 ESTABLISHMENT OF A 10-CM TERRESTRIAL COORDINATE SYSTEM

In the words of the Williamstown study, "The terrestrial system will be defined by coordinates assigned to a number of stations and their time variations. This system should have as its origin the earth's center of mass and as Z-axis the principal axis of inertia, as determined from satellite dynamics considerations." Thus, the satellite must be designed to be used for observations in such a way that its orbit can be determined to an accuracy consistent with the accuracy needed to define the coordinate system.

#### 1.3.3 EARTH PHYSICS SATELLITE REQUIREMENTS

A satellite that is optimum for EPP geometric measurements would be characterized in the following way:

- a. Completely passive to attain maximum operating life. Acquired by camera (photographing reflected sunlight against star background). Equipped with retroreflectors for ranging with ground-based lasers.
- b. Compact and rigid to minimize changes in spacecraft geometry.
- c. Spherical so geometry of retroreflector array versus spacecraft center of mass will not change with aspect. Spherical shape also necessary to minimize errors in corrections for solar-radiation pressure and drag.
- d. Maximum feasible mass-to-area ratio to reduce perturbations caused by nongravitational forces (mainly radiation pressure). This is needed to permit the computation of extremely accurate short (24-hour) arcs to relate geographically remote locations.
- e. Orbital altitude high enough to reduce to an acceptable level orbit errors resulting from uncertainties in geopotential models.
- f. Orbital altitude low enough to provide strong geometry, i.e., altitude comparable to baselines of interest.
- g. Inclination large enough to provide global coverage.



#### 1.4 APPROACH AND LIMITED PHASE B STUDY OBJECTIVES

The basic approach adopted for the launch vehicle portion of the limited Phase B study was to utilize MSFC in-house manpower to define the Satellite shroud, Satellite supporting structure and the Satellite ejection mechanism, to accomplish the Satellite mission analysis, to estimate overall cost and to publish the limited Phase B study final report. The launch vehicle was defined by in-house manpower, supplemented by the Saturn Program contractors' "off-peak" manpower. This consisted of selecting existing available stages, identifying their respective required modifications, accomplishing the vehicle mission analysis and formulating a Phase C/D schedule compatible with on-going NASA programs.

Meanwhile, tasks directly involving the Satellite definition were being accomplished by the Smithsonian Astrophysical Observatory (SAO) under contractual arrangements with OSSA-SR. These tasks were to accomplish the Satellite core and retroreflector design, to establish ground handling procedures and equipment design, to formulate test and checkout procedures, to provide Phase C/D schedules and to estimate Satellite costs.

Figure 1-1 depicts the overall management relationships for this study and Figure 1-2 depicts the MSFC Study Working Group.

The objectives of this limited Phase B study were to define the Satellite and its interfaces and to determine the merit and feasibility of using the Saturn IB launch vehicle to place the proposed Satellite into a 3720-km circular orbit at a 55-degree inclination.

#### 1.5 STUDY ASSUMPTIONS

In order to take full advantage of existing assets, the following ground rules were established:

- a. Use the Skylab Program as the institutional base for the Smithsonian Earth Physics Satellite Project.
- b. Use "off-peak" Skylab contractor effort for launch vehicle modification.
- c. Use the Skylab launch facilities.
- d. Launch as soon as possible after the Skylab A.

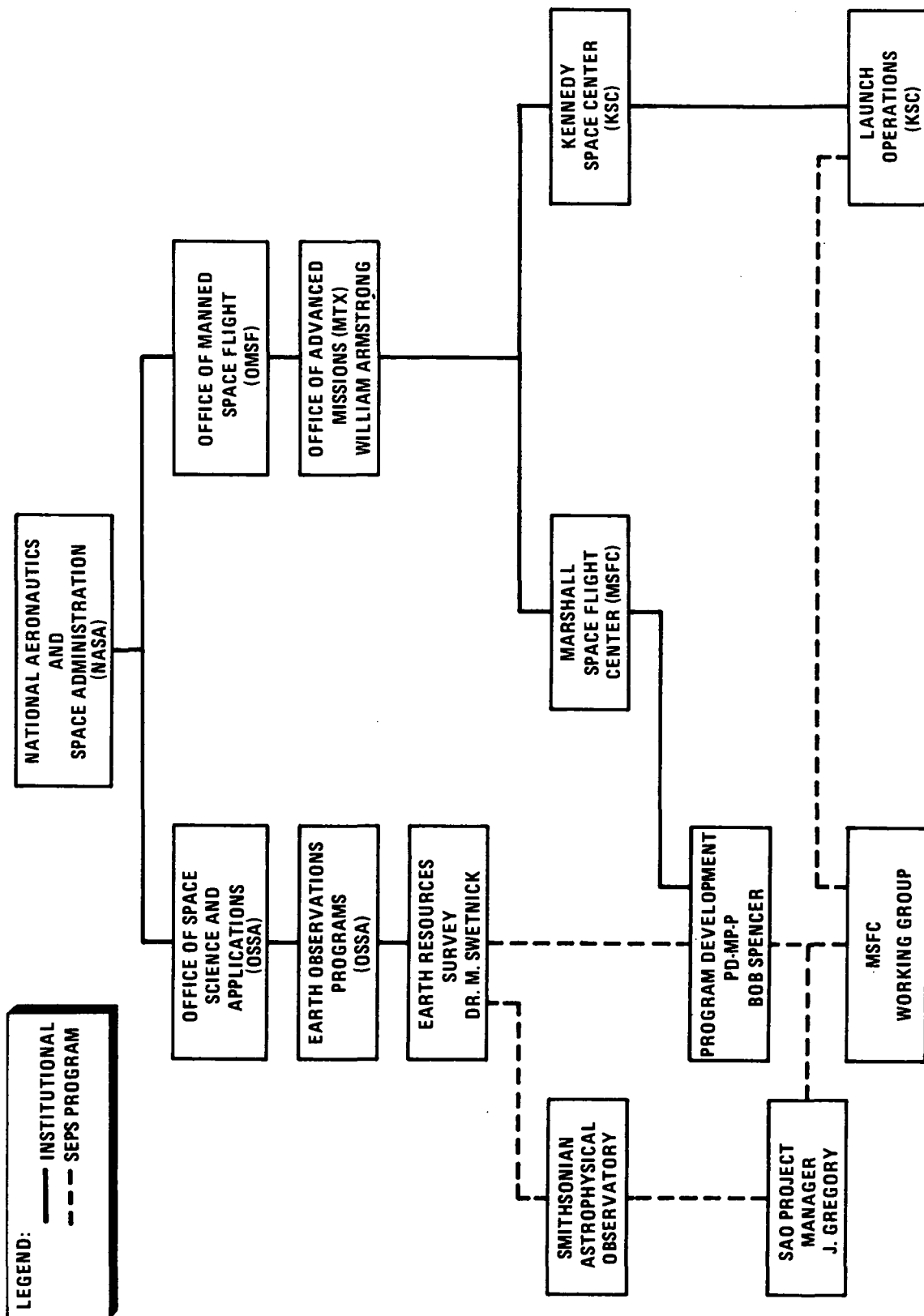


FIGURE 1-1. Management Relationships.

BOB SPENCER (PD-MP-P) - STUDY COORDINATOR

Dr. J. L. RANDAL (S&E-ASTR) - SCIENTIFIC ADVISOR

PAYLOAD DEFINITION

LAUNCH VEHICLE DEFINITION

JIM HEYER/STEVE DENTON (PD-DO)  
 Define:  
     Satellite Shroud  
     Satellite Support Structure  
     Satellite Ejection Mechanism  
     Accomplish Satellite Mission Analysis

LUCIAN BELL/BOB BEAMAN (PM-SAT-E)  
 Define:  
     The Launch Vehicle  
     The LVGSE  
     Monitor "Off-Peak" Contractor Effort

HAROLD TREXLER (PD-PP)  
 Prepare Cost Estimates  
 Prepare Phase C/D Schedules  
 Publish Volumes III and IV of Final Report

GEORGE MCKAY (S&E-CSE)  
 Coordinate Launch Vehicle  
 Activities Within S&E  
 Publish Volume II of Final Report

ROY MCFOLIN (PD-PS)  
 Prepare Mfg. Q&RA Plans  
 Assess Facilities Required  
 Develop Facilities Plans

FRED VREULS (S&E-P)  
 Coordinate Payload  
 Activities Within S&E

JOHN GREGORY (SAO)  
 Project Manager for SAO

FIGURE 1-2. MSFC working group.

## 1.6 RELATIONSHIP TO OTHER NASA EFFORTS

It is anticipated that the Smithsonian Earth Physics Satellite Project can be carried out with little or no impact on any on-going NASA program. A significant relationship identified is the manner in which the Skylab Program can be used to advantage in keeping launch costs to a minimum. If the launch date can be scheduled within four months after the last Skylab A launch, regardless of whether there are follow-on Skylab programs, significant savings, if not the major part of launch costs, can be assimilated by utilizing "off-peak" Skylab manpower.

Additional savings can be achieved by a timely initiation of the Instrument Unit (IU) reprogramming and modifications. This task would be relatively expensive if initiated late in the schedule; however, it would be considered IU contractual "scope-of-work" early in the schedule.

## 1.7 PHASE C/D SCHEDULE

The Phase C/D schedule, presented in Figure 1-3, is designed to provide maximum utilization of contractor "off-peak" manpower during this time frame. The beginning of each bar represents the latest time that the respective task can get underway and effectively key into the existing Skylab Program with maximum utilization and minimum impact.

## 1.8 ESTIMATED COSTS

It is estimated that the overall cost to accomplish this program is 8.3 million dollars. This includes modifications to existing launch vehicle, manufacture and test of the Satellite, the Satellite support structure, and the Satellite ejection mechanism, as well as launch operations and program integration.

The dollar estimates for this study are based on the following ground rules:

- o 1971 dollars
- o Only costs to modify the Saturn IB vehicle to the SEPS configuration are included.
- o Support structure, ejection mechanism and handling equipment to be designed and produced in-house.
- o An existing LM adapter (SLA) and nose cone will be used for payload fairings; only modification costs are included.

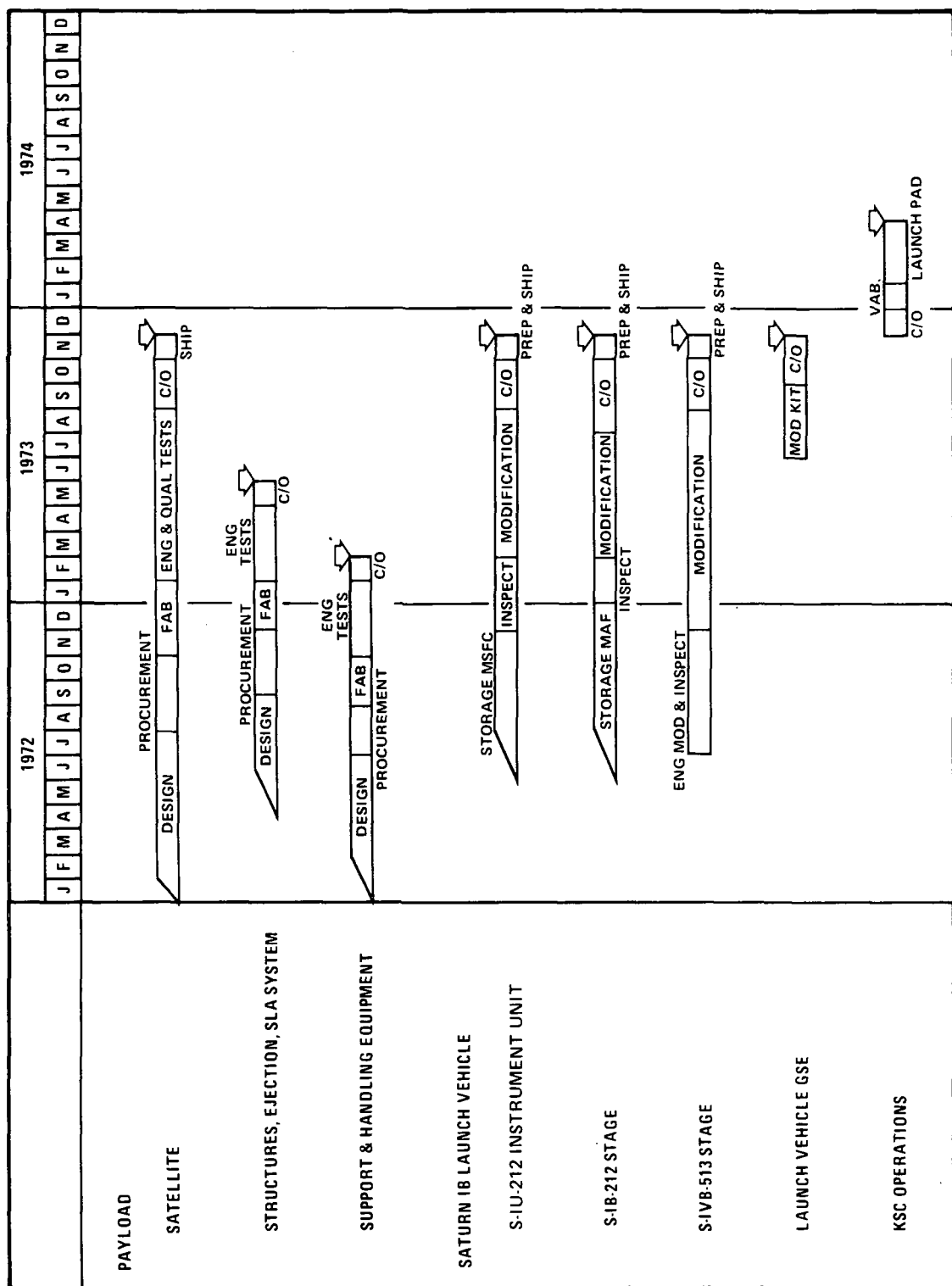


FIGURE 1-3. SEPS development and production schedule.

- o Satellite contractor will provide satellite test article required by MSFC.
- o Assume a planned launch in March 1974.
- o Assume the existence of post Skylab A program (e.g., alternate IA) to carry required launch support levels.
- o Assume launch vehicle will be made up of the SA-212 S-IB stage; the SA-212 Instrument Unit; and the SA-513 S-IVB stage.

## 1.9 CONCLUSIONS

Based on the data generated during this limited Phase B study, the MSFC Working Group has concluded the following:

- o A composite\* launch vehicle can be assembled which makes maximum use of unassigned hardware.
- o The satellite core design and retroreflector array, as proposed by the SAO, offer high probabilities of providing the earth physics data required to fulfill the Earth Physics Program objectives.
- o The use of the launch vehicle and satellite, as defined in this study and keyed properly into the Skylab Program Schedule, forms a very viable project.

---

\* Stages and hardware from both the Saturn IB and Saturn V launch vehicles.

## SECTION 2. TECHNICAL SUMMARY

### 2.1 LAUNCH VEHICLE CONFIGURATION DEFINITION

#### 2.1.1 CONFIGURATION SUMMARY

This study considers only the Saturn IB configuration for the SEPS launch vehicle. This launch vehicle consists of an S-IB for the first stage, a Saturn V or Saturn IB/S-IVB as the second stage and a Saturn IB Instrument Unit. The payload (everything above the Instrument Unit) consists of a SLA/nose cone, which has an external configuration similar to SA -204, with the 3628-kg (8000-lb) SEPS enclosed within the SLA (Figure 2-1).

The desired SEPS orbit requires an S-IVB capable of restarting to circularize the orbit at the proper altitude. A Saturn IB/S-IVB may be modified to obtain this restart capability or a Saturn V/S-IVB with this capability already existing may be modified to mate with the S-IB stage.

The launch vehicle recommended based upon availability, performance characteristics, and cost consists of the SA -212 S-IB stage, the SA-513 S-IVB stage, and the SA -212 Instrument Unit (Figure 2-1).

#### 2.1.2 STUDY GROUND RULES

a. The SA-204 external configuration will be used for aerodynamic studies.

b. Existing flight environment data similar to SA-203 and SA -204 will be used for structural, vibration, and accoustical analyses.

c. The IU will provide all sequencing of events.

d. The APS will provide attitude control for the mission duration.

e. Launch will be from LC-39, Pad B, into a 55-degree-inclination orbit.

f. The payload will not impose any mechanical or electrical requirements on the launch vehicle.

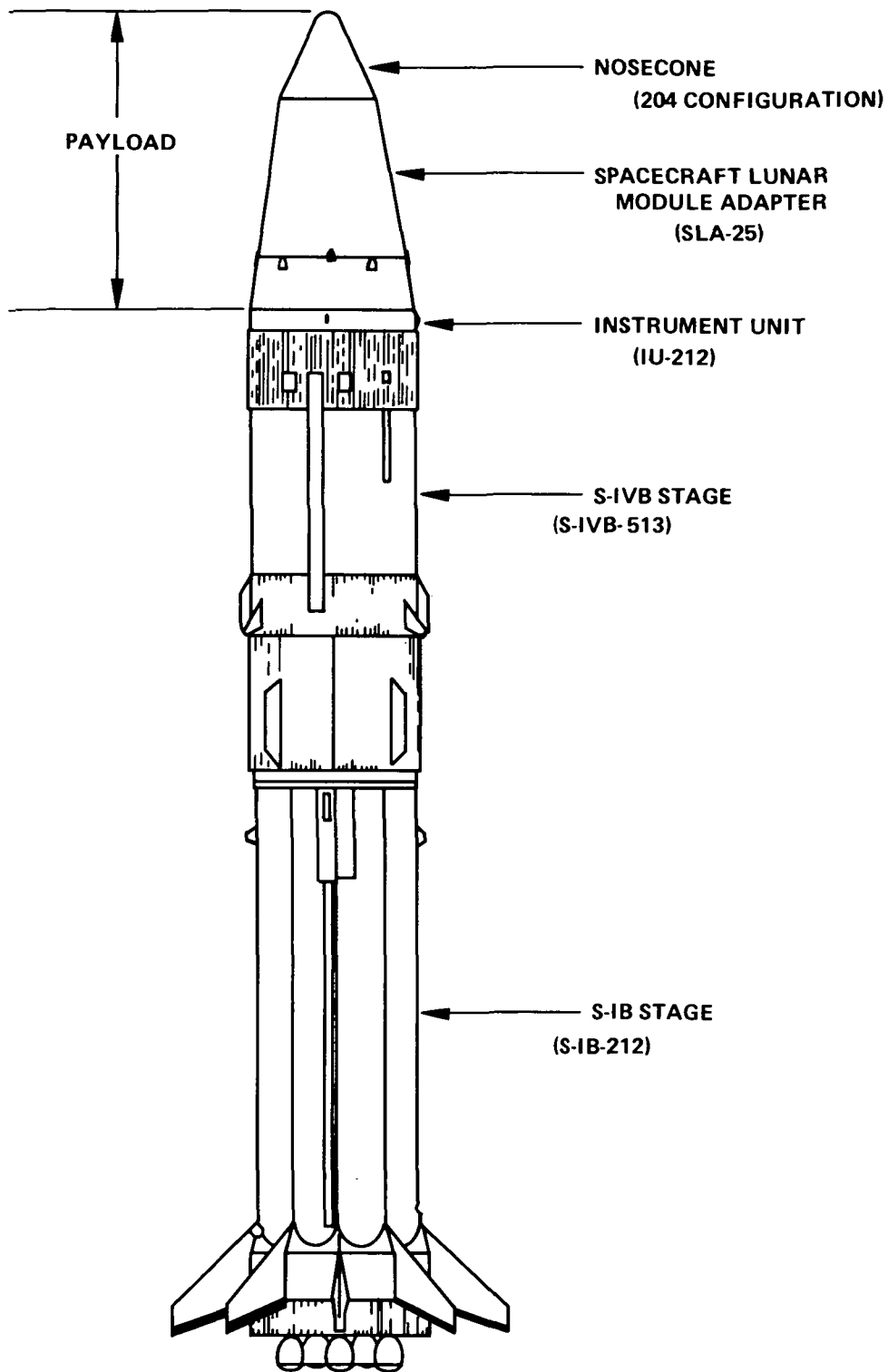


FIGURE 2-1. Launch vehicle configuration.



- g. Gross payload at lift-off will be approximately 6220 kg.
- h. Launch vehicle stages that have the least probability of manned flight assignment will be selected.
- i. Stage selection will be from both Saturn IB and Saturn V configurations.
- j. The S-IVB stage APS will orient the spin axis of the satellite normal to the ecliptic plane and impart the required spin to the satellite upon ejection.

#### 2.1.3 S-IB STAGE SELECTION

The present S-IB stage availability status indicates that there are nine S-IB stages in some state of readiness from which a selection can be made for the SAO Earth Physics Satellite mission. S-IB stages SA-206 through SA-212 are complete stages, and stages SA-213 and SA-214 have no firm commitment; however, several options are being considered to utilize some of the available stages.

All completed S-IB stages (SA-206 through SA-212) have available an S-IVB stage, with the exception of SA-212. The S-IVB stage for SA-212 was modified to accommodate the Saturn Work Shop (SWS) and is presently scheduled as part of the SA-513 mission. The SA-212 currently has no S-IVB stage assigned to complete the stack, and therefore would not impact other planning if selected for the Earth Physics Satellite mission.

The SA-212 S-IB stage was static fired on July 25, 1968, and placed in storage at MAF on June 30, 1969, and transferred into storage at MSFC on August 20, 1970. No mission-peculiar modifications are required for this stage, assuming that all electrical interfaces will be made compatible on the selected S-IVB stage.

#### 2.1.4 S-IVB STAGE SELECTION

The present S-IVB stage availability status indicates six complete Saturn IB/S-IVB stages and five complete Saturn V/S-IVB stages available for consideration. The SA-212 S-IVB and the SA-515 S-IVB were reworked for Saturn Workshops. Of the six Saturn IB/S-IVB stages available, four have firm mission plans and the other two are being considered as visit missions in the second Skylab program. Of the Saturn V/S-IVB stages available, three have firm Apollo missions and

two have no present assignment. One of the two unassigned Saturn V / S-IVB stages completes the stack for a complete Saturn V launch vehicle and is available for future mission applications. The other Saturn V / S-IVB stage would be available for Earth Physics Satellite mission consideration.

The S-IVB stage to be utilized for the Earth Physics Satellite mission must be capable of restarting to circularize the orbit at the proper altitude. The Saturn IB /S-IVB would require extensive modification to provide this capability, while the Saturn V /S-IVB has the capability already. The Saturn V /S-IVB stage, however, does require modification to interface with the S-IB stage. A Saturn V /S-IVB stage is recommended based upon availability without interference with present planning or breaking up a stacked vehicle in either program and lower modification cost due to the restart package already being available on the Saturn V /S-IVB stage. (See Table 2-1.)

Present manned flight planning does not include the Saturn V / S-IVB stages SA -513 and -514. The SA-513 S-IVB stage is presently matched with the SA-514 launch vehicle; however, a performance comparison of the two S-IVB stages revealed the SA-514 S-IVB stage to be the higher performer. Performance of the SA-513 S-IVB stage is adequate to meet the requirements for this mission; therefore, this stage was selected, leaving the high performing stage for a more sophisticated type mission.

#### 2.1.5 INSTRUMENT UNIT (IU) SELECTION

The current Instrument Unit (IU) status indicates that seven Saturn IB IUs and five Saturn V IUs are available. All Saturn V IUs are assigned to a launch vehicle. Three of these vehicles are planned for Apollo; one is the Skylab backup launch vehicle; the remaining vehicle is unassigned. All Saturn V launch vehicles with an assigned mission require an IU and any future mission plans for the unassigned Saturn V will require an IU. All Saturn IB IUs are assigned to a complete launch vehicle with the exception of SA-212. No S-IVB stage presently exists in the Saturn IB SA-212 stack. Of the Saturn IB launch vehicles, four have firm missions and the two remaining complete vehicles are tentatively planned for manned missions associated with Skylab B or with other manned missions presently being considered. The IU for Saturn IB SA-212 is presently being assembled. This IU, when complete, will not be a part of any present mission since the Saturn IB SA-212 is not a complete launch vehicle. The SA-212 IU will meet all the requirements for this mission with very few modifications.

TABLE 2-1. SATURN V S-IVB STAGE MODIFICATIONS

<u>Description</u>	<u>Justification</u>	<u>Mandatory?</u>	<u>Weight (lb<sub>m</sub>)</u>
Add LOX Baffle	To attenuate first burn cutoff initiate liquid disturbances and thus provide stable propellant surface for restart.	Yes	+40
Install LH <sub>2</sub> Baffle at Restart Level		Yes	+29
Remove LH <sub>2</sub> Baffle and Deflector	Payload improvement and provides better access for other LH <sub>2</sub> tank modifications.	No	-199
Modify Repressurization System (Provide Ambient LH <sub>2</sub> & Cryogenic LOX)	Provide necessary ullage pressure (NPSH for J-2) prior to restart.	Yes	-16
S-IB Interstage Modification	Provides compatibility of Saturn V S-IVB aft skirt to S-IB after interstage (bolt hole locations).	Yes	+56
J-2 Restart Mods	Provides restart after 60 min of coast.	Yes	NIL
Add Modification Packages	Incorporates ECPs authorized subsequent to placing stage in long-term storage	Yes	

The modifications required are mostly in the area of telemetry and electrical networks. Filters for the FCC must be designed, and a new flight program must be written for this mission. The IU software is scheduled far enough in advance to allow development without significant additional cost.

#### 2.1.6 SATELLITE SHROUD SELECTION

The selected baseline payload shroud configuration consists of an Apollo Spacecraft LM Adapter (SLA) and an existing nose cone of the SA-204 configuration. The major considerations for the selection of this configuration are as follows:

- a. The required shroud components are existing, flight qualified hardware and can be utilized without modification.
- b. The resulting vehicle external configuration is the same as SA-204 for which aerodynamic and flight data are available.
- c. The SLA provides a suitable structural interface, through the four LM support points, for the payload support structure.
- d. The selected shroud weights are compatible with the Saturn IB vehicle performance capability and the target satellite weight.

Alternate payload shroud configurations which were considered and investigated prior to baseline selection are the following:

- a. Modified Skylab nose cone.
- b. SA-204 type nose cone with a newly designed conical section to interface with the Saturn IB IU and with support points for the payload support structure.
- c. SA-204 type nose cone and the lower frustum of the SLA with a newly designed conical section to interface with the SLA lower frustum. The SLA lower frustum contains the LM support points which would be utilized for the structural interface of the payload support structure.

Consideration of use of a modified Skylab nose cone was eliminated due to the very heavy construction of the cone and the extensive redesign which would be required. The other two alternate shrouds

provide weight advantages over the selected baseline estimated at 957 kg for shroud b. and 698 kg for shroud c.; however, these weight advantages do not appear to warrant the cost and development effort which would be required in view of the acceptable payload capability of the Saturn IB with the baseline shroud.

## 2.2 SATELLITE SUPPORT STRUCTURE

The satellite support structure, as indicated in Figure 2-2, consists primarily of two deep I-section beams, a support frame, and four holddown arms. The deep I-beams attach to the four LM attach points located in the SLA and are oriented to intersect at 90 degrees at the vehicle centerline. The beams are built-up aluminum 7075-T6 construction, of T-section flanges, sheet web, and angle section lateral and vertical stiffeners. At their intersection, the beams are attached to a cylindrical tube which also adapts the payload support frame and encloses a compressed spring utilized for ejection of the satellite. The payload support frame provides the structural support points for the satellite, which are four pads having spherical surfaces, and provides the load path from the satellite to the deep I-beams. Four holddown arms are provided to hold the satellite in place against lateral and negative acceleration and are hinged near the ends of the members of the payload support frame. A screw jack is provided in the upper end of each hold-down arm to preload the structure and prevent the satellite from lifting from its support points under negative acceleration. The payload support frame adapts to the deep I-beams through a cylindrical tube which fits concentrically with the tube attaching the beams at their intersection. This tube is also preloaded to prevent the support frame from lifting from the deep I-beams under negative acceleration.

## 2.3 SATELLITE EJECTION SYSTEM

Ejection of the satellite is accomplished by releasing the tubular portion of the payload support frame from the main support beam structure using a single pin puller and linkage arrangement located at the lower end of the tube. A spring enclosed within the tubular members translates the support frame and the satellite from the main support beam structure. After a small vertical travel, the holddown arms slip off their support points and are free to rotate back; releasing and providing clearance for the satellite. This action, with the support frame in its fully extended position, is illustrated in Figure 2-3.

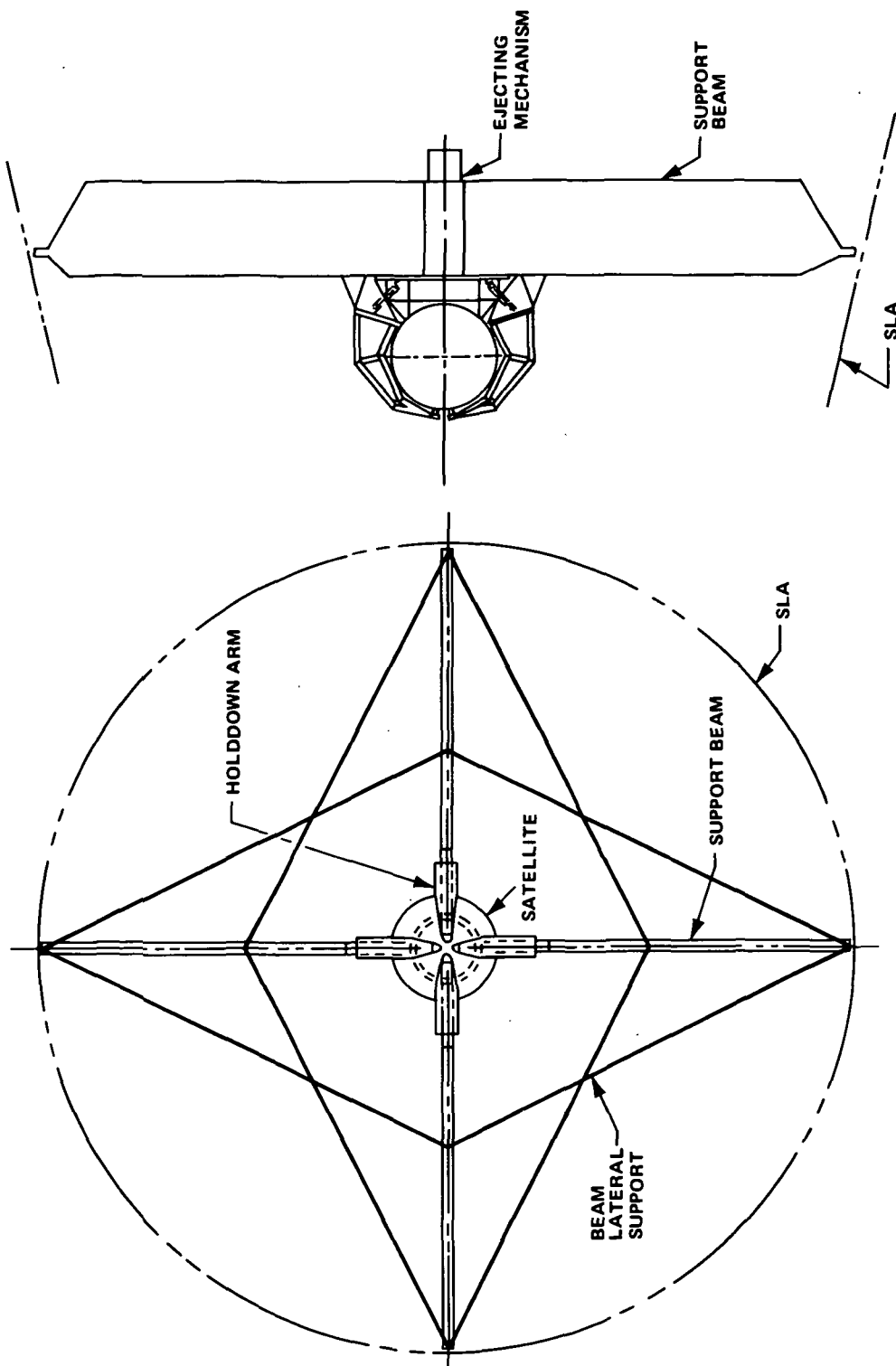


FIGURE 2-2. Satellite support structure.

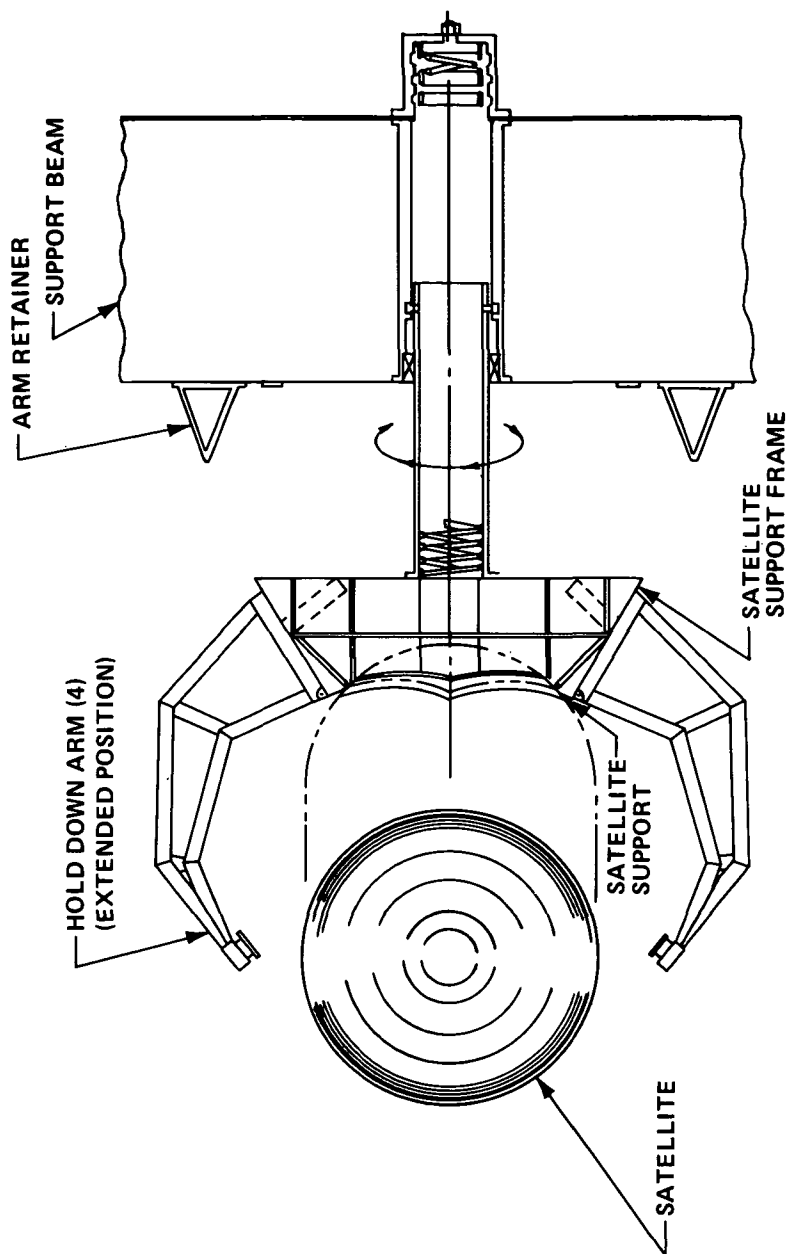


FIGURE 2-3. Satellite support and separation mechanism.

## 2.4      SATELLITE ASSEMBLY DESCRIPTION

The satellite sphere will be composed of a cubical inner core and six spherical caps. The cube core will be 38.1 cm on an edge and the caps added to the core faces will complete the 76.2-cm-diameter sphere. Each spherical cap will be positioned on its corresponding cube core face by a centrally located 3.8-cm-diameter shear pin and held in place by four 1.59-cm-diameter bolts. The bolts are positioned on the cap such that their heads are within counterbores which are located directly under the retroreflector cavities (Figure 2-4).

The cube core will also contain three balance counterweights which allow final adjustment of the center of mass to be coincident with the geometric center. Each of the counterweights will be 7.6 cm in diameter and 22.9 cm in length; they are positioned on three mutually perpendicular, but non-intersecting, axes with an axial adjustment travel of plus-or-minus 7.6 cm (Figure 2-4).

There will be 144 retroreflectors, and hence 144 cavities, in each of the spherical caps for a total of 864 retroreflectors. Figure 2-5 depicts a cross section of a retroreflector mounted in a cavity. Some parameters of the retroreflectors are listed in Table 2-2.

Figure 2-6 is a summary chart of the Satellite configuration and launch vehicle configuration.



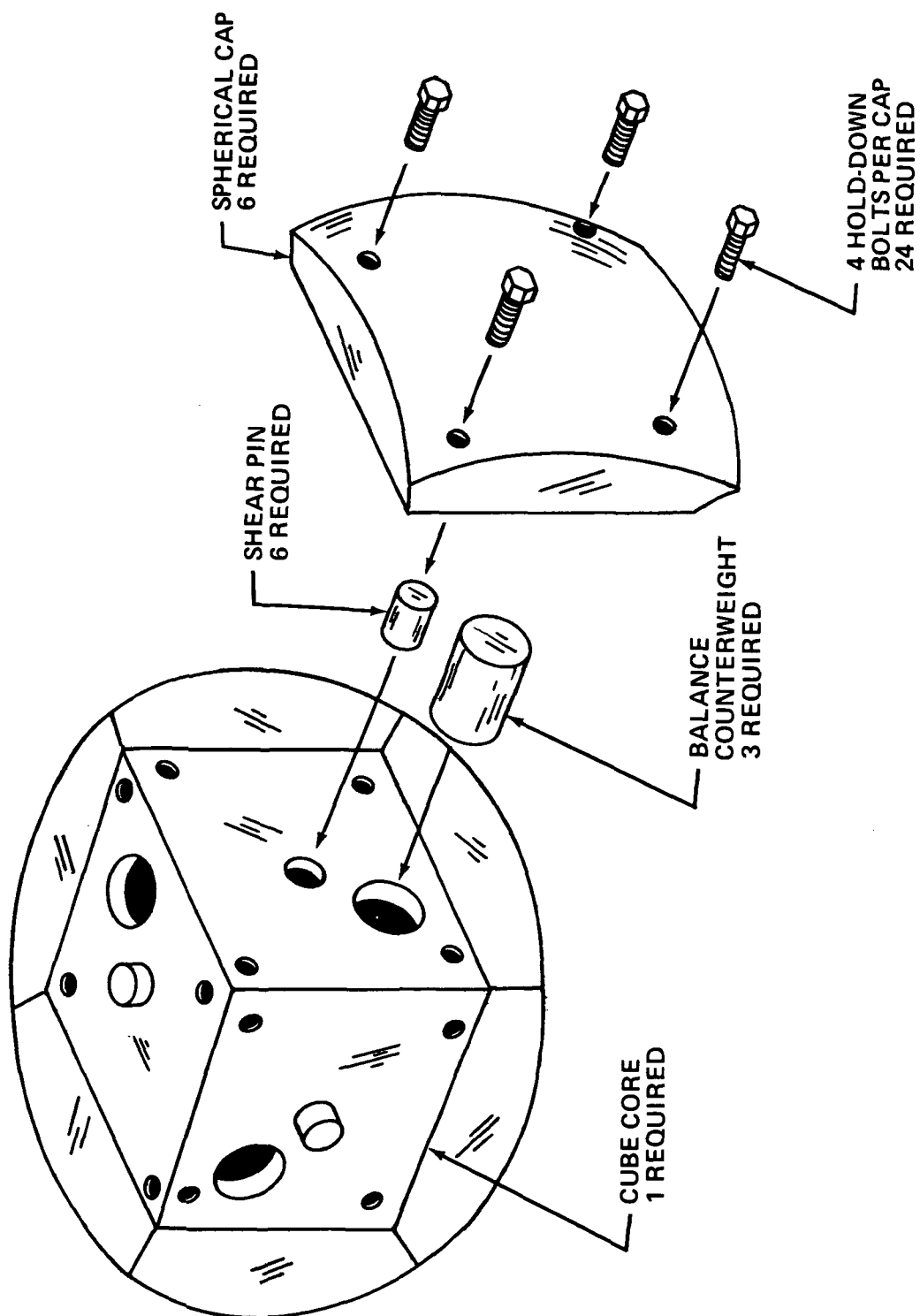


FIGURE 2-4. Assembly configuration of cube core.

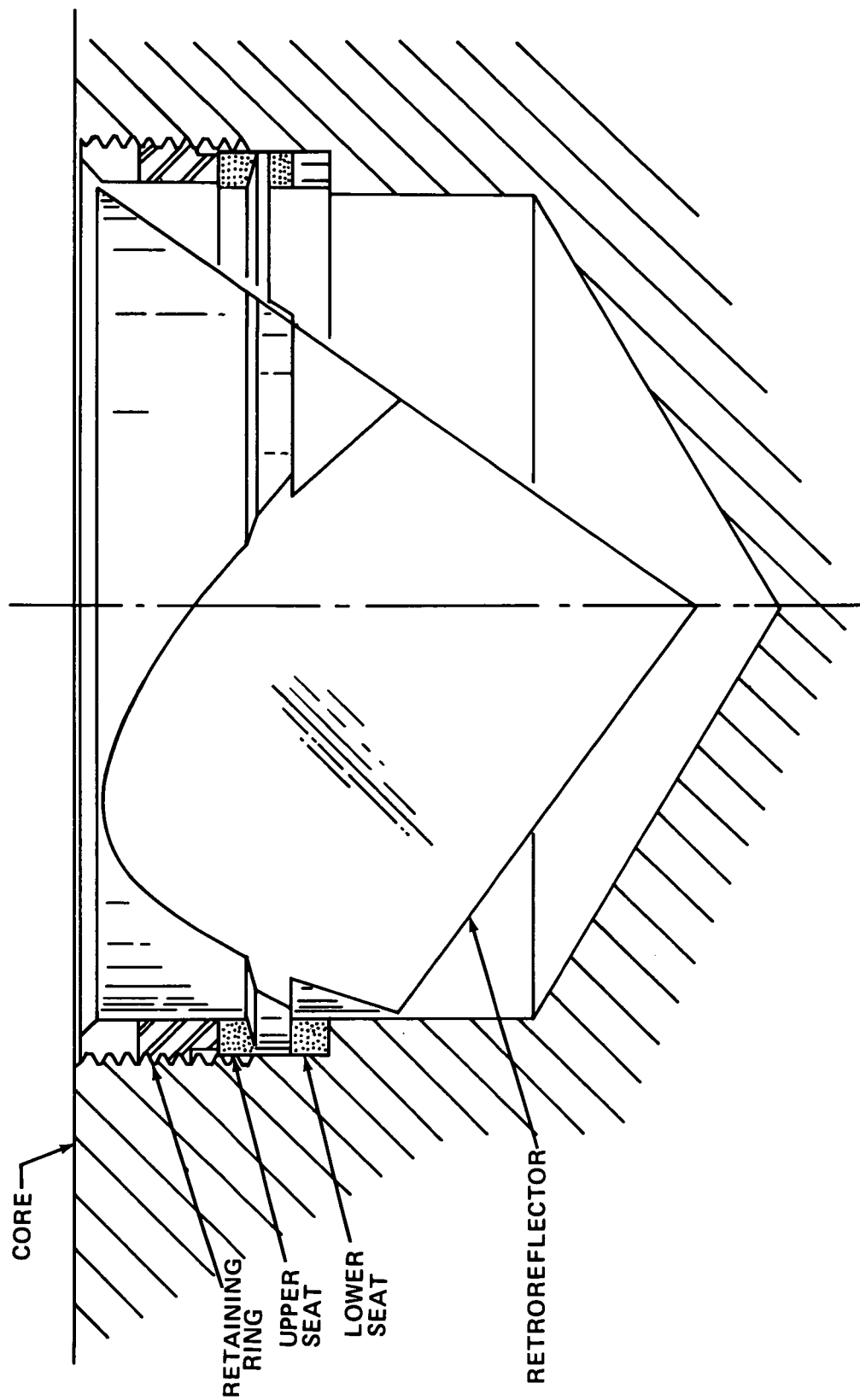


FIGURE 2-5. Cross section of retroreflector mounted in cavity.

TABLE 2-2. RETROREFLECTOR PARAMETERS

Number:	864 Total
Size:	1.438-inch (3.65 cm) Diameter
Material:	High-grade Fused Silica
Configuration:	Cylindrical Cube Corner
Dihedral Angles:	90° 00' 2.5"    +0.0" -0.5"
Surface Accuracy:	Flat Within $\lambda/20$
Surface Coating:	Aluminized Reflective Surfaces with No Overcoating
Entrance Face:	No Anti-reflection Coating
Mounting:	Similar to Lunar Retroreflectors
Pattern on Sphere:	General Triangular Pattern in Each Quadrant of Each Gap

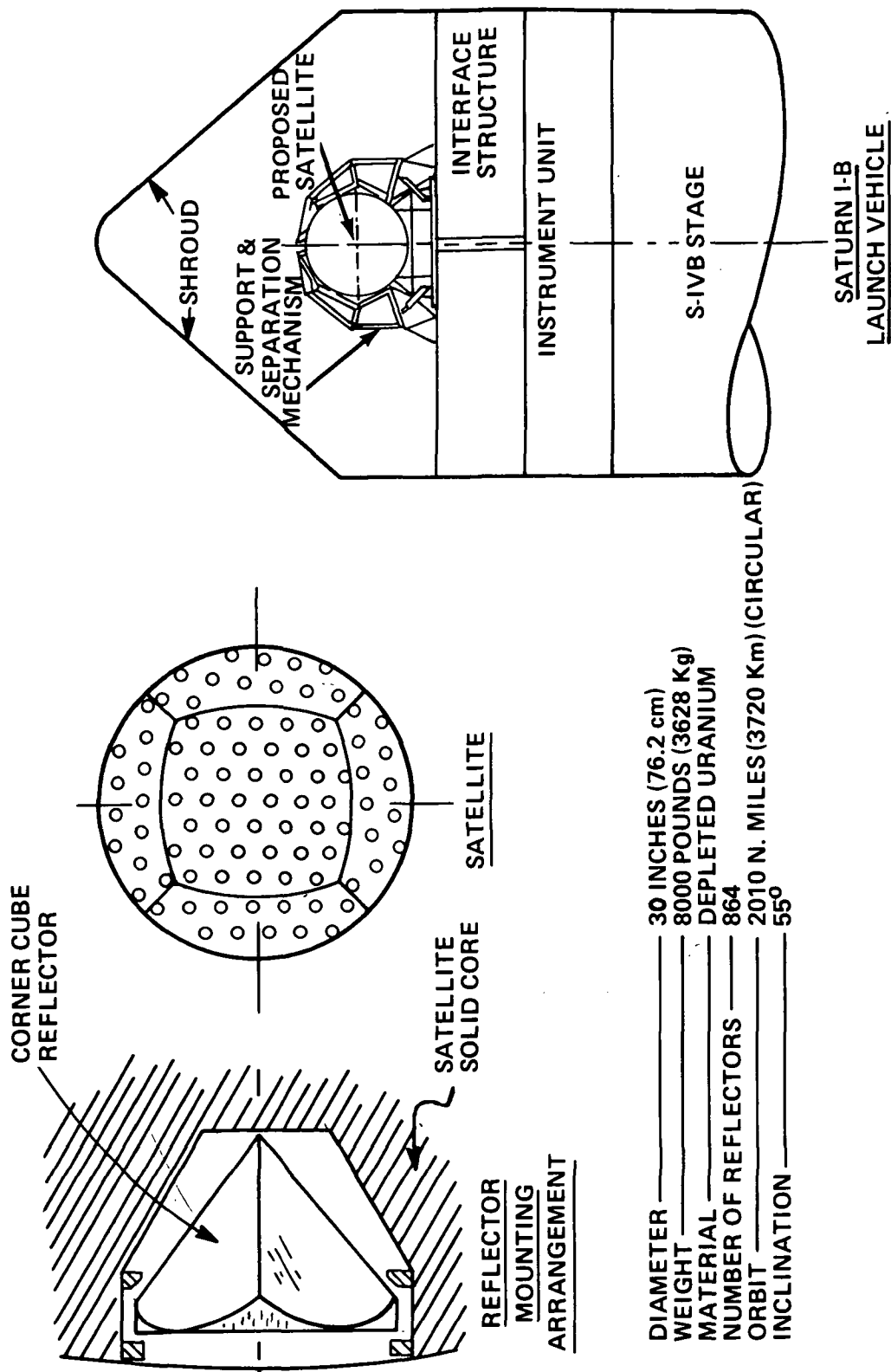


FIGURE 2-6. Satellite and launch vehicle configurations and parameters.

The launch vehicle trajectory calls for insertion of the payload in a 3720-km circular orbit, inclined at 55 degrees. Launch is from Pad 39B at Kennedy Space Center, using a launch azimuth of 37.94 degrees to provide a planar boost flight to insertion in a 55-degree-inclination elliptical orbit at 150 km by 3720 km altitude. Following orbit insertion, a portion of the payload enclosure (SLA/nose cone) is jettisoned; and the S-IVB/IU payload coasts until the S-IVB stage restart, which is planned to occur as the vehicle approaches the first apogee. The S-IVB stage second burn then establishes a circular orbit at 3720 km with a period of 167.96 minutes. (See Figure 2-7.) The payload is separated from the S-IVB/IU at the first equatorial crossing (ascending node) following the apogee burn. Two APS retroburns are then performed to maneuver the S-IVB/IU into an orbit below the payload. (See Figure 2-8.)

Since the IU will be programmed to handle all mission functions, communications networks will not be required; however, the Skylab communications network will be available for all critical events during launch vehicle flight if it is desired. The Skylab network coverage would be as follows: The launch phase of flight to insertion in the initial 150-km by 3720-km orbit would have continuous coverage by MILA, Bermuda, and an insertion ship. The Madrid station would provide coverage of the jettison of the payload enclosure. During subsequent orbital flight, the S-IVB restart for the apogee circularization burn would have coverage from the Australian stations. Near continuous coverage would then be provided for both the S-IVB/IU and the payload during flight in the 3720-km orbit. Separation of the payload at the ascending node following the S-IVB restart would be covered from Hawaii. The first of two auxiliary propulsion system (APS) retroburns utilized to maneuver the S-IVB/IU into an orbit below the payload would be covered by Ascension Island and Canary Island, while the second would be covered from Guam and Honeysuckle.

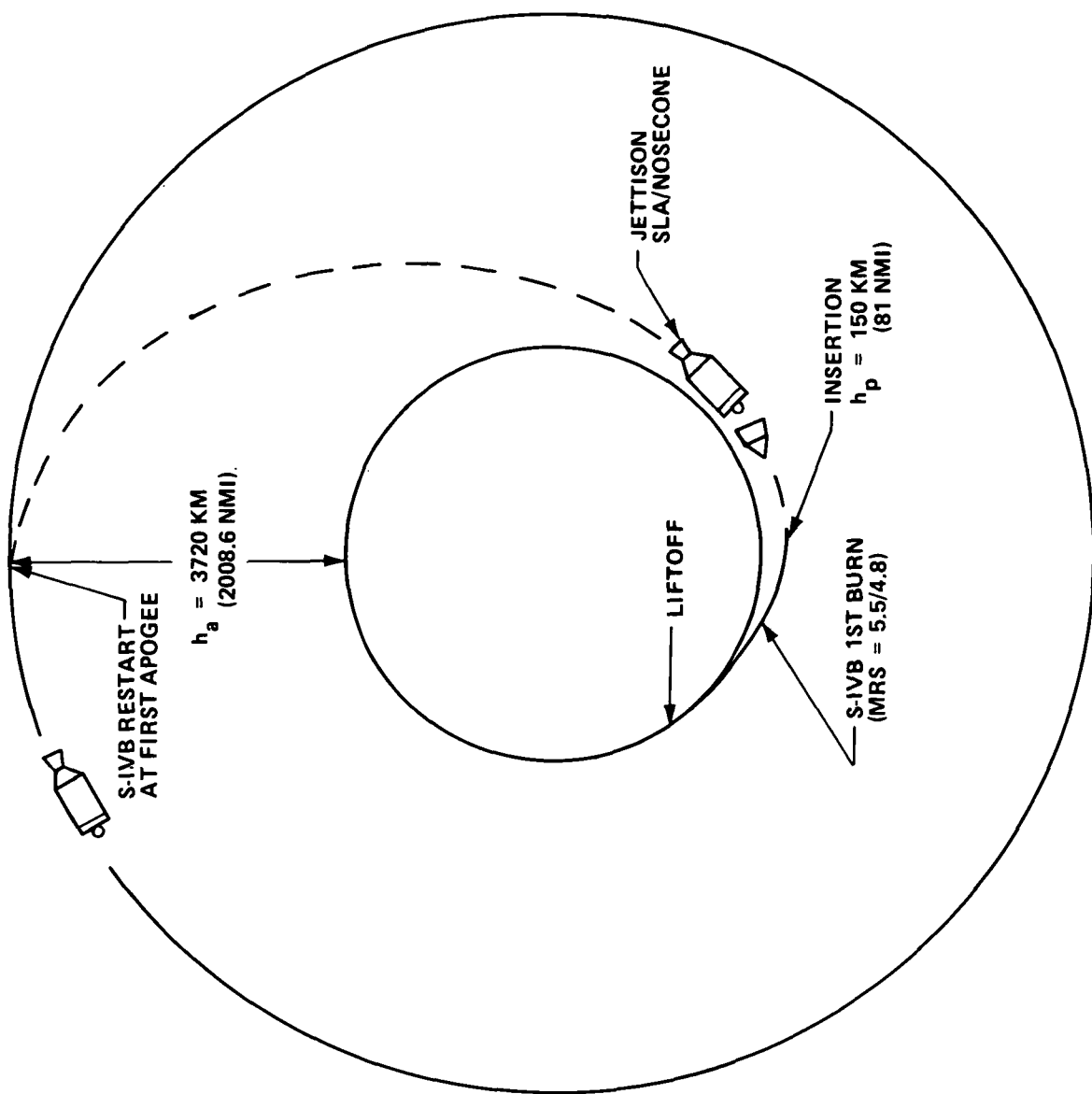


FIGURE 2-7. Flight profile.

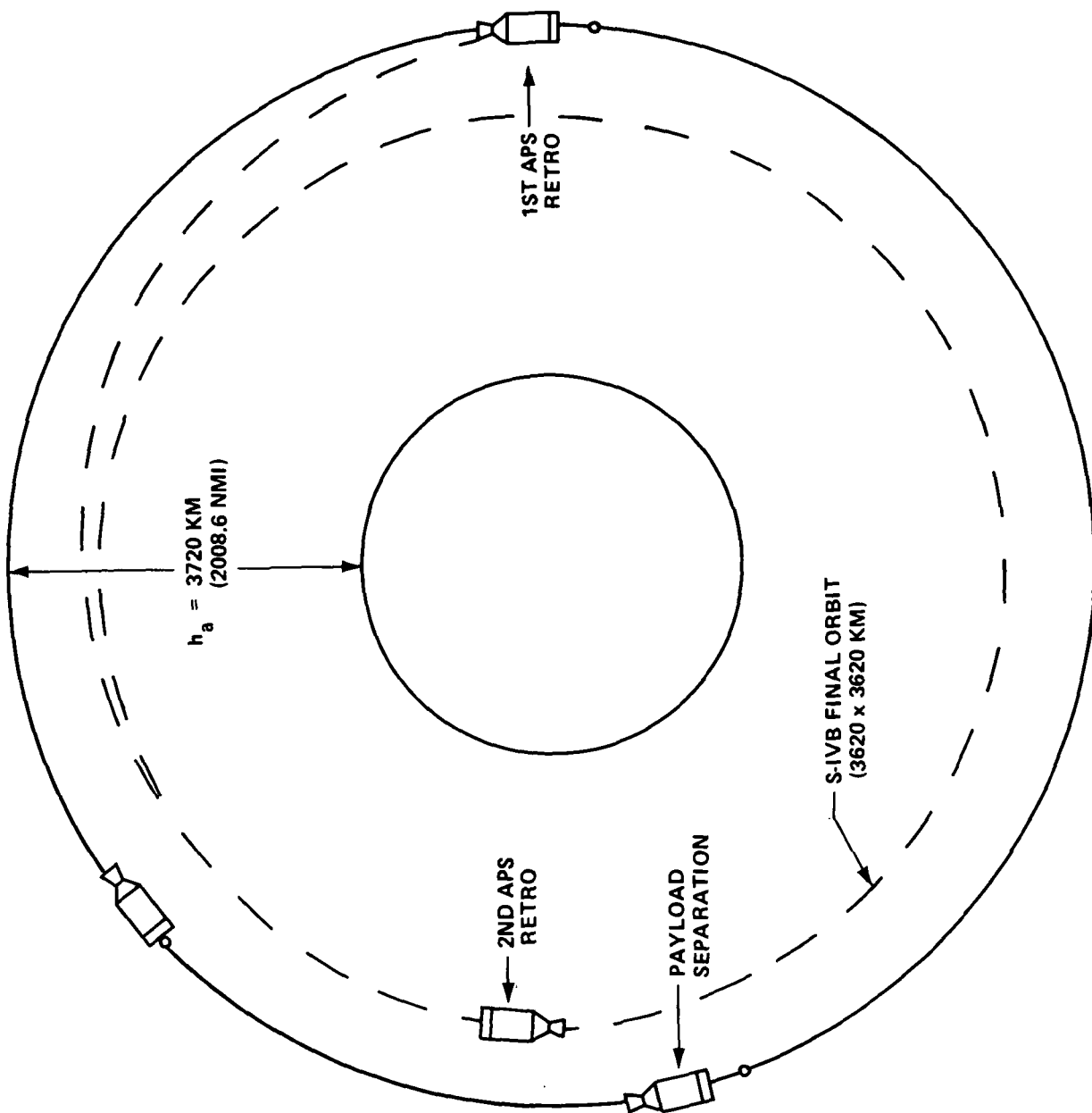


FIGURE 2-8. Orbital flight profile.

VOLUME II

PRELIMINARY DESIGN AND TRADE STUDIES SUMMARY



## TABLE OF CONTENTS

1.0	INTRODUCTION	1-1
1.1	PURPOSE AND APPLICATION	1-1
1.2	CRITERIA	1-2
1.2.1	SEPS CONFIGURATION	1-2
1.2.2	SEPS REQUIREMENTS	1-3
1.2.3	SYSTEM ACCURACY REQUIREMENTS	1-4
1.2.4	GROUND RECEIVING STATION PLACEMENT	1-5
1.2.5	PAYLOAD SYSTEMS DESIGN	1-5
1.2.6	LAUNCH VEHICLE SELECTION	1-6
2.0	SATELLITE	2-1
2.1	INTRODUCTION	2-1
2.2	SATELLITE REQUIREMENTS	2-1
2.2.1	SCIENTIFIC REQUIREMENTS	2-1
2.2.2	RANGING REQUIREMENTS	2-2
2.3	SATELLITE DESIGN	2-9
2.3.1	GENERAL RETROREFLECTOR ARRAY CONSIDERATIONS	2-9
2.3.2	SPECIFIC RETROREFLECTOR DESIGN	2-17
2.3.3	CORE	2-31
2.3.4	SATELLITE ACCURACY	2-38
2.3.5	MASS AND BALANCE	2-40
2.3.6	LAUNCH VEHICLE INTERFACE	2-41
2.4	THERMAL ANALYSIS	2-45
2.4.1	GENERAL THERMAL CONSIDERATIONS	2-45
2.4.2	CORE	2-45
2.4.3	RETROREFLECTORS	2-46
2.4.4	THERMAL CONCLUSIONS	2-49
2.5	DETAIL DESIGN	2-49
2.5.1	CORE DETAILS	2-49
2.5.2	RETROREFLECTOR DETAILS	2-59
2.5.3	RETROREFLECTOR MOUNTING DETAILS	2-59
2.5.4	OTHER DESIGN DETAILS	2-59
2.6	MANUFACTURING	2-60
3.0	PAYLOAD SYSTEMS PRELIMINARY DESIGN	3-1
3.1	PAYLOAD SHROUD	3-1
3.1.1	PAYLOAD SHROUD CONFIGURATION	3-1

## ABSTRACT

Presented in this volume are the considerations applicable to the design and launch of a passive satellite for laser ranging measurements in an earth physics program. Criteria, applications, requirements, and configurations are explained in detail for the satellite, the support and ejection mechanism, the launch vehicle stages, and the flight mission.

The report shows that the selected design configurations are feasible for accomplishing the program mission objectives.

## TABLE OF CONTENTS (Continued)

3.1.2	SATELLITE SUPPORT STRUCTURAL INTERFACE	3-1
3.1.3	PAYLOAD SHROUD SEPARATION SYSTEM	3-1
3.2	SATELLITE SUPPORT SYSTEM	3-5
3.2.1	STRUCTURAL SUPPORT SYSTEM	3-5
3.2.2	SATELLITE SUPPORT STRUCTURE AND EJECTION MECHANISM	3-5
3.2.3	SATELLITE EJECTION SYSTEM ORDNANCE AND ELECTRICAL SYSTEMS	3-13
3.3	SATELLITE ANTI-CONTAMINATION SYSTEM	3-16
3.3.1	ANTI-CONTAMINATION SYSTEM CONCEPT	3-16
3.3.2	ANTI-CONTAMINATION ENCLOSURE	3-18
3.3.3	ANTI-CONTAMINATION PURGE SYSTEM	3-21
3.4	SUPPORT SYSTEM STRUCTURAL ANALYSES	3-38
3.4.1	FLIGHT LOADS	3-38
3.4.2	PRE-LOADS AND LOAD PATHS	3-39
3.4.3	STATIC LOAD ANALYSES	3-41
3.4.4	STRESS ANALYSES AND MEMBER SIZING	3-46
3.4.5	FINITE ELEMENT ANALYSIS OF SUPPORT STRUCTURE	3-53
3.4.6	ACOUSTIC ENVIRONMENT	3-67
3.5	PAYLOAD SYSTEMS WEIGHT SUMMARY	3-75
4.0	LAUNCH VEHICLE CONFIGURATION DEFINITION	4-1
4.1	CONFIGURATION SUMMARY	4-1
4.2	S-IB STAGE MODIFICATION DEFINITION AND INTERFACES	4-1
4.2.1	S-IB STAGE MODIFICATIONS	4-1
4.2.2	S-IB STAGE SELECTION FOR SEPS	4-1
4.3	S-IVB STAGE	4-3
4.3.1	S-IVB STAGE MODIFICATIONS	4-3
4.3.2	SATURN IB/S-IVB STAGE	4-8
4.3.3	SATURN V/S-IVB STAGE	4-13
4.3.4	S-IVB STAGE SELECTION FOR SEPS	4-17
4.4	S-IU STAGE	4-19
4.4.1	S-IU STAGE MODIFICATION	4-19
4.4.2	S-IU STAGE SELECTION FOR SEPS	4-21
4.5	GROUND SUPPORT EQUIPMENT MODIFICATION DEFINITION	4-21
5.0	MISSION ANALYSIS	5-1
5.1	MISSION PROFILE	5-1
5.1.1	LAUNCH SEQUENCE	5-1

## TABLE OF CONTENTS (Concluded)

5.1.2	PAYLOAD SEPARATION	5-1
5.1.3	S-IVB EVASIVE MANEUVERS	5-1
5.2	MISSION TIMELINE	5-3
5.3	PERFORMANCE ANALYSIS	5-3
5.3.1	LAUNCH VEHICLE BOOST TRAJECTORY	5-3
5.3.2	LAUNCH VEHICLE DISPERSIONS	5-15
5.3.3	TRADE STUDIES	5-23
5.3.4	ORBITAL STUDIES	5-31
5.4	TRACKING AND COMMUNICATIONS	5-47
5.4.1	COVERAGE WITH SKYLAB NETWORK	5-47
5.4.2	MINIMUM COVERAGE FOR ASSURANCE OF MISSION OBJECTIVES	5-53
5.5	SUBSYSTEMS ANALYSIS	5-54
5.5.1	THRUST VECTOR CONTROL SYSTEM	5-54
5.5.2	STRUCTURAL ANALYSIS	5-64
6.0	CONCLUSIONS AND RECOMMENDATIONS	6-1
6.1	CONCLUSIONS OF PRESTUDIES	6-1
6.2	SATELLITE CONCLUSIONS	6-1
6.2.1	CORE	6-1
6.2.2	RETROREFLECTOR ARRAY	6-2
6.3	PAYLOAD SYSTEMS CONCLUSIONS	6-3
6.3.1	INTERFACE	6-3
6.3.2	PAYLOAD SHROUD	6-4
6.3.3	SUPPORT SYSTEM	6-4
6.3.4	EJECTION SYSTEM	6-4
6.3.5	ANTI-CONTAMINATION SYSTEM	6-5
6.4	LAUNCH VEHICLE CONFIGURATION CONCLUSIONS	6-5
6.5	MISSION PROFILE CONCLUSIONS	6-6
6.6	RECOMMENDATIONS	6-7

## REFERENCES

## LIST OF FIGURES

FIGURE		PAGE
2-1	THE "SCINTILLATION" EFFECT	2-4
2-2	THE "QUANTIZATION" EFFECT	2-4
2-3	CALCULATED RETURN PULSE (100 ELECTRONS)	2-5
2-4	CALCULATED RETURN PULSE (1,000 ELECTRONS)	2-5
2-5	EXPERIMENTALLY DETERMINED RANGE ERROR	2-6
2-6	RAY SYMMETRY	2-10
2-7	CUBE CORNER	2-10
2-8	OUTPUT APERTURE	2-11
2-9	HEXAGONAL RETROREFLECTOR	2-11
2-10	EFFECTIVE REFLECTING AREA VISUALIZATION	2-11
2-11	SIDE MOVEMENT CUTOFF	2-11
2-12	CORNER MOVEMENT CUTOFF	2-11
2-13	CIRCULAR FACE	2-11
2-14	CIRCULAR ORIENTATION INDEPENDENCE	2-11
2-15	DIELECTRIC EFFECT	2-12
2-16	CRITICAL ANGLE FOR UNCOATED SIDES	2-12
2-17	EXCLUDED ANGLE VISUALIZATION	2-13
2-18	Y-SHAPED PERMISSABLE AREA	2-13
2-19	ACTIVE RETROREFLECTORS	2-13
2-20	RETURN PULSES	2-14
2-21	BEAM SPREAD	2-16
2-22	RETROREFLECTOR ARRAY GEOMETRY	2-19
2-23	SPHERICAL CAP	2-21
2-24	RETROREFLECTOR	2-22
2-25	SEPS FLIGHT SATELLITE ASSEMBLY	2-36
2-26	ASSEMBLY CONFIGURATION OF CUBE CORE	2-35
2-27	CUBE CORE	2-50
2-28	BALANCE COUNTERWEIGHT	2-51
2-29	SHEAR PIN	2-52
2-30	CLOSURE PLUG	2-53
2-31	BUSHING	2-54
2-32	STEM	2-55
2-33	RETAINER RING	2-56
2-34	LOWER SEAT	2-57
2-35	UPPER SEAT	2-58
3-1	PAYLOAD SHROUD CONFIGURATION	3-2
3-2	LM SUPPORT AND HOLDDOWN FITTING	3-3
3-3	NOSE CONE/SLA SEPARATION INTERFACE	3-4
3-4	STRUCTURAL SUPPORT SYSTEM	3-6
3-5	STRUCTURAL SUPPORT SYSTEM	3-7

# LIST OF FIGURES (Continued)

FIGURE		PAGE
3-6	STRUCTURAL SUPPORT SYSTEM	3-8
3-7	SATELLITE SUPPORT AND HOLDDOWN STRUCTURE	3-9
3-8	SATELLITE RELEASE MECHANISM	3-12
3-9	EJECTION SYSTEM ORDNANCE SCHEMATIC	3-14
3-10	EBW FIRING UNIT AND POWER SUPPLY	3-15
3-11	EBW ELECTRICAL INTERFACE	3-17
3-12	ANTI-CONTAMINATION ENCLOSURE - SECTION VIEW	3-19
3-13	ANTI-CONTAMINATION ENCLOSURE - SECTION VIEW	3-20
3-14	PRESSURE-REGULATED PURGE SYSTEM	3-23
3-15	BLOW DOWN PURGE SYSTEM	3-25
3-16	PRESSURE IN THE ANTI-CONTAMINATION ENCLOSURE VERSUS TIME FOR THE FIRST 150 SECONDS OF FLIGHT	3-28
3-17	PRESSURE IN THE ANTI-CONTAMINATION ENCLOSURE AND ATMOSPHERIC PRESSURE VERSUS TIME FOR THE FIRST 50 SECONDS OF FLIGHT	3-29
3-18	PRESSURE IN THE ANTI-CONTAMINATION ENCLOSURE AND ATMOSPHERIC PRESSURE VERSUS TIME FROM 50 SECONDS TO 150 SECONDS INTO THE FLIGHT	3-30
3-19	PRESSURE IN THE ANTI-CONTAMINATION ENCLOSURE VERSUS TIME FROM 150 TO 1000 SECONDS INTO THE FLIGHT	3-31
3-20	PRESSURE IN THE ANTI-CONTAMINATION ENCLOSURE VERSUS TIME FROM 1000 TO 8000 SECONDS INTO THE FLIGHT	3-32
3-21	PRESSURE IN THE STORAGE SPHERE VERSUS TIME FROM LAUNCH THROUGH SATELLITE RELEASE	3-34
3-22	ANTI-CONTAMINATION ENCLOSURE PRESSURE RELEASE PURGE SYSTEM	3-36
3-23	PRE-LOADS AND LOAD PATHS	3-40
3-24	MAIN BEAM SHEAR-MOMENT DIAGRAM	3-44
3-25	MAIN BEAM SHEAR-MOMENT DIAGRAM	3-45
3-26	MAIN BEAM TYPICAL CONSTRUCTION	3-47
3-27	MAIN BEAM TENSION ROD ARRANGEMENT	3-48
3-28	TENSION ROD LOAD DISTRIBUTION	3-51
3-29	TENSION ROD SIZING MODEL	3-52
3-30	FINITE ELEMENT MODEL	3-55
3-31	TYPICAL GRID POINTS AND STRUCTURAL ELEMENTS	3-56
3-32	SLA ATTACH POINT MODEL	3-58
3-33	MODE SHAPE, MODE 1	3-61
3-34	MODE SHAPE, MODES 2 AND 3	3-62

# LIST OF FIGURES (Continued)

FIGURE		PAGE
3-35	MODE SHAPE, MODES 4 AND 5	3-63
3-36	MODE SHAPE, MODES 6 AND 7	3-64
3-37	MODE SHAPE, MODES 8 AND 9	3-65
3-38	MODE SHAPE, MODES 10 AND 11	3-66
3-39	LATERAL AMPLIFICATION FACTOR VERSUS FREQUENCY	3-68
3-40	LONGITUDINAL AMPLIFICATION FACTOR VERSUS FREQUENCY	3-69
3-41	SOUND PRESSURE LEVEL VERSUS FREQUENCY SATURN S-IB/S-IVB/ATM-SLA	3-74
4-1	APS PERFORMANCE CAPABILITY	4-6
4-2	S-IVB/IB/SEPS MODIFICATIONS	4-9
4-3	S-IVB SLOSH BAFFLE INSTALLATIONS	4-11
4-4	S-IVB/V/SEPS MODIFICATIONS	4-15
4-5	SAT IB/S-IVB INTERSTAGE MODIFICATIONS	4-18
5-1	LAUNCH VEHICLE FLIGHT PROFILE	5-2
5-2	ALTITUDE VS. TIME - S-IB STAGE FLIGHT	5-6
5-3	VELOCITY VS. TIME - S-IB STAGE FLIGHT	5-7
5-4	PITCH ATTITUDE VS. TIME - S-IB STAGE FLIGHT	5-8
5-5	ACCELERATION VS. TIME - S-IB STAGE FLIGHT	5-9
5-6	DYNAMIC PRESSURE VS. TIME - S-IB STAGE FLIGHT	5-10
5-7	AERO-HEATING INDICATOR VS. TIME - S-IB STAGE FLIGHT	5-11
5-8	ALTITUDE VS. TIME - S-IVB FIRST BURN	5-12
5-9	VELOCITY VS. TIME - S-IVB FIRST BURN	5-13
5-10	PITCH ATTITUDE VS. TIME - S-IVB FIRST BURN	5-14
5-11	DELTA-PAYLOAD VS ALTITUDE AND INCLINATION	5-24
5-12	DELTA-PAYLOAD & FLIGHT ENVIRONMENT VS. INSERTION ALTITUDE	5-25
5-13	INSTANTANEOUS IMPACT PREDICTION TRACE OVER NEWFOUNDLAND	5-27
5-14	INSTANTANEOUS IMPACT PREDICTION TRACE OVER EURASIA	5-28
5-15	PAYLOAD PENALTY FOR BOOST FLIGHT YAW STEERING TO 55 DEGREE INCLINATION	5-29
5-16	PAYLOAD INCREASE BY JETTISONING SLA/NOSECONE DURING BOOST FLIGHT	5-30
5-17	PRELIMINARY ORBIT ERROR ANALYSIS	5-32
5-18	TIME OF LAUNCH FOR ORBITAL NODE OF 180 DEGREES	5-35

## LIST OF FIGURES (Concluded)

FIGURE		PAGE
5-19	LAUNCH WINDOW VS. YAW MANEUVER	5-36
5-20	LATITUDE AT SEPARATION VS. YAW MANEUVER	5-37
5-21	APOGEE CHANGE DUE TO SEPARATION VELOCITY	5-38
5-22	HORIZONTAL SEPARATION TIME HISTORY	5-39
5-23	MAXIMUM VERTICAL SEPARATION	5-40
5-24	S-IVB DELTA-VELOCITY REQUIRED TO ESTABLISH ORBIT BELOW PAYLOAD	5-41
5-25	TOTAL DELTA-VELOCITY CAPABILITY OF S-IVB APS SYSTEM	5-42
5-26	EFFECT OF ONE S-IVB RETRO IMPULSE	5-44
5-27	EFFECT OF TWO S-IVB RETRO IMPULSES	5-45
5-28	TIME HISTORY OF SOLAR LOOK ANGLE	5-46
5-29	TRACKING COVERAGE - LIFTOFF THROUGH S-IVB RESTART	5-49
5-30	TRACKING COVERAGE FOLLOWING S-IVB RESTART	5-50
5-31	COMMUNICATION TIMELINES	5-51
5-32	AERODYNAMIC DISTURBANCE MOMENT COEFFICIENT TIME HISTORY	5-55
5-33	RECOMMENDED FIRST STAGE PITCH/YAW CONTROL GAINS	5-56
5-34	FIRST STAGE PITCH/YAW STABILITY MARGINS	5-57
5-35	ROOT LOCI FOR FIRST AND SECOND COUPLED VEHICLE/PEDESTAL/PAD MODES	5-59
5-36	SECOND STAGE PITCH/YAW SLOSHING ROOT LOCI	5-60
5-37	BOOST FLIGHT HEAD-TAIL WIND SPEED LIMITS	5-62
5-38	BOOST FLIGHT LEFT-RIGHT CROSSWIND SPEED LIMITS	5-63
5-39	NATURAL FREQUENCY VERSUS FLIGHT TIME	5-70
5-40	INSTABILITY GAIN VERSUS EXCITATION FREQUENCY	5-71
5-41	S-IVB MAXIMUM $q\alpha$ LOADS	5-72
5-42	LIMIT RUNNING LOAD (MAX $q\alpha$ )	5-76



## LIST OF TABLES

TABLE		PAGE
2-1	SIGNAL - STRENGTH VALUES	2-3
2-2	TYPICAL ATMOSPHERIC CORRECTION	2-7
2-3	ELECTRONS GENERATED WITHIN 15 NSEC	2-8
2-4	RETURN STRENGTH FOR CIRCULAR RETROREFLECTORS	2-17
2-5	SEPS RETROREFLECTOR ARRAY	2-30
2-6	DENSITIES OF SOME HEAVY METALS	2-31
2-7	POTENTIAL HAZARDS OF DEPLETED URANIUM	2-33
2-8	ENGINEERING PROPERTIES OF SELECTED METALS	2-34
2-9	GEOMETRIC ERROR BUDGET	2-39
3-1	EJECTION SPRING CHARACTERISTICS	3-11
3-2	PRESSURE REGULATED SYSTEM MASS STATEMENT	3-26
3-3	BLOW DOWN SYSTEM MASS STATEMENT	3-33
3-4	ANTI-CONTAMINATION ENCLOSURE PRESSURE RELEASE SYSTEM MASS STATEMENT	3-37
3-5	FLIGHT LOAD CONDITIONS	3-39
3-6	SUPPORT STRUCTURE LOADS	3-43
3-7	LM-SEPS ATTACH POINT LIMIT LOAD COMPARISON	3-54
3-8	SUPPORT STRUCTURE NATURAL FREQUENCIES	3-59
3-9	DESIGN SPECIFICATION FOR SINUSOIDAL VIBRATION FOR SATURN S-IB/S-IVB/ATM AT THE SLA OUTRIGGER	3-60
3-10	LONGITUDINAL AXIS ACCELERATION RESPONSE	3-70
3-11	LONGITUDINAL AXIS DISPLACEMENT RESPONSE	3-71
3-12	LATERAL AXIS ACCELERATION RESPONSE	3-72
3-13	LATERAL AXIS DISPLACEMENT RESPONSE	3-73
3-14	PAYLOAD SYSTEMS MASS SUMMARY	3-76
4-1	EARTH PHYSICS SATELLITE-PHASE B STUDIES VEHICLE MASS BREAKDOWN	4-2
4-2	SMITHSONIAN SATELLITE MISSION-SEPS MISSION APS USAGE	4-4
4-3	J-2 ENGINE SEPS MODIFICATIONS	4-7
5-1	MISSION TIME LINE	5-4
5-2	FLIGHT ENVIRONMENT	5-15
5-3	SATURN IB L/V DISPERSION ANALYSIS PROPELLANT RESERVES REQUIRED TO OFFSET ERROR SOURCE EFFECTS ON PERFORMANCE	5-16

# LIST OF TABLES (Concluded)

TABLE		PAGE
5-4	SATURN IB L/V DISPERSION ANALYSIS ERROR SOURCE CONTRIBUTION TO FLIGHT PERFORMANCE RESERVES	5-19
5-5	SATURN IB L/V DISPERSION ANALYSIS AXIAL ACCELERATION, COMPARISONS	5-20
5-6	SATURN IB L/V DISPERSION ANALYSIS DYNAMIC PRESSURE COMPARISONS	5-21
5-7	SATURN IB L/V DISPERSION ANALYSIS AERO-HEATING INDICATOR COMPARISONS	5-22
5-8	TRAJECTORY PARAMETERS	5-23
5-9	TRACKING AND COMMUNICATIONS NETWORK	5-48
5-10	MAXIMUM LONGITUDINAL LOAD FACTORS ON S-IB PROPELLANT TANKS DURING LAUNCH	5-65
5-11	MAXIMUM HOLD-DOWN LOADS DURING LAUNCH	5-65
5-12	BASE BENDING MOMENT	5-65
5-13	STRESS RATIO SUMMARY FOR PRIMARY STRUCTURE	5-66
5-14	STRESS RATIO SUMMARY-LAUNCH CONDITIONS	5-68
5-15	COMPARISON OF S-IVB LOADS AND S-IVB/IB STRUCTURAL CAPABILITY	5-73
5-16	PRELIMINARY BENDING MODE CHARACTERISTICS COMPARISON OF FIRST STAGE BENDING MODE FREQUENCIES	5-79

## SECTION 1. INTRODUCTION

This is the second of four volumes designed to present a total summation of the Smithsonian Earth Physics Satellite (SEPS) study. This volume (Volume II) presents the technical results of the study, defining the basis for the recommendations and conclusions. Briefly, Volume II covers the technical evaluation and design concepts for the satellite, satellite support structure, Saturn IB launch vehicle configuration modification, mission analysis and conclusions and recommendations.

### 1.1 PURPOSE AND APPLICATION

The Earth Physics Satellite program is a laser ranging system using a fixed object in space for sighting to provide global measurements at heretofore unattainable accuracy. This concept developed as a result of a recommendation of the Williamstown Study on Solid-Earth and Ocean Physics, which expressed the need for ranging the satellite to an accuracy of  $\pm 2$  cm for the detection of variation in the geometry of the earth such as those resulting from body tides, continental drift, etc. A satellite such as SEPS would allow very accurate range measurements from the earth's surface to an object in an extremely stable orbit, permitting global measurements of ground stations positions to an accuracy of 10 cm or better and could possibly be uprated to obtain the accuracy desired through improved laser ranging techniques. This concept will provide a gain in accuracy of two orders of magnitude over existing satellite configurations.

The basic objectives of the Earth Physics Program (EPP), utilizing the SEPS satellite, are to make observations which will provide measurements of the following:

1. Rotation of the earth.
2. Polar motion.
3. Earth body tides and tidal loading.
4. Tectonic motions.
5. Establishment of a 10-cm terrestrial coordinate system.

It is postulated that this system will provide a basis for earthquake investigation by measuring earth movements before, during, and after earthquakes. Other uses will be to measure the continental mass deformation due to tides and due to the recession and advancement of glaciers, and to measure more accurately the earth's rotation.

## 1.2 CRITERIA

### 1.2.1 SEPS CONFIGURATION

In considering satellites for EPP, interest has generally centered on multipurpose spacecraft in synchronous (usually geostationary) or near-synchronous orbits. Although this may be a preferred choice for some EPP missions, such as satellite/satellite tracking, it is not suitable for the high-precision geometric objectives noted above. There are three fundamental reasons for this conclusion: restricted geographic coverage, unfavorable satellite/ground-station geometry, and unfavorable satellite configuration.

If the spacecrafts are geostationary, full global coverage is not afforded even by a three satellite constellation. If a limit of  $10^\circ$  on the lower elevation angle is adopted (to avoid excessive errors resulting from atmospheric propagation), regions above  $70^\circ$  latitude are excluded even at the longitude of each satellite. More serious is amplification of the geometric error in and near the orbital plane; it prevents accurate determinations of latitude in a band around the earth's equator and longitude in regions around the subsatellite points. This effect applies not only to ranging systems but also to Very Long Baseline Interferometry systems, which are essentially range difference devices. These gaps in coverage can be avoided by the use of inclined orbits, but then some of the advantages of synchronous orbits are lost--such as the possibility of using fixed directional antennas or telescopes for observing the satellites.

The use of multipurpose spacecraft for EPP geometrical observations unavoidably complicates the measurements. As an example, consider the case of the Applications Technology Satellites -F and -G, whose linear dimensions are more than 3 orders of magnitude greater than the desired accuracy. Relating the satellite center of mass to the observed range for each of a number of lasers viewing these satellites from various aspects and at different times may be solvable in principle; but surely it introduces formidable practical problems; a matter further complicated by the changing spacecraft attitude. The reasonable assumption that the entire error budget ought not to be devoted solely to uncertainties in spacecraft geometry produces the requirement that the pertinent spacecraft geometric parameters be known to an accuracy of a few

millimeters on a structure some  $10^4$  mm in size. This is an improbable expectation for a structure that has been exposed to the launch environment, unfolded in orbit, and then subjected to temperature variations that, at this level of precision, inevitably produce distortions of the satellite geometry.

The suggested satellite is a completely passive, solid sphere fitted with retroreflector cube corners. It is a 3628-kg (8000-pound) sphere of 76.2 cm (30.0-inch) diameter and very high mass-to-area ratio ( $7980 \text{ kg/m}^2$ ). In the suggested orbit of  $55^\circ$  inclination, 3720-km (2010-nm) altitude, and low eccentricity ( $e \sim 0.01$ ), the orbital lifetime is extremely long. The useful life in orbit will be limited only by degradation of the cube corners, so many decades of operation can be expected.

### 1.2.2 SEPS REQUIREMENTS

A satellite that is optimum for EPP geometric measurements has the following characteristics:

1. Completely passive to attain maximum operating life. Acquired by camera (photographing reflected sunlight against star background). Equipped with retroreflectors for ranging with ground-based lasers.
2. Compact and rigid for maximum stability of spacecraft geometry.
3. Spherical so geometry of retroreflector array vs. spacecraft center of mass will not change with aspect. Spherical shape also is necessary to minimize errors in corrections for solar-radiation pressure and drag.
4. Maximum feasible mass-to-area ratio to reduce perturbations caused by nongravitational forces (mainly radiation pressure). This is needed to permit the computation of extremely accurate short (24 hour) arcs to relate geographically remote locations.
5. Orbital altitude high enough to reduce to an acceptable level orbit errors resulting from uncertainties in geopotential models.
6. Orbital altitude low enough to provide best attainable geometry, i. e., altitude comparable to baselines of interest.
7. Inclination large enough to provide global coverage.

### 1.2.3 SYSTEM ACCURACY REQUIREMENTS

Consideration of the scientific objectives clearly substantiates the recommendation of the Williamstown study and the Space Science Board that an earth-physics program will need ranging accuracies of  $\pm 2$  cm. This requirement is due to the fact that secular motions as slow as 1 cm per year exist. The fact that each ground station in the program will be subject to all of the complex motions discussed above -- tidal, earth rotation, polar wander, tectonic, etc. -- and that the motion resulting from each phenomenon must somehow be sorted out before the observations can be fully exploited emphasizes the need for this level of accuracy.

One of the more important factors in designing the SEPS is the total range error that the satellite is allowed to contribute to the 2-cm total of the laser observations. To establish a design goal for this satellite error, the magnitudes of the errors contributed by other sources must be estimated; that is, an error budget must be formulated that anticipates the future state of the art in laser ranging. Although predictions of this kind are always somewhat uncertain, the following are reasonable expectations for a period some 5 to 10 years from now:

#### Tropospheric-propagation velocity

Uncertainties	15 mm
---------------	-------

#### Laser

Pulse detection	10 mm
Range counter	5 mm
Cables, mechanical, calibration-target survey, calibration propagation velocity, etc.	5 mm

Satellite	5 mm
-----------	------

Root Sum Square	20 mm
-----------------	-------

The most pertinent question about this error budget that can be examined at this time is the feasibility of attaining the 5-mm level with the satellite. The conclusion is that this accuracy can surely be attained through careful design and fabrication.

#### 1.2.4 GROUND RECEIVING STATION PLACEMENT

A complication in the interpretation of tectonic observations is the difficulty in finding a "fixed" point whereon to stand. Observing with respect to a satellite should be very helpful--if the orbit is sufficiently stable that it can be determined to the needed accuracy.

The frequencies of tectonic motions can be broadly conceived to be comprised of the entire range from earthquakes to continental drift, i.e., seconds to millenia. However, the averaging times in the satellite data need not encompass the high frequency end, as high-frequency (seismic) phenomena are more amenable to observation by ground instruments. Note that this does not exclude from the province of the proposed satellite the measurement of position before and after earthquakes, since each determination, before and after, can be comprised of an average of data taken over a period of time far longer than the duration of the earthquake. Measurements of the latter type will be quite valuable for measuring displacements at distances of a few hundred kilometers or more from an earthquake and for measuring displacements in island arc regions where surface geodetic techniques cannot be used.

Tectonics places one additional requirement on the SEPS system. The ground stations must be placed in rather particular geographic locations. As an example, a three-station net within the Canadian shield, probably the most stable area in the world, is desirable to serve as an "anchor." As this triad is too closely spaced for good orbit-determination geometry, three more stations should be added within a larger, but reasonably stable, region of North America. Stations must also be placed in tectonically active regions (a necessity to observe tectonic motion) such as the eastern Mediterranean, Ethiopia, and Japan. Baselines should be established within these regions and related to the stable networks. The latter places a difficult accuracy requirement on orbit determination.

Specifying a ground-station network is an involved and complex subject and will not be pursued further except to note that the station separations and geographic deployment dictated by tectonic considerations are important determinants in the selection of satellite altitude and inclination.

#### 1.2.5 PAYLOAD SYSTEMS DESIGN

The SEPS must be adapted to the Saturn IB launch vehicle. Due to the relative sizes between the payload and the launch vehicle an adapter must be designed that will secure the satellite above the IU. The adapter must restrain the satellite during powered flight and must eject the satellite when the proper orbit is reached. The satellite must also be protected from any pre-launch or

launch environments which may degrade the quality of the laser reflectors. A nosecone must be selected that will enclose the satellite and eliminate any aerodynamic forces on the satellite during atmospheric flight.

#### 1.2.6 LAUNCH VEHICLE SELECTION

To boost the candidate SEPS satellite into the desired orbit requires a launch vehicle of the Saturn IB class. However, the Saturn IB, as designed, is not capable of performing the second burn necessary to circularize the orbit at 3720 km (2010 nm). The S-IVB stage of the Saturn V has a restart capability and could be substituted for the non-restartable Saturn IB S-IVB stage.

A prime purpose of the Phase B study is to determine the capability of a modified Saturn IB in placing the SEPS satellite into the desired orbit. Secondary considerations include the selection of the hardware that will perform the mission with minimum cost and impact on existing space programs (Skylab, Lunar Exploration, etc.). Therefore the hardware selection will revolve around whether a Saturn IB S-IVB may be modified for a restart capability or a Saturn V S-IVB may be modified to interface with the S-IB stage. Within each of the above options a choice may then be made as to which of the available hardware will have minimum impact on existing space programs.



## SECTION 2 SATELLITE

### 2.1 INTRODUCTION

The broad requirements of the limited phase-B study of the (Smithsonian) Earth Physics Satellite (EPS) program imply an engineering effort having its own specific goals. These goals are to

1. Evolve a detailed design and associated specifications for a functional EPS matched to the scientific and other requirements of the overall program;
2. Establish a manufacturing plan for producing an actual flight satellite to this design and these specifications;
3. Identify, define, and recommend action on any unresolved problems beyond the scope of the present study.

These goals have been achieved. The individual tasks that have resulted in the attainment of these goals are discussed below.

### 2.2 SATELLITE REQUIREMENTS

The satellite design has been derived primarily from scientific considerations and laser-ranging requirements. In addition, practical aspects such as feasibility of manufacture and costs have influenced the design. While the satellite has been designed to meet the scientific and laser-ranging requirements in a nearly optimum manner, it must be understood that certain trade-off considerations involving characteristics of the launch vehicle and orbital limitations have necessarily been incorporated.

#### 2.2.1 SCIENTIFIC REQUIREMENTS

The requirements imposed on the EPS as a result of scientific considerations have been presented in Section 1. Those that apply directly to the satellite design are the following:

1. The satellite must be passive;
2. The satellite must be compact and rigid;
3. The satellite must be spherical;
4. The satellite must have as large a mass-to-area ratio as is feasible;
5. The satellite centers of mass and geometry must coincide;
6. The satellite must have no detrimental magnetic characteristics.

Others, such as orbit altitude, high inclination, and low eccentricity, apply directly to the orbital requirements of the satellite and hence influence the design of the launch vehicle. This aspect is discussed in detail elsewhere; however, the combined effect of these and other considerations has been to establish an initial maximum satellite weight of 3628 kilograms (8000 pounds).

In summary, the scientific objectives of the EPS program dictate that the satellite must be a rigid, symmetrical, spherical, non-magnetic, passive satellite having as small a diameter as is feasible within other considerations and weighing no more than 3628 kg (8000 lb).

## 2.2.2 RANGING REQUIREMENTS

Since laser ranging has been established as the means for realizing the scientific objectives of the EPS program, requirements for optimum laser ranging must be incorporated into the satellite design.

In addition, since general orbital parameters must be established before laser ranging, the satellite must incorporate provisions for photographic tracking by reflected sunlight.

### 2.2.2.1 GENERAL RANGING CONSIDERATIONS

The range equation (1) is used to calculate S, the number of photons that reach the receiving telescope from the retro-reflector array on the satellite, when the quantities defined are specified. This equation takes care of the geometric attenuation through the  $R^{-4}$  term and the atmospheric attenuation through the  $T^2$  term. For a ruby-laser system,  $h\nu$ , the energy of a single photon, is  $2.9 \times 10^{-19}$  J.

$$S = \frac{E}{h\nu} G_T A_S G_S A_R \frac{T^2}{R^4} \quad , \quad (1)$$

where

- E = energy of each transmitted pulse,
- $h\nu$  = energy per photon,
- T = atmospheric transmission factor,
- R = laser-to-satellite range,
- $A_S$  = effective aperture of satellite retroreflector array,  
and
- $A_R$  = effective aperture of ground receiver, and
- $G_T$  and  $G_S$  are the "gain" functions for transmitter and  
satellite retroreflector, respectively.

The values of S in Table 2-1 are obtained from the range equation. Here E is used to refer to the satellite's elevation angle, and the respective values of R and T correspond to the angle values listed in the first column. A typical laser energy is assumed to be 5 J and the full width of the laser beam, 3 arcmin. The latter value is smaller than that used with some satellites now in orbit, because the EPS will be in a highly stable orbit from which the azimuth and elevation settings can be predicted with significantly increased accuracy. The number of photon counts, N, is given numerically in the last column. A factor of 58 photons/

electron was used in obtaining N from S. This value includes the effects of the quantum efficiency of a typical photomultiplier tube and the losses in the optical system of a typical receiving telescope. However, newer cathode materials are now being used by the manufacturers of photomultipliers to increase the response several fold at the laser wavelength. The use of a tube with such a cathode would lead to N values as much as 5 times those listed in Table 2-1.

TABLE 2-1 SIGNAL-STRENGTH VALUES

E	R (Mm)	T	S	N
10°	6.803	0.186	270	4.7
15°	6.354	0.318	1040	18
20°	5.948	0.418	2300	40
25°	5.588	0.493	4200	70
30°	5.268	0.550	6600	110
45°	4.528	0.655	17000	300
60°	4.062	0.707	31000	530
75°	3.802	0.733	43000	740
90°	3.723	0.741	48000	830

This range equation contains the variables that have significant and readily represented effects on the strength of the return. There are, however, other variables not easily identified and accounted for. Their effects are shown by the experimental data plotted in Figure 2-1. Here, the differences between the signal calculated from the range equation and typical measured signals are plotted on a logarithmic scale. It is probably not significant that the average of this difference is greater than zero, because not all the range-equation parameters can be precisely determined. The important point is the "scintillation" or variation from one pulse to the next. Hence, it should be realized that there will be statistical effects whose origin is probably the mutual interference of the coherent beams reflected from the individual cube corners that make up the retroreflector array on the satellite.

The finite number of photon counts associated with a given return leads to the "quantization" effect, shown schematically in Figure 2-2. The photomultiplier's generation of discrete electrons distorts the received pulse in a random manner. Hence, the intersection of the pulse's leading edge with  $V_2$ , the threshold level of the range counter, will vary even when the received energy remains constant. This effect will be noted as a variation in  $T_c$ , the two-way propagation time over a fixed distance. There are two ways to eliminate the quantization effect. The first involves a receiver modification that records, either electrically or photoelectrically, the structure of the received pulse. Then  $T_2$ , the time between the threshold intersection corresponding to the stopping of the range counter and the centroid, or other invariant point on the pulse can be obtained and applied as a correction. The second method requires an increase in system sensitivity with a consequent improvement in the pulse shape. Figures 2-3 and 2-4 are computed

examples that show how the pulse's leading edge smooths out under a tenfold increase in the number of photon counts. When the pulse is smooth, the structure of the received pulse need not be determined for increased accuracy, since  $T_c$  can be derived from a measurement of the energy in the received pulse and the known configuration of the transmitted pulse.

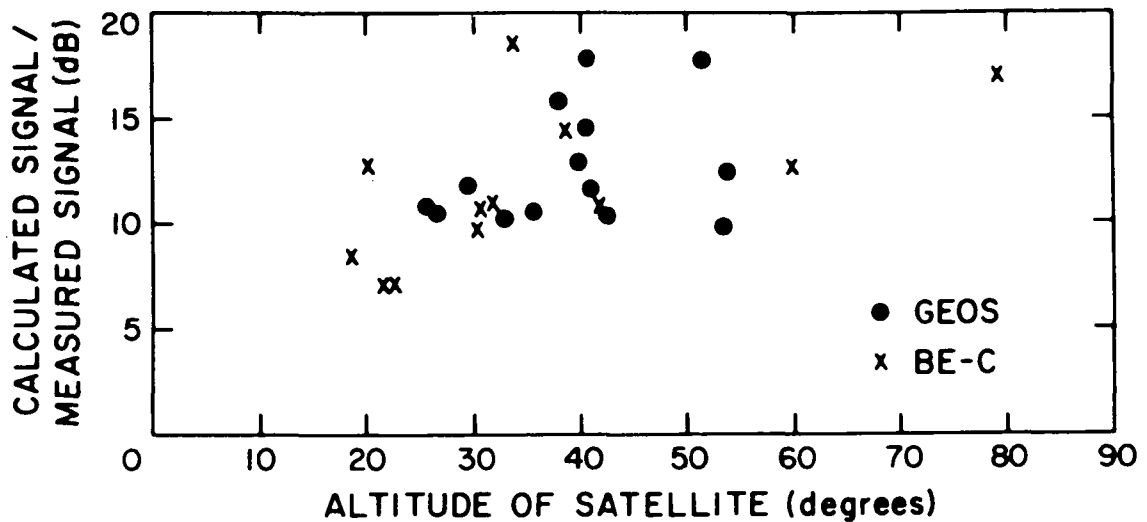


FIGURE 2-1 THE "SCINTILLATION" EFFECT.

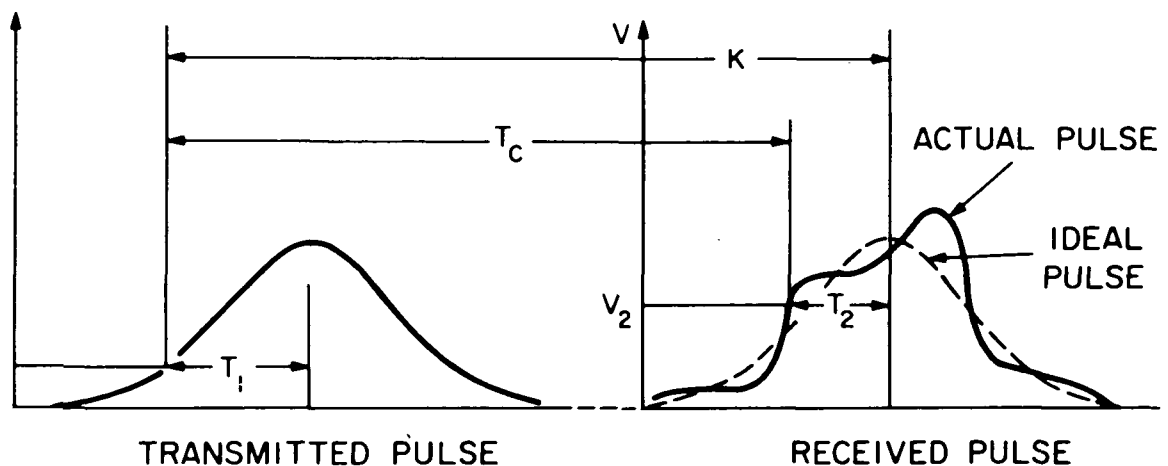


FIGURE 2-2 THE "QUANTIZATION" EFFECT.

Figure 2-5 shows what the ultimate accuracy of a typical laser might be if the receiving technique were modified to record the structure of the returned pulse. This accuracy is dependent, of course, on the laser's pulse duration, which is about 15 nsec in this example. Lasers with considerably shorter pulse durations are now available commercially

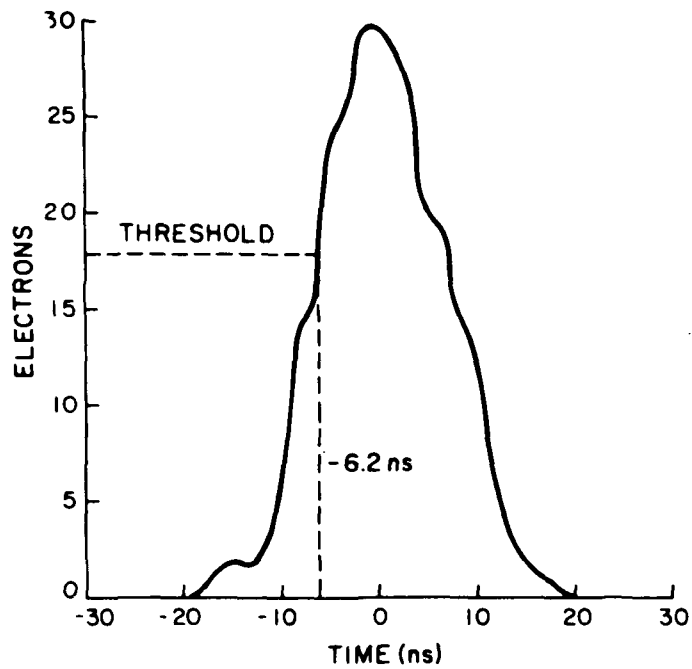


FIGURE 2-3 CALCULATED RETURN PULSE (100 ELECTRONS).

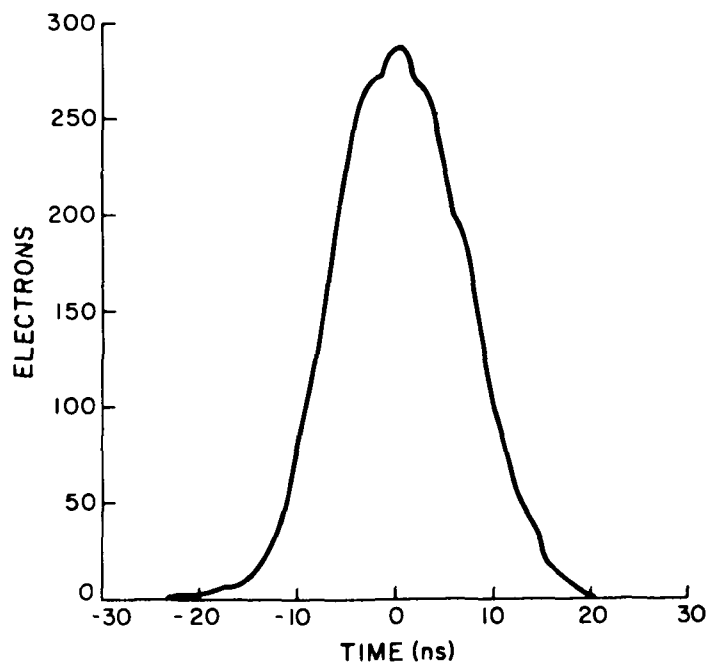


FIGURE 2-4 CALCULATED RETURN PULSE (1,000 ELECTRONS).

and can be used when greater accuracy is required. The experimental data leading to the results shown in Figure 2-5 were obtained by ranging on a reflector at a fixed distance, scaling  $T_2$  values from oscilloscope photographs, and correcting the range-counter readings accordingly. Although the reflector was less than 1 km from the laser system, the return was attenuated to correspond to a satellite return of 30 photon counts. As might be expected, the error, which is about 30 cm at high threshold settings, increases to about 50 cm at lower thresholds, where the slope of the pulse's leading edge is less steep.

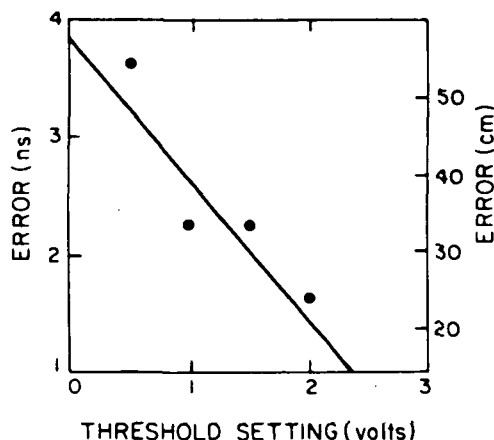


FIGURE 2-5 EXPERIMENTALLY DETERMINED RANGE ERROR.

The formula (3) is currently being used for the atmospheric correction. Subsequent investigations have improved the theoretical base from which such formulas are derived, and these new formulas appear to give even better agreement with experiment. However, the error relation:

$$\sigma_r = \frac{0.018}{\sin \alpha + 10^{-3} \cot \alpha} \text{ [m]} \quad (2)$$

shows that the formula now being used is more than accurate enough for present work. This fact is substantiated by the numbers given in Table 2-2.

For maximum effectiveness, a laser system should be capable of both nighttime and daytime operation. Daytime operation is, of course, the more stringent condition because the sky-background radiation is  $10^7$  higher than it is at night. If the noise pulses generated by this radiation are either too large or too frequent, the receiver cannot discriminate them from satellite returns. However, the effect of daylight noise can be reduced by decreasing the receiver's field of view, by using a narrow passband filter centered at the laser wavelength, and by incorporating a photomultiplier tube with a good single-electron distribution.

With the brightness of the sunlit sky being of fourth magnitude per square arc sec or  $7. \times 10^{16}$  photons  $\text{sec}^{-1} \text{ m}^{-2} \text{ sr}^{-1}$  within a 0.6 - nm bandwidth, the average number of electrons generated will be 0.4 electrons in 15 nanoseconds for a 0.5 meter diameter telescope with a 1.5 arc minute field and a conversion ratio of 58 photons per electron.

Table 2 -3 shows that the probability is only 0.0001 that, under these conditions, a noise pulse would stop a counter whose threshold level was set at a voltage equivalent to 5 electrons.

$$r_m = r_v - \frac{2.238 + 0.0414PT^{-1} - 0.238h_s}{\sin \alpha + 10^{-3} \cot \alpha} \quad \text{for } \theta_0 > 5^\circ \quad (3)$$

$\lambda = 694.3 \text{ nm}$

where:

- P = the atmospheric pressure (mbar),
- T = the temperature ( $^\circ\text{K}$ ),
- h = the laser's elevation above mean sea level (km),
- $\alpha^s$  = the elevation angle of the satellite,
- $\theta_0$  = the apparent elevation angle (i. e. , the elevation angle uncorrected for atmospheric bending), and
- $r_m$  and  $r_v$  are range values (m).

TABLE 2-2  
TYPICAL ATMOSPHERIC CORRECTION

$\alpha$	RANGE CORRECTION	ERROR IN RANGE CORRECTION
$90^\circ$	1.8 m	2 cm
$20^\circ$	5.2 m	5 cm

TABLE 2-3 ELECTRONS GENERATED WITHIN 15 NSEC

Number of Electrons	Probability of Generation
0	0.7
1	0.3
2	0.05
3	0.007
4	0.0007
5	0.0001

#### 2.2.2.2 SPECIFIC RANGING REQUIREMENTS

Requirements as evolved elsewhere in this report are here restated:

1. The satellite must incorporate a large number of identical optical retroreflectors uniformly distributed over the entire spherical surface of the satellite at equal radii from its center of mass;
2. The retroreflectors must be tailored to maximize the reflected energy of an incident beam of light in a conical region that is symmetrical about that incident beam and that has a conical half-angle matched to the range of the velocity aberration associated with the satellite in its orbit;
3. The portion of the spherical surface devoted to retroreflectors must be maximized within the constraint that the remaining surface area is sufficient to allow photographic tracking;
4. The characteristics of the satellite surface not occupied by retroreflectors or their mounting devices must ensure photographic tracking.

#### 2.2.3 OTHER REQUIREMENTS

The EPS design must take into account other requirements. Chief among these is that the satellite must be readily manufactured; i. e., that its component parts do not require new or exotic machining, casting, plating or other fabrication processes, that it is easily assembled, and that it can be practically and safely handled with conventional lifting, moving, and manipulating techniques.

In addition, the satellite and its manufacture must be compatible with established reliability and quality assurance requirements as presented and discussed elsewhere. Also, the cost of the satellite must be a consideration wherever technical requirements can allow alternative choices or trade-offs.



## 2.3 SATELLITE DESIGN

The EPS consists of two principal parts - the retroreflector array and the core - and each is discussed in detail below. In addition, several other aspects of the satellite such as accuracy, weight and balance, interface with the launch vehicle, thermal analysis, etc., require specific treatment.

### 2.3.1 GENERAL RETROREFLECTOR ARRAY CONSIDERATIONS

In the present design, the EPS is a sphere, of 76.2 cm (30 in.) in diameter, carrying 864 retroreflectors distributed as evenly as possible over the surface. When a laser beam strikes the satellite, the return pulse will be composed of returns from many individual retroreflectors. A transfer function must be constructed for predicting the characteristics of this return signal. This transfer function will depend on the design of the retroreflectors. The characteristics of various types of retroreflectors have been studied to determine the design most suitable for obtaining the desired return, which must be strong enough to be measurable and consistent enough so that the variations in the measured range are within the required tolerances.

Many different designs of retroreflectors are possible, each with its advantages and disadvantages. Of course, each design consists of a set of three mutually perpendicular reflecting surfaces. When a light ray hits the system, each surface reverses one of the components of the velocity vector of the light ray so that it will, after three reflections, be returned in the same direction as the incoming beam. The incident and the reflected rays are symmetrical with respect to the vertex of the retroreflector (Figure 2-6). The vertex is halfway between the lines of the incident and the reflected rays. This symmetry allows fairly easy computation of the effective reflecting area for a given design.

The simplest type of retroreflector can be formed by cutting a corner off a cube (Figure 2-7). The aperture is an equilateral triangle. If a beam is incident normally on the face of this reflector, the symmetry of the incident and the reflected rays requires that the reflected rays also be contained in a triangle, which can be constructed by moving each point on the input aperture to the opposite side of the vertex (Figure 2-8). The new triangle, which is rotated  $180^\circ$  with respect to the old triangle, may be called the output aperture. Since the input and the output apertures do not coincide, the effective reflecting area is the intersection or overlap of the two triangles, which is a regular hexagon.

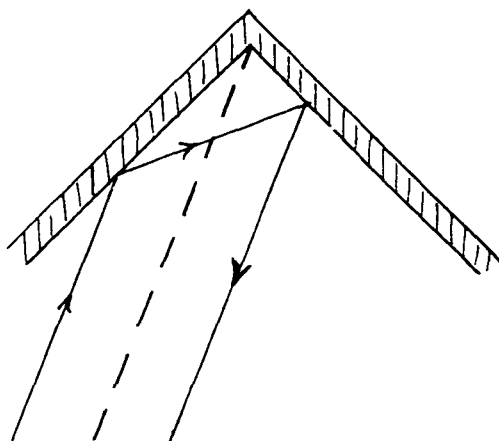


FIGURE 2-6 RAY SYMMETRY

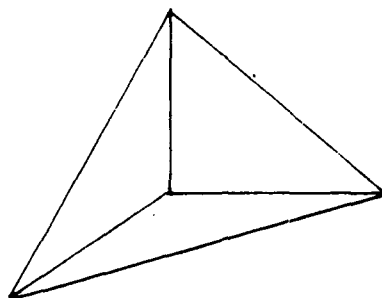


FIGURE 2-7 CUBE CORNER

The corners of a triangular face do not contribute at normal incidence. A hexagonal retroreflector can be formed by slicing off the corners by cuts perpendicular to the face (Figure 2-9). The input and the output apertures coincide for this geometry at normal incidence.

Instead of thinking of the output aperture as being in the same plane as the input aperture, one can think of the output aperture as being an equal distance in back of the vertex. In fact, when one looks into a retroreflector, one sees an image of the input face in back of the vertex, almost as if there were a mirror at the vertex. This leads to a useful method of visualizing the effective reflecting area of a retroreflector. If one constructs a tube with the input aperture on the front end and the output aperture on the back and with a length twice the distance from the vertex to the face, then the space that one sees by looking through the tube from various angles is the same as the reflecting area of the corresponding retroreflector (Figure 2-10).

The reflecting area of the hexagonal retroreflector is the intersection of two hexagons. The strength of the return signal depends both on the angle between the incident beam and the normal to the face and on the orientation angle of the retroreflector about the normal to the face. The cutoff occurs quickest when the input and the output apertures move away from each other perpendicularly to a side of the hexagon (Figure 2-11). The greatest cutoff angle is obtained when the hexagons move away along a corner (Figure 2-12).

One can make the retroreflecting area independent of the orientation of the reflector about the normal to the face by cutting the face in the form of a circle (Figure 2-13). The input-output apertures are then circles at normal incidence, and the reflecting area at other incidence angles is the intersection of two ellipses (Figure 2-14).

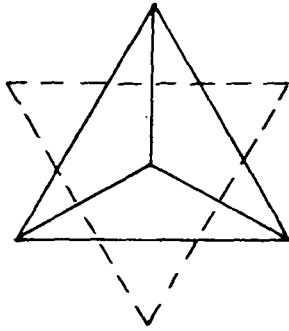


FIGURE 2-8  
OUTPUT APERTURE

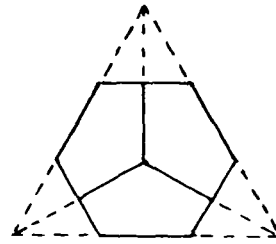


FIGURE 2-9  
HEXAGONAL RETROREFLECTOR

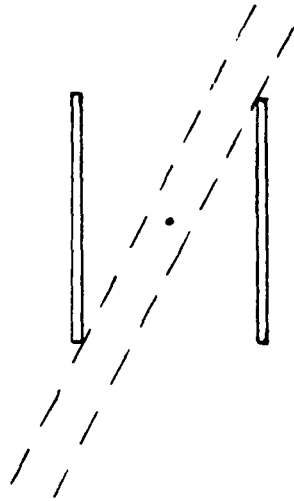


FIGURE 2-10 EFFECTIVE REFLECTING AREA VISUALIZATION

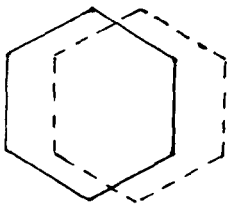


FIGURE 2-11  
SIDE MOVEMENT CUTOFF

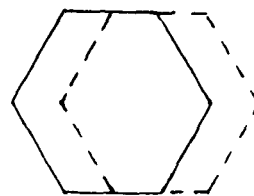


FIGURE 2-12  
CORNER MOVEMENT CUTOFF

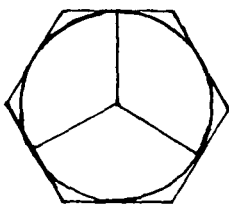


FIGURE 2-13  
CIRCULAR FACE

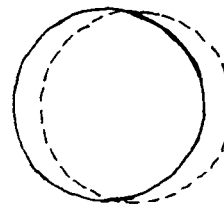


FIGURE 2-14  
CIRCULAR ORIENTATION INDEPENDENCE.

The cutoff angle for a retroreflector is the angle beyond which the incoming beam can no longer reach the vertex. This is obvious from the fact that the incident and the reflected rays are symmetrical with respect to the vertex. If the retroreflector is filled with a dielectric, the cutoff angle is increased since the ray is bent toward the normal to the plane and can reach the vertex from a greater incidence angle (Figure 2-15).

If the retroreflector consists of a prism whose three mutually perpendicular sides are coated with a reflecting material, then there will be nearly complete reflection at all surfaces, regardless of the angle of incidence at any of the surfaces.

If the surfaces are uncoated, then there will be total internal reflection at each of the three surfaces as long as the angle that the ray makes with the normal to the reflecting surface is greater than the critical angle. For an index of refraction of 1.46, a ray must have an incidence angle greater than  $43^{\circ}14'$  for total internal reflection to occur. The forbidden incidence angles are contained in a cone about the normal to the surface (Figure 2-16).

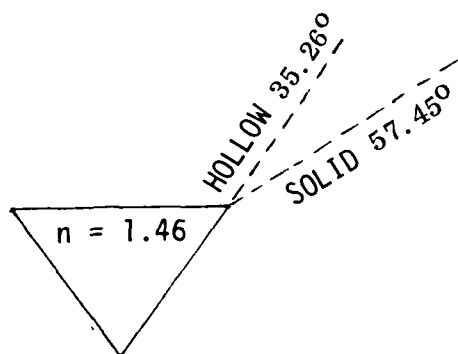


FIGURE 2-15  
DIELECTRIC EFFECT.

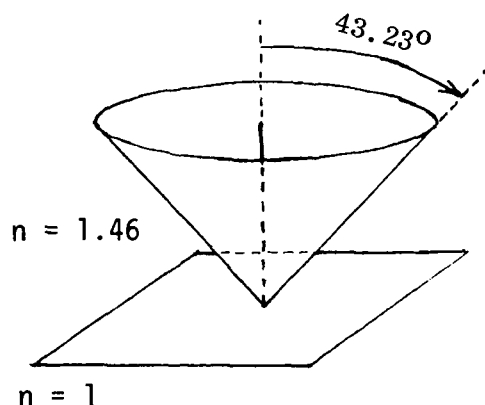


FIGURE 2-16  
CRITICAL ANGLE FOR UNCOATED SIDES.

To calculate the return from an uncoated retroreflector, one must know the angles of incidence with each of the three reflecting faces. Whenever the angle of incidence measured from the normal is too small, there will be only the ordinary reflection and no total internal reflection. The incoming ray may strike any of the three faces first and either of the remaining two faces second, so that there are three or six ways a beam can go through the retroreflector. In whatever order the reflections occur, the angle of reflection at each face is always the same. In the cartesian coordinate system defined by the three corners of the reflector, the effect of each reflection is to reverse the component of the velocity vector normal to the plane. Since the magnitude of the vector and the normal component to each face are constant, the angle of reflection at each face is constant and is the same as the angle between the incident beam and each face.

One can picture the excluded angles of incidence in an uncoated retroreflector by drawing a quarter cone about the normal to each face (Figure 2-17). Any incidence angle contained within any of these three cones will not undergo total internal reflection. Looking at the face of a circular retroreflector, one sees a Y-shaped area of permissible incidence angles for getting a return with total internal reflection at each face (Figure 2-18). With an index of refraction of 1.46, the cutoff angle varies from  $16.9^\circ$  to  $57.4^\circ$  for the uncoated retroreflector.

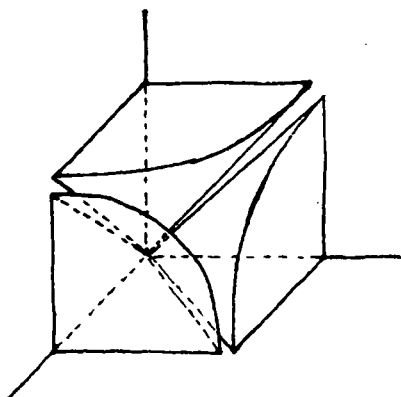


FIGURE 2-17

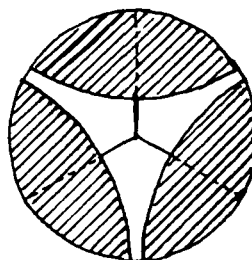


FIGURE 2-18

EXCLUDED ANGLE VISUALIZATION. Y-SHAPED PERMISSABLE AREA.

The purpose of laser ranging is to measure the distance to the center of mass of the satellite. If there were only one retroreflector at the center of mass, this distance could be measured directly. However, the retroreflected beam from the EPS is a combination of returns from a number of retroreflectors on the surface of the sphere. In Figure 2-19, the range to two representative retroreflectors is different from the range to the center of mass by the distances  $D_1$  and  $D_2$ . One must calculate a range correction to be applied to the return signal in order to obtain the range to the center of mass.

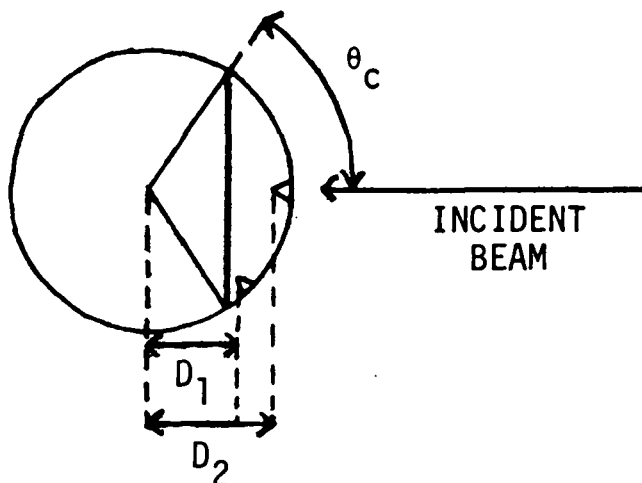


FIGURE 2-19 ACTIVE RETROREFLECTORS.

When a beam of light hits a retroreflector, the strength of the return is a maximum when the incident beam is perpendicular to the face of the retroreflector. As the angle of incidence increases, the strength of the return signal decreases until it reaches zero at some cutoff angle  $\theta_c$ . Therefore, when a laser beam hits the EPS, each retroreflector whose face is at an angle less than the cutoff angle with respect to the incident beam will give a return. In Figure 2-19, the active retroreflectors are located on a cap of half-angle  $\theta_c$  as measured from the center of the sphere.

The cutoff angle depends on the design of the retroreflector and can be varied from 0 to 90°. The larger the cutoff angle is, the stronger the return signal because of the larger number of retroreflectors participating and the greater reflecting area of each. Greater signal strength gives a better defined return pulse, because of the larger number of photons, and therefore greater accuracy from each return. However, increasing the cutoff angle of the retroreflectors also increases the spread in range of the retroreflectors, so that the potential uncertainty in the range corrections is greater.

The laser emits a pulse whose energy is nearly a gaussian as a function of time and distance. The return signal from the satellite is therefore a combination of gaussian-shaped pulses from each retroreflector. Each pulse has a different amplitude and phase and arrives at a time determined by the range to each retroreflector. In Figure 2-20, two return pulses are shown as solid lines. The pulse at the origin is the pulse that would have been received from a retroreflector placed at the center of mass. The sum of the two solid lines is shown as a dotted line above them. Since the beams are coherent, the two pulses actually interfere with each other, depending on their relative phase. Adding the intensities gives the combined intensity for incoherent waves. Adding the intensities is also the same as averaging over all possible phase differences for coherent waves.

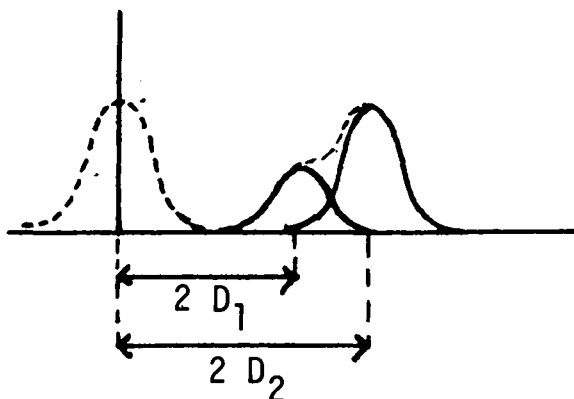


FIGURE 2-20 RETURN PULSES.

In practice, averaging over phase differences will be done by repeated ranging to the satellite. Since the wavelength of light is very small compared to the dimensions of the satellite, very slight changes in viewing angle or rotation of the satellite will give completely different relative phases between the components of the return signal as repeated range measurements are made.

The total return signal is not a gaussian-shaped curve and is wider than the pulse sent out by the laser. Whatever pulse shape is received, one can determine its centroid. To determine the range to the center of the satellite, one must apply a correction for the difference between the centroid of the return pulse and the center of an imaginary pulse received from a retroreflector at the center of mass.

The range correction is computed by calculating the return signal that should be generated by the retroreflector array. The return signal is a function of the direction of the incident beam, the positions and orientations of the retroreflectors, the active reflecting area of each retroreflector, and the diffraction pattern of each reflector.

Since the retroreflectors are nearly uniformly placed on the sphere, the direction of the incoming beam does not make much difference in the return signal. The positions of the retroreflectors will be known to about 10 mils or better, and the active reflecting area as a function of incidence angle has been calculated. When the final specifications of the retroreflectors have been set, the diffraction pattern of the retroreflectors can be calculated. The laser and the receiver will be collocated, and therefore, the return signal is always measured away from the center of the return beam by the amount of the velocity aberration, which is about 8.5 arcsec for the EPS. The retroreflector must be designed so that the beam spread is at least as large as the velocity aberration.

The diffraction pattern depends on factors such as the exact dihedral angles between the reflecting faces, the type of reflecting surface, the angle of incidence of the laser beam, and temperature gradients within the retroreflector. A. D. Little, Inc. (ADL) has investigated the thermal conditions and their effect on the diffraction pattern (see Reference 1).

The diffraction pattern can be described by a normalized function  $f(x, y)$  that gives the relative intensity of the beam at each point in a plane perpendicular to the direction of the beam. The plane is located at a large distance from the retroreflector.

As shown in Figure 2-21, the return beam from each retroreflector is initially a separate pencil of light. At large distances from the satellite, the beams spread and overlap until eventually the width of each beam is much larger than the separation between the beam centers, which can be neglected. Let us consider the oversimplified case of two uniform circular spots of light of different diameters coming from two retroreflectors. A detector in the ring between the inner and outer circles

would receive energy only from the retroreflector with the larger beam spread. The range measured by timing the pulse would be the range to that retroreflector. On the other hand, if the detector is located inside the smaller circle, the energy measured is coming from both reflectors. The range measured by timing this pulse would be intermediate between the ranges to the two reflectors.

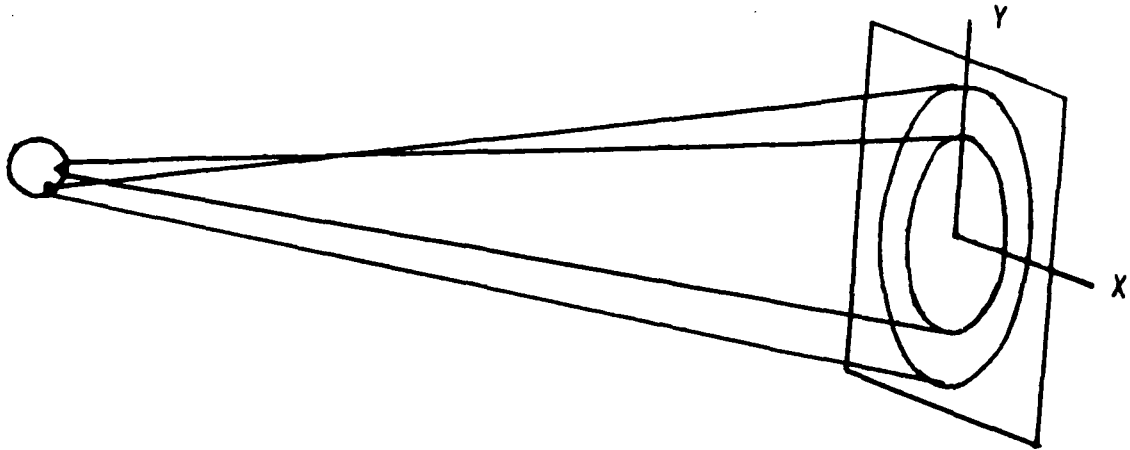


FIGURE 2-21 BEAM SPREAD.

In calculating the return signals measured by a detector at a point  $(x, y)$  in the plane, one must evaluate the diffraction pattern of each retroreflector at that point. The radial distance of the detector from the beam center is determined by the velocity aberration. Since the orientation of the satellite will not be known, the total return must have reasonably good rotational symmetry.

Since, because of velocity aberration, the detector is never at the center of the diffraction pattern, any energy in the center is wasted. It would therefore be desirable to have the energy distributed in a ring whose radius is comparable to the amount of velocity aberration.

If the dihedral angles of the retroreflector are all made different from  $90^\circ$  by the same small amount, the energy distribution will shift away from the center of the beam. From geometrical optics, the beam is split into six beams. For normally incident light, the six beams form the corners of a regular hexagon. At other incidence angles, the pattern changes so that one no longer has a regular hexagon. When diffraction effects are taken into account, one finds that the minimum intensity is not exactly at the points predicted by geometrical optics.

Even though changing the dihedral angles does not make the diffraction pattern into a perfect circular ring, it should be possible by properly orienting the retroreflectors to produce a total return signal that is a fair approximation to a circular ring-shaped pattern with the desired radius.



As a first approximation to the transfer function, the return signal from the EPS has been calculated for the simplified case where the diffraction pattern is the same for all retroreflectors, regardless of incidence angle. The intensity of the return from each retroreflector is proportional to the active reflecting area of the retroreflector as a function of the particular incidence angle. Table 2-4 shows the strength of the return in terms of the equivalent number of retroreflectors at normal incidence for three different types of circular retroreflector. The solid coated retroreflector gives the strongest return and is therefore the most desirable in terms of signal strength.

TABLE 2-4 RETURN STRENGTH FOR CIRCULAR RETROREFLECTORS

	Cutoff Angle (Degrees)	Active Reflectors	Total Return
Hollow	35.2	76	18.1
Solid; Coated	57.4	196	38.5
Solid; Uncoated			
Maximum	57.4	196	38.5
Average	16.9-57.4	50	22.1
Minimum	16.9	20	14.6

The centroid of the return pulse from the solid coated circular retroreflectors has been computed for several angles of incidence on the satellite. For the incoherent return, the variation of the centroid with incidence angle is on the order of 1 mm. Using a random-number generator, a dozen coherent returns have been calculated. The variation in the centroid between different coherent returns is about 2 or 3 cm. This error must be reduced to the desired level of less than 5 mm by averaging over many range measurements. The value of the range correction (about 34 cm under the assumption of constant diffraction patterns) will change significantly when the actual diffraction pattern is computed.

It is recommended that the transfer function be further refined by taking into account the actual diffraction pattern of the retroreflectors as a function of incidence angle, thermal conditions, deviation of the dihedral angles from 90°, and type of reflective coating.

### 2.3.2 SPECIFIC RETROREFLECTOR ARRAY DESIGN

The three major aspects involved in the design of the retroreflector array are the positional pattern of the retroreflectors, the retroreflects themselves, and their mounting.

### 2.3.2.1 POSITION PATTERN

Because accurate interpretation of the laser return signal requires that the retroreflectors be uniformly positioned over the spherical surface of the satellite, their positioning resolves into the simple problem of geometrically dividing the surface of a sphere into a large number of equal and similarly shaped areas. We have chosen near-equilateral spherical triangles as the basic area shape since they are compatible with the spherical surface and with the triangular configuration of the basic cube-corner retroreflectors.

To divide the spherical surface in this way, a number of schemes have been evolved; however, only the latest one has proved to be geometrically compatible with the satellite assembly configuration and to provide a practical and workable number of retroreflectors in response to the requirement for a large number of them. The basic scheme is to divide the entire spherical surface into 6 equal spherical squares having vertex angles of  $120^\circ$  (these are the 6 spherical caps of the satellite core discussed elsewhere) and to subdivide each square into 4 equal triangles for a total of 24, each having  $60^\circ$  base angles and a  $90^\circ$  apex angle. Further subdivision of these large triangles into smaller but similar triangles by use of equally spaced lines parallel to all three sides is geometrically compatible with the use of retroreflectors of triangular aperture. Since such retroreflectors have not been selected as the final configuration (see next subsections), this method of subdivision is not directly applicable.

By extending this subdivision, however, to a large number of small triangles and recombining the majority of them into hexagonally shaped groups touching each other at their vertices and with appropriate sides coincident with the sides of the large triangle, we have a convenient method to uniformly locate retroreflectors of hexagonal or circular aperture by centering them in the middle of each hexagonal group. This procedure, illustrated in Figure 2-22, provides for the location of 3, 6, 10, 15, 21, 28, 36, 45, or more retroreflectors in each large triangle and consequently 72, 144, 240, 360, 504, 672, 864, 1080, or more over a complete spherical surface.

By balancing the laser-ranging requirements, which dictate a large number of retroreflectors, against practical considerations such as machining complexity, tolerance buildup, handling, and testing, we chose 864 as the total number of retroreflectors. This requires 144 per spherical square or cap, which is 36 in each large spherical triangle. This gives a statistically large enough number of retroreflectors contributing to the laser return signal while still providing a reasonably small enough number to satisfy practical considerations.

The placement pattern described above uniformly positions the retroreflectors in each spherical square or cap, but results in a pattern mismatch at the interface between adjacent squares. This mismatch is readily corrected by rotating the whole pattern within each

DIVISION OF BASIC SPHERICAL TRIANGLE  
INTO LARGE NUMBER OF SMALL TRIANGLES  
AND RECOMBINING OF GROUPS OF SMALL  
TRIANGLES INTO HEXAGONS, EACH REPRESENTING  
A RETROREFLECTOR LOCATION

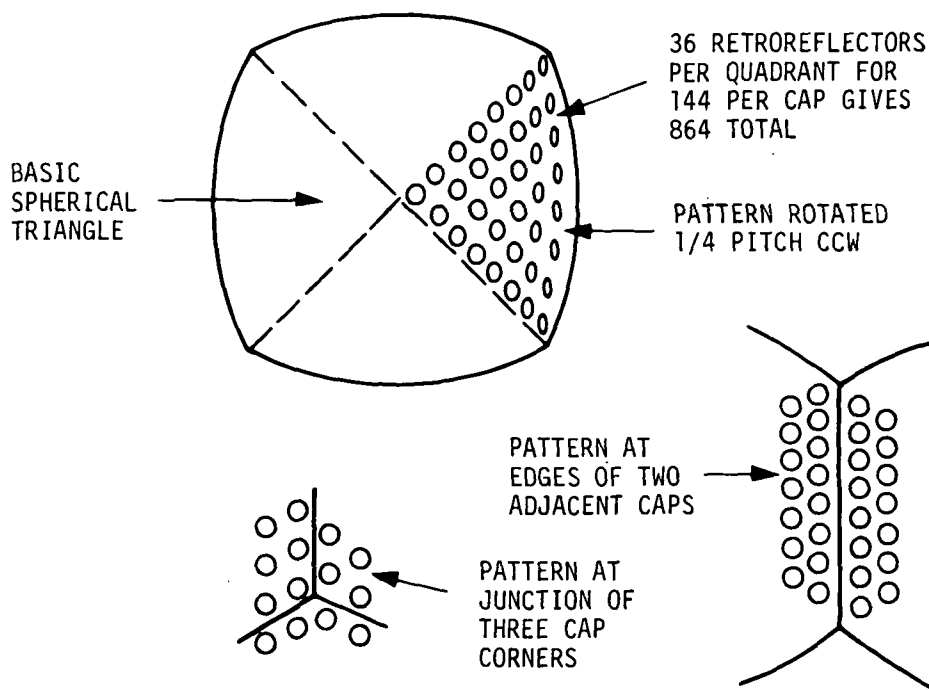
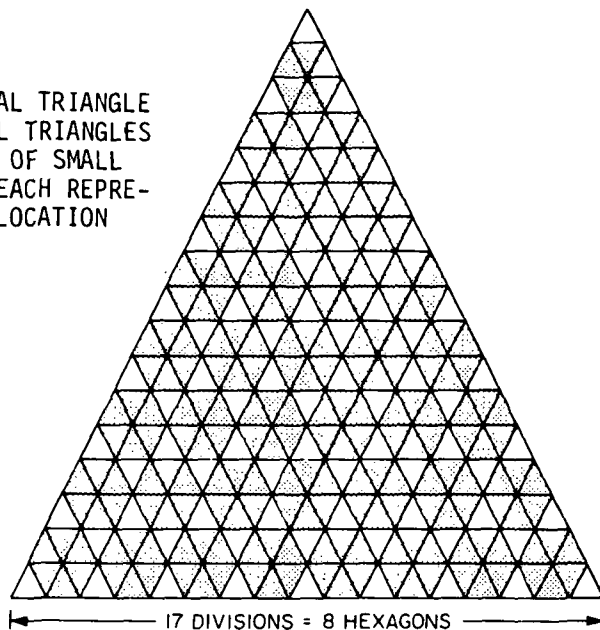


FIGURE 2-22 RETROREFLECTOR ARRAY GEOMETRY.

square — all in the same sense or direction — by the equivalent of one-fourth of the spacing of adjacent retroreflectors at the square's edges. This, in effect, continues the pattern within the squares across their common boundary and maintains overall uniformity of the array, as illustrated in Figure 2-22.

A final small adjustment of each retroreflector position beyond that described above is made to equalize center-to-center distances between adjacent retroreflectors in the most crowded direction and to provide an adequate center-to-edge distance for all retroreflectors adjacent to the edges of the square or cap. This adjustment is on the same order as the tolerance allowed in positioning of the retroreflectors for machining purposes and has been shown to be acceptable with respect to its influence on the laser return signal and its interpretation.

The final positions of each of the 36 retroreflectors in each of the 4 large triangles within a spherical square or cap have been expressed in terms of a polar angle from the radial through the center of the spherical square and a plus or minus azimuth angle from each of the 4 meridians normal to the sides of the spherical square. These polar and azimuth angles are tabulated on drawing E-CBS-101, Figure 2-23.

#### 2.3.2.2 RETROREFLECTOR CONFIGURATION (Dwg C-CBS-105, Fig. 2-24)

In determining the optimum retroreflector configuration for the EPS design, we find a large number of alternatives within the limitations and requirements set forth in the preceding section. These alternatives include choices of type (solid or open); general shape (triangular, hexagonal, or circular aperture); size; material; reflective coating or not; type of coating if used; method for tailoring return beam; and others. The proper choice of any one of these alternatives is not a simple decision, for it is interrelated with considerations of many of the others. As a result, the retroreflector configuration determination has been an involved reiterative process and as such is not easily documented. Consequently, in each case the alternative choices are discussed below along with reference to any additional applicable factors affecting that choice.

Retroreflector Type. A basic decision for the EPS was between an open or a solid retroreflector. We have chosen the latter for the following reasons:

1. The state of the art in design, fabrication, and testing of solid retroreflectors is well advanced — certainly beyond the requirements for the EPS. On the other hand, the techniques for manufacture of open retroreflectors of the configuration, quality, and precision required have not yet been established. There is some evidence, however, of reasonable progress toward this goal by means of replication and electroforming processes.





2. A solid retroreflector will provide retroreflection over a greater incidence angle than will an open one because the material of the former has an index of refraction greater than unity, the value inherent for an open retroreflector.

3. The effects of thermal gradients and other temperature influences on the performance of a solid retroreflector have been thoroughly analyzed and tested and have been verified by experience with the lunar retroreflector arrays. No similar situation exists for open retroreflectors. Although the thermal influence on the performance of a solid retroreflector is complicated and can be substantial, it is well understood and is amenable to corrective measures through proper design, material selection, and mounting configuration. Alternatively, even though for open retroreflectors no change of the index of refraction occurs with temperature, other temperature and thermal gradient effects associated with differential-expansion distortion, material instability, and strain induced by the mounting are likely to be present.

4. A solid retroreflector is considered to be more amenable to reasonable mounting configurations than is a thin-shelled open one. For any practical mounting scheme proposed, mechanical and thermal-induced strains will affect the solid retroreflector less than an open one. In addition, experience with the lunar retroreflector array has validated the use of a reasonable mounting configuration for solid retroreflectors and, as such, has been the basis for our selected design.

In summary, solid retroreflectors have been selected mainly because of their known state of the art, whereas the use of open retroreflectors on the EPS would require an extensive analysis, development, and testing program to approach satisfactory performance; even then, attaining such a goal would not be guaranteed.

Retroreflector Shape. Early EPS concepts utilized triangular-aperture, solid retroreflectors because of their better retroreflection characteristics at high-incidence angles within certain azimuth directions, as compared to retroreflectors of hexagonal or circular aperture. However, this advantage is now considered to be more than offset by the problems associated with the actual mounting of these triangular retroreflectors, such as aperture shadowing, mechanical distortion, reduced packing density, and difficult thermal control, along with the greater difficulty in fabrication and hence higher cost per aperture area. Consequently, the triangular-aperture retroreflector has been eliminated as a contender.

A comparison of retroreflectors with hexagonal apertures and those with circular apertures shows that the small additional aperture area potentially available with the former is not generally realizable in a closely packed pattern. Also, the simplicity and flexibility of the mounting for a circular retroreflector as compared with a hexagonal one are attractive practical considerations. Consequently, a circular configuration has been chosen for the EPP satellite. This choice has additional advantages in that this configuration is the same

as that earlier selected for the lunar retroreflector arrays, and so, a significant amount of related valuable experience, analysis, and design data can be utilized in the EPS program.

Retroreflector Size. In keeping with the laser-ranging requirements, the size of the retroreflector's circular aperture has been maximized within the constraints imposed by other requirements. The array pattern evolved (see Section 2. 3. 2. 1) would permit somewhat more than half of the spherical surface to be an active retroreflector area before interference between adjacent retroreflectors becomes a limiting factor as their diameters are increased. However, because some small radial distance is required to provide for a reasonable mounting configuration, the retroreflector diameter must be reduced somewhat. Consequently, a practical maximum of about one-half of the spherical surface area can be devoted to active retroreflector area.

As the final size of the EPS has evolved, as described elsewhere, to its present final diameter of 76.2 cm (30.0 inches), the size of the individual retroreflector has been determined by the total number of them (864) and the area coverage (~50%). The diameter of the aperture has thus been established as 3.65 cm (1.438 inches).

This size is only slightly smaller than the 3.810 cm (1.500 in) dia. of retroreflectors selected for the lunar retroreflector arrays to date and thus lends credibility to the use of applicable analyses, test data, and experience derived from that program.

Retroreflector Material. The selection of solid retroreflectors over open ones immediately imposes stringent requirements on the material to be used. It must be optically homogeneous, have good optical transmissibility in the visible spectrum, and possess high long-term mechanical and thermal stability. Properties such as low coefficient of thermal expansion, adequate workability, high resistance to moisture, and to chemical, radiational, and thermal degradation, reasonably high index of refraction but low coefficient of refractive index change with temperature, and ready availability at reasonable cost are additional important requirements. Of the potential candidate materials such as the traditional optical glasses, the new tailored optical materials, and natural materials like quartz and sapphire, one material, synthetic, fused silica, best meets all these requirements.

Fused silica has been used extensively for high-quality, precision optical elements in many applications and was selected for the lunar-array retroreflectors. Consequently, a vast amount of data and experience has been accumulated on characteristics, workability, and quality testing of fused silica and is directly applicable to the design, fabrication, and testing of the EPS retroreflector.

A number of grades of fused silica are available from the several manufacturers of such optical material. The grades differ in two important factors: chemical purity and optical clarity. Low



chemical purity results in changes in color and transparency on exposure to ultraviolet and other radiation. Since the EPS is expected to remain in orbit a very long time, we must select the most pure fused silica reasonably available to minimize the long-term degradation due to radiational exposure.

A more vexing problem is optical clarity. All optical materials have inherent internal inhomogeneities and minute inclusions such as striae, bubbles, and seeds; these should be held to a minimum consistent with the operational requirements of the retroreflectors. The net result of these inhomogeneities and inclusions is a distortion of the wavefront of the incident laser beam as it progresses through the retroreflector with a consequent distortion of the reflected beam such that the performance of the retroreflector can be significantly altered and even degraded. In addition, since a complete analysis of the influence of the retroreflector characteristics on the overall laser-beam transfer function for the EPS has not yet been undertaken, no definitive basis yet exists on which to judge what is acceptable degradation of retroreflector performance.

Since the availability, and hence the cost, of optical materials, including fused silica, have a strong inverse relationship to the density and size of the inhomogeneities and inclusions, it is prudent not to overspecify the optical clarity or grade of material to be used. The present selection of a grade of fused silica is judged to be acceptable in terms of cost, availability, and optical performance, but it has not been determined in any quantitative way to be an acceptable grade. In fact, actual quantities of the fused silica may have to be selectively chosen from a larger sample within a grade on the basis of a quantitative measurement of the effect of nonhomogeneities and inclusions. Interferometric testing is available to make such a differentiation.

The final specification of a suitable grade of fused silica must, in any case, be subject to verification by actual tests of representative retroreflectors, using acceptance criteria based on a complete analysis of the laser-beam transfer function, before procurement of the total number of retroreflectors required by the satellite. Such a testing program and the associated procurement of representative prototype retroreflectors, as well as the transfer function analysis required to establish acceptable performance criteria, are beyond the scope of the present study and therefore are discussed here only as the basis of recommendations discussed elsewhere in this report.

Retroreflector Geometry. The geometry of a theoretically perfect retroreflector is essentially fixed. It has three reflective surfaces and an entrance face that are perfectly flat; the dihedral angles between each pair of the three reflective faces are exactly right angles; and the angles each of the three reflective faces makes with the entrance face are all equal. The reflected beam from such a perfect retroreflector is exactly coaxial with the incident beam, has the

minimum reflected beam divergence possible, and has a symmetrical far-field energy distribution that is in accord with the Fraunhofer diffraction pattern.

For an actual retroreflector having departures from the perfect geometry, the return beam will deviate in direction or have greater divergence from or differ in energy distribution or symmetry, or, more likely, the beam will contain some combination of all these effects. Past experience with precision retroreflectors, particularly those used in the lunar retroreflector arrays, has shown that present fabrication techniques are suitable to provide, at reasonable costs, retroreflectors having geometric accuracy sufficiently close to the perfect case that no significant performance degradation occurs.

The requirements of laser ranging on the EPS dictate, however, that the reflected beam be tailored to match the velocity aberration associated with the actual orbit of the satellite rather than to approach the performance of a perfect retroreflector. Accordingly, the energy distribution in the reflected beam must be optimized within a symmetrical conical zone coaxial with the incident beam. The half angles of this conical zone for the predicted satellite orbit are approximately between 30 to 40  $\mu$ rad, and it is desirable that the distribution be most dense at the greater angle.

The best method to tailor the reflected beam to this requirement is to change the three dihedral angles between the three reflective faces. (There are numerous mentions of this technique in the literature.) This produces six individual reflected beams that are symmetrically and equally displaced from a normal incident beam if all three dihedral angles deviate from a perfect right angle by the same amount and in the same direction. Owing to the diffraction pattern of each of the six individual beams, there is a certain amount of overlapping between adjacent beams, and the net effect is to approach closely the symmetrical conical-zone energy distribution required of the reflected beam. The quantitative relationship for the conical half angle,  $\phi$ , between a normal incidence beam and the reflected beam and the deviation,  $\delta$ , of the three dihedral angles from a right angle is

$$\phi = \frac{4\sqrt{2}}{\sqrt{3}} n\delta \quad , \quad (\text{see Reference 1}) \quad (4)$$

where  $n$  is the refractive index of the retroreflector material. For fused silica at 0.6943  $\mu$  (the wavelength of ruby-laser energy),  $n = 1.45546$  and thus  $\phi = 4.751 \delta$ . From this relation for the desired half-cone angles of  $\phi = 30$  to 40  $\mu$ rad, the required dihedral-angle deviations are  $\delta = 6.3$  to 8.4  $\mu$ rad or 1.27 to 1.70 arcsec. The effect on the reflected beam is theoretically obtained for the angle  $\delta$  being added to or subtracted from the right-angle dihedral angles. Since thermal gradients within the retroreflector also alter the distribution pattern of the reflected beam energy and in a preferred direction, as discussed elsewhere, the optimum combined effect is obtained when the angular deviation  $\delta$  is added to the right-angle dihedral angles.

All the above is pertinent for an incident beam normal to the entrance face of the retroreflector; however, for the EPS most retroreflectors will be reflecting an incident beam of some inclination from the normal. This incidence angle has the effect of foreshortening the hexagonal pattern of the six individual beams in the direction of the incident beam proportional to its incidence angle. This effect will be taken into account in the overall transfer-function analysis and optimized for a better determination of the dihedral-angle deviation,  $\delta$ , required for the actual flight EPS retroreflectors.

A retroreflector that has been tailored to produce a specific energy distribution pattern in the reflected beam as described above must still adhere closely to the perfect retroreflector geometry in all other respects; i. e., the reflective and entrance faces must all be flat, and the angles between each reflective face and the entrance face must be equal. Deviations from these geometric ideals will also alter the energy distribution pattern of the reflected beam but in a manner more complex, less desirable, and difficult to control. Consequently, the retroreflector geometry has been specified to be acceptably close to the theoretically perfect retroreflector geometry for all aspects except one; the dihedral angles are specified to be greater than an exact right angle by the required small deviation angle.

Retroreflector Coating. Two distinct and separate decisions on coating must be made for the EPS retroreflectors:

1. Should the reflective faces be coated, and if so, what type of coating should be applied?
2. Should the entrance face be coated?

Relative to the first, a solid retroreflector with no coating of its faces will retroreflect an incident beam of light by total internal reflection at these faces. However, the retroreflection is limited to cases where the incidence angle at any one face of the ray as it passes through the retroreflector is within the internal reflection angle for that material. This limits the incidence angle of the incident beam for which retroreflection will occur; for fused silica, this angle ranges from  $16.9^\circ$  to  $57.4^\circ$ , depending on the azimuth angle of the incident beam.

If, however, the faces have a reflective coating (usually metallic), the ray, as it passes through the retroreflector, will be reflected at each face no matter what its incidence angle. Accordingly, retroreflection is obtained over a larger angle of the incident beam. This angle is  $57.4^\circ$  for a fused silica retroreflector with a circular entrance face or aperture and is independent of the azimuth angle of the incident beam. Thus, a reflective coating greatly enhances the retroreflection at the larger incidence angles, a significant advantage for the EPS.

The use of metallic reflective surfaces brings up the question of their adherence, especially for a long period in the space environment. Present experience indicates that a properly applied metallic coating will survive the space environment for a satisfactorily long time

and should not be affected by the small background radiation from a core made from depleted uranium. Micrometeoroid impacts are not considered to be a problem, since the metallic coatings are applied to the back or inward facing surfaces of the retroreflector as it is mounted; hence, the coatings are shielded by the retroreflector itself. Satisfactory adherence of the coatings must be ensured by the judicious application of quality-control techniques in the actual coating process and in all assembly and test processes thereafter. Cleanliness of the substrate and material to be coated, as well as the residual gas in the vacuum coating tank, is of utmost importance in obtaining a coating with good adherence; techniques and methods are now known and employed to ensure these conditions.

Several other considerations relative to the use of metallic reflective coatings are of consequence in the EPS application. For example, such coatings are important relative to the solar heating of the retroreflector and to the thermal coupling between the retroreflector and its surrounding cavity. These thermal considerations have been included in the overall thermal analysis, but have been found to produce no undue implications.

Additionally, the use of a metallic reflective coating on the three reflective faces of a solid retroreflector minimizes the polarization effects of the reflections within a retroreflector, but this factor is of small significance in the EPS application.

The choice of possible metallic reflective coatings is wide, but only two, silver and aluminum, are appropriate. Both have higher reflectivities over the visible spectrum than do other potential choices. Silver has the higher reflectivity but is rather quickly degraded to a lower overall reflectivity by reactive contaminants always present in the atmosphere. The reflectivity of aluminum, on the other hand, is not degraded significantly with time or exposure to any of the reactive contaminants in the atmosphere. Although the retroreflectors will be exposed to the earth's atmosphere and its constituents for only a relatively short time, the degree of immunity offered by aluminum over silver to degradation due to such exposure or to any other contamination by handling or during orbit injection and subsequent events makes it the optimum choice for the EPS.

No protective overcoating will be applied, because it is important to provide a low-emissivity surface to minimize radiative coupling between the retroreflector and the surrounding satellite core and because an overcoating might have a tendency to flake or peel off and thereby produce disturbing debris and possibly remove the reflective coating at the same time.

The second area for coating considerations is the retroreflector entrance face. An antireflection coating on this face could increase the overall intensity of the reflected beam by reducing the loss due to reflection as the incident beam strikes the entrance face. This increase in efficiency is small, however.

Since there is a possibility that direct exposure to solar and other radiation might in time seriously degrade such a coating and hence reduce its transmissibility, the probability is high that the small gain in efficiency will be more than offset by a potentially larger loss in efficiency. Hence, no coating will be used on the entrance face of the EPS retroreflectors.

### 2.3.2.3 RETROREFLECTOR MOUNTING

The mounting for the retroreflectors must accomplish three specific tasks while satisfying the requirements and surviving the rigors of all phases of assembly, testing, shipping, prelaunch activities, launch, orbit injection, and subsequent orbital lifetime of the satellite: It must 1) hold and position the retroreflectors; 2) provide thermal contact between the retroreflector and the core within the range required by thermal analysis; and 3) provide a means for adjusting the retroreflectors to a predetermined azimuth orientation. We have selected a mounting configuration similar to that employed in the lunar retroreflector array and have thereby benefited from the analysis and test experience of that program.

The retroreflector is held by means of three integral tabs sandwiched between two Teflon seats or rings, which in turn are held between a circular ledge machined into the retroreflector cavity in the core and a threaded retaining ring. The three tabs on the retroreflector are what remains of a cylindrical ridge on the outside diameter of the retroreflector after the three reflecting faces intersect and hence remove portions of it. Each of the three equally spaced tabs occupies approximately  $30^\circ$  of the retroreflector circumference, and each has a bottom surface that is normal to the axis of symmetry of the retroreflector and a top surface that is a portion of a very flat cone — an apex half-angle of  $81^\circ$  — concentric with the symmetry axis. The  $9^\circ$  slope of the top face provides a thermally compensated mount whereby differential expansion or contraction between all elements within the mount system in the axial direction is balanced by a corresponding expansion or contraction in the lateral direction. This slope thus maintains an axial clearance, as set during assembly, for all isothermal temperature levels of the mount system. This eliminates temperature-induced strain on, and hence distortion of, the retroreflectors and maintains a reasonably constant thermal conductance of the mount to ensure adequate passive temperature control of the retroreflector.

The top Teflon seat has a conical bottom face that matches the slope of the tops of the tabs. The bottom Teflon seat has three cutout sections, which the three retroreflectors tabs engage, while the remaining uncut portions of the seat prevent the retroreflector from turning relative to the seat. The bottom seat also has a series of slots cut into it at specific intervals; one of these engages a small pin installed in the cavity ledge. This arrangement prevents the seat, and hence the retroreflector, from turning within the cavity and thereby eliminates the possibility of Teflon debris being produced during launch vibration; such

debris could cause partial optical blockage of the retroreflector aperture. In addition, because of the several slots available, the azimuth of each retroreflector can be selected when it is installed to optimize the laser return signal from the overall retroreflector array.

The threaded retaining ring engages an internally threaded portion of the retroreflector cavity and thereby retains the whole assembly in place. The ring will be seated and then backed off a predetermined amount and locked against further rotation by staking. This will provide a small axial clearance on the order of 0.002 cm (0.001 in), which is large enough to ensure that no distorting strain is applied to the retroreflector yet small enough that no detrimental impacting will take place during vibration.

From analysis, it has been determined that the thermal conductance of the retroreflector mount may vary over a wide latitude while still providing satisfactory thermal performance. Although this mount conductance will obviously be dependent on such factors as the contact area of the retroreflector tabs, the thickness of the Teflon seats, and the contact pressure of the mount system, an analytical prediction of the value of the conductance for the orbital situation is difficult to make with any degree of accuracy. The present mount design has been proportioned from that used on the lunar retroreflector array and thus should be reasonably within the acceptable limits for mount conductance. However, it is very desirable and thus strongly recommended that adequate thermal simulation tests be undertaken with prototype hardware to measure the actual mount conductance and verify that it will be satisfactory.

Other aspects of retroreflectors, such as the amount of corner chamfering, etc., play a role in the selection of the overall configuration for the EPS retroreflector, but they are secondary to those itemized above. Table 2-5 summarizes the significant parameters of the retroreflector array as it is currently established.

TABLE 2-5 EPS RETROREFLECTOR ARRAY

Number:	864 Total
Size:	3.65 cm Diameter (1.438-In.)
Material:	High-Grade Fused Silica
Configuration:	Cylindrical Cube Corner (see Fig. 2-24)
Mounting:	Similar to that of Lunar Retroreflectors
Accuracy:	Tailored for conical return beam within 30 to 40 $\mu$ rad. half angle
Coating:	Cube Surfaces Reflective Coated with No Overcoating; Entrance Surface not Coated
Pattern on Sphere:	General Triangular Pattern in Each Quad- rant of Each Cap (see Fig. 2-23)

It is of primary importance to note that, owing to the limited scope of this phase-B study, a number of choices and decisions had to be made without benefit of experiment or test and that such a verification program should be undertaken before any full-scale procurement phase.

### 2. 3. 3 CORE

The three major aspects involved in the design of the EPS core are the core material, the core configuration, and the core surface.

#### 2. 3. 3. 1 CORE MATERIAL

High-density materials from which to make a satellite having the required high mass-to-area ratio are limited to a relatively few metals. A list of some such metals with their densities is given in Table 2-6. Others exist in such extremely small quantities or are so highly radioactive that they are not considered to be potential candidate materials in any sense and are hence not included in the list. Metals such as platinum and gold are so expensive that the cost of a satellite of the mass required would outweigh the advantages gained by the resultant relatively small increase in overall density. Other metals, such as lead and silver, although of low enough cost, have densities significantly below other candidate metals that would be reasonably economical choices. Consequently, two metals — tungsten and uranium — were selected as the optimum potential materials on the basis of cost, availability, and properties for the EPS core. Fortunately, both of these metals are readily available in forms having reasonable engineering properties and at acceptable costs.

TABLES 2-6 DENSITIES OF SOME HEAVY METALS

Osmium	22.5 g/cm <sup>3</sup>
Iridium	22.4
Platinum	21.4
Gold	19.3
Tungsten	19.3
Uranium	19.0
Tantalum	16.6
Mercury	13.5
Lead	11.3
Silver	10.5

Tungsten has been utilized in many applications where high-density material is required; hence, a complete family of tungsten-based alloys have been formulated with varying properties. Of these, Mallory 2000 material (Mallory Metalurgical Co.) appears to have a good combination of the properties necessary for the EPS core. It is readily machined, can be satisfactorily plated, has no detrimental magnetic characteristics, is resistant to general corrosion, and, of course, has high density. However, it is a sintered material, and the high-pressure presses and strong forming dies required make the fabrication of large sized pieces an expensive process. Assembly of a large number of small pieces to make the large sizes required also poses potential problems and is thus not an attractive alternative. None the less, tungsten-based alloys are considered potential candidate materials for the EPS core.

"Depleted" uranium is readily available in sufficient quantities and at a reasonably low cost (it can be made available in the raw material form to government contracts on a cost free basis) that it is considered a good potential material for the core. It can be easily cast in sizes and shapes that are suitable, it is readily machined, it can be alloyed to improve specific properties, it can be plated, it has no detrimental magnetic properties, it can be satisfactorily protected against corrosion, and it has the high density required. Depleted uranium alloyed with a small amount of molybdenum to enhance its machining properties and increase its hardness to where it can be readily handled is known in the industry as "dilute U." It appears to be the optimum choice of uranium-based material for the EPS core.

Uranium in its depleted form, although considered by many uninformed to be a highly reactive and dangerous material, is neither. Depleted uranium is basically the stable, nonradioactive isotope  $U^{238}$ . It is stockpiled by the U. S. Government in huge quantities as a by-product of plants that extract the radioactive isotope  $U^{235}$  by the gaseous diffusion process. Depleted uranium contains less than 0.2% of  $U^{235}$ ; hence, its residual radioactivity is extremely low - a level approximately equivalent to that from a luminous dial of a wristwatch. Although depleted uranium is less toxic than beryllium or even lead and is less pyrophoric than magnesium, its processing, handling, and shipping are closely controlled by regulations of the Atomic Energy Commission (AEC). These regulations permit the licensing of certain qualified facilities to process depleted uranium under AEC-maintained controls. A number of such licensed facilities, both private-commercial and government-contractor operated, in the U. S. and Canada can handle the pieces required for the EPS core.

Numerous additional questions are raised by the potential choice of a uranium-based material for a massive satellite with an expected lifetime in orbit of 10 or more years. These range from whether the uranium core might become a miniature atomic bomb in orbit to what are the geopolitical implications of placing a mass of uranium into orbit. The latter type of question must be left to others to answer. The former have been anticipated to the extent that we have engaged a recognized nuclear engineer as a consultant to study the overall problem and to determine if any such dangers exist and, if so, to what degree. This study concludes that there are no technical problems associated with placing a massive depleted-uranium core in orbit for an extended period of time. A summary of the results appear in Table 2 -7 , and a complete analysis in Reference 2.

Table 2 -8 lists the comparative engineering and other properties of Mallory 2000 and "dilute U." We have chosen the latter as the primary material for the core, with the Mallory 2000 as a technically acceptable alternative. Subsequent detail design accomplished within the scope of this limited phase-B study and the cost estimates presented have been based on the use of "dilute U."



TABLE 2 -7 POTENTIAL HAZARDS OF DEPLETED URANIUM

---

Controlled by AEC through Regulations and Licensing of Fabrication Facilities

**PYROPHORICITY:**

Similar to Magnesium but not to Same Degree  
No Hazard if not being Machined

**TOXICITY:**

Similar to Beryllium but not to Same Degree  
No Hazard if not being Machined  
Unlike Lead it is not Cumulative in Body

**RADIOACTIVITY:**

Beta Radiation: Body Contact for 320 Hours Results in Yearly Acceptable Dose. Low Energy, hence Short Range  
Gamma Radiation: Very Low Dosage; No Hazard

**NUCLEAR CRITICALITY:**

Multiplication Factor for  $U^{238}$  Sphere  $\ll 1.0$ ; No Hazard

**INDUCED ACTIVITY:**

Fission Rate due to Proton Flux of Inner Van Allen Belt Less Than Natural Decay Rate; No Hazard

---

**2.3.3.2 CORE CONFIGURATION**

The primary requirements on the core configuration are that the satellite be spherical, compact, rigid, and symmetrical (i. e., the centers of mass and geometry must coincide). The first three requirements are readily met, and the last is satisfied within a reasonable degree by the use of a solid metallic sphere composed of or built up from only a few pieces. Additional requirements, such as provisions for mounting of the retroreflectors, reasonable feasibility of manufacture, and suitable cost and schedule implications, are also adequately satisfied by this concept. The use of a one-piece solid sphere seems reasonable at first thought but upon further consideration it is evident that it makes machining and assembly difficult, precludes the adoption of suitable trim or counterweights, and unnecessarily restricts the fabrication to a single large mass difficult to cast.

A number of configurations were studied and evaluated for a multipiece core: assemblies of two hemispheres, four quarterspheres, eight eighth-spheres, and all combinations of a regular polyhedron (tetrahedron, cube, octahedron, icosahedron, and dodecahedron) inner core with spherical caps on each face to complete the sphere. These were evaluated on the basis of 10 factors:

1. Compatibility of the size and weight of the individual pieces with respect to casting and other fabrication processes involved.
2. Ease of machining.

TABLE 2 -8 ENGINEERING PROPERTIES OF SELECTED METALS

Base Metal	Depleted Uranium	Tungsten
Designation	"Dilute U"	Mallory 2000
Composition	U <sup>238</sup> + 0. 2% U <sup>235</sup> + 0. 2% Mo	W + 3. 5% Ni + 1. 5% Cu
Density, g/cm <sup>3</sup> and lb/in <sup>3</sup>	18. 8 and 0. 683	17. 8 and 0. 642
Yield Strength, psi	35, 000	85, 000
Young's Modulus, psi	24 × 10 <sup>6</sup>	45 × 10 <sup>6</sup>
Thermal Expansion, °C-1	7. 5 × 10 <sup>-6</sup>	4. 4 × 10 <sup>-6</sup>
Thermal Conductivity, $\frac{\text{cal}}{\text{sec cm } ^\circ\text{K}}$	0. 057	0. 328
Hardness	80 R B	27 R C
Magnetic Properties	Nil	Nil
Method of Basic Forming	Cast	Sintered
Machinability	Excellent	Good
Electroplatability	Good	Good
Raw-Material Cost - Approx.	\$2 per Pound	\$8 per Pound

3. Ease of assembly.
4. Compatibility with a reasonable geometry for the retro-reflectors.
5. Ease of including trim weights or balance adjustments.
6. Heat-transfer considerations.
7. Repairability of individual pieces.
8. Schedule implications (or possibility of concurrent fabrication of identical pieces).
9. Compatibility of two different materials for the core (should serious drawbacks to having an outer surface of uranium been uncovered).
10. General compatibility with geometric accuracy requirements.

On the basis of this comparative evaluation, a cubical inner core surrounded by six spherical caps was chosen as the best configuration for fabrication of the EPS core (see dwg. C-CBS-100, Fig. 2-25). Subsequent detailed design has confirmed this choice. The retroreflector geometry described earlier fits well and indeed is based on these six identical spherical caps, each with 144 cavities for retroreflectors. The cube core is well adapted for the inclusion of balancing counterweights, while the whole configuration is excellent for precision machining and a rugged bolted assembly. The exploded view of Figure 2-26 shows this selected configuration

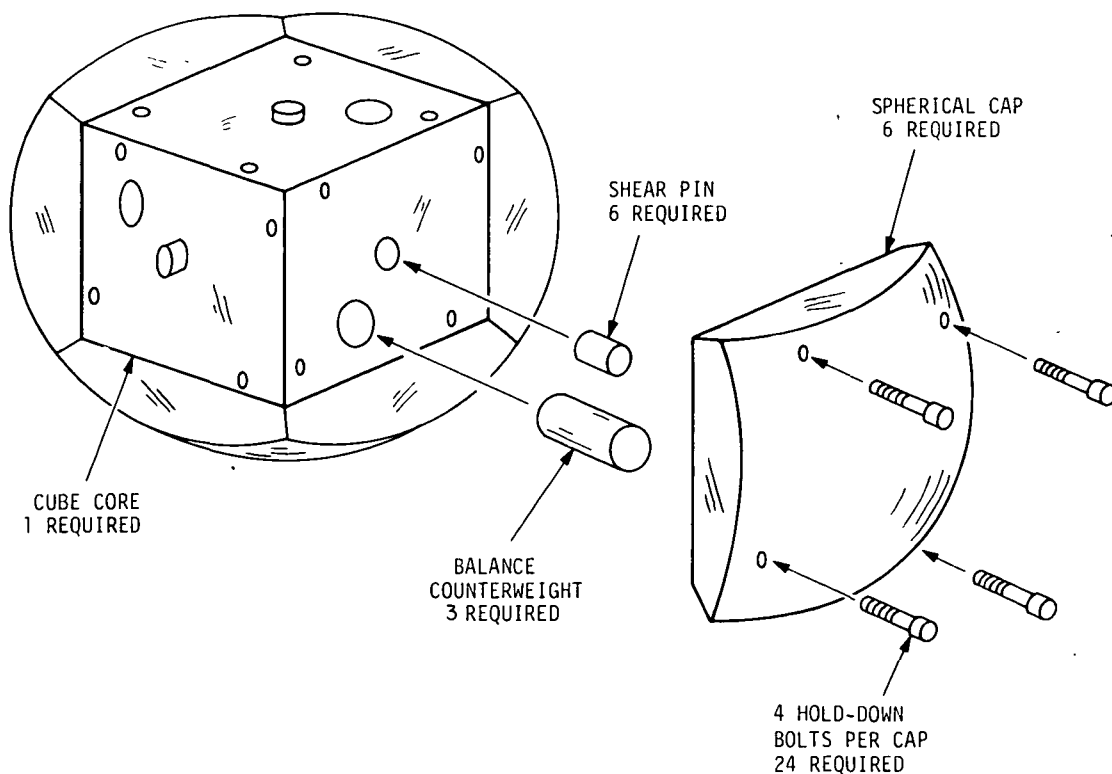
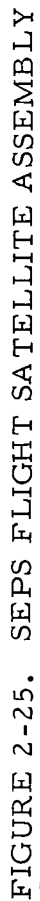


FIGURE 2-26 ASSEMBLY CONFIGURATION OF CUBE CORE.



### 2. 3. 3. 3 CORE SURFACE

The characteristics of the outer surface of the core are primarily dictated by the requirement of suitable reflective properties to enable acquisition by photographic tracking due to reflected sunlight and by the overall requirement for providing the retroreflectors with a satisfactory thermal environment. A secondary requirement of any core surface process is that it provide adequate protection of the basic uranium core material against corrosion and oxidation until the satellite is in orbit, where such processes cease; any of the surface treatments under consideration will satisfy this requirement.

The photographic tracking by reflected sunlight requires that the surface reflect in a highly diffuse manner and have an overall reflectivity for the solar wavelength of approximately 40% or more. Such a surface would cause the EPS to have a brightness approximately between 10 to 15 mag, depending on the sun/satellite/tracking-station location geometry and other noncontrollable variables. Since the Baker-Nunn cameras, which will be utilized for this program, routinely track satellites of 13 mag and with special procedures, can track satellites dimmer than 15 mag, it would appear that such surface characteristics would be satisfactory.

Of the candidate materials for achieving a proper surface treatment for the uranium core, it would appear that aluminum, nickel, and rhodium are the better choices. The first is readily applied by vacuum deposition or ion plating, and the latter two by conventional electroplating.

With respect to a proper surface treatment for thermal considerations, the thermal analysis indicates that the surface should have a relatively low absorptance-to-emittance ratio. In conjunction with the requirement for a high solar reflectivity and hence low solar absorptance, this condition is further ensured by a surface having a reasonably high emittance. Actual measurements of gritblasted aluminum and other metallic surfaces indicate that a satisfactorily high emittance is obtainable, while adequate reflectivity and diffusivity are also provided. Presumably, similar surfaces of nickel and rhodium would exhibit the same characteristics.

Another requirement identified by the thermal analysis is that the cavity surfaces that "see" the back surface of the installed retroreflectors should be radiatively decoupled and thus have a low emittance. Hence, the requirements on the spherical surface and the cavity surfaces are opposite with respect to emittance. This implies either different materials or different preparation for the two surfaces. Fortunately, the gritblasted aluminum has a satisfactorily high emittance, while plain aluminum has a suitably low emittance; hence, it appears that these two conflicting requirements may be met by the same material by using a different preparation for each of the underlying surfaces.

A vapor-deposited material does not produce any measurable buildup of thickness, whereas an electroplated material may do so. Also, a vapor-deposited material "throws" or deposits well into deep and narrow holes, while electroplating into such re-entrant geometries requires special electrodes. On the basis of all these considerations, we have chosen vacuum deposition (i. e., ion plating) of aluminum as the optimum process and material for the surface treatment of the uranium core. We also recognize the necessity for some predeposition or post deposition treatment of the spherical surface (as opposed to the as-machined cavity surfaces) to achieve the required diffusivity and increased emittance. Gritblasting or some similar process may be satisfactory; however, it is highly recommended that the resultant surface characteristics be verified by actual testing and that such a test program be undertaken before satellite fabrication.

#### 2.3.4 SATELLITE ACCURACY

The accuracy required of the EPS is basically a geometric accuracy, i. e., it involves ensuring that the centers of mass and geometry coincide within an allowable amount and that the retroreflectors are accurately positioned with respect to the center of mass and to each other within an allowable amount.

##### 2.3.4.1 GENERAL ACCURACY CONSIDERATIONS

The geometric inaccuracies that will exist will be due to one or a combination of the following factors:

1. The satellite outer surface will not be an exact sphere; hence, there will not be an exact location of a geometric center.
2. The trimming or balancing process with which the center of mass is positioned will not be exact because of a limit to the resolution of the adjustment or the balance indication.
3. The actual positions of the retroreflectors on the satellite surface will not be exactly at their true positions, owing to setup, machining, and measuring errors.
4. The true positions determined for the retroreflectors on the satellite surface are not theoretically uniformly distributed, but are somewhat distorted to provide even centerline-to-centerline spacing along the most crowded directions and to provide adequate centerline-to-edge distances along the sides of the spherical caps.
5. The radial location of the retroreflectors will not all be identical, owing to machining tolerances and the fact that the geometric reference center is not an exact location.
6. The retroreflectors will be neither exact nor identical.

Some of these factors are more directly associated with the actual satellite accuracy than are others. For instance, the deviations of the true positions of the retroreflectors in 4. above are at least symmetrical about the satellite and will be taken into account in the determination of the overall transfer function. On the other hand, although most of the other inaccuracies will exist within certain set limits, they

cannot be readily measured or easily identified so that they cannot be routinely accounted for and hence must be accepted.

#### 2.3.4.2 GEOMETRIC ERROR BUDGET

The allowable overall geometric inaccuracy of the EPS is here established to be 1 mm or less and defined as the limit of the sum of:

1. The worst-case combination in any direction of the variation in the actual position of the reference point of any retroreflector (the theoretical sharp apex formed by the tri-intersection of the three reflecting faces) with respect to the mean location of the reference point of all retroreflectors when referred to a common geometric center for the "best-fit" sphere;

2. the maximum variation of the actual satellite surface from the surface of a "best-fit" sphere;

3. the maximum eccentricity of the mass center from the geometric center of the "best-fit" sphere.

The single reference point common to all three of the above factors is the "best-fit" sphere. This is not a physical entity and thus is not directly measurable; however, we will define it for our purposes as the theoretically perfect sphere having a diameter of exactly 76.200 cm (30.000 in), which most closely represents the actual spherical surface.

The relative proportions of the 1-mm inaccuracy allotted to each of these main factors and a breakdown within each factor of major individual contributions are presented in a quantified error budget for the geometrical EPS in Table 2-9.

TABLE 2-9 GEOMETRIC ERROR BUDGET  
(mil = 0.0254 mm = 0.001 inch)

1. Variation of Actual Retroreflector Apex Position from Mean Position = $\sqrt{A^2 + B^2}$	=	0.457 mm (18 mil)
where A = Transverse Variation of Apex from True Position	=	0.381 mm (15 mil)
B = Radial Variation of Apex from Mean Radial Position	=	0.254 mm (10 mil)
2. Variation of Actual Surface from "Best-Fit" Sphere Surface	=	0.254 mm (10 mil)
3. Eccentricity of Mass Center from Geometric Center of "Best-Fit" Sphere = (C + D)	=	0.152 mm (6 mil)
where C = Equivalent Resolution of Balance-Trim Adjustment.	=	0.025 mm (1 mil)
D = Equivalent Accuracy of Balance Measurement	=	0.127 mm (5 mil)
Sum (< 1 mm)		0.863 mm (34 mil)

The relative apportionments indicated by this error budget were determined by judgment of the relative difficulties and costs associated with equivalent machining and fabrication tolerances.

### 2.3.5 MASS AND BALANCE

The mass restriction of 3628 kg (8000 lb) derives from the baseline capability of the launch vehicle for the selected orbit. The balance consideration is the result of the accuracy requirement that the centers of mass and geometry coincide within an allowable eccentricity of 0.15 mm (6 mils).

#### 2.3.5.1 MASS CONTROL

The EPS mass will be controlled by maintaining up-to-date mass data on all components in the assembled flight satellite and then removing from the flat face side of each of the six spherical caps the mass required to bring the final assembled mass to agree with the established payload mass. The present design is calculated as 3936 kg (8678.5 lb) on the basis of a number of published masses for hardware and certain assumptions on the density of the uranium material as cast. Since this is 308 kg (678.5 lb) over the currently established baseline payload mass, approximately  $2725.2 \text{ cm}^3$  ( $166.3 \text{ in}^3$ ) of material must be removed from each of the six spherical caps, assuming a density of  $18.84 \text{ g/cm}^3$  ( $0.680 \text{ lb/in}^3$ ) for "dilute U." This is the equivalent of a cylindrical cavity of 30.480 cm (12.000 in.) outside diameter by 10.160 cm (4.000 in.) inside diameter by 4.229 cm (1.665 in.) deep which will readily fit within the spherical cap without degrading its strength or detrimentally altering its thermal profile.

The present detailed design does not include the necessary provisions for implementing this mass-control scheme, since the established payload mass limit is not yet considered to be a final number, nor has the mass, and hence density, of the cast uranium material been established. Firm numbers for these conditions will not exist until the program is into the satellite fabrication phase; at that point, ample opportunity will exist to establish final quantities and their allowable tolerances and then to initiate the final mass-control concept.

#### 2.3.5.2 BALANCE CONTROL

The EPS balance, i.e., the eccentricity of the centers of mass and geometry, will be controlled by the proper adjustment of three counter-masses contained within the cubical inner core along three mutually orthogonal - or perpendicular - axes. Each counter-mass is approximately 18.1 kg (40 lb) and has an adjustment range of  $\pm 7.6 \text{ cm}$  ( $\pm 3.0 \text{ in.}$ ) so that an imbalance of approximately 13.6 N-m (10 ft-lb) in any direction can be compensated for. Analysis of the potential and



probable source and amount of imbalance in the assembled EPS indicates that 13.6 N-m (10 ft-lb) of balancing capability will be sufficient.

The resolution of the counter-mass adjustment to the equivalent of a 0.025 mm (1 mil) eccentricity of the mass center appears quite simple since it requires only 0.5 cm (0.2 in) resolution in the longitudinal motion of the counter-mass or a resolution of only 2 turns of the counter-mass, since it is actuated by a 4 turn/cm (10 turn/in) thread. Likewise, the accuracy of the balance measurement to the equivalent of a 0.127 mm (5 mil) eccentricity of the mass center or total imbalance within approximately 4.8 N-m (3.5 ft-lb) appears to be feasible.

Additional discussion of the balance principles, determination, technique, and equipment is contained in a later section.

### 2.3.6 LAUNCH-VEHICLE INTERFACE

Considerations of the interface between the launch vehicle (L/V) and the EPS design, other than allowable payload weight, encompass four specific areas:

1. The geometry of the payload support on the launch vehicle and its ejection from it.
2. Orbital altitude, pressure, thermal and radiational environment, micrometeoroid impact, etc.
3. The influence of the launch environment such as mechanical vibration, acoustic energy, acceleration, and time-dependent pressure and thermal profiles.
4. Satellite spin, spin rate, and spin-axis orientation.

L/V interface considerations for this limited study have been based on the probable use of a Saturn IB launch vehicle.

#### 2.3.6.1 GEOMETRIC L/V INTERFACE

The geometric L/V interface for the EPS is very simple and straightforward. It has been established to be the external spherical surface of the satellite as mutually agreed upon by those responsible for the L/V and by SAO as the agency responsible for the EPS. This requires that the payload support structure and ejection mechanism (PSS/EM) be designed to bear only against the outside spherical surface of the EPS and in a manner that does not damage the surface or structure. There is the limitation, however, that the satellite handling rig designed by SAO and utilized to place the satellite into the PSS/EM cannot encroach on the space below a horizontal plane intersecting the sphere at the equivalent of 35° S latitude. This will ensure no mechanical interference when the payload is mated to the launch vehicle.

An additional requirement that enters into the EPS-L/V interface definition and that must be taken into consideration in the PSS/EM design is a spin of a given rate and with a preferred spin-axis orientation be imparted to the EPS. This requirement is discussed in detail in a later portion of this section.

A secondary aspect of the EPS-L/V interface is that the PSS/EM must mechanically enclose the EPS and protect it with a pressurized atmosphere of contaminant-free inert gas from the time that it is mated with the L/V until orbit injection.

#### 2.3.6.2 ORBIT L/V CONSIDERATIONS

The selected orbit does not impose any serious limitations on the EPS design beyond the usual outgassing, long-term radiation exposure, nominal thermal environment, and micrometeoroid considerations. Since the satellite is passive, many of the usual orbital considerations are not applicable or exert only a minimum influence.

Outgassing will be controlled by strict quality assurance of cleanliness during fabrication, assembly, testing, and handling and by the selection of "clean" materials for the actual satellite hardware. All materials selected for the EPS (uranium, aluminum, stainless steel, fused silica, and Teflon) have very low vapor pressures and are considered to be adequately "clean" in terms of outgassing for the expected long orbital lifetime.

Long-term exposure to solar radiation and to the Van Allen belt has been determined to have no detrimental effect on the uranium core material (see Table 2-7), and it is likewise not expected to affect in any way the aluminized spherical surface of the satellite. As discussed in an earlier section, the fused silica material for the retroreflectors will be specifically chosen to minimize any radiational effects upon it; in addition, specific samples of the retroreflector material will be tested in an accelerated manner to verify that the expected radiation will not cause detrimental effects such as discoloration and transmissibility reduction.

The thermal environment imposed on the EPS is not particularly severe for a passive satellite. The thermal analysis shows that satisfactory passive thermal control can be provided for a spinning EPS by the proper choice of certain satellite and material parameters within a reasonably wide range of values and that, even for a nonspinning satellite, the proper values within these ranges can still result in satisfactory thermal control.

The problem of micrometeoroid impact on the EPS is a potentially serious one in terms of the expected long useful orbital lifetime. Such micrometeoroid action will undoubtedly cause a gradual mechanical deterioration of the surface of the retroreflectors and thereby reduce their optical efficiency. No quantitative predictions have yet been made of the probable rate of this action and, hence, of the useful lifetime of the EPS, but it is considered that the satellite will be useful for significantly more than 10 years. As this gradual decay of optical retroreflection efficiency occurs, equal or greater compensating increases in the ground-based laser transmitting and receiving equipment will undoubtedly take place so that a greater useful lifetime is likely.

All schemes considered to date for eliminating, or even slowing down, the micrometeoroid action suffer from exactly the same result. Any protective "window" must be transparent to visible optical wavelengths, but the transparency of all such known materials will be also degraded by micrometeoroid action. Consequently, we are resigned to accepting this apparently inevitable conclusion and allowing the EPS useful lifetime to thereby cease when it will.

#### 2.3.6.3 LAUNCH ENVIRONMENT

The launch environment will primarily impose mechanical and acoustic vibration, shock, and acceleration on the EPS. In addition, the launch will impose time-dependent thermal and pressure profiles on the satellite but it is considered that these will have no effect since the passive EPS is a large thermal mass, is relatively well insulated within its pressurized PSS/EM, and contains no temperature- nor pressure-sensitive components.

Preliminary estimates based on L/V and PSS/EM analyses indicate that vibration, shock, and acceleration levels will be reasonably low. Maximum vibration input levels are anticipated to be in a range up to 15 to 20 G's with the first natural frequency of the PSS/EM at approximately 11 Hz in the axial mode and 19 Hz in the transverse mode. Acceleration values have been predicted to be at about the 5-G level.

The EPS as currently designed has been checked for susceptibility to vibration and acceleration. Analysis and tests on similar retro-reflector mountings for the lunar array indicated that no problems will exist in this area for the EPS at the expected vibration input levels and frequencies. Initial analysis indicates that the only location to be concerned about is the interface between the cube core and any one of the spherical caps. Two modes of vibration-induced resonance may occur: the cap, as a solid body, may resonate against the four hold-down bolts as springs; and the cap may resonate in its first dish-like bending mode. Initial calculations show that the natural frequency for the former mode will be on the order of 700 Hz, and for the latter about 600 Hz. Experience and judgment indicate that both modes would have relatively high damping due to energy absorbing phenomenon such as friction.

Also, the tightening torque on the four hold-down bolts for each cap provides sufficient pretension that cap separation will not occur at acceleration levels below about 35 G's.

The natural frequencies of both of the potential EPS resonant modes are well above the high transmission band of the PSS/EM, as indicated by the low axial and transverse first natural frequencies. The EPS, being a very large concentrated mass, will remain relatively stationary, while the PSS/EM will absorb the vibrational energy transmitted from the L/V.

Although no specific analysis has been undertaken, these results indicate that there will likely be no problems with random or acoustic vibration inputs.

The area of the EPS least immune to shock will be the retroreflectors, but prior experience on the lunar retroreflector array indicates that this will not be a problem. Acceleration is likewise considered not to be of consequence to the retroreflectors or any other portion of the satellite.

#### 2.3.6.4 SPIN CONSIDERATIONS

The questions of whether to spin or not to spin the EPS and, if spin, what spin rate and what spin-axis orientation are difficult to answer. A spinning satellite with proper rate and axis orientation provides the optimum thermal environment for the retroreflectors, but with too slow a rate or the wrong axis orientation, the thermal environment quickly worsens for particular groupings of retroreflectors. On the other hand, a spinning EPS with an oriented axis will subject a certain band of retroreflectors to greater exposure to other potentially detrimental effects, such as solar radiation and micrometeoroid impact.

Furthermore, if the EPS is injected into orbit with a given spin rate and axis orientation, it will be exposed to influences that can significantly change its spin rate and spin-axis orientation over its extended lifetime. Eddy-current damping due to the earth's magnetic field will cause a gradual decay in spin rate, while other forces such as solar photon pressure may affect the spin rate in either or both directions, depending on the geometric imbalance of the EPS and other nonsymmetrical factors. These forces may also cause precession of the spin axis so that the spin-axis orientation is likely to change considerably over the satellite's lifetime.

All these detrimental effects are significant in that they affect some preferential group or band of retroreflectors differently from others; this, in turn, causes a bias in the laser return signal that will be extremely difficult to detect or correct. As a result, a preferable satellite motion would be a random tumbling that would subject the EPS to random disturbing influences only and thus presumably balance out all of the problems discussed above for the lifetime of the satellite. Such a desired tumbling motion is considered difficult if not impossible to achieve, and any attempts are likely to result in an overly complicated ejection mechanism or require unattainable maneuvers from the final L/V stage, and lead to only an approximation to true random tumbling motion in the end.

Consequently, we have proposed, for the purposes of this limited phase-B study, to require for the EPS at orbit injection a spin rate and a spin-axis orientation based only on considerations of the short-range thermal environment. This requirement is for a minimum spin rate of 0.1 RPM and a spin-axis orientation normal to the ecliptic plane within 3°. It is evident, however, that more analysis and study

must be undertaken to determine the overall optimum orbit-injection motion and any potential passive means for stabilizing or controlling it.

## 2.4 THERMAL ANALYSIS

It was recognized early in the EPS program that a thorough thermal analysis would be required to understand fully and to prepare adequately for the thermal interaction of the massive uranium core and the precision retroreflectors during the lengthy orbital lifetime. For the Phase B studies the thermal analysis was restricted to an initial overview of the thermal situation for the EPS in orbit and to several specific worst cases for the thermal/optical performance of retroreflectors. The results have generated guidelines for a number of specific design decisions and have verified that adequate optical performance can be obtained from the retroreflectors even for extreme conditions.

### 2.4.1 GENERAL THERMAL CONSIDERATIONS

Since the EPS is a completely passive satellite, only passive means to control temperatures in critical areas are possible. On the other hand, the allowable temperature limits are generally broader than for active satellites. Additionally, because of the very simple, symmetrical geometry of the EPS, the thermal analysis resolves into a reasonably straightforward problem, with the thermal influence on the optical performance of the retroreflectors becoming the governing criterion.

Accordingly, the results of the thermal analysis can be readily separated into two distinct categories: (1) the thermal aspects of the core, and (2) the thermal aspects of the retroreflectors. These are covered in more detail in the following sections.

### 2.4.2 CORE

The average temperature of the core is the equilibrium temperature established when the energy absorbed by the EPS from the sun, earth, and moon is balanced by the energy radiated into space. Since by design the EPS is spherically symmetrical in all respects, the average temperature of the core is independent of the satellite's orientation, i. e., whether the satellite is spinning or not and whatever the pointing direction of the spin axis is. However, for a nonspinning satellite or one whose spin axis is not oriented properly with respect to the sun, there will be temperature gradients established through the core, even though the average temperature will be the same as before. However, these gradients appear to be within acceptable limits.

The amounts of energy absorbed and radiated by the core and hence its temperature are highly dependent on the characteristics of the spherical surface not covered by retroreflectors and on the thermal coupling of the retroreflectors to the core. Using reasonable ranges for these parameters, the average core temperature will be maintained satisfactorily at approximately 0°C or slightly colder and that the maximum temperature gradient across a solid core under the worst conditions would be only about 6°C. The core thus becomes a stable, nearly isothermal heat sink independent of the satellite orientation and thereby tends to minimize any thermal effects on the retroreflectors that would result from a varying ambient temperature.

There appear to be no additional significant temperature gradients within the core due to the interfaces between the several component pieces that make up the spherical core, provided reasonable interface surface pressures are maintained; this condition is ensured by the pretensioning of the assembly bolts to provide satisfactory survival of vibration during the launch.

The spherical surface need have only a low solar absorptance-to-emittance ratio to ensure that these thermal conditions exist. The optical reflecting characteristics to provide reflected sunlight tracking capability appear to be compatible with the low absorptance-to-emittance ratio surface and can be reasonably achieved by several candidate surface finishes. A textured surface of nickel or aluminum will satisfy both requirements, and either can be readily applied to the uranium core. Aluminum would appear to be the better choice.

#### 2.4.3 RETROREFLECTORS

The retroreflectors, being the most operationally critical part of the EPS, are also the most thermally influenced.

The degradation of the retroreflector optical characteristics depends basically on the temperature gradients that exist within them, both radially and axially, but is generally independent of their average temperature level. On the other hand, the average temperature level of the retroreflectors is coupled to the core temperature in that they provide a significant path for EPS energy loss due to thermal radiation to space.

##### 2.4.3.1 AVERAGE RETROREFLECTOR TEMPERATURE

The retroreflector average temperature does not influence its optical characteristics to any significant degree and hence is not as important a factor as are the temperature gradients within the retroreflectors. However, since the retroreflectors occupy one-half of the EPS surface, their average temperature is involved in the overall energy balance for the system and hence must be reasonably controlled. Since the retroreflectors will have a lower absorptance-to-emissivity

ratio than will the remainder of the core surface, their average temperature will generally be lower than that of the core. Thus, they essentially cool the core by reradiating the energy it receives.

This energy is transferred from the core to the retroreflectors by the thermal coupling of the retroreflectors to the core. There are two basic paths: the conductive path through the mounting tabs, and the radiative coupling between the back surfaces of the retroreflectors and the enclosing surfaces of their cavities. The latter path is purposefully minimized to reduce axial gradients as discussed in the next section; the conductive path is thus the only means of controlling the overall thermal coupling. However, the considerable range in the conductivity of this path will result in satisfactory average temperatures as well as proper radial thermal gradients. Calculations indicate that a range of nearly 2 orders of magnitude in the retroreflector-mount conductance results in only about a 50% change in thermal energy transferred from the core to the retroreflectors. This relatively small range of energy transferred produces in turn satisfactory average temperatures of the retroreflector and also results in radial thermal gradients in the retroreflector that are both small enough and in the proper direction.

The assurance that the mount conductance falls within this acceptance range must be demonstrated by thermal simulation testing.

#### 2.4.3.2 TEMPERATURE GRADIENTS OF THE RETROREFLECTORS

The optical performance of the retroreflectors has been determined to be much more influenced by temperature gradients within the retroreflector than by its average temperature. This is due mainly to the fact that the retroreflector optical material — in this case, fused silica, but also true for all optical materials — exhibits a change of refractive index with temperature,  $dn/dT$ . Although this is a small effect, the optical performance can be significantly affected.

An average temperature change will alter the index of refraction everywhere within the retroreflector on an equal basis and hence will change the speed of the entire optical wavefront equally as it progresses through the retroreflector, hence producing no differential effect that would cause wavefront distortion and that would, in turn, degrade optical performance. On the other hand, temperature gradients within the retroreflector material will produce refractive-index gradients that will affect different portions of the wavefront differently as it progresses through the retroreflector. This results in wavefront distortion that, in effect, alters the optical performance.

From a comparison of different rays, such as a central ray and an edge ray, through a retroreflector in a geometric ray-tracing exercise, it is obvious that the effects of symmetrical radial gradients in the index of refraction on an incident wavefront filling the aperture always tend to cancel out, whereas those due to axial gradients are

additive and hence do not cancel out. Consequently, it is most important that the axial temperature gradients be maintained at a satisfactorily low level, while the magnitude and direction of the radial temperature gradients are also controlled.

The thermal analysis shows that even a 2°C gradient from the apex to the entrance face of a retroreflector will spread the return beam to the extent that the central irradiance will drop to half of its original value and will essentially fall to zero at a 5°C difference. Hence, in an application such as the EPS where high efficiency of the reflected energy and close control of its return direction are required, all means to minimize the axial temperature gradients in the retroreflector must be employed.

Further calculations show that this can be effectively accomplished by minimizing the radiative coupling between the back surfaces of the retroreflector and the surrounding cavity walls of the core. Providing both these surfaces with a low-emissivity coating fulfills this requirement. This is ensured if the aluminized back side is a highly reflective, low-emissivity surface not covered by a protective overcoating as is conventionally done and if the surrounding core surfaces of the cavity walls are also aluminized.

Although the effect of the radial temperature gradients on the optical performance of the retroreflector is not as pronounced, proper choice of mounting conductance ensures satisfactory magnitude and proper direction so as not to degrade materially the performance. The analysis indicates that such a situation will exist within the previously mentioned wide acceptable range of mount conductances.

#### 2.4.3.3 THERMAL/OPTICAL INTERACTION

The thermal influence on the optical performance of the retroreflectors is critical: the analysis shows that it can be satisfactorily controlled by ensuring that axial temperature gradients are minimized and that radial gradients are in the proper direction and maintained to a reasonable magnitude. Nonetheless, some gradients will exist and their influence on the optical performance of the retroreflector must be understood.

Consequently, the theoretical far-field diffraction pattern was derived for retroreflectors of the type to be used - i.e., solid fused silica with aluminized reflective surfaces and slightly opened dihedral angles - under expected as well as extreme thermal conditions. The results are machine plotted as three-dimensional representations of the intensity of the far-field, return-beam diffraction pattern over the lateral plane normal to the beam axis; the plots appear as Figures 4 through 11 in Reference 1. These plots show that, for retroreflectors having specific deviations of the dihedral angle the return-beam energy at the selected beam-spread angle (to compensate for the velocity aberration) does not vary beyond what appear to be reasonable



limits except possibly for the case of a retroreflector looking at free space from a nonrotating satellite. These results are encouraging but not necessarily conclusive and hence must be confirmed by an experimental effort using prototype hardware items.

#### 2.4.4 THERMAL CONCLUSIONS

The conclusions resulting from the thermal analysis are basically as follows:

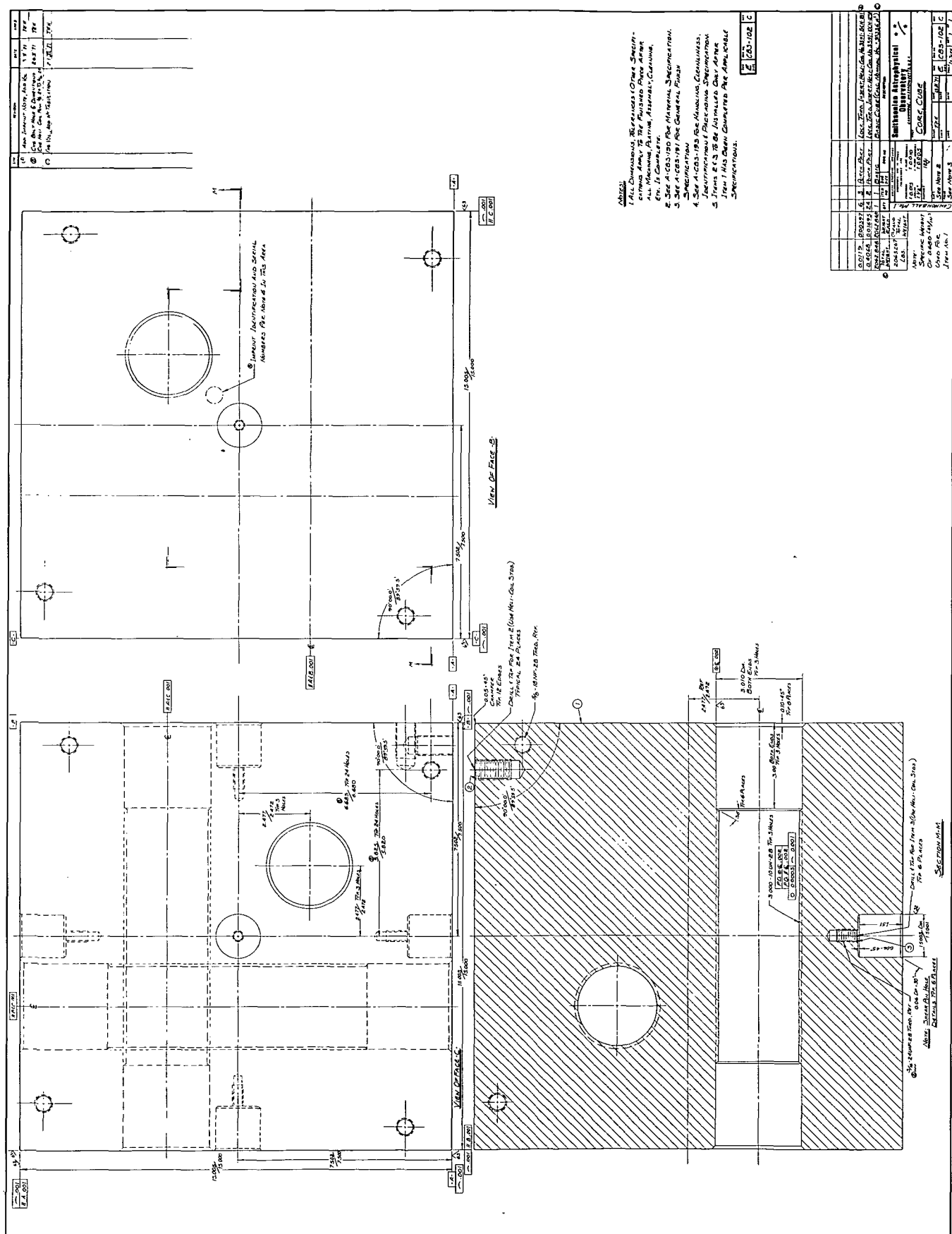
1. Temperature gradients within the retroreflectors will degrade their optical performance, but their thermal environment can be properly controlled, with the result that satisfactorily high optical performance can be attained.
2. Proper control of the thermal environment of the retroreflector can be achieved within the operational requirements of the EPS with a reasonably wide range in several of the more critical aspects such as the conductance of the retroreflector mounting and the EPS spin rate and spin-axis orientation.
3. There are no critical thermal problems within the core itself, and several potentially suitable finishes for the spherical surface have been identified.
4. There is a definite need to determine more precisely by experiment the quantitative values of several of the more important parameters involved in the overall thermal picture so that a more accurate prediction can be made of in-orbit performance. These include measurements of the solar absorptance and infrared emittance of the actual surface treatment to be used, a more thorough analysis of the thermal/optical performance of retroreflectors under all expected operational conditions, and an experimental verification of that thermal/optical performance based on simulated orbital conditions imposed on prototype hardware items.

#### 2.5 DETAIL DESIGN

On the basis of the requirements, design considerations, and thermal analysis, a detailed design for a EPS has been completed. It is represented by the assembly drawing and the group of detail fabrication drawings, along with the associated specifications, available upon request.

##### 2.5.1 CORE DETAILS

Detail drawings of main core items include the spherical cap E-CBS-101 (Fig. 2-23), the cube core E-CBS-102 (Fig. 2-27), the balance counterweight C-CBS-103 (Fig. 2-28), and the shear pin C-CBS-104 (Fig. 2-29). Additional special hardware items associated with the core are presented in drawings B-CBS-109 through -111 (Figs. 2-30 through 2-32). All these core items are shown in the drawing of the assembled core E-CBS-100. Additional standard hardware items are shown on drawings CBS-106 through -108 (Figs. 2-33 through 2-35). Self-locking stainless-steel screw-thread inserts are specified for all threaded holes.





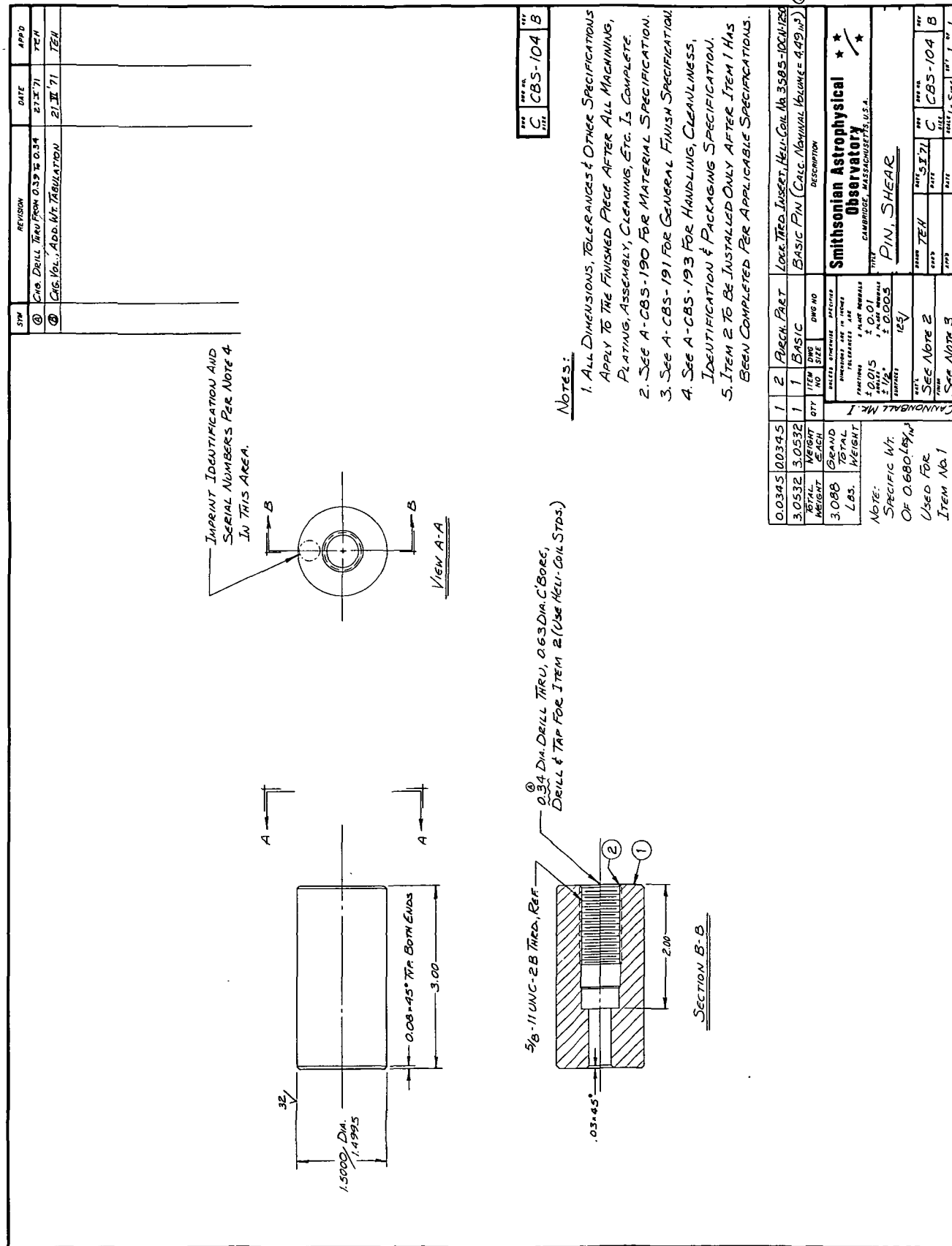


FIGURE 2-29. SHEAR PIN

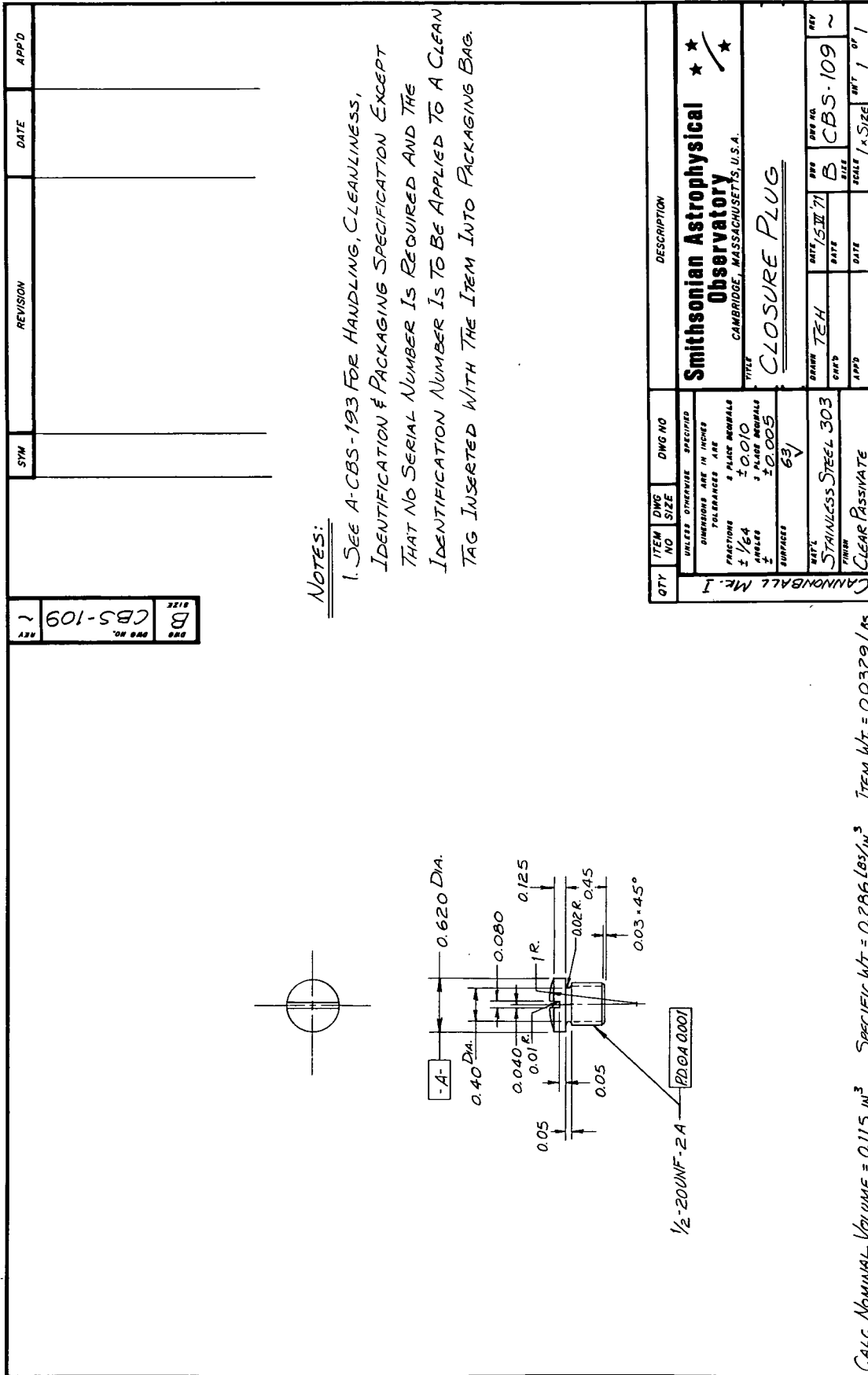


FIGURE 2-30. CLOSURE PLUG

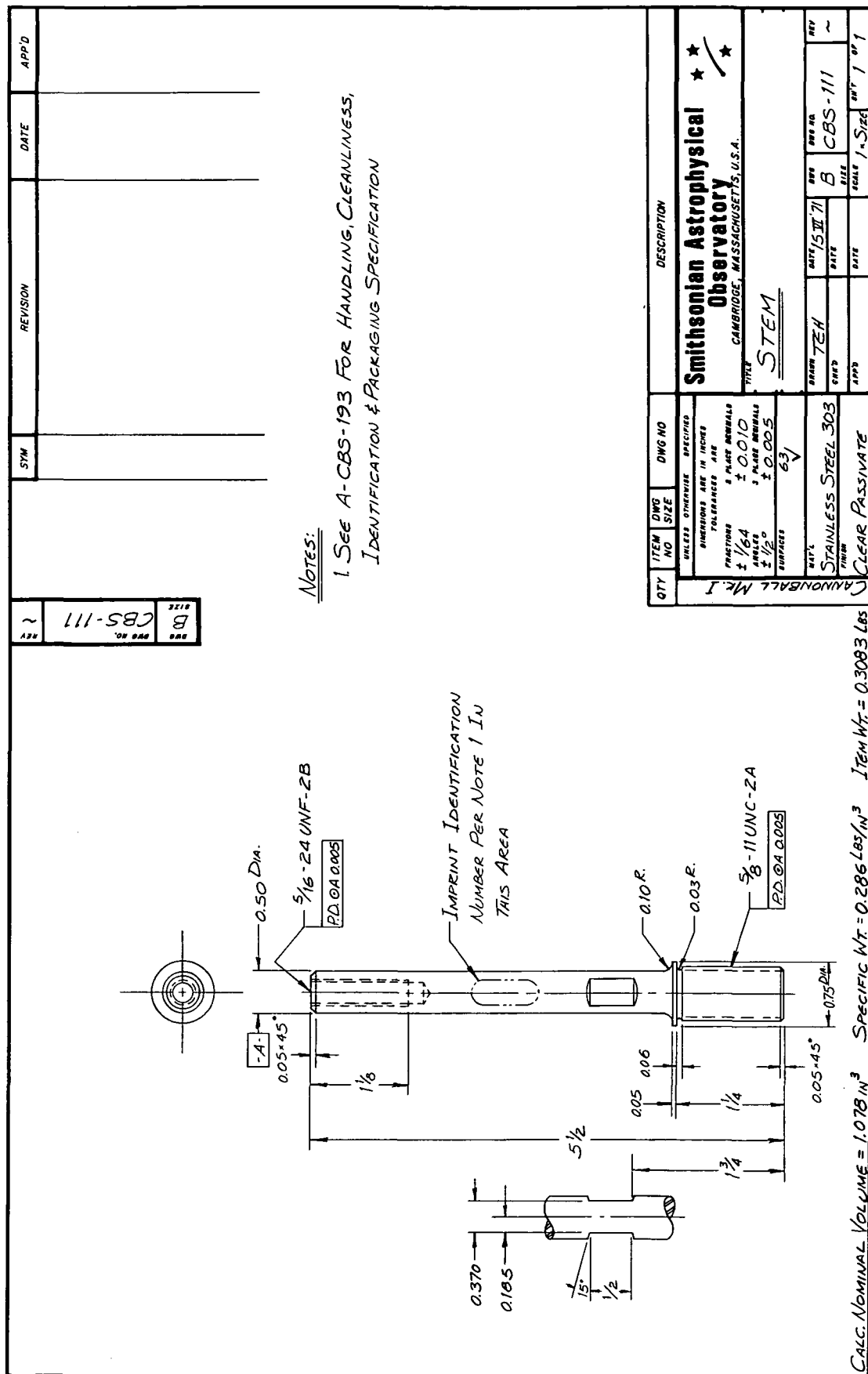


1. SEE A-CBS-193 FOR HANDLING, CLEANLINESS, IDENTIFICATION & PACKAGING SPECIFICATION EXCEPT THAT NO SERIAL NUMBER IS REQUIRED AND THE IDENTIFICATION NUMBER IS TO BE APPLIED TO A CLEAN TAG INSERTED WITH THE ITEM INTO THE PACKAGING BAG.

REV	CBS-110	B SIZE
-----	---------	-----------

QTY	ITEM NO	DWG NO	DWG SIZE	DESCRIPTION
UNLESS OTHERWISE SPECIFIED DIMENSIONS ARE IN INCHES TOLERANCES ARE FRACTIONS 3 PLACE DECIMALS ANGLES ± 0.010 SURFACES ± 0.005 ± 1/64 ± 1/8"				
CANNONBALL ME. I BUSHING 63				
DRAWN T.E.H. DATE 15 VII 71 CHECKED DATE APP'D DATE				REV ~ DWG NO B C.B.S.-110 SCALE 1" = SIZE SHEET 1 OF 1
Smithsonian Astrophysical Observatory CAMBRIDGE, MASSACHUSETTS, U.S.A.				

FIGURE 2-31. BUSHING







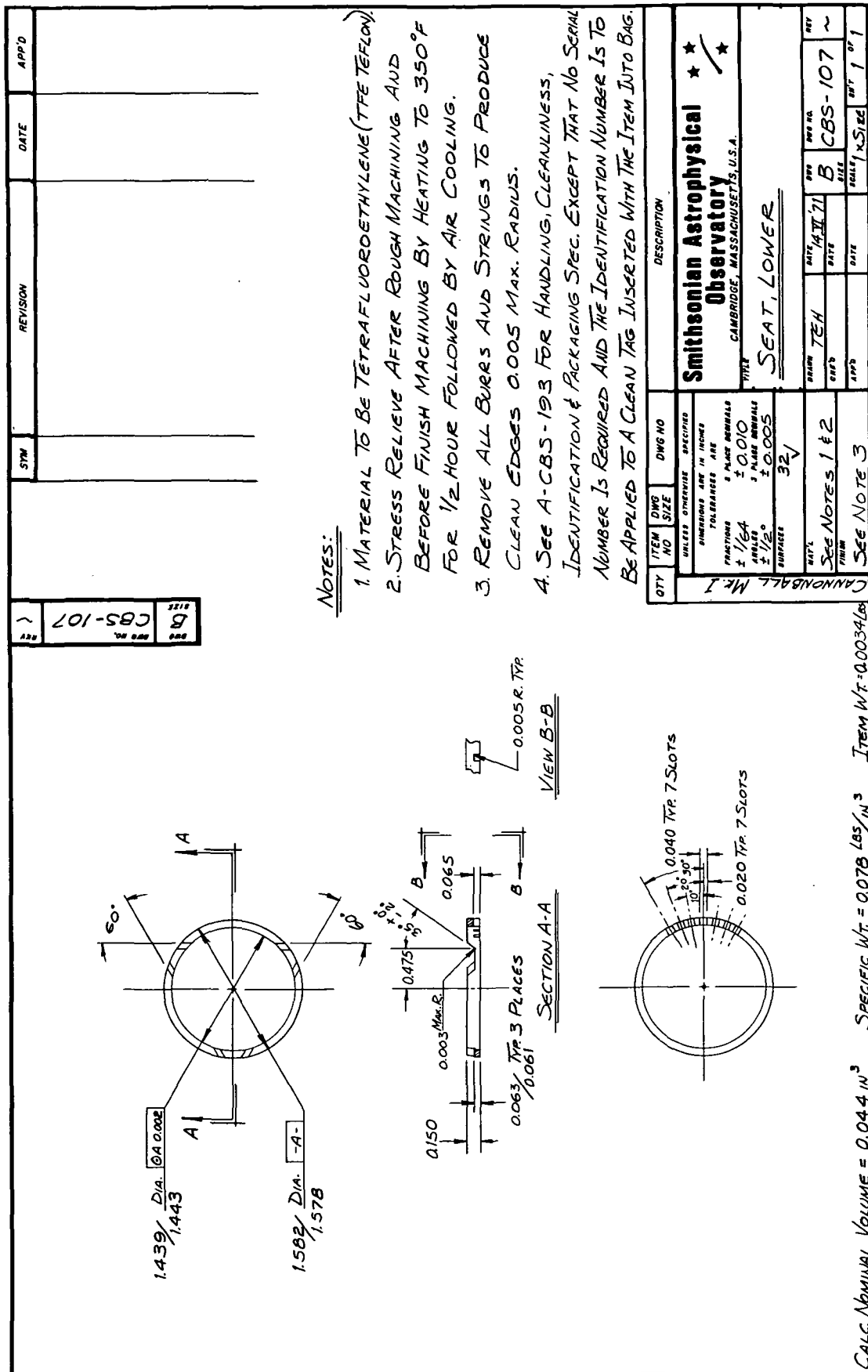


FIGURE 2-34. LOWER SEAT

REV B CBS-108	SYM	REVISION	DATE	APP'D

**NOTES:**

1. MATERIAL TO BE TETRAFLUOROETHYLENE (TFE TEFLON)
2. STRESS RELIEVE AFTER ROUGH MACHINING AND BEFORE FINISH MACHINING BY HEATING TO 350°F FOR 1/2 HOUR FOLLOWED BY AIR COOLING.
3. REMOVE ALL BURRS AND STRINGS TO PRODUCE CLEAN EDGES 0.005 MAX. RADIUS.
4. SEE A-CBS-193 FOR HANDLING, CLEANLINESS, IDENTIFICATION & PACKAGING SPECIFICATION EXCEPT THAT NO SERIAL NUMBER IS REQUIRED AND THE IDENTIFICATION NUMBER IS TO BE APPLIED TO A CLEAN TAG INSERTED WITH THE ITEM INTO PACKAGING BAG.

SECTION A-A

QTY	ITEM NO	DWG NO	DESCRIPTION												
1	1	1	Smithsonian Astrophysical Observatory CAMBRIDGE, MASSACHUSETTS, U.S.A.												
<p style="text-align: center;"><u>SEAT, UPPER</u></p>															
<p>UNLESS OTHERWISE SPECIFIED DIMENSIONS ARE IN INCHES TOLERANCES ARE</p> <table style="width: 100%;"> <tr> <td>FRACTIONS</td> <td>± PLACES</td> <td>DECIMALS</td> </tr> <tr> <td>± 1/64</td> <td>± 0.010</td> <td></td> </tr> <tr> <td>± 1/32</td> <td>± 0.005</td> <td></td> </tr> <tr> <td>SURFACES</td> <td>32</td> <td></td> </tr> </table>				FRACTIONS	± PLACES	DECIMALS	± 1/64	± 0.010		± 1/32	± 0.005		SURFACES	32	
FRACTIONS	± PLACES	DECIMALS													
± 1/64	± 0.010														
± 1/32	± 0.005														
SURFACES	32														
<p>WGT/LB SEE NOTES 1 &amp; 2</p>															
<p>THRU SEE NOTE 3</p>															

Calc. Nominal Volume = 0.010 in<sup>3</sup>

Specific Wt = 0.078 lbs/in<sup>3</sup>    Item Wt = 0.0008 lbs

FIGURE 2-35. UPPER SEAT

The assembly drawing clearly indicates the spherical core consisting of the cubical inner core and the six spherical caps and the shear pin and the bolted construction for their assembly. It also shows the balancing counterweights in place and the method employed for locking them after adjustment.

The specifications associated with the core are given in the following: A-CBS-190, which specifies the basic depleted uranium core material; A-CBS-191, the general finish required on the depleted uranium to control satisfactorily its oxidation during fabrication, assembly, testing, and until orbit injection; A-CBS-192, the particular finish for the core spherical surface required to permit optical tracking and to produce the proper thermal environment; A-CBS-197, the finish for the cavity surfaces necessary for proper thermal control; and A-CBS-193, the necessary handling, cleanliness, identification, and packaging requirements. It is anticipated that these specifications, especially those of A-CBS-192 and -197, will be updated after results are available from actual thermal testing of preprototype hardware items.

#### 2.5.2 RETROREFLECTOR DETAILS

The retroreflectors are completely specified by drawing C-CBS-105 and by associated specifications A-CBS-194, which calls out the retroreflector fused silica material; A-CBS-195, the reflectance coating to be applied to the three back surfaces of the retroreflector; and A-CBS-196, the performance requirements of the retroreflector. The general specifications of A-CBS-193 also apply to the retroreflectors.

It is anticipated that these specifications will be revised according to the results of optical/thermal testing and the final outcome of the overall transfer-function analysis for the reflected laser beam.

#### 2.5.3 RETROREFLECTOR MOUNTING DETAILS

The mounting of the retroreflectors in their cavities is shown in the large-scale detailed assembly view on the overall assembly drawing E-CBS-100, along with the necessary assembly instructions. The required hardware items for the mounting are shown in detailed drawings C-CBS-106 through -108 while the cavity details are shown on drawing E-CBS-101 of the spherical cap. Although not anticipated, the retroreflector mounting may change in some small details as a result of the optical/thermal and vibration testing on preprototype hardware items.

#### 2.5.4 OTHER DESIGN DETAILS

One goal of this limited study program was to evolve a complete detail design for a EPS satellite. This has been done within the limitations discussed; however, because of the definition of this phase-B program, a number of design tasks have had to be postponed until the initial phase of the EPS fabrication. These include the detailed and

assembly drawings for the dummy satellite and the required detail design and drawings for the several special tools required and the necessary handling jigs and fixtures.

## 2.6 MANUFACTURING

Manufacture of the flight satellite and the dummy satellite will be conducted according to the plans presented and discussed in Volume III of this study.

## SECTION 3. PAYLOAD SYSTEMS PRELIMINARY DESIGN

### 3.1 PAYLOAD SHROUD

#### 3.1.1 PAYLOAD SHROUD CONFIGURATION

The payload shroud configuration selected as a baseline for this study consists of the Apollo Spacecraft LM Adapter (SLA) and an existing nose cone of the AS-204 configuration, as shown in Figure 3-1. The major considerations for the selection of this configuration are as follows:

(a) The required shroud components are existing flight-qualified hardware and can be utilized without modification.

(b) The resulting vehicle external configuration is the same as AS-204 for which aerodynamic and flight data are available.

(c) The SLA provides a suitable structural interface, through the four LM support points, for the payload support structure.

(d) The resulting shroud weights are compatible with the Saturn IB vehicle performance capability and the target satellite weight.

#### 3.1.2 SATELLITE SUPPORT STRUCTURE INTERFACE

The existing LM holddown support fittings, located on the lower section of the SLA, were selected for support and holddown of the Satellite support structure. This holddown fitting is shown in Figure 3-2. The only modification that may be desirable is the replacement of the LM separation devices on the holddown fittings with non-ordnance devices.

#### 3.1.3 LAUNCH VEHICLE STRUCTURAL INTERFACE

The SLA, which supports the Satellite structure, structurally interfaces with the forward end of the Instrument Unit. This interface is structurally the same as used on the Apollo flights. There are no modifications required for this interface.

#### 3.1.4 PAYLOAD SHROUD SEPARATION SYSTEM

Two separations are required for this configuration, both of which are flight qualified. The first separation involves the ejection of the nose cone from the SLA. The nose cone/SLA separation interface is shown in Figure 3-3, and is the same design as used on the AS-204 vehicle.

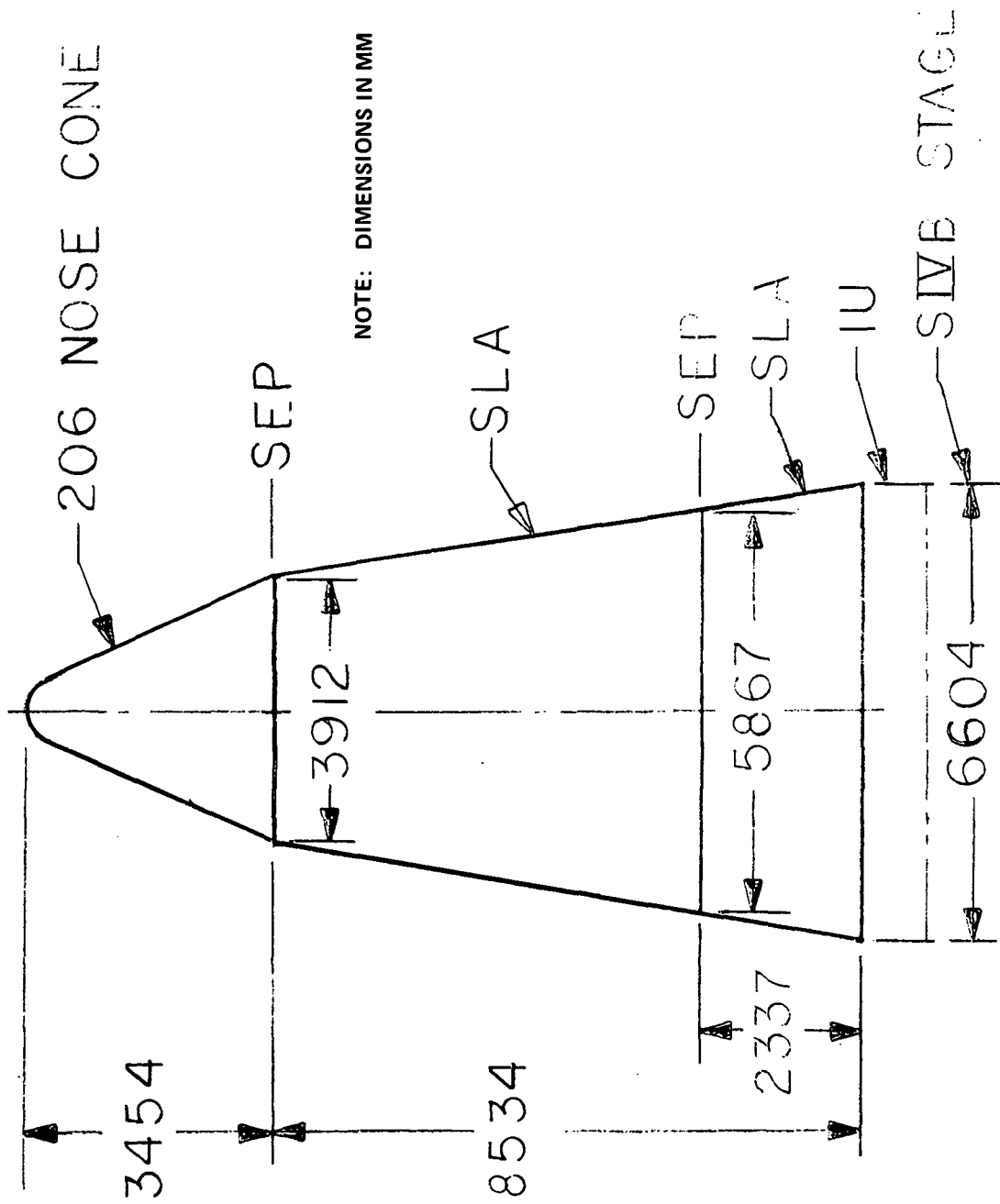


FIGURE 3-1. PAYLOAD SHROUD CONFIGURATION

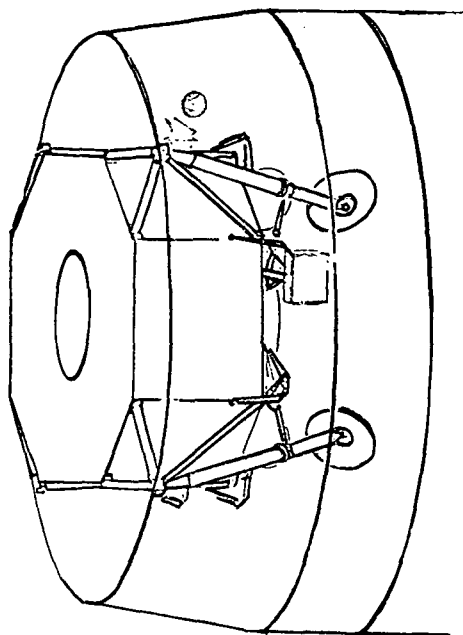
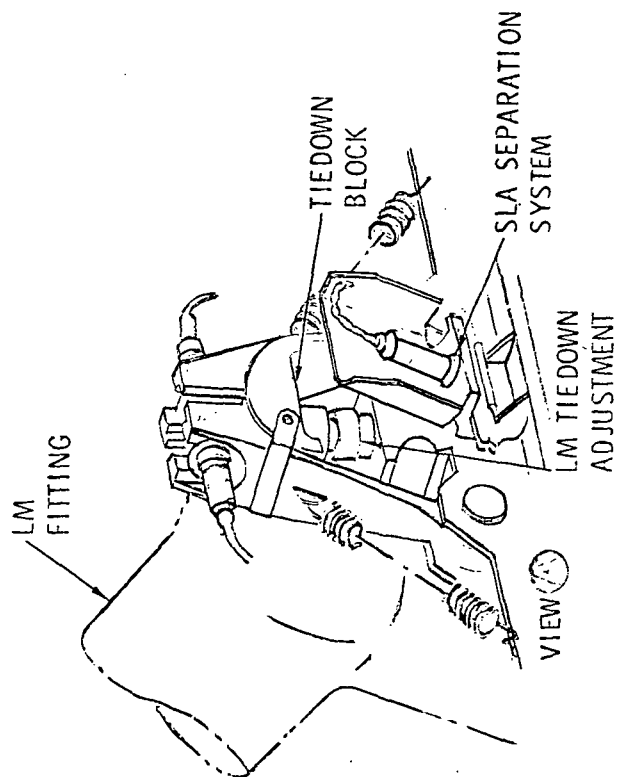
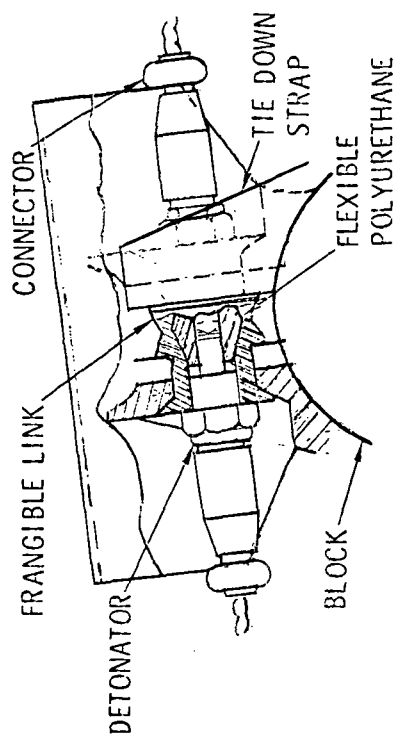


FIGURE 3-2. LM SUPPORT AND HOLDDOWN FITTING

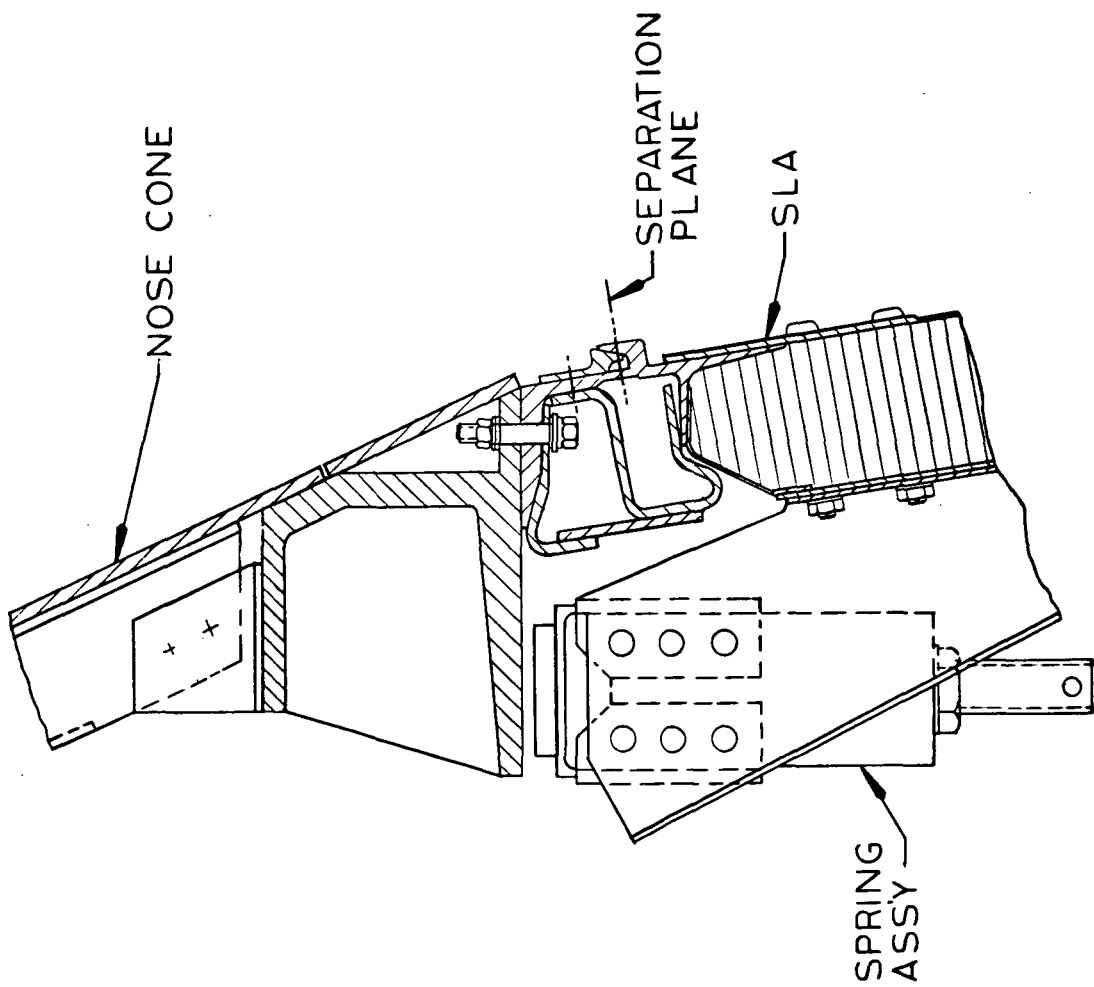


FIGURE 3-3. NOSE CONE/SLA SEPARATION INTERFACE



After the nose cone is ejected, the upper portion of the SLA is divided into four equal panels and ejected by the SLA separation system to expose the Satellite for ejection. The SLA separation system is suitable as currently exists and no modifications are required for this payload application.

### 3.2 SATELLITE SUPPORT SYSTEM

#### 3.2.1 STRUCTURAL SUPPORT SYSTEM

As described in 3.1.2, there are four points available in the SLA for the introduction of the payload support loads. The support structure consists, therefore, of a set of two built-up I-beams which intersect each other at the center of the vehicle cross section, as shown in Figure 3-4. The upper and lower flanges of these beams are supported against lateral buckling by tie rods, also shown in Figure 3-4. In addition, these tie rods improve the distribution of horizontal loads from the Satellite (i.e., at the point of intersection of the cross beams) into the four support points by reducing the local support point loads to amounts compatible with their capability. At their point of intersection, the beams are penetrated by a tube enclosing the payload-ejection system. As shown in Figure 3-5 and Figure 3-6, the required load paths around the resulting hole are provided by gusset plates for the top and bottom flanges, and by the tube with attachment fins for the webs, the tube having a somewhat larger diameter than the ejection tube.

The upper gusset plate is provided with a bearing surface which guides the ejection tube, and at its four outer ends it is designed to provide the contact pads for the payload support frame and ejection structure. The lower gusset plate has a circular cutout for the payload release mechanism.

The outer ends of the beams are provided with fittings designed to adapt to the existing support and holddown fittings of the lower SLA.

#### 3.2.2 SATELLITE SUPPORT STRUCTURE AND EJECTION MECHANISM

The spherical satellite is supported at four points which are located 45 degrees below its equator, as shown in Figure 3-7. The cruciform structure, which interconnects these points underneath the sphere, consists of machined aluminum parts which are welded together. An aluminum tube, 190 mm (7.5 in.) in diameter is welded to the center portion of the cruciform structure and extends downward through the main support beams.

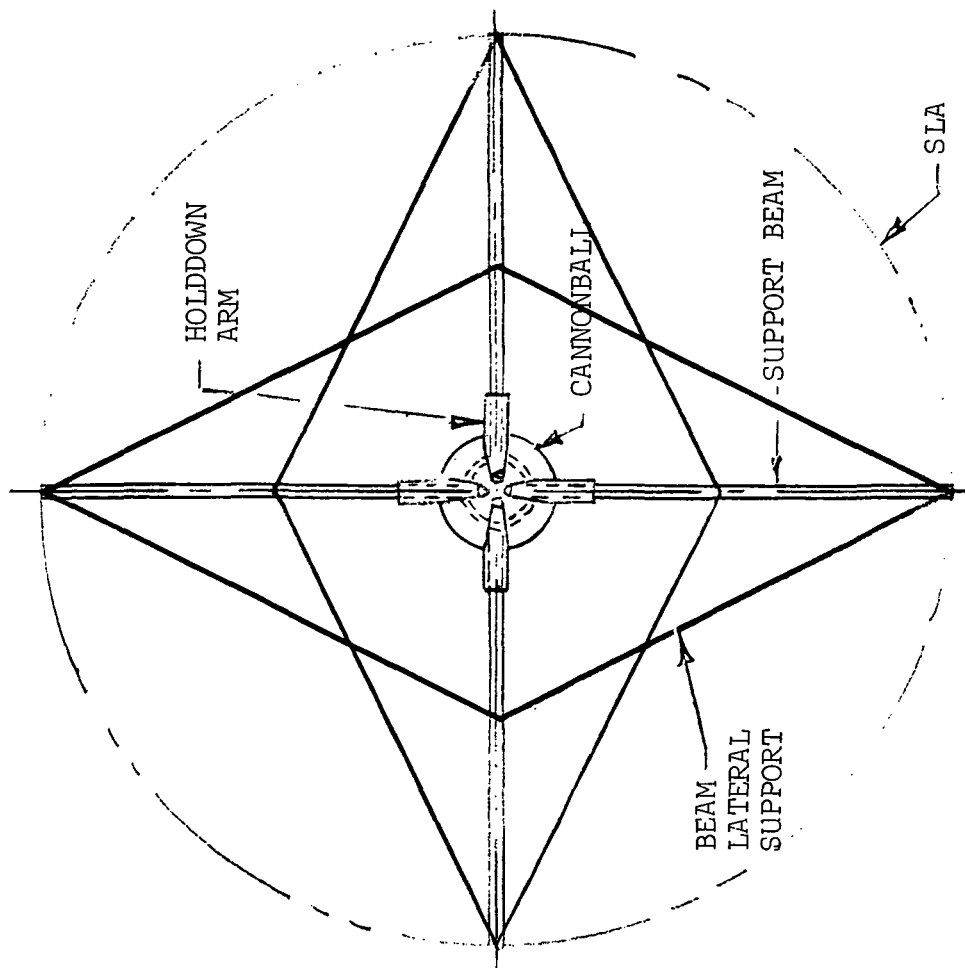


FIGURE 3-4. STRUCTURAL SUPPORT SYSTEM

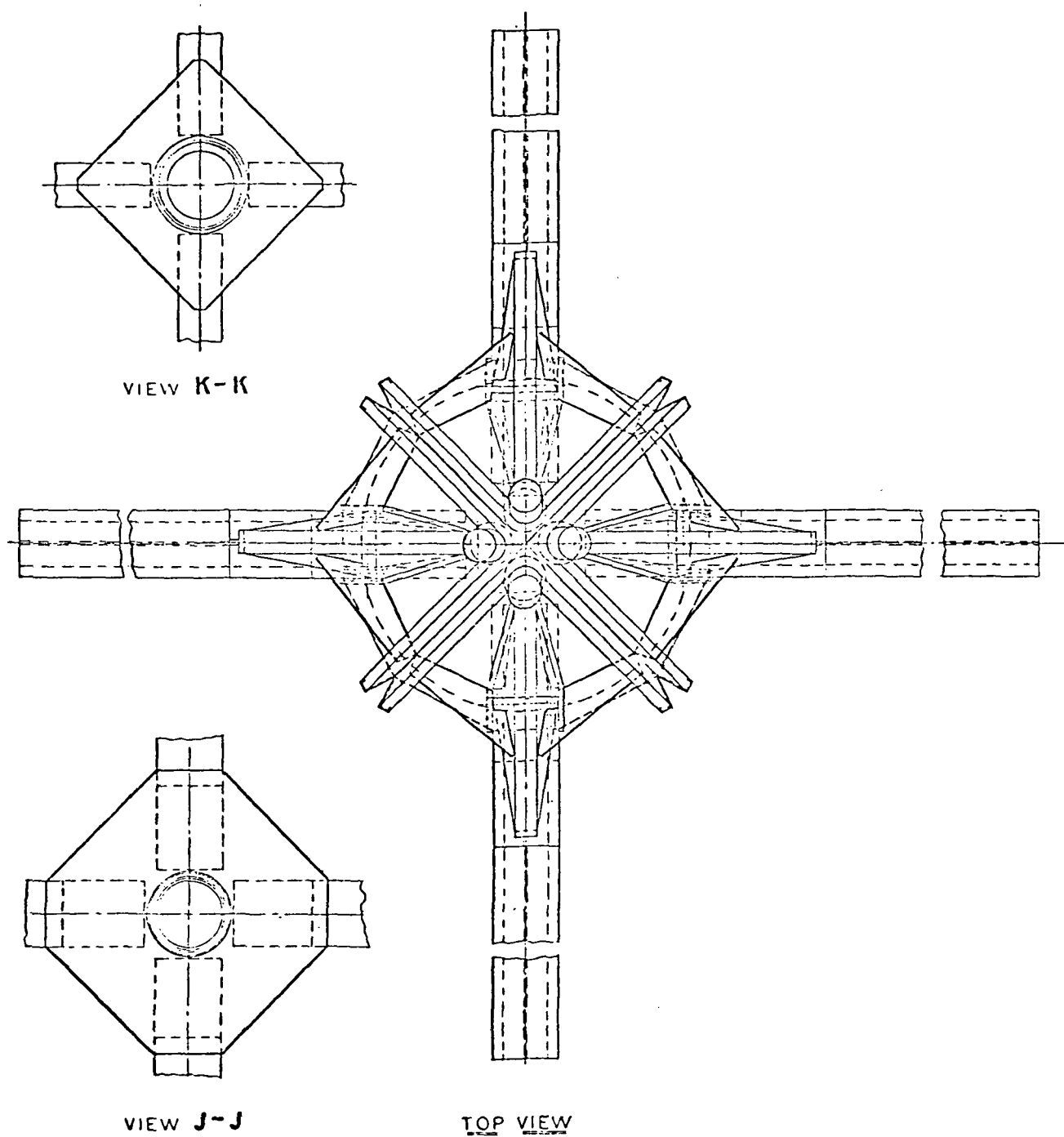


FIGURE 3-5. STRUCTURAL SUPPORT SYSTEM

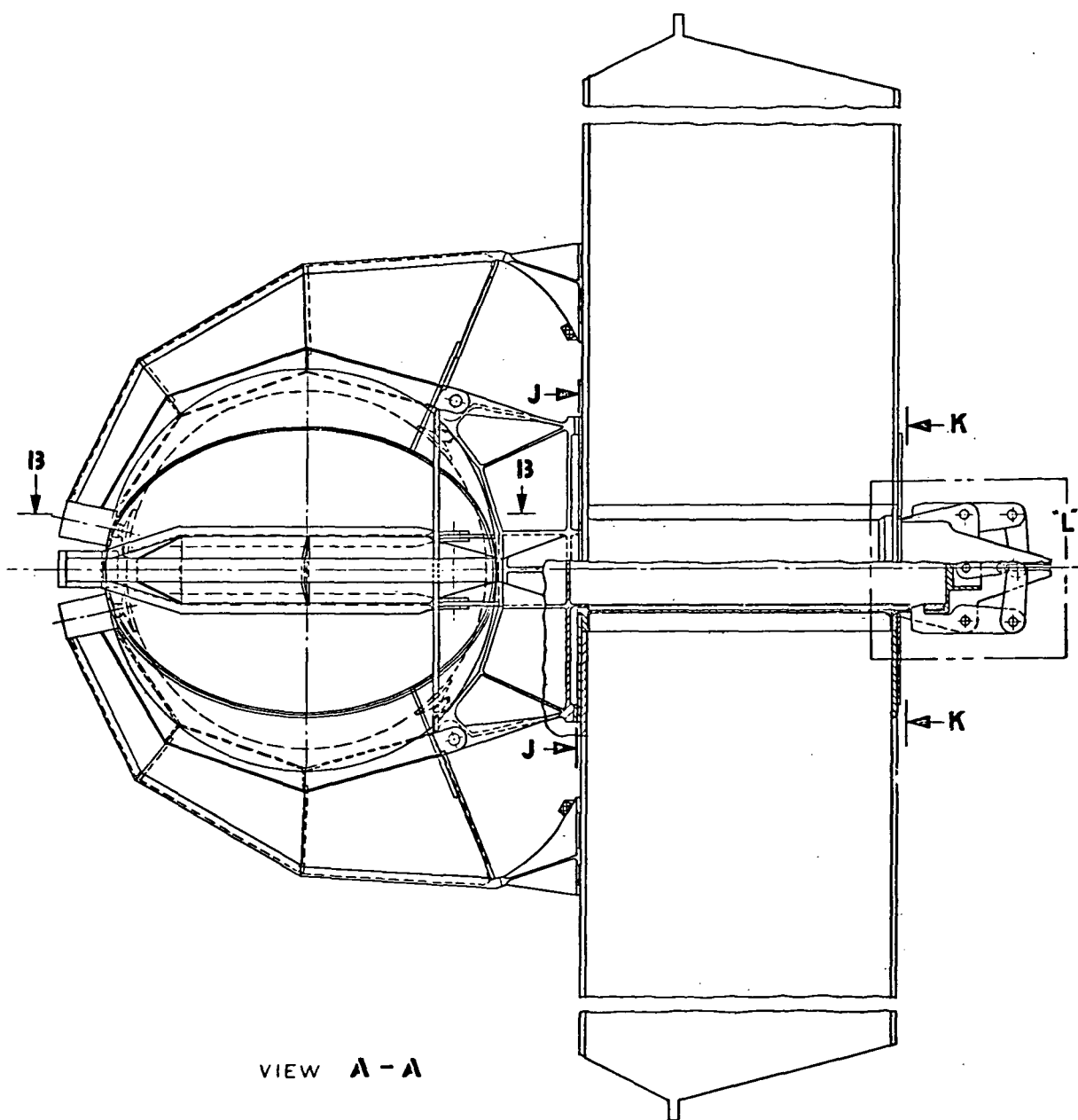


FIGURE 3-6. STRUCTURAL SUPPORT SYSTEM

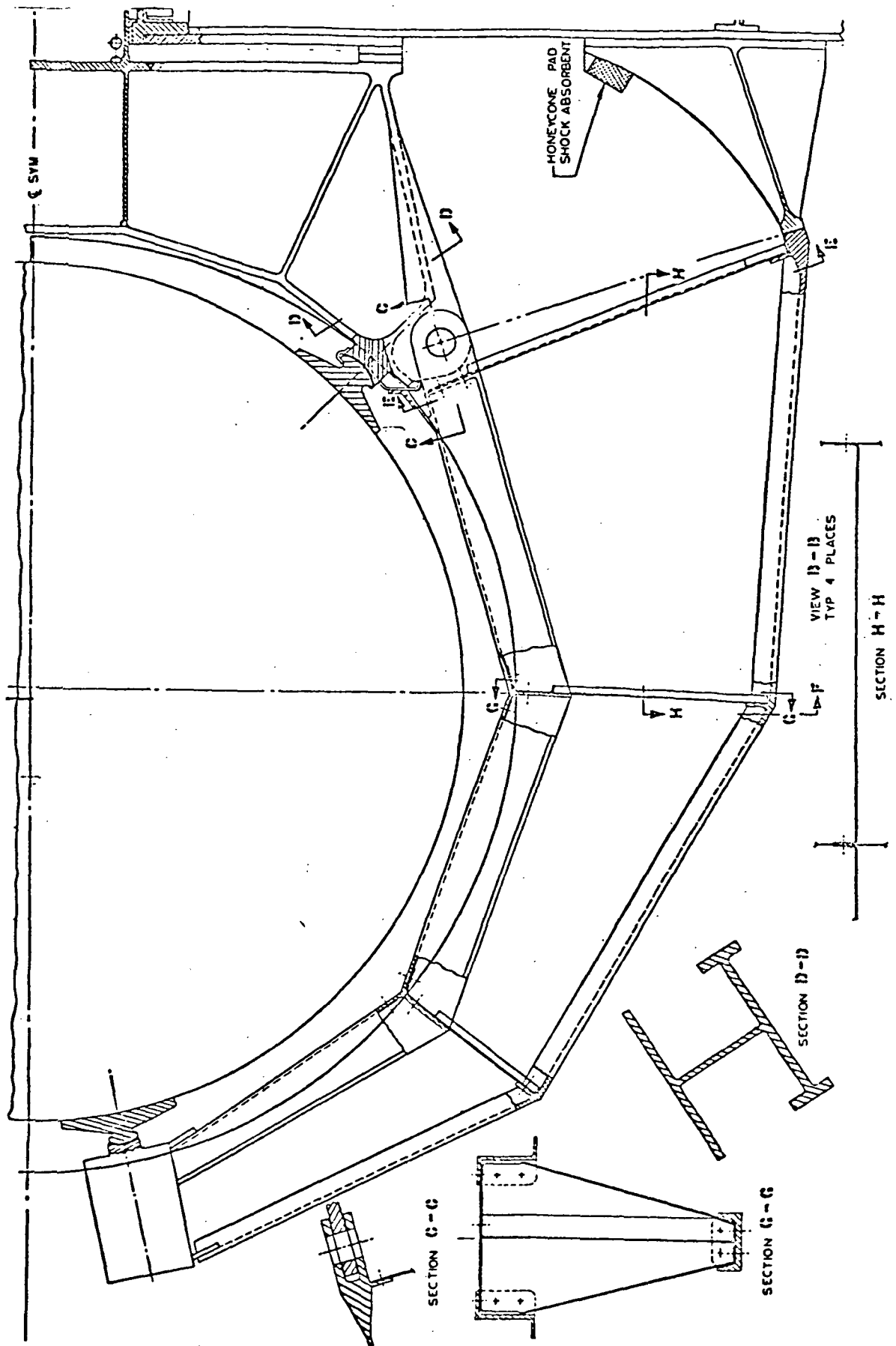


FIGURE 3-7. SATELLITE SUPPORT AND HOLDDOWN STRUCTURE

The diameter of the support pads for the satellite is made rather large to ensure sufficient contact area with the unperforated portion of the satellite surface. To allow for small angular deviations between support structure and satellite due to deflections under the various g-loads, the interfaces between pads and support structure are spherical. Each pad is held to the support structure by leaf springs which permit slight angular changes but prevent the pads from flying away at Satellite separation.

Four identical holddown arms, one of which is shown in Figure 3-7, are provided to hold the Satellite in place against lateral and negative g-loads. These arms are hinged near the support pads at the outer ends of the cruciform support structure. Close to the upper end of each holddown arm is located a screw-type fixture to which a pad is attached which is of the same type as those used for the main support. This fixture provides for applying the amount of preload necessary to prevent the Satellite from lifting off its lower support points under any loading condition.

The arm itself is not curved but has straight members between the break points in order to achieve a minimum arm deflection under the preload applied at its end. The cross section of the arm has the shape of a T ; its inner and outer flanges are machined pieces interconnected by a sheet metal web and sheet metal ribs.

The outer support at the lower end of the arm consists of a bearing surface only, which rests against a small pedestal mounted on the main support beam. This arrangement has the following purpose: Immediately after Satellite release, when the entire Satellite support structure begins to move along its vertical axis, the bearing face at the outer end of the arm begins to slide towards the vehicle center, and slips off the pedestal after a Satellite travel of approximately 50 mm. That makes the entire holddown arm free to rotate away from the Satellite and clear its way for ejection. Although the outward motion of the arms may already be achieved by the acceleration of the ejection process and the preload stresses, it is expected that additional spring action is required. At this time, no investigation has been made whether the spring action of the preloaded and now released holddown arm is sufficient, or whether a separate spring is needed. If the latter should be the case, such a spring can be easily added. A honeycomb crush pad is provided at the foot of the pedestal to absorb the impact of the arm and prevent rebound.

For installation of the sphere on the Satellite support structure, the arms are completely removed by taking out the bolts at the arm hinge points. This provision precludes the Satellite handling ring from having any support structure related restrictions.

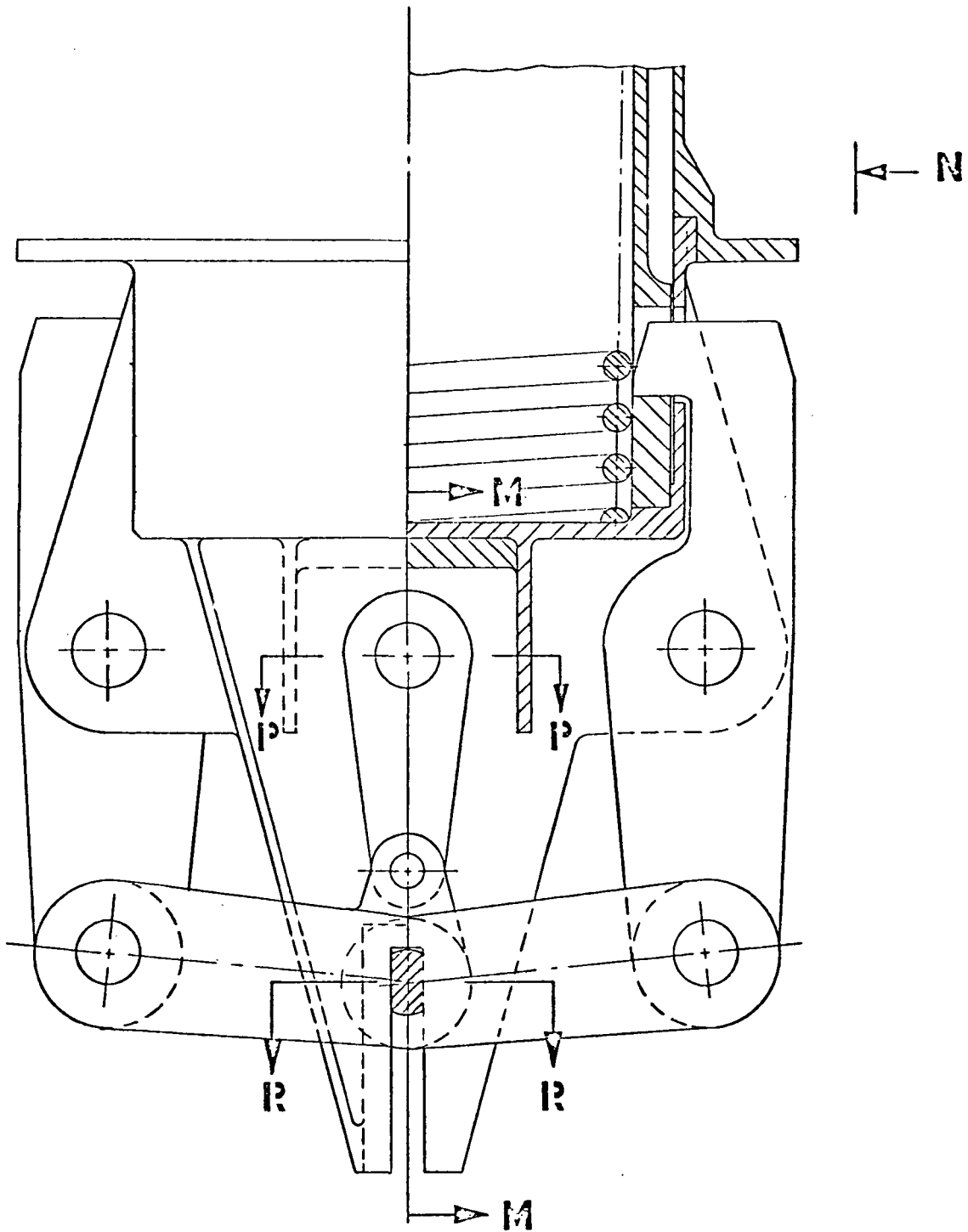
For ejection, the Satellite support structure is released by the mechanism shown in Figure 3-8. The ejection spring, which is located inside the 190-mm-diameter tube, rests with its lower end at the bottom of a cup-like element. This cup is screwed into the lower end of the larger diameter tube which provides the shear-tie among the webs of the main support beams. Two parallel ribs extend across and below the cup bottom. These ribs support hooks which engage into respective cutouts in the ejection tube. The geometrical relation between the contact face between each hook and the tube, and the hook's pivot point is such that a tensile load in the 190-mm-diameter tube will rotate the hook in an outward direction. A linkage system, which connects the lower ends of the hooks and provides a tie to a pin puller, prevents such motion as long as the pin puller is in an extended position. Activation of the pin puller eliminates the central support of the linkage system, and the hooks will release the ejection tube. The two-pronged lower extension of the cup ribs ensures a symmetrical motion of the hooks, and, therefore, the proper release of the tube.

The spring, which is located inside the 190-mm-diameter tube, will then push the Satellite support structure, and through it the Satellite, in an upward direction. Stops for stroke limitation, and guides for proper motion of the ejection tube are provided for in the space between the two tubes.

As currently defined, the ejection spring characteristics are as indicated in Table 3-1.

TABLE 3-1. EJECTION SPRING CHARACTERISTICS

COIL DIAMETER	152 mm
WIRE DIAMETER	9.5 mm
STROKE	420 mm
AVERAGE LOAD	59994 N
EJECTION VELOCITY	0.6 m/sec



DETAIL L

ROTATED 90° C W

FIGURE 3-8. SATELLITE RELEASE MECHANISM



### 3.2.3 SATELLITE EJECTION SYSTEM ORDNANCE AND ELECTRICAL SYSTEMS

#### 3.2.3.1 ORDNANCE SYSTEM CONCEPT

As described in 3.2.2, the Satellite ejection system incorporates a pin puller as the device to initiate ejection of the Satellite. The ordnance system associated with the pin puller is illustrated schematically in Figure 3-9. Although a single pin puller is utilized, complete redundancy is provided in the ordnance system and the pin puller incorporates dual pressure cartridges for redundant actuation. A second pin puller could be incorporated by providing a second release point within the release mechanism linkage, but is considered to be an unwarranted complication at this time. As currently defined, all components in the system have off-the-shelf availability.

#### 3.2.3.2 EXPLODING BRIDGEWIRE (EBW) FIRING UNIT

As indicated in Figure 3-9, the ordnance system is initiated by Exploding Bridgewire (EBW) firing units which deliver high-energy pulses to fire the pyrotechnics. The EBW requires 28 Vdc for operation and a 28-Vdc trigger signal. The EBW does not contain explosives and does not require special storage or handling. The unit is illustrated in Figure 3-10.

When power is applied to the EBW firing unit, a 1-microfarad capacitor is charged to 2300 Vdc through an oscillator and step-up transformer. A 4.8-Vdc monitor signal is provided to telemetry for ground and in-flight monitoring. A 28-Vdc trigger signal supplies a spark voltage to a three-element gap tube through a second oscillator and step-up transformer. The gap tube delivers the stored capacitor energy into a small diameter, low resistance wire. The wire fuses and vaporizes to create high temperatures and a shock wave which detonates a confined detonating fuse (CDF).

#### 3.2.3.3 ELECTRICAL POWER

Electrical power is provided by one 3-ampere-hour silver-zinc primary battery. Physical size of the battery is indicated in Figure 3-10. The battery is sized to deliver 25 milliamperes to the two EBW firing units for 10 minutes of prelaunch tests and 140 minutes in orbit. The battery is assumed to operate to an 80-percent depth-of-discharge, and an allowance of 5 percent is made for a line loss between the battery

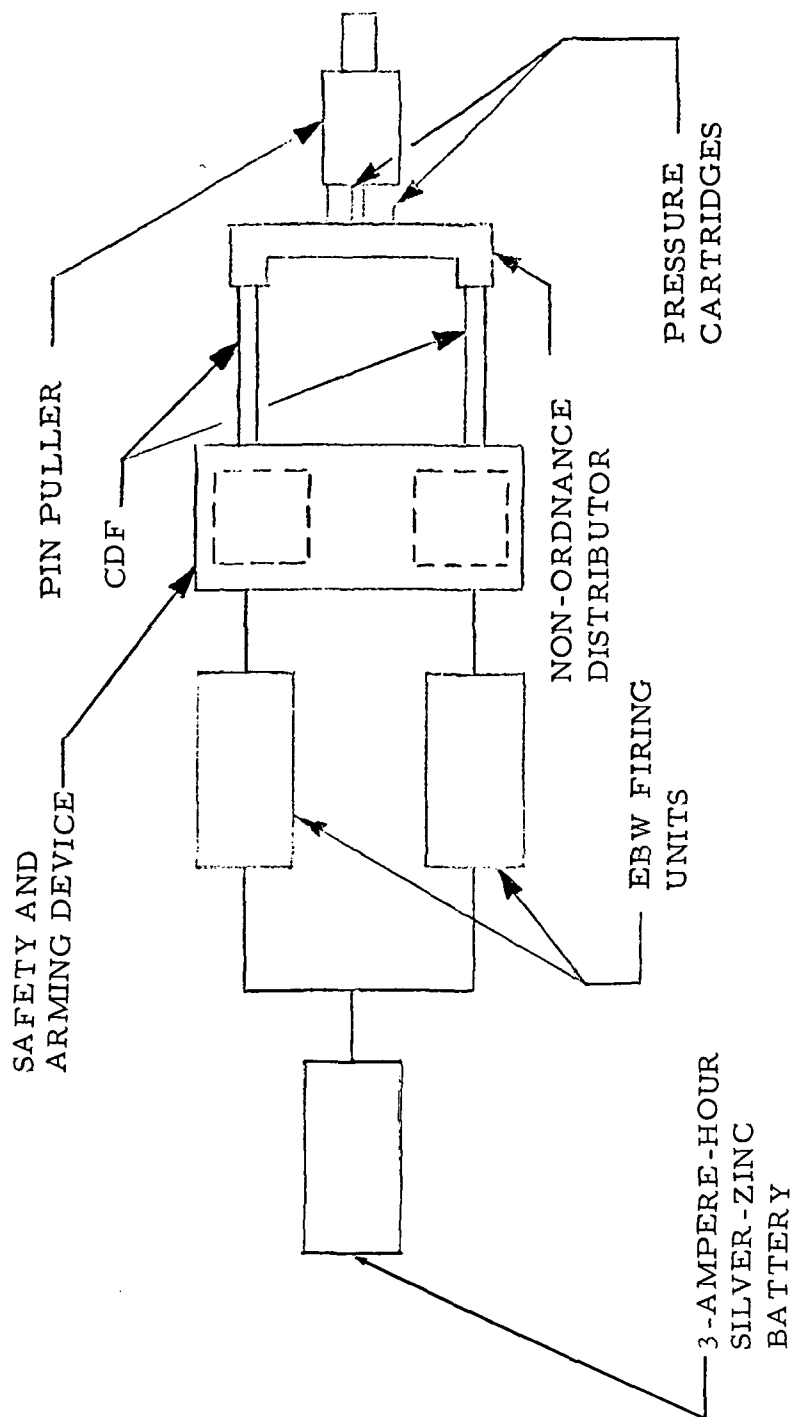


FIGURE 3-9. EJECTION SYSTEM ORDNANCE SCHEMATIC

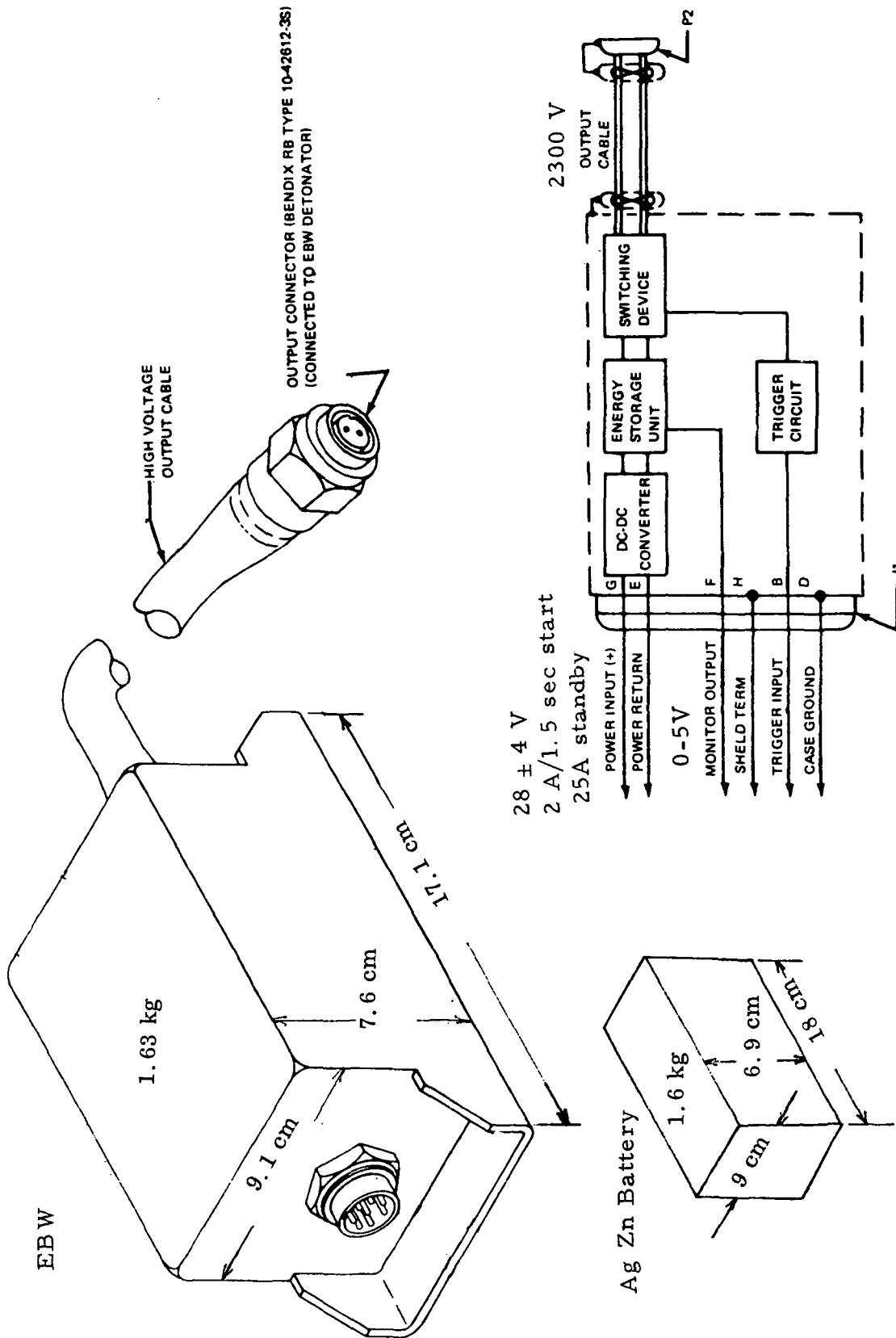


FIGURE 3-10. EBW FIRING UNIT AND POWER SUPPLY

and the EBW. A 50-percent contingency is added to account for self-discharge after activation, temperature effects, and possible additional telemetry or signal conditioning power requirements. With allowance for a 5-percent line voltage loss, voltage to the EBW firing units will be approximately 32 Vdc at full charge and 27 Vdc at 80 percent discharge.

#### 3.2.3.4 ELECTRICAL INTERFACE

The EBW firing unit and battery interface with the IU for in-flight control and monitoring and with the SLA umbilical for preflight operations. It is assumed that existing wires at the IU interface and SLA swing arm can be utilized for the EBW. Wiring for one EBW and one battery is shown in Figure 3-11. Duplicate control and monitor signals are required for operation of the second EBW from the IU, but the ESE control shown can operate both units.

Prelaunch power is furnished from ESE power supply 7D110. Existing AWG 14 control wire on the swing arm will be adequate for the expected 28-Vdc EBW load of 4 amperes starting current and 0.5 amperes operating current. Ground power is applied to the EBW and pulse sensor during simulated flight tests. "Lift-off" and "Arm" commands are given from the IU switch selector and the "ESE Power On" command is given by ESE command. The relay coils are for latching relays. The relays are of the latching type with a set and reset coil. The relay contacts are shown in position, assuming the coil marked with a dot was energized last. An "ESE Power On" indicating light is required to determine the position of the relay. The EBWs are fired by switch selector command into an EBW pulse sensor. If both units fire, an indication is supplied to the ESE. The pulse sensor is removed prior to launch.

### 3.3 SATELLITE ANTI-CONTAMINATION SYSTEM

#### 3.3.1 ANTI-CONTAMINATION SYSTEM CONCEPT

Prior to and during launch, the Satellite is subject to a contaminating environment that could be detrimental to its reflective surfaces. The magnitude of the success of the mission can be determined by how well the reflective surfaces are kept clean. Some of the contaminating environments include particles present in the atmosphere during launch preparation and boost phase; particles produced by shroud separation; and particles produced by the S-IVB during the long coast, and during maneuvers required prior to release of the Satellite.

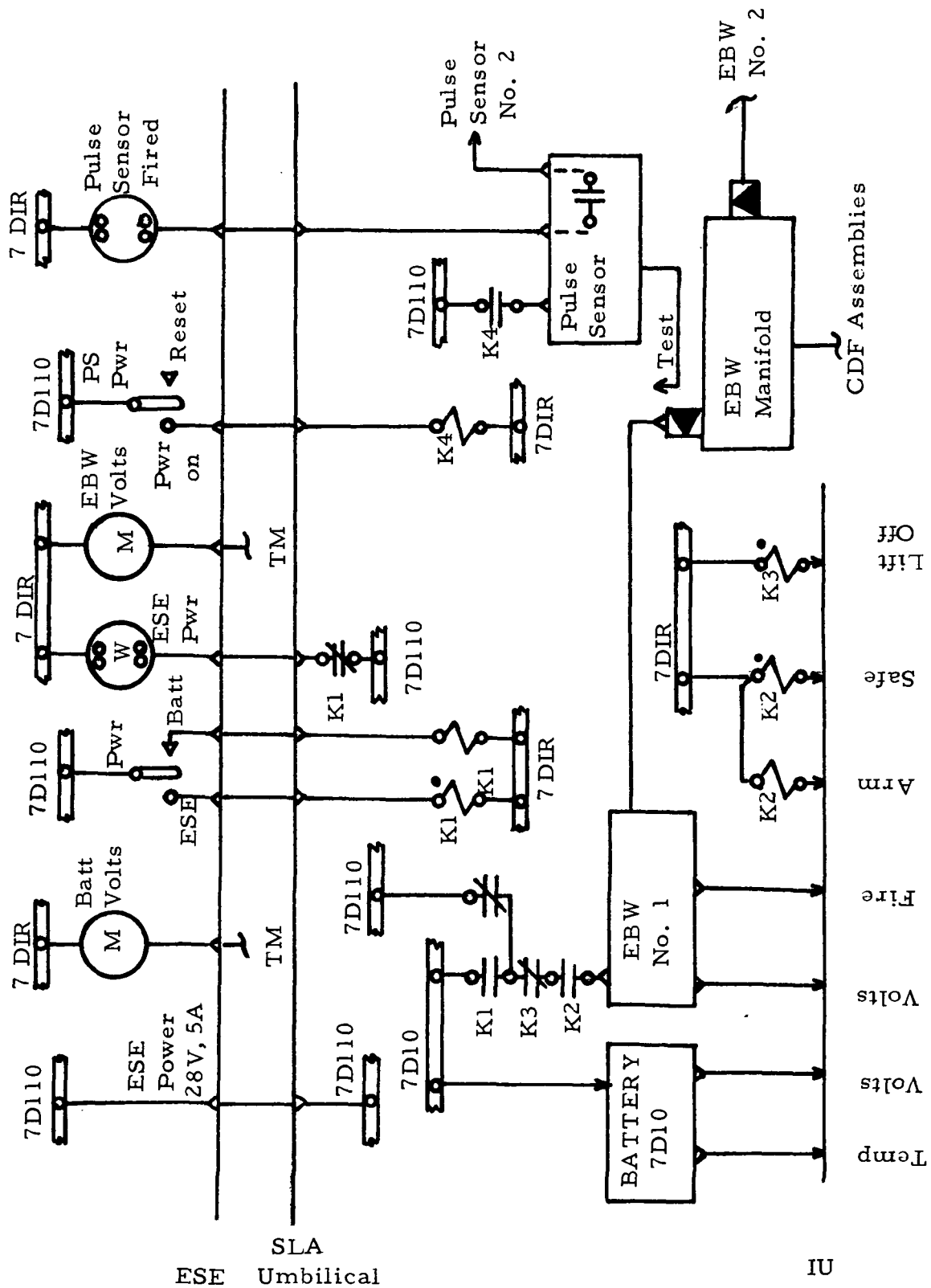


FIGURE 3-11. EBW ELECTRICAL INTERFACE

To protect the Satellite against contaminating environments, an anti-contamination enclosure and purge system will be required. The requirements of the purge system, however, are not well defined; therefore, three purge system concepts were considered to cover the expected range of requirements. One of these systems is recommended as a baseline based on some assumed actual requirements.

### 3.3.2 ANTI-CONTAMINATION ENCLOSURE

The enclosure is essentially a closed cover surrounding the Satellite, and serves to contain the purge gas and preclude entrance of contaminants. It consists of two major portions: a lower, permanently-mounted bowl; and an upper, deployable structural shell. All parts of these structures are of lightweight design because the maximum differential pressure they have to withstand is only about  $1.4 \text{ N/cm}^2$  (2 psi).

The lower bowl consists of thin sheet metal and a ring located near the payload support pads and attached to the machined cruciform ejection structure as shown in Figure 3-6. The ring has an unsymmetrical cross section which carries the bending and torsional moments resulting from the load and support conditions. The upper face of the ring lies in a horizontal plane which separates the lower from the upper portion of the enclosure, and serves as the interface for the horizontal seal between lower and upper parts of the enclosure.

The upper structure is subdivided into four segments, each of which consists of the movable arm described in 3.2.2, and lightweight shell structures welded to the arm, as shown in Figures 3-5 and 3-7. The sheet metal stiffeners extending along the outer edges of each segment in meridional direction are relatively stiff in order to avoid large dynamic deflection. The meridional interfaces between the segments are provided with seals. One of the segments is equipped with a relief valve which limits the pressure differential across the enclosure to about  $1.4 \text{ N/cm}^2$  (2 psi).

All seals are attached to the upper, movable segments. They are L-shaped, as indicated in cross sections of the enclosure presented in Figures 3-12 and 3-13, to ensure proper sealing at the low pressures involved. Sealing capability can be improved by proper selection of the angle between the legs of the seal profiles, so that they are preloaded before any pressure is applied.

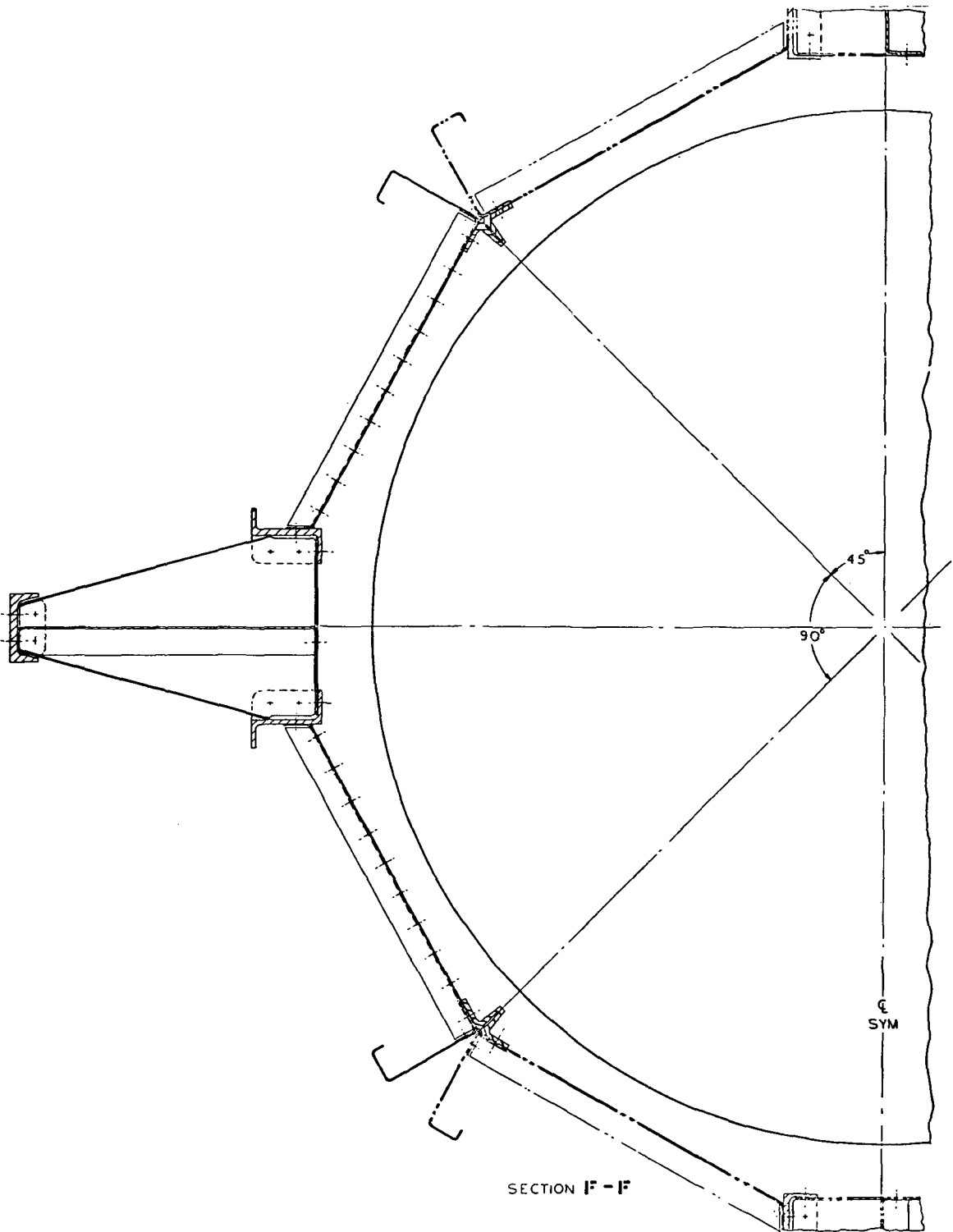
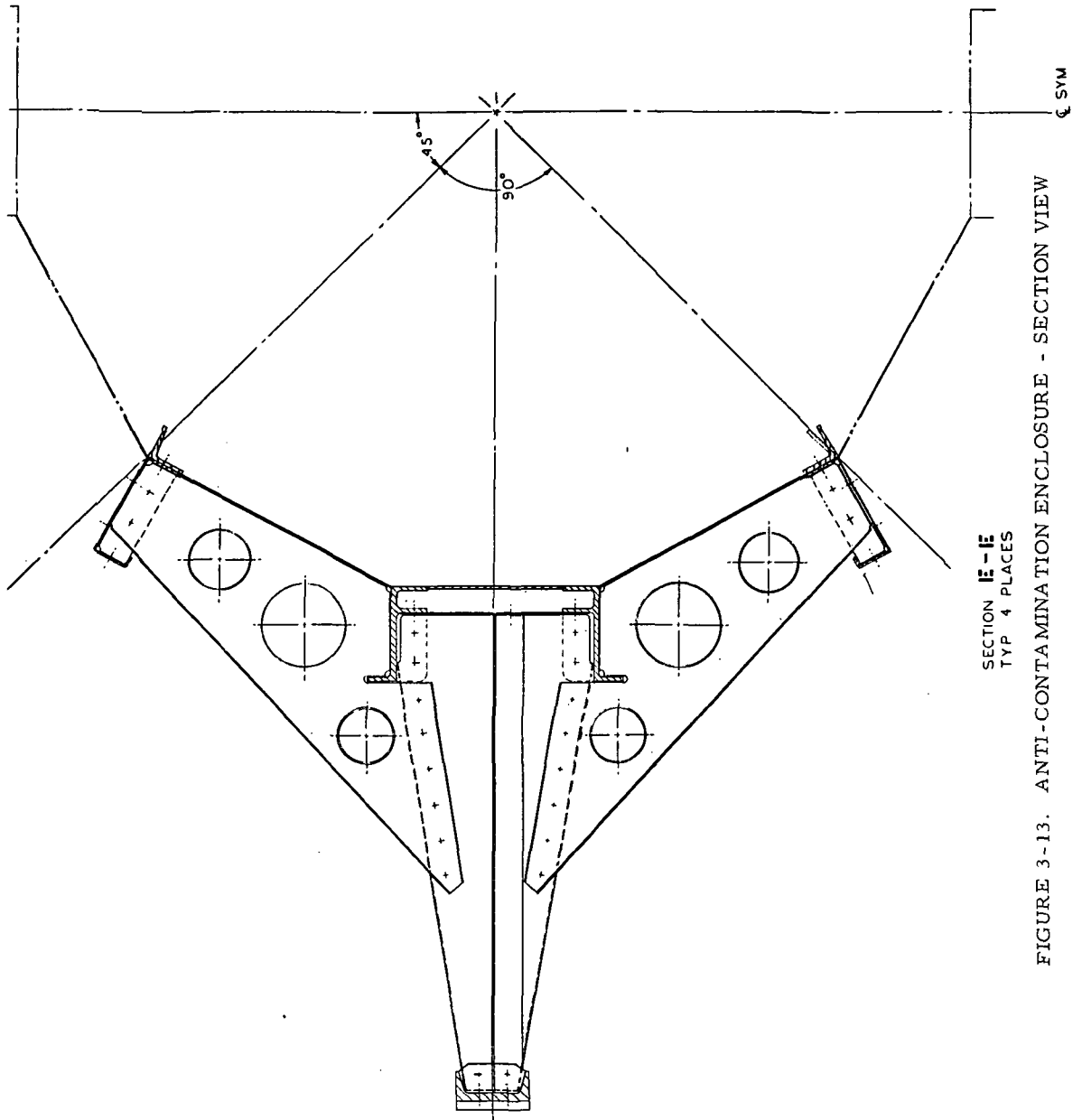


FIGURE 3-12. ANTI-CONTAMINATION ENCLOSURE - SECTION VIEW  
3-19





### 3.3.3 ANTI-CONTAMINATION PURGE SYSTEM

#### 3.3.3.1 GUIDELINES AND ASSUMPTIONS

In designing a purge system for the Satellite, the following guidelines and assumptions were considered:

(a) The Satellite will be protected from contaminants until it is released in orbit.

(b) Effective use will be made of existing and proven components, i.e., those components used on previous flights or proven by ground tests.

(c) The purging gas is nitrogen.

(d) The purging system is assumed to undergo an adiabatic irreversible process as a worst case.

(e) The temperature in all pressurized vessels at launch is 294.26°K (530°R).

(f) The discharge coefficient for all orifices is 0.65.

(g) The volume of the purge space between the Satellite and the anti-contamination enclosure is 0.1056 cubic meters (3.728 cubic feet). This volume is based on the assumption that the average distance between the Satellite and the anti-contamination enclosure is 5.08 cm (2 inches).

(h) The accumulative leakage area of the anti-contamination enclosure shall not exceed 1.6 square centimeters (0.25 square inches). This total leakage area is assumed to function as an orifice with an effective diameter of 1.432 centimeters (0.564 inches). Where applicable, data presented in this report are based on an anti-contamination enclosure accumulative leakage area of 1.6 square centimeters.

(i) The pressure inside the anti-contamination enclosure shall not exceed 1.37 newtons per square centimeter gage (2.0 psig). The anti-contamination enclosure will not be designed to take an excessive pressure load.

### 3.3.3.2 PURGE SYSTEMS DESCRIPTION

During this study, three purge system types were considered as possible candidates for use in protecting the Satellite against contaminants:

- o Pressure-regulated system
- o Blow-down system
- o Anti-contamination enclosure pressure release system.

Each of these will be discussed in detail.

#### 3.3.3.2.1 PRESSURE-REGULATED SYSTEM

A schematic of this system is presented in Figure 3-14. With the exception of the pressure regulator, relief valve, and separation joint, all components of the system are identical to components presently used to supply  $\text{GN}_2$  to the gas bearings of the stabilization platform in the IU. The pressure regulator is slightly modified for application to the purge system. The other two components are relatively common, and it is expected that a search of components used in other space applications will yield suitable, qualified units. The pressure regulator is modified to sense atmospheric pressure as a reference rather than the pressure in the anti-contamination enclosure or the gas bearing area in the case of the IU. By sensing atmospheric pressure, the pressure regulator is also modified to regulate the gas flow to the anti-contamination enclosure to maintain a constant pressure in that space of  $1.379 \text{ N/cm}^2$  gage (2 psig).

Figure 3-14 shows the system in the prelaunch purge mode of operation. Prior to launch, a GSE  $\text{N}_2$  gas supply line and an electrical lead line are connected to the purge umbilical plate located on the IU. The fill valve is opened by supplying a current of 1.5 amperes at 24 volts dc from GSE. Current is supplied continually to the valve to keep it open until launch. Gaseous  $\text{N}_2$  is fed from GSE through the two storage spheres up to the pressure regulator. The volume of each storage sphere is 0.05663 cubic meters (2  $\text{ft}^3$ ). A  $2.0 \times 10^{-7}$  meter (20-micron) filter is installed upstream of the pressure regulator for protection of the regulator. When the pressure in the storage spheres reaches about  $137.9 \text{ N/cm}^2$  (200 psi) the pressure regulator will begin to allow gas to flow to the anti-contamination enclosure. The pressure regulator is

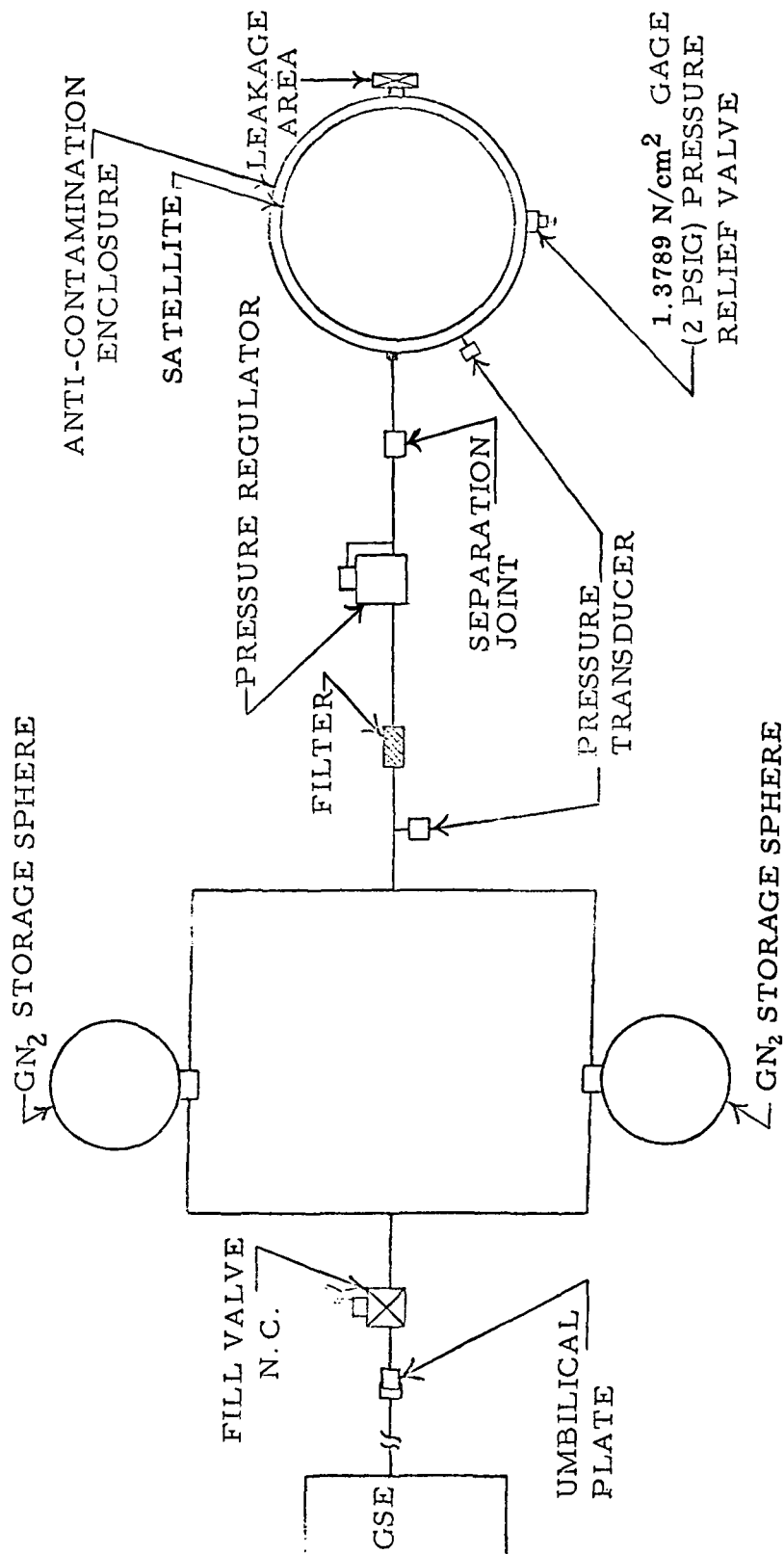


FIGURE 3-14. PRESSURE-REGULATED PURGE SYSTEM

designed to operate within an inlet pressure range of  $137.9 \text{ N/cm}^2$  (200 psi) and  $2,275.37 \text{ N/cm}^2$  (3300 psi). To maintain a pressure of  $11.514 \text{ N/cm}^2$  (16.7 psi) in the anti-contamination enclosure while on the launch pad, a flow rate of approximately 0.9557 standard cubic meters per minute (33.75 scfm) through the assumed enclosure leakage area of  $1.6 \text{ cm}^2$  ( $0.25 \text{ in}^2$ ) is required. Since GSE will supply gas to the storage spheres at a much faster rate than it is being taken out, the two storage spheres will be pressurized to approximately  $2,275.37 \text{ N/cm}^2$  (3300 psi). To maintain this peak operating pressure until launch, GSE will continually resupply the storage spheres.

At launch ( $T = 0$ ), the fill valve is closed by opening its circuit and the umbilical is separated. During ascent the pressure regulator senses the decrease in atmospheric pressure and adjusts the flow rate to the anti-contamination enclosure to maintain a constant pressure of  $1.379 \text{ N/cm}^2$  gage (2 psig). Should for some reason during the purge the pressure in the enclosure exceed this level, the  $1.379 \text{ N/cm}^2$  gage (2 psig) pressure relief valve will open to release the excess pressure. During the purge, pressure transducers will monitor the pressure regulator inlet pressure conditions and the pressure conditions inside the anti-contamination enclosure.

After about 75 seconds of flight, the flow out of the enclosure becomes choked. At about 130 seconds into the flight, pressure in the enclosure levels off at a constant  $1.379 \text{ N/cm}^2$  (2 psi) with a constant flow out the enclosure of 0.177 standard cubic meters per minute (6.25 scfm). The Satellite is released at 7068 seconds into the flight and the amount of  $\text{GN}_2$  needed by this system to maintain a purge for this length of time is approximately 29.95 kg (66.00 lb). When the Satellite is released, the holddown arms are pulled back, taking segments of the anti-contamination enclosure with them. The Satellite is then pushed forward and the purge supply line is disconnected at the separation joint.

Table 3-2 presents a mass statement for the pressure regulated system.

#### 3.3.3.2.2 BLOW DOWN SYSTEM

A schematic of this system is presented in Figure 3-15. The components of this system are identical to the components used in the pressure regulated system, except an orifice is used in place of the pressure regulator. The  $\text{GN}_2$  in the storage sphere blows down through the orifice into the anti-contamination enclosure. The function

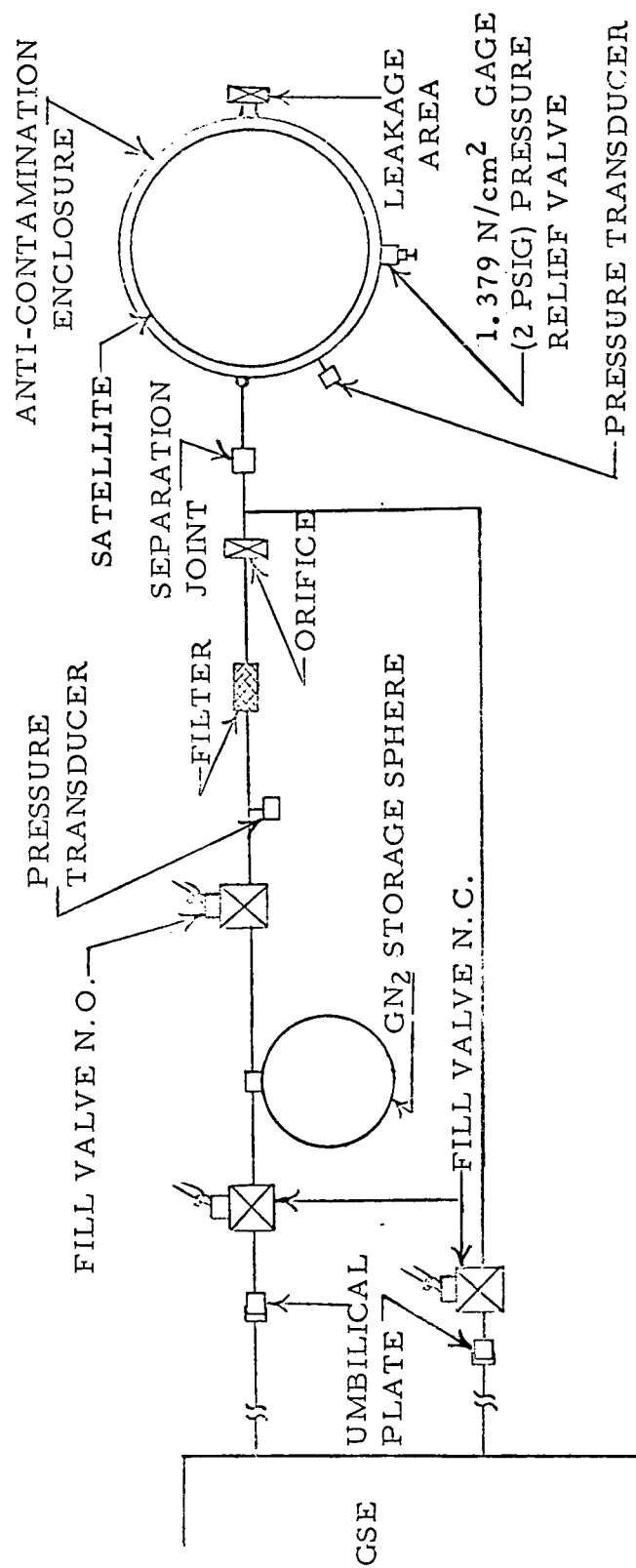


FIGURE 3-15. BLOW DOWN PURGE SYSTEM

TABLE 3-2. PRESSURE-REGULATED SYSTEM  
MASS STATEMENT

<u>Item</u>	<u>Mass (kg)</u>	<u>Mass (lbm)</u>
Fill Valve	1.59	3.50
GN <sub>2</sub> Pressure Storage Sphere (2)	42.19	93.00
Pressure Transducer (2)	0.46	1.00
Filter	0.34	0.75
Pressure Regulator	1.02	2.25
Plumbing, Separation Joint, and Miscellaneous	7.26	16.00
Pressure Relief Valve	0.46	1.00
Pressurant GN <sub>2</sub>	29.94	66.00
Total System Mass	83.26	183.50

of the orifice is to regulate the flow to the anti-contamination enclosure and was sized to meet the worst case flow requirement which occurs at launch ( $T = 0$ ). The diameter of the orifice is 0.381 mm (0.015 in.).

Prior to launch, two GSE N<sub>2</sub> gas supply lines and electrical lead lines are connected to the purge umbilical plates located on the IU. Two purge supply lines lead to the anti-contamination enclosure. Through one line, a purge is provided in the enclosure by GSE while the vehicle is on the launch pad. This purge is maintained until launch ( $T = 0$ ). The other line provides a purge to the enclosure during flight by using the on-board GN<sub>2</sub> storage sphere.

The fill valve in the GSE purge line is opened by supplying a current of 1.5 amperes at 24 volts dc from GSE. Current is supplied continually to keep the valve open until launch ( $T = 0$ ). The anti-contamination enclosure is then pressurized to 11.514 N/cm<sup>2</sup> (16.7 psi) by gaseous N<sub>2</sub> fed from GSE. The accumulative leakage area of the

enclosure is assumed to be  $1.6 \text{ cm}^2$  ( $0.25 \text{ in}^2$ ), and this total leakage area is assumed to function as an orifice with an effective diameter of 1.432 centimeters ( $0.564 \text{ in.}$ ). Under these conditions, the  $\text{GN}_2$  will flow out of the enclosure at the rate of 0.9557 standard cubic meter per minute (33.75 scfm). Thus, GSE must continually replenish this loss to maintain a constant pressure of  $11.514 \text{ N/cm}^2$  (16.7 psi) in the enclosure.

While the anti-contamination enclosure is being purged by the GSE purge supply line, the  $\text{GN}_2$  storage sphere is filled through the other umbilical. A current of 1.5 amperes at 24 volts dc is continually supplied by GSE to a fill valve downstream and upstream of the storage sphere. Electric power is supplied to the upstream fill valve to keep it open and to the downstream valve to keep it closed. The storage sphere is pressurized with  $\text{GN}_2$  to about  $2,068.4 \text{ N/cm}^2$  (3000 psi). At launch ( $T = 0$ ), the current is removed from the fill valve in the GSE purge supply line closing that valve, and that umbilical is separated. Simultaneously, the current to the valve downstream of the storage sphere is also removed and that valve opens, causing flow to proceed out of the storage sphere into the anti-contamination enclosure.

Figure 3-16 presents a plot of pressure in the anti-contamination enclosure versus time for the first 150 seconds of flight.

Figure 3-17 presents a plot of pressure on the anti-contamination enclosure and atmospheric pressure along the flight trajectory versus time for the first 50 seconds of flight. The large decrease in pressure shown in the enclosure during the first 5 seconds is due to the difference in flow rates supplied by GSE and the storage sphere. At approximately 5 seconds, the pressure in the enclosure drops to about  $0.069 \text{ N/cm}^2$  (0.1 psi) above ambient. After 5 seconds, however, the delta pressure between the enclosure and the atmosphere increases.

Figure 3-18 presents the same plot as Figure 3-17 from 50 seconds to 150 seconds into the flight. The gas flow out of the enclosure becomes choked at approximately 75 seconds. At approximately 130 seconds atmospheric pressure is zero.

Figure 3-19 presents a plot of the pressure in the enclosure versus time from 150 seconds to 1000 seconds into the flight.

Figure 3-20 presents a plot of the pressure in the enclosure versus time from 1000 seconds to 8000 seconds. The Satellite is to be released at approximately 8000 seconds and at that time the pressure in the anti-contamination enclosure is about  $0.13789 \text{ N/cm}^2$  (0.2 psi).

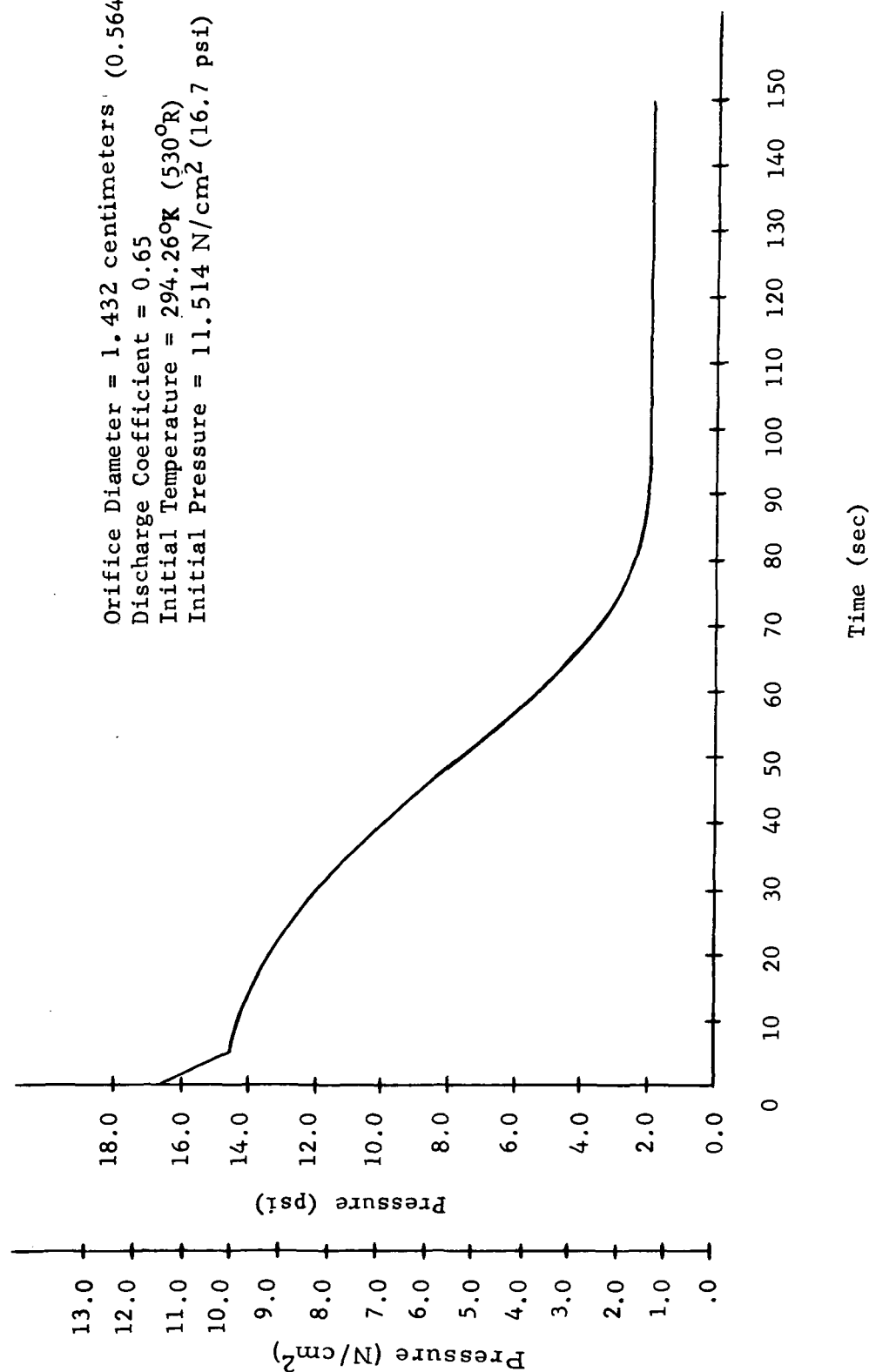


FIGURE 3-16. PRESSURE IN THE ANTI-CONTAMINATION ENCLOSURE VERSUS TIME FOR THE FIRST 150 SECONDS OF FLIGHT



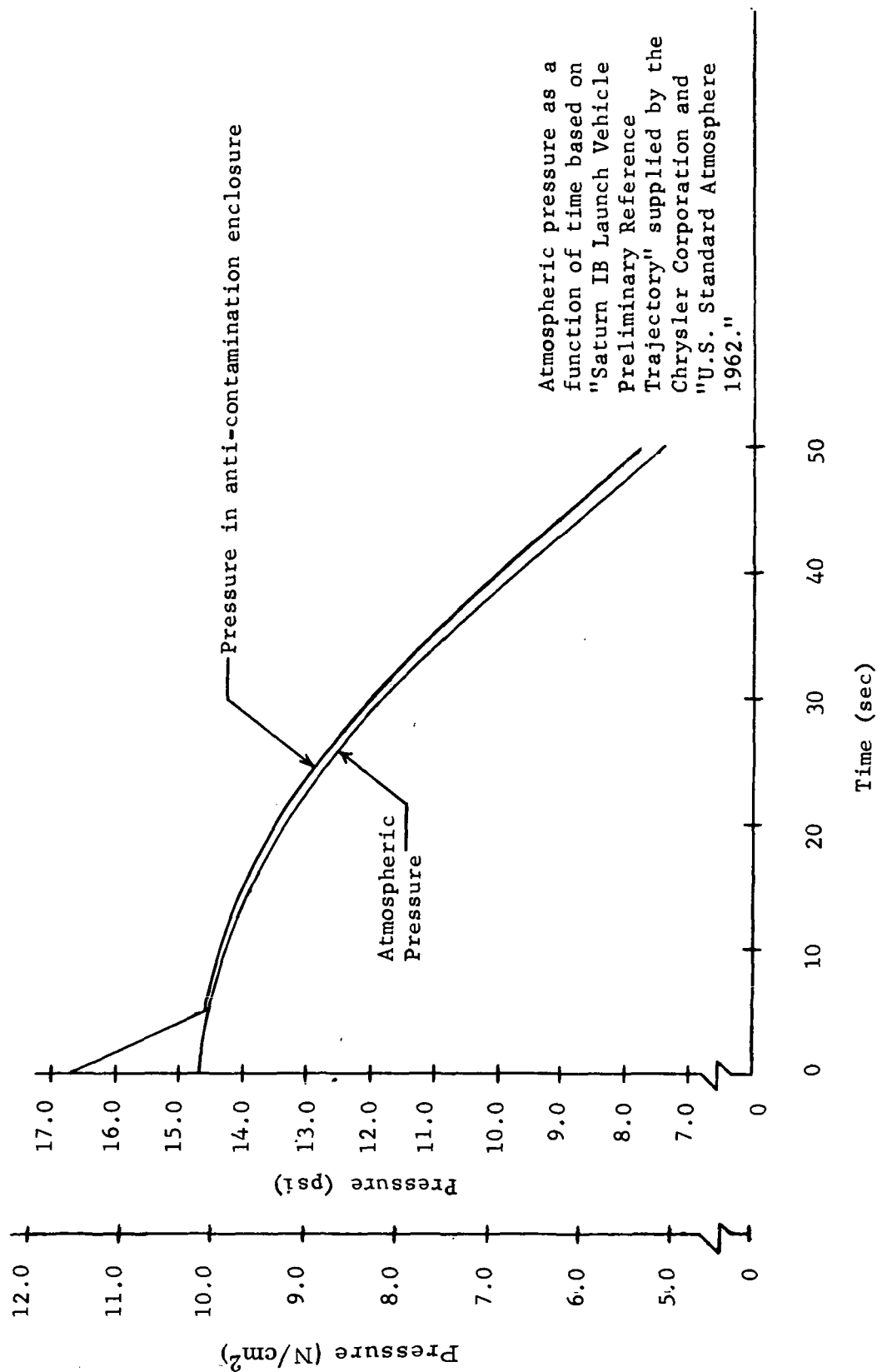


FIGURE 3-17. PRESSURE IN THE ANTI-CONTAMINATION ENCLOSURE AND ATMOSPHERIC PRESSURE VERSUS TIME FOR THE FIRST 50 SECONDS OF FLIGHT

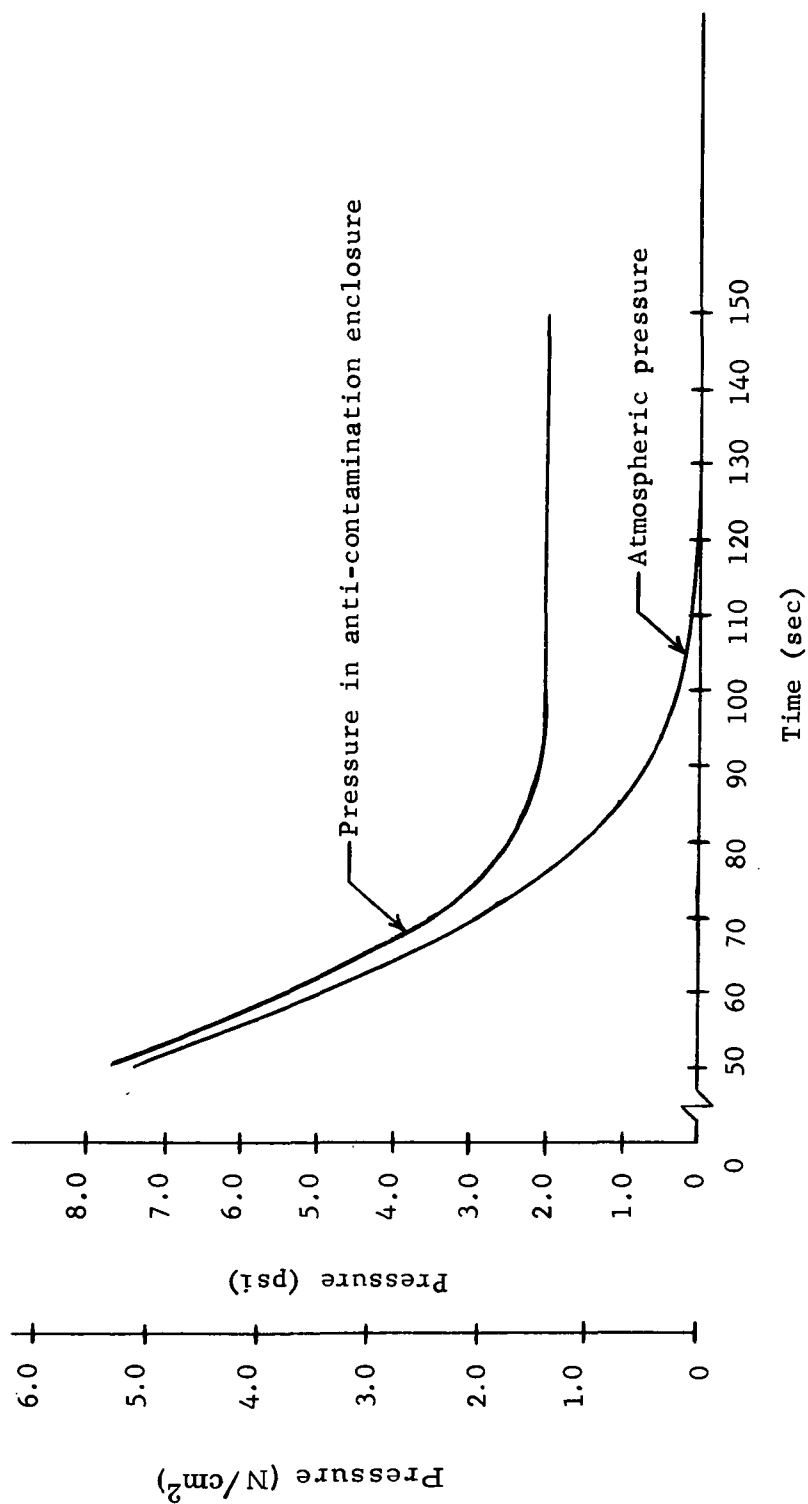


FIGURE 3-18. PRESSURE IN THE ANTI-CONTAMINATION ENCLOSURE AND ATMOSPHERIC PRESSURE VERSUS TIME FROM 50 SECONDS TO 150 SECONDS INTO THE FLIGHT

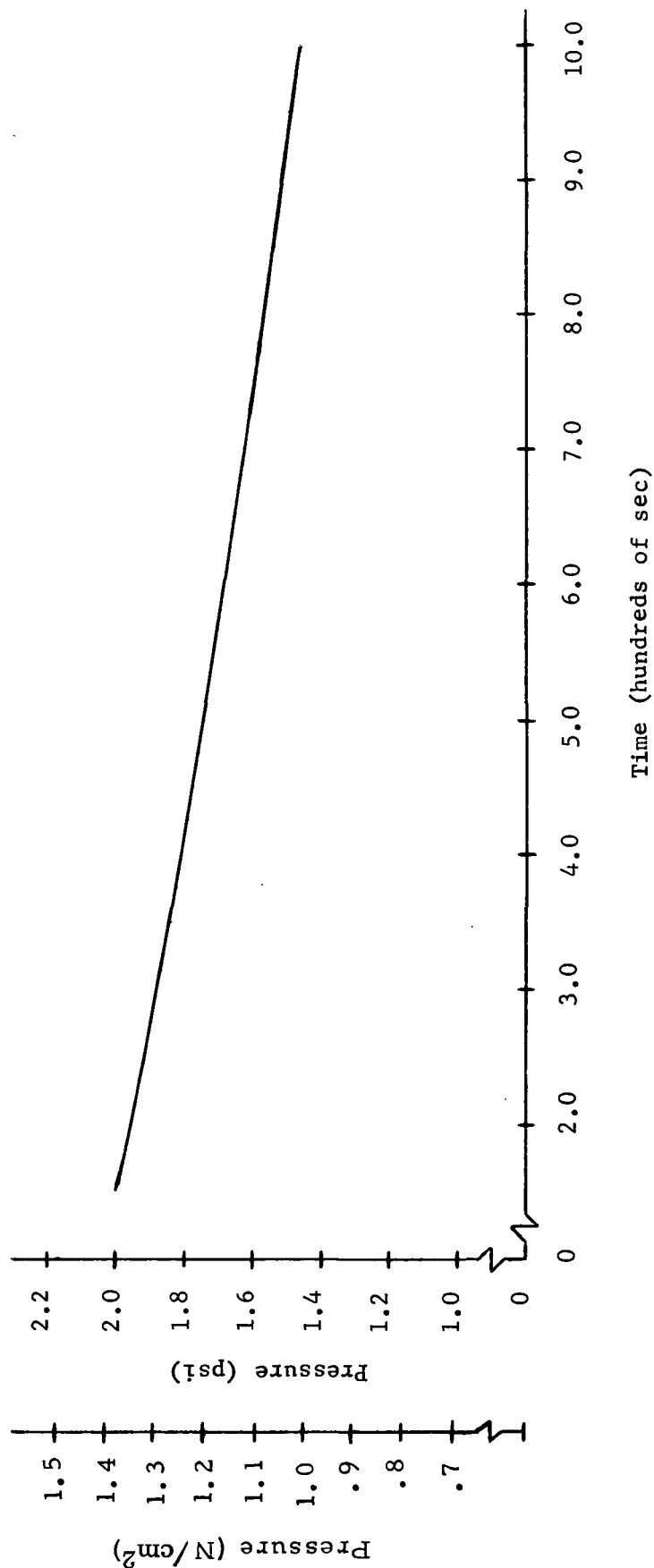


FIGURE 3-19. PRESSURE IN THE ANTI-CONTAMINATION ENCLOSURE VERSUS TIME FROM 150 SECONDS TO 1000 SECONDS INTO THE FLIGHT

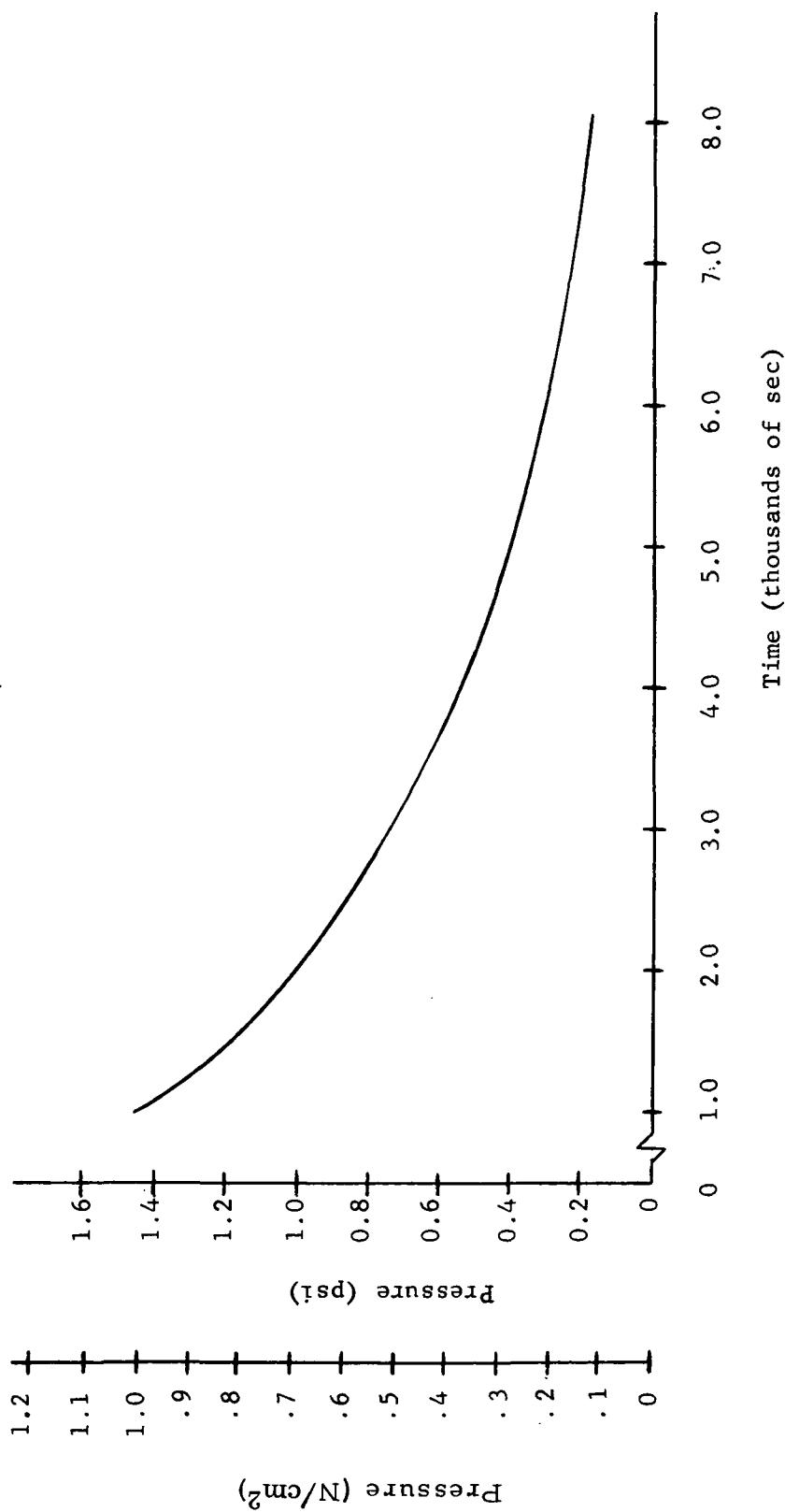


FIGURE 3-20. PRESSURE IN THE ANTI-CONTAMINATION ENCLOSURE VERSUS TIME FROM 1000 SECONDS TO 8000 SECONDS INTO THE FLIGHT

Figure 3-21 presents a plot of the pressure in the storage sphere versus time from launch through Satellite release. The pressure in the storage sphere at the time of release is approximately  $172. \text{ N/cm}^2$  (250 psi).

A  $5.0 \times 10^{-7}$  meter (20-micron) filter is installed upstream of the orifice to prevent the orifice from becoming plugged with foreign matter. Pressure transducers monitor the pressure of the gas entering the orifice and the pressure of the gas inside the anti-contamination enclosure. The relief valve functions as a safety device to release the pressure inside the enclosure should it exceed  $1.37895 \text{ N/cm}^2$  gage (2 psig). When the Satellite is released, the holddown arms are pulled back, taking segments of the anti-contamination enclosure with them. The Satellite is then pushed forward, and the purge supply line is disconnected at the separation joint.

Table 3-3 presents a mass statement for the blow down system.

TABLE 3-3. BLOW DOWN SYSTEM MASS  
STATEMENT

<u>Item</u>	<u>Mass (kg)</u>	<u>Mass (lbm)</u>
Fill Valve (3)	4.76	10.50
GN <sub>2</sub> Pressure Storage Sphere	21.09	46.50
Pressure Transducer (2)	0.46	1.00
Filter	0.34	0.75
Orifice	1.11	1.25
Pressure Relief Valve	0.46	1.00
Plumbing, Separation Joint, and Miscellaneous	7.26	16.00
Pressurant GN <sub>2</sub>	<u>13.61</u>	<u>30.00</u>
Total System Mass	48.09	106.00

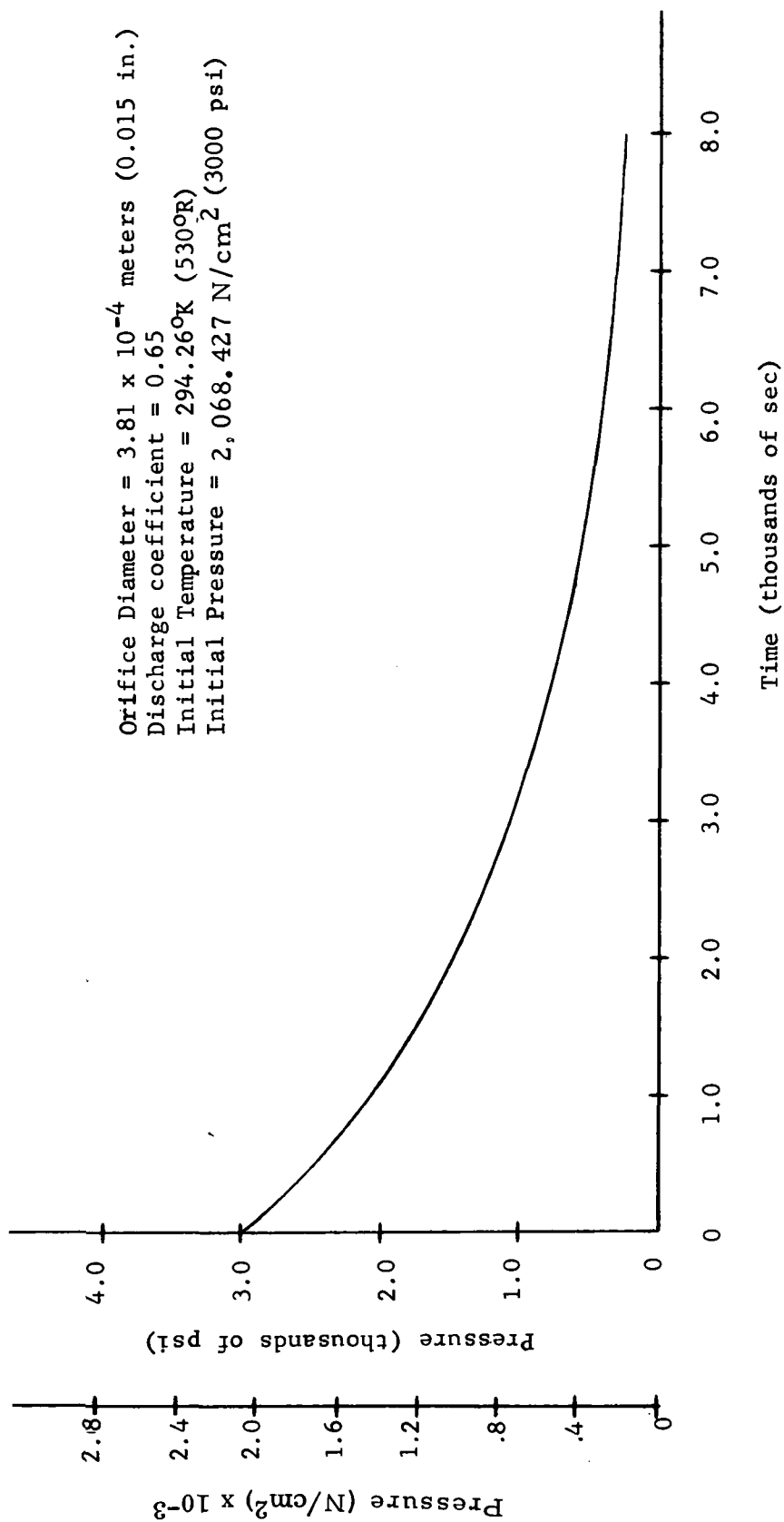


FIGURE 3-21. PRESSURE IN THE STORAGE SPHERE VERSUS TIME FROM LAUNCH THROUGH SATELLITE RELEASE

### 3.3.3.2.3 ANTI-CONTAMINATION ENCLOSURE PRESSURE RELEASE SYSTEM

A schematic of this system is presented in Figure 3-22. The components of this system are identical to the components used in the pressure-regulated system and the blow down system. The requirements of this system, however, are assumed different from those of the other two. First, this system does not require a continuous gas flow from a supply source to maintain a purge. Second, a pressure over ambient in the anti-contamination enclosure is not required to last until the Satellite is released.

Prior to the launch, a GSE GN<sub>2</sub> supply line and an electrical lead line are connected to the purge umbilical plate located on the IU. The fill valve in the purge supply line is opened by supplying it with a current of 1.5 amperes at 24 volts dc from GSE. Current is supplied continually until just prior to launch to keep the valve open. The anti-contamination enclosure is then pressurized to 11.51424 N/cm<sup>2</sup> (16.7 psi), with GN<sub>2</sub> supplied from GSE, and this pressure is maintained by GSE until just prior to launch. During pressurization, the gas flows through a  $5.0 \times 10^{-7}$  meter (20-micron) filter upstream of the enclosure to protect the Satellite from any contaminants that might be present in the gas. The anti-contamination enclosure is assumed to be designed such that little or no leakage will occur.

Just prior to launch, the fill valve is closed by removing the current, and the umbilical is separated. As the vehicle ascends, the atmospheric pressure decreases. The pressure inside the anti-contamination enclosure is not to exceed 1.37895 N/cm<sup>2</sup> (2 psi) above ambient; therefore, a 1.37895 N/cm<sup>2</sup> gage (2 psig) pressure relief valve mounted on the enclosure cycles during the ascent to release any over pressure. In orbit, the pressure inside the enclosure is constant at 1.37895 N/cm<sup>2</sup> (2 psi). During the flight, a pressure transducer monitors the pressure conditions in the enclosure at all times.

Should a small leak exist in the enclosure, the purge pressure will probably be lost before the Satellite is released. However, should this occur, the anti-contamination enclosure is assumed to protect the Satellite sufficiently from outside contaminants.

When the Satellite is released, the holddown arms are pulled back, taking segments of the anti-contamination enclosure with them. The Satellite is then pushed forward, and the purge supply line is disconnected at the separation joint.

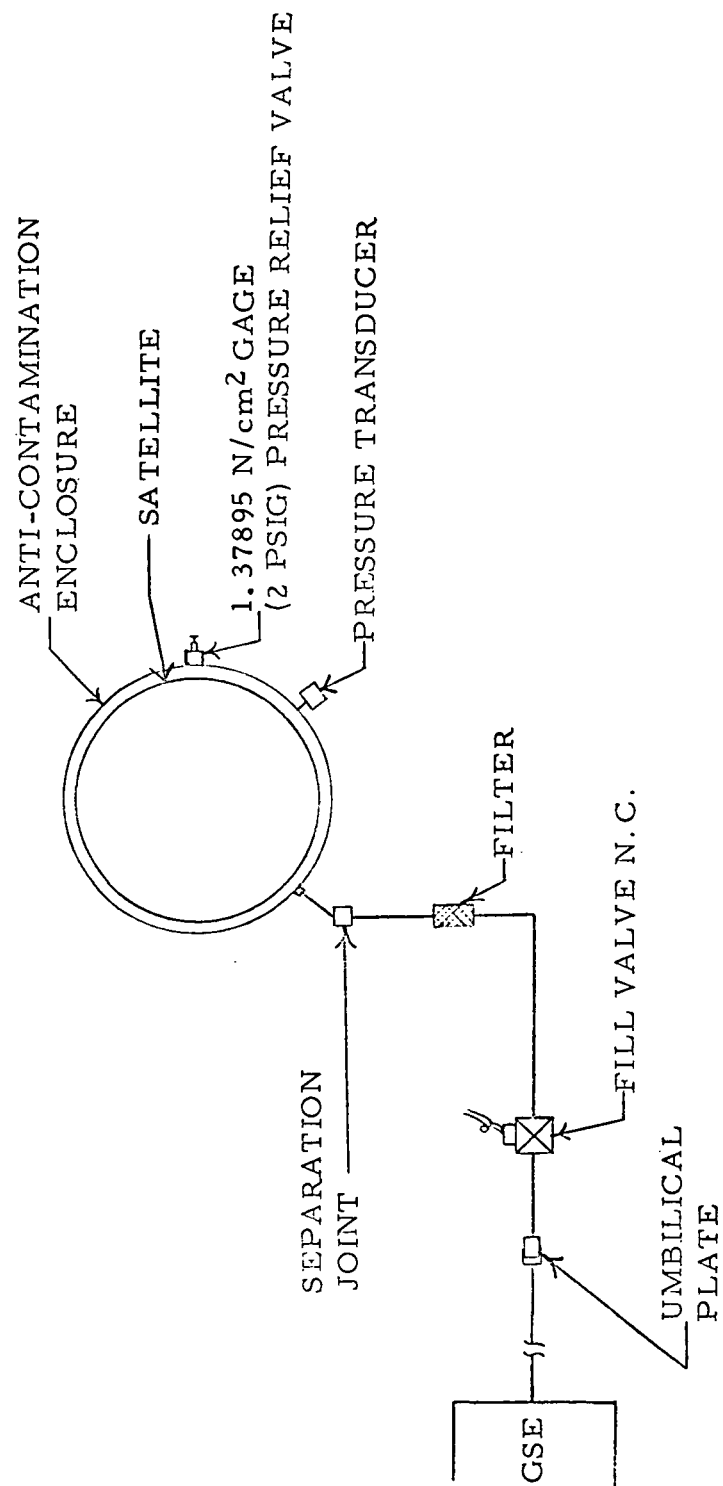


FIGURE 3-22. ANTI-CONTAMINATION ENCLOSURE  
PRESSURE RELEASE PURGE SYSTEM



Table 3-4 presents a mass statement for the anti-contamination enclosure pressure release system.

TABLE 3-4. ANTI-CONTAMINATION ENCLOSURE PRESSURE RELEASE SYSTEM MASS STATEMENT

<u>Item</u>	<u>Mass (kg)</u>	<u>Mass (lbm)</u>
Fill Valve	1.59	3.50
Filter	0.34	0.75
Pressure Transducer	0.22	0.50
Pressure Relief Valve	0.46	1.00
Plumbing, Separation Joint, and Miscellaneous	3.63	8.00
Pressurant GN <sub>2</sub>	0.22	0.50
Total System Mass	6.46	14.25

### 3.3.3.3 COMPARISON AND RECOMMENDATION

Of the three purge system types proposed, the pressure-regulated system is the heaviest and is considered to be the most complex and costly. The pressure regulator associated with this system will have to be modified to meet the purge requirements and results in high cost. The high flow rate of this system requires the use of two supply spheres which results in cost and weight. The number of components and the operation of this system makes it complex. However, if the Satellite should require a constant positive purge pressure of  $1.37895 \text{ N/cm}^2$  (2 psi) above ambient in the anti-contamination enclosure from launch to Satellite release, then the pressure regulated system can satisfy this requirement.

The blow down system is considered to be moderately complex, especially the GSE interface. All components for this system are

obtainable with no major modifications to them required. Comparatively, the weight of this system is moderate, and the cost should be much less than the pressure-regulated system. Should the Satellite require only a small positive purge pressure above ambient (less than  $1.37895 \text{ N/cm}^2$  (2 psi) maximum) in the anti-contamination enclosure that decreases as a function of time from launch to Satellite release, then the blow down system can satisfy this requirement. A big disadvantage of both the pressure-regulated system and the blow down system is that the function of both systems is dependent upon the accumulative leakage area of the anti-contamination enclosure, 1.6 square centimeters ( $0.25 \text{ in}^2$ ). Should this area increase significantly, then the purge could become completely ineffective in a short time or deplete before Satellite release.

The anti-contamination enclosure pressure release system is simple, lightweight, and has very few components, which results in low cost. It is required that the anti-contamination enclosure be designed tight enough such that the pressurized purge gas will not readily be lost through leakage, at least until the launch vehicle reaches orbit. If the pressurized purge gas is lost prior to Satellite release, the enclosure should be sufficient to protect the Satellite against contamination of a detrimental nature. This requirement is expected to be the more realistic for the Satellite anti-contamination purge system; therefore, the anti-contamination enclosure pressure release system is recommended as the baseline.

### 3.4 SUPPORT SYSTEM STRUCTURAL ANALYSES

#### 3.4.1 FLIGHT LOADS

Flight load design conditions include both rigid body and transient accelerations. Rigid body loads are basically vehicle accelerations, while transient loads include dynamic response characteristics of the vehicle. Table 3-5 presents flight load conditions for payload-critical flight events. Payload-critical conditions exist during lift-off, at end of first stage burn, and at cutoff and separation.

Flight load conditions are presented in three columns of Table 3-5 in terms of earth g's. The first two load columns give the rigid body and transient loads, respectively, where the rigid body loads were obtained from flight trajectory and the transient loads were calculated based on preliminary Saturn IB/ATM analyses. Design loads, in the last column, are obtained by algebraically summing the corre-

TABLE 3-5. FLIGHT LOAD CONDITIONS

<u>Flight Condition</u>	<u>g Level Rigid Body</u>	<u>g Level* Transient</u>	<u>Design g Level</u>
<u>Longitudinal</u>			
Lift-off	1.13	$\pm 3.5$	+4.63 - 2.37
End First Stage	4.76	-	4.76
Cutoff and Separation	2.1 $\rightarrow$ 0	$\pm 3.5$	+5.64 - 3.5
<u>Lateral</u>			
Lift-off	0.0153	$\pm 1.5$	$\pm 1.5$
Cutoff	0.0153	$\pm 1.5$	$\pm 1.5$

\* Based on Saturn IB/ATM Preliminary Analyses.

sponding rigid body and transient loads. Worst case combined design loads occur during cutoff and separation. They are +5.64 g's longitudinal in combination with  $\pm 1.5$  g's lateral, and - 3.5 g's longitudinal in combination with  $\pm 1.5$  g's lateral. These worst case load conditions were used in the structural analyses for sizing primary structural members.

#### 3.4.2 PRE-LOADS AND LOAD PATHS

Primary load paths are shown in Figure 3-23 which is a schematic showing major structural elements and forces in the X - Y plane. The schematic is shown for the condition of 3.5 g's negative longitudinal acceleration and 1.5 g's negative lateral acceleration.  $F_{cv}$  and  $F_{ch}$  represent the net reactions of the 3628 kg (8000 lbm)

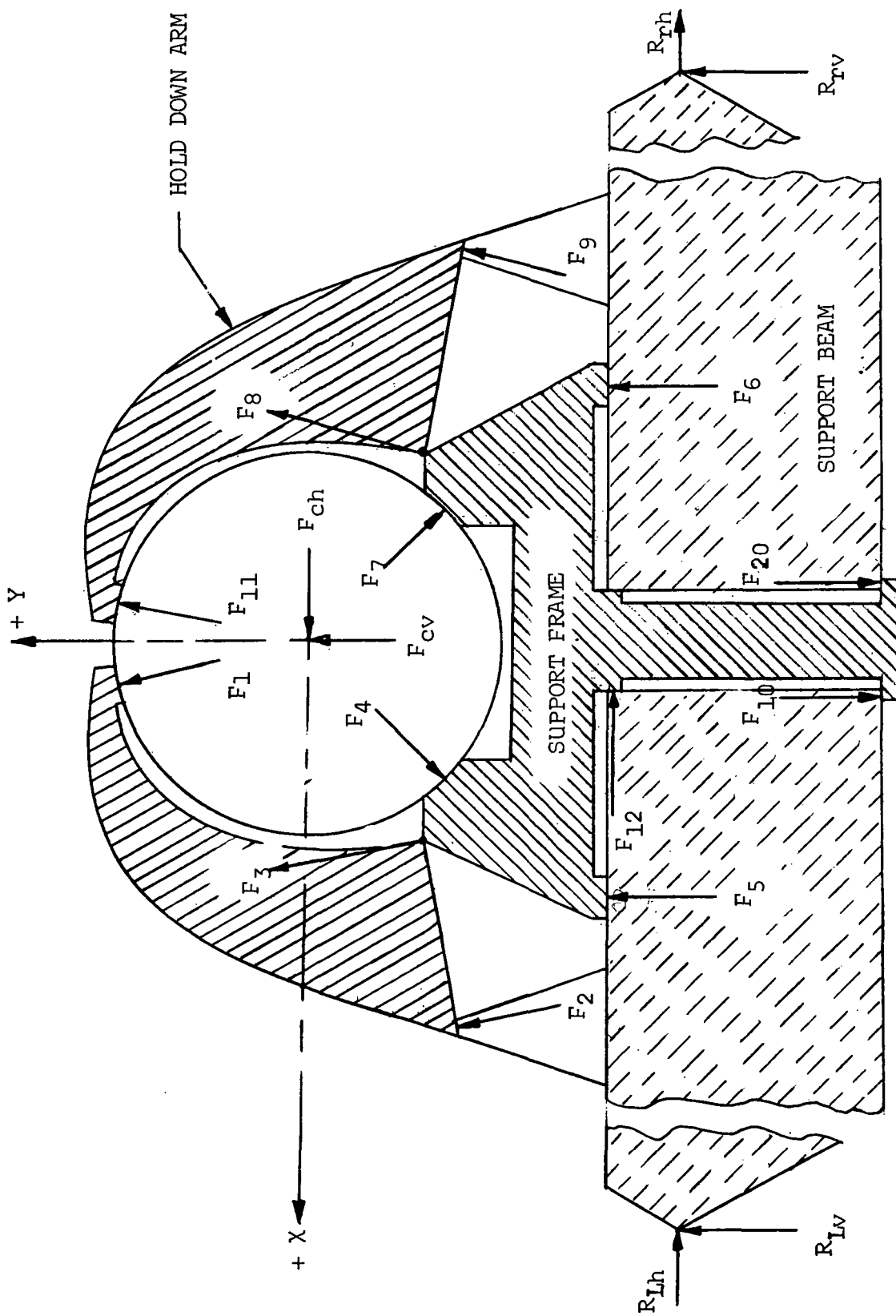


FIGURE 3-23. PRE-LOADS AND LOAD PATHS

Satellite mass during longitudinal and lateral acceleration.  $F_{cv}$  is 124,550 Newtons (28,000 lb<sub>f</sub>), and  $F_{ch}$  is 53,379 Newtons (12,000 lb<sub>f</sub>) for this load condition.

Certain simplifying assumptions were made in determining loads. One was to neglect the mass of the support structure and consider only the Satellite mass in determining structural loads during worst case load conditions. Another assumption was to ignore the effects of structural deflection in determining loads. It was also assumed that, during times of negative g's, the net lateral reaction on the Satellite support pads would be resisted by a single support pad. This reaction is represented in Figure 3-23 by  $F_{4H}$  (not shown) which is the lateral component of  $F_4$ . The lateral component of  $F_4$  is equal in magnitude to  $F_{ch}$  during periods of combined negative longitudinal and lateral acceleration.

Holddown forces  $F_1$  and  $F_{11}$  are referred to as preload forces since a minimum preload force is required at the holddown pads to prevent the Satellite from lifting off its support pads during periods of negative acceleration. Therefore, the minimum required holddown force is that value which prevents  $F_7$  from becoming negative during maximum negative acceleration. With  $F_7$  set equal to zero, and  $F_4$ ,  $F_{cv}$ , and  $F_{ch}$  known, the holddown forces  $F_1$  and  $F_{11}$  can be readily determined. By knowing  $F_1$  and the holddown arm geometry,  $F_2$  and  $F_3$  are readily determined.

Pre-load forces  $F_{10}$  and  $F_{20}$  were determined much the same as were  $F_1$  and  $F_{11}$ . The worst-case loading conditions for pre-load forces  $F_{10}$  and  $F_{20}$  occur during maximum acceleration in the negative direction as was the case in determining  $F_1$  and  $F_{11}$ . Minimum values for  $F_{10}$  and  $F_{20}$  were obtained by setting  $F_6$  equal to zero during maximum negative acceleration and solving for  $F_5$  and  $2F_{10}$  ( $F_{10} = F_{20}$ ). Note that  $F_{12}$  is equal to  $F_{ch}$ . End reactions on the main support beam are solved for in the usual manner, except that the horizontal reactions  $R_{Lh}$  and  $R_{rh}$  take into consideration the spring rate of the SLA attach points.

#### 3.4.3 STATIC LOAD ANALYSES

The static load analysis was performed for candidate worst-case structural loading conditions. Effects of elastic bending of the

integrated structure were not generally considered in the static analysis except where it was necessary to balance static forces to account for a shared point of deflection of two or more intersecting structural elements. An example is the longitudinal shear interaction which occurs between the main beams when lateral g-loads predominate in one of the primary coordinate planes during periods of negative longitudinal g's.

Table 3-6 lists the Satellite support structure interface loads employing the same force notations as in Figure 3-23. Forces are noted in newtons with secondary notations in  $lb_f$  (shown in parentheses).

Acceleration is in g's with the sign convention established by the coordinate system of Figure 3-23. The extreme left column of Table 3-6 is designated "shear moment diagram reference numbers." Reference numbers appearing in this column are used as references to identify corresponding shear moment diagrams used in the analysis. References 1 and 2 of Table 3-6 pertain to the shear moment diagrams for the main support beam during periods of maximum negative and maximum positive longitudinal acceleration. The remaining reference numbers are associated with shear moment diagrams for the Satellite support frame. Support frame g-loading conditions for references 3 and 4 are the same as for the main beam (references 1 and 2). The three additional g-loading conditions for which the support frame was investigated are defined in the footnotes of Table 3-6. These three additional loading conditions were significant in the support frame analysis. For example, the maximum bending moment imposed on the frame was calculated to occur during the pre-launch phase with the Satellite removed and the frame pre-loaded to the main beam.

Worst-case loadings of the main beam occur during periods of maximum negative and positive longitudinal acceleration, and are illustrated in the shear and moment diagrams of Figures 3-24 and 3-25. An interacting shear force of 26,689 **Newtons** occurs at the intersection of the main beams during conditions of maximum negative g's. This shear force appears at 0-station of the shear diagram of Figure 3-25.

It is apparent from the moment diagrams of Figures 3-24 and 3-25 that the main beams are more heavily loaded in bending moment during conditions of maximum positive longitudinal acceleration than during maximum negative longitudinal conditions. For this reason the top flange of the main beam was made wider than the bottom flange, and the maximum compressive stress experienced by the two flanges is more nearly the same.

TABLE 3-6. SUPPORT STRUCTURE LOADS

Shear Moment Dia. Ref. No.	Acceleration (g's)		Forces - Kilo Newton and (lb <sub>f</sub> )							
	Long.	Lat.	F <sub>4</sub>	F <sub>7</sub>	F <sub>5</sub>	F <sub>6</sub>	F <sub>12</sub>	R <sub>LV</sub>	R <sub>HT</sub>	R <sub>RV</sub>
1 & 3	-3.5	1.5	75.48 (16,969)	0 (0)	101.37 (22,789)	0 (0)	53.38 (12,000)	-23.82 (-5,354)	53.38 (12,000)	-38.46 (-8,646)
2 & 4	5.64	1.5	171.61 (38,579)	96.12 (21,609)	169.34 (38,070)	67.97 (15,280)	53.38 (12,000)	57.50 (12,926)	53.38 (12,000)	42.85 (9,634)
5	-3.5	0.0	0 (0)	0 (0)	23.99 (5,359)	23.99 (5,395)	0 (0)	31.14 (7,000)	0 (0)	31.14 (7,000)
6	1.0	0.0	25.16 (5,657)	25.16 (5,657)	127.97 (28,769)	127.97 (28,769)	0 (0)	- -	- -	- -
7	1.0	0.0	-	-	110.18 (24,769)	110.18 (24,769)	0 (0)	- -	- -	- -

Ref. (5) Pad forces 4 and 7 are zero due to lateral acceleration of 1.5 g's in perpendicular plane.

Ref. (6) Pre-launch condition, Satellite rests on two opposing pads.

Ref. (7) Pre-launch condition, Satellite removed from frame.

Pre-load forces:  $F_1 = F_{11} = 46.04$  (10,350),  $F_2 = F_9 = 41.70$  (9,374)

$F_3 = F_8 = 88.60$  (19,918),  $F_{10} = F_{20} = 110.18$  (24,769)

$R_{HT}$  = Total horizontal reaction on main beam.

LONGITUDINAL ACCELERATION = 5.64 g

LATERAL ACCELERATION = 1.5 g

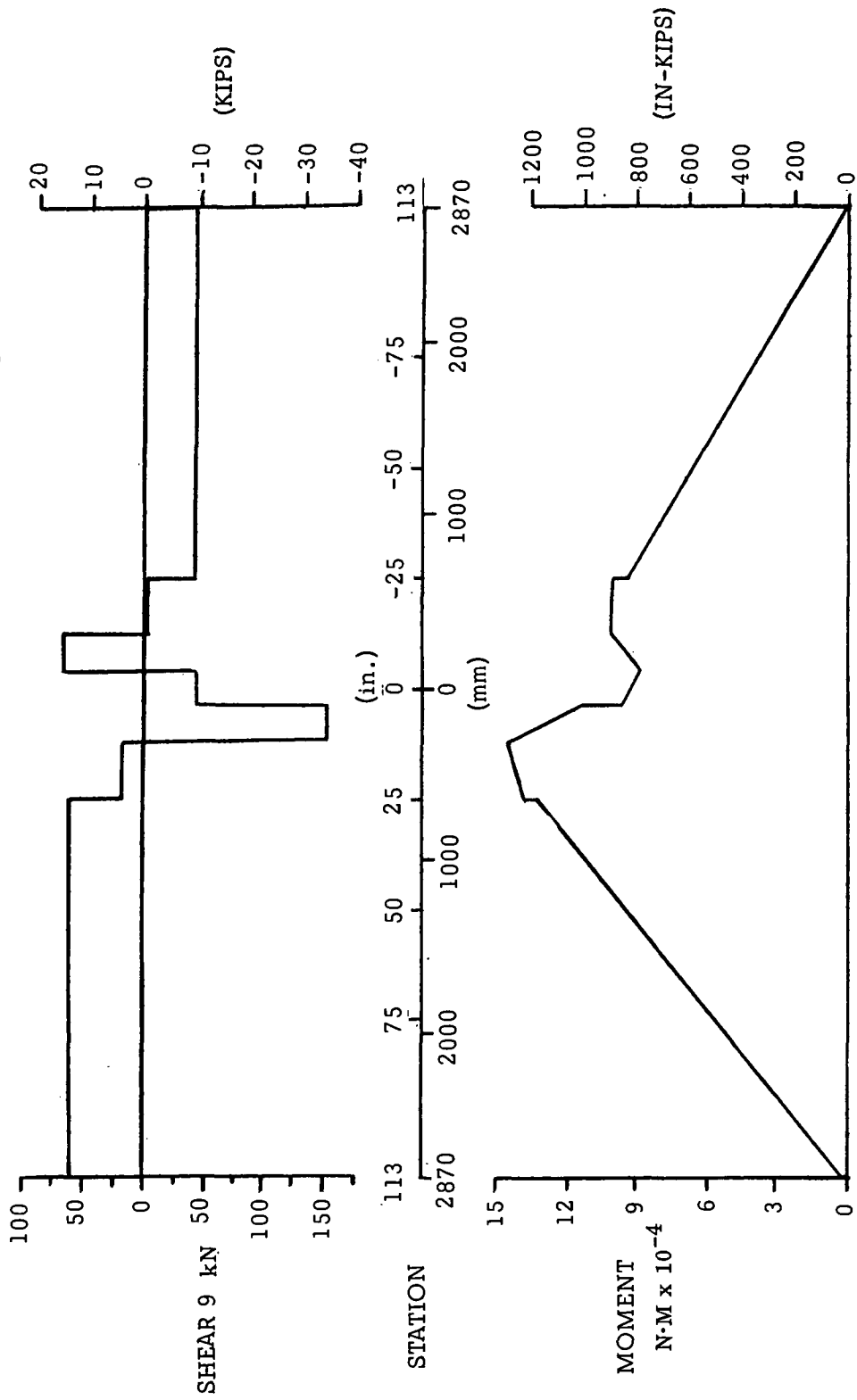


FIGURE 3-24. MAIN BEAM SHEAR - MOMENT DIAGRAM



LONGITUDINAL ACCELERATION = -3.5 g

LATERAL ACCELERATION = 1.5 g

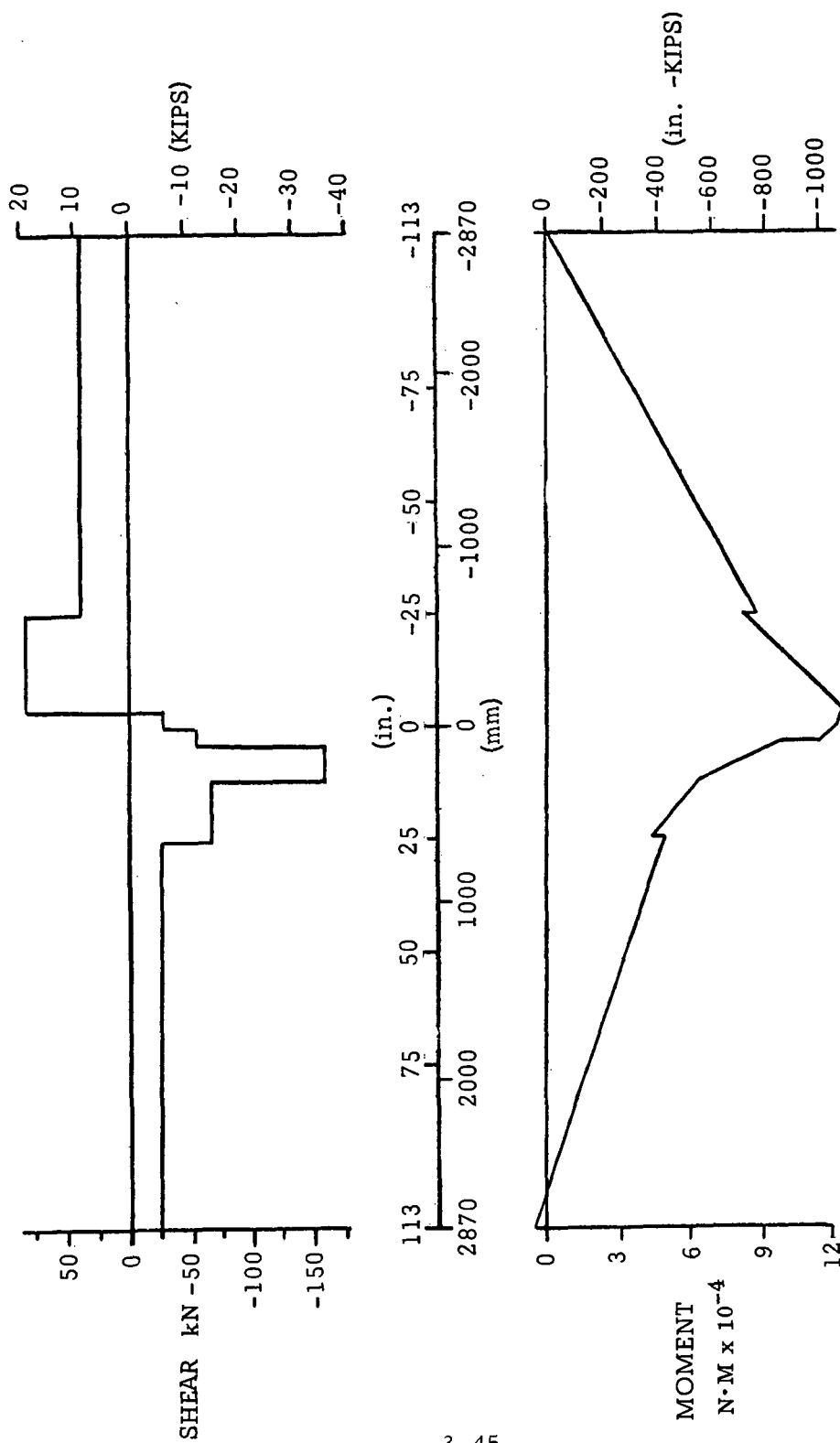


FIGURE 3-25. MAIN BEAM SHEAR - MOMENT DIAGRAM

### 3.4.4 STRESS ANALYSES AND MEMBER SIZING

#### 3.4.4.1 MAIN CROSS BEAMS

The initial sizing of the main cross beams was based on an assumed allowable buckling stress of approximately  $207 \times 10^6 \text{ N/m}^2$  (30,000 psi). 7075-T6 aluminum was selected as the material for the main cross beam structural members because of its high strength to weight properties. Primary components of the main cross beams are flat shear webs, tee flanges, and bulb angles used as longitudinal and lateral web stiffeners. These main beam members are assembled with fasteners since 7075-T6 aluminum has poor welding qualities. The shear webs of the main cross beams are fastened to a common structural element called the outer cylinder. The outer cylinder is designed to take the shear load from the main beam shear webs and distribute it as shown in the shear diagrams of Figures 3-24 and 3-25. Bending moments are resisted at the main beam intersection by gusset plates which are attached to the top and bottom beam flanges. The main beams are stabilized against lateral buckling by tension rods attached at the top and bottom flanges of each beam at its quarter span and the support point fitting at each end. This stabilizing arrangement effectively reduces the beam lengths for purposes of calculating allowable buckling stress. Thus, a higher allowable buckling stress and lighter beam weight results. Figure 3-26 is an isometric sketch showing dimensions of the main beam structural elements. Figure 3-27 is a sketch showing the stabilizing arrangement of the tension rods on the main beams.

#### 3.4.4.2 SATELLITE SUPPORT FRAME

The Satellite support frame assembly is of welded 2219-T87 aluminum construction and has the dual function of supporting the Satellite during launch and acting as a Satellite jettisoning platform in orbit. The Satellite is cradled in the support frame by four equally-spaced support pads which have ball socket joints. By neglecting structural deflection of the support frame and assuming zero friction in the support pad ball joints, all reactions at the support pads pass through the pivot points of the pads, radial to the Satellite surface. The inner cylinder is an integral part of the Satellite support frame assembly and is positioned within the outer cylinder during launch. It contains the payload ejection spring. The inner cylinder is normally loaded in axial tension with the pre-load force required to hold the support frame against the main beam assembly during launch. It also acts as a spring-driven piston during Satellite ejection. The inner cylinder walls are

Technical drawing of a rectangular frame structure, likely a mold or tray, showing dimensions in millimeters. The drawing includes a perspective view of the frame and a cross-sectional view. Key dimensions are labeled:

- Overall length: 152.4
- Overall width: 101.6
- Internal length: 686
- Internal width: 254
- Frame thickness: 5.80
- Internal width of the central channel: 3.30
- Height of the side walls: 50.8
- Height of the central channel: 5.80 mm

**DIMENSIONS IN mm**

FIGURE 3-26. MAIN BEAM TYPICAL CONSTRUCTION

CONVERSIONS	
mm	in.
3.30	0.130
5.80	0.228
50.8	2
101.6	4
152.4	6
254	10
686	27

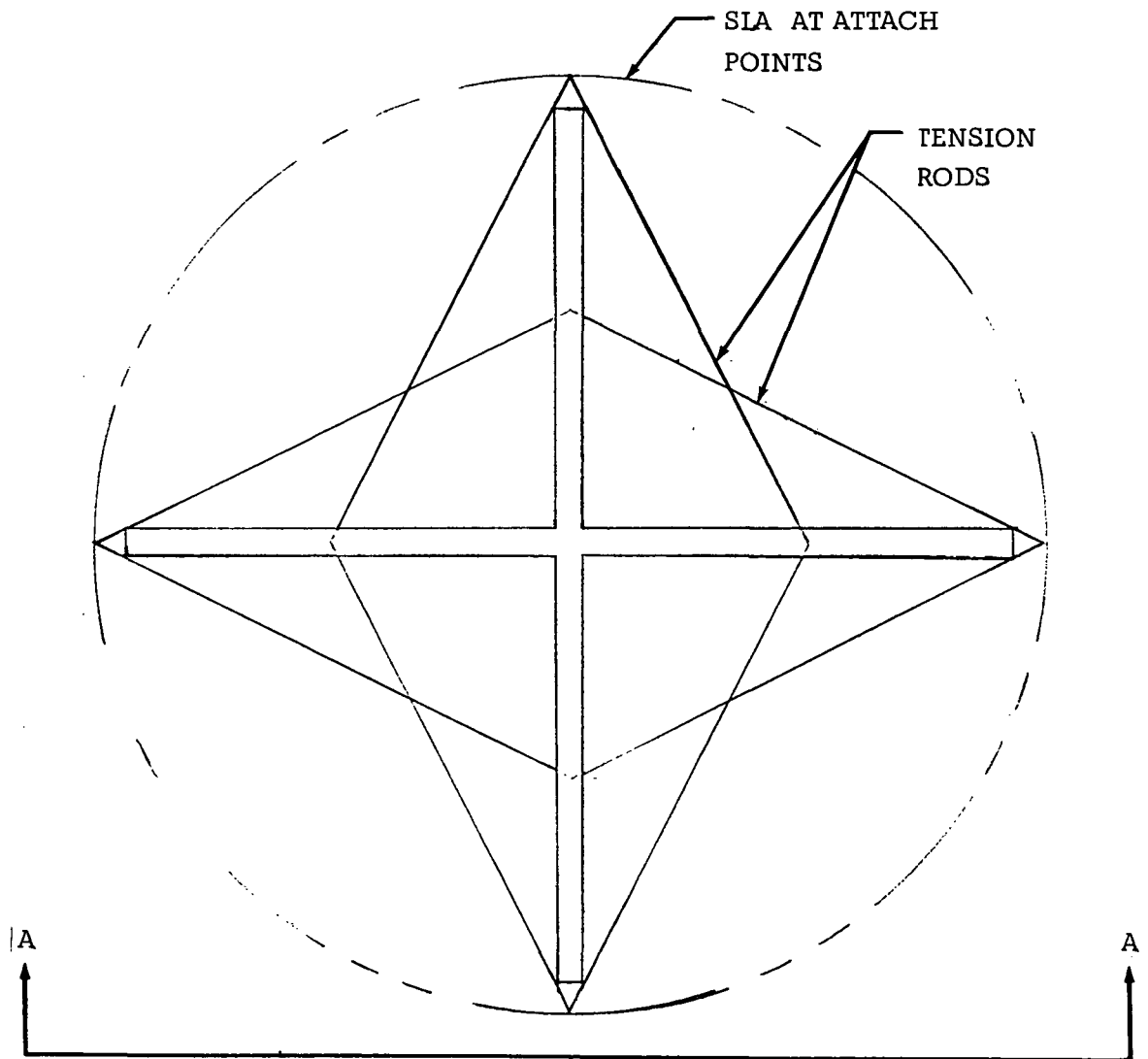
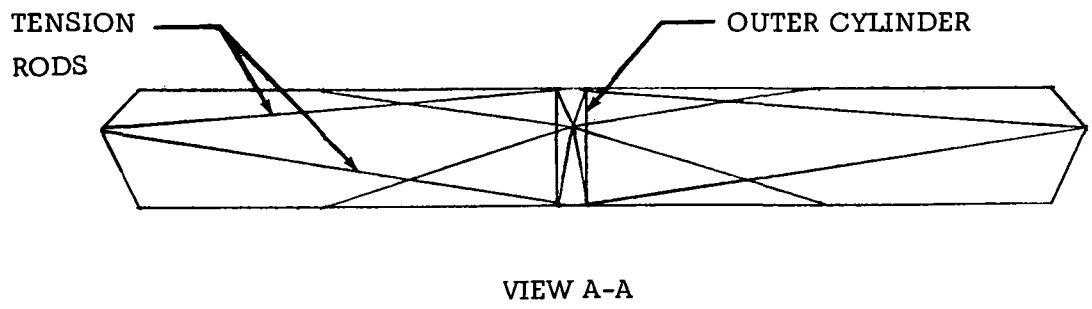


FIGURE 3-27. MAIN BEAM TENSION ROD ARRANGEMENT

designed to take a tension load of 444,822 Newtons (100,000 lb<sub>f</sub>) during launch, or in the pre-load condition. The wall thickness of the inner cylinder is greater at the top where the four beam-type elements of the frame are welded to it. This provides additional strength to distribute web shear from the beam-type elements to the inner cylinder. The lower end of the inner cylinder is an integral ring approximately 12.7 mm (0.5 in.) thick by 76.2 mm (3 in.) high. The ring is machined in two places to receive two latches of the payload release mechanism which are required to carry the pre-load forces totaling 444,822 Newtons.

#### 3.4.4.3 SATELLITE RELEASE MECHANISM

The Satellite release mechanism is fabricated from aluminum except for pins, release latches, and two toggle links which require high-strength steel. The analysis of the payload release method was cursory in that detailed analysis was not attempted to the point of optimizing each individual dimension. Instead, a conservative approach was taken in sizing the individual parts and the conclusion is that the mechanism is structurally sound in its concept.

#### 3.4.4.4 HOLDDOWN ARMS

The holddown arms were structurally analyzed based on the pre-load forces of Table 3-6. Web thickness requirements were computed to be 1.02 mm (0.040 in.) for the center web and 2.79 mm (0.110 in.) for the top web. The bottom web thickness was computed to be 2.16 mm (0.085 in.). Ribs were found to develop tension loads of up to 44,500 Newtons (10,000 lb<sub>f</sub>) adjacent to the channel-shaped flange of the holddown arm.

These heavy rib loads make it impractical to join the ribs to the flanges with fasteners. For this reason a welded aluminum structure is recommended for the holddown arms. Another area of high load concentration where a welded joint appears to be more desirable is the juncture of the flanges with the holddown pad assembly. The material selected for this assembly and all other welded structure was 2219-T87 aluminum.

#### 3.4.4.5 ANTI-CONTAMINATION ENCLOSURE

The payload protective shield is required to withstand a differential pressure of 1.4 N/cm<sup>2</sup> (2 psi). The material selected for the pressure membrane is 2219-T87 aluminum, with a nominal thickness of 0.406 mm (0.016 in.). This thickness is well above that required solely on a basis of tensile strength. However, a thinner gage would present a

problem in that it would be highly vulnerable to accidental damage during assembly, checkout, and preflight operations.

#### 3.4.4.6 TENSION RODS

The isometric sketch (Figure 3-28) shows how the tension rods are attached to the main beams to stabilize them against lateral buckling. The primary intent of the tension rods was to give the main beam lateral stability, but it is also apparent that as the structure deflects during periods of lateral g-loading this deflection is resisted in part by the tension rods. The percentage of this side load that is reacted through the tension rods at any given time is a function of the structural geometry, direction of side-loading, and spring rates of the affected structural elements.

The model used in sizing the main beam tension rods is illustrated in Figure 3-29. The lateral g-load is shown being reacted at the intersection of the main beams along a line passing through two opposing end-attach points. This model shows the main beams pinned to the SLA which is represented as a phantom circle. The horizontal beam is represented as a one-piece rigid element with tension rods attached midway on the left half of the beam. The other (cross) beam is comprised of two equal segments each modeled with pinned ends. Modeling the cross beam as two pinned elements can be justified since the lateral spring rate of the beam, based on a force applied to the beam end and parallel to  $F_3$ , is insignificant compared to  $k_3$ , the tangential spring rate of the SLA attach point. Also, the axial spring rate of the main beams is several times higher than the corresponding radial spring rate of the SLA attach points, and therefore, axial strain effects of the main beams were discounted in sizing the tension rods and in calculating deflections at the SLA attach points.

Based on the above assumptions and on the reaction loads chosen for the SLA attach points the maximum deflections, as shown in Figure 3-29, at the attach points is 0.016 mm (0.0006 in.) for  $\Delta_3$  and  $\Delta_4$  and 3.835 mm (0.151 in.) for  $\Delta_1$  and  $\Delta_2$ . The internal forces diagram, which is the bottom sketch of Figure 3-28, shows a maximum main beam axial compressive load of 31,138 Newtons (7,000 lb<sub>f</sub>). The effect of this compressive load on the quartersection of the beam is to shorten it by approximately 0.178 mm (0.007 in.). The other three quarter-sections of the same beam experience changes in length accordingly. The overall change in length in the X direction is a decrease of 0.051 mm (0.002 in.). The other main beam has a uniform compressive loading

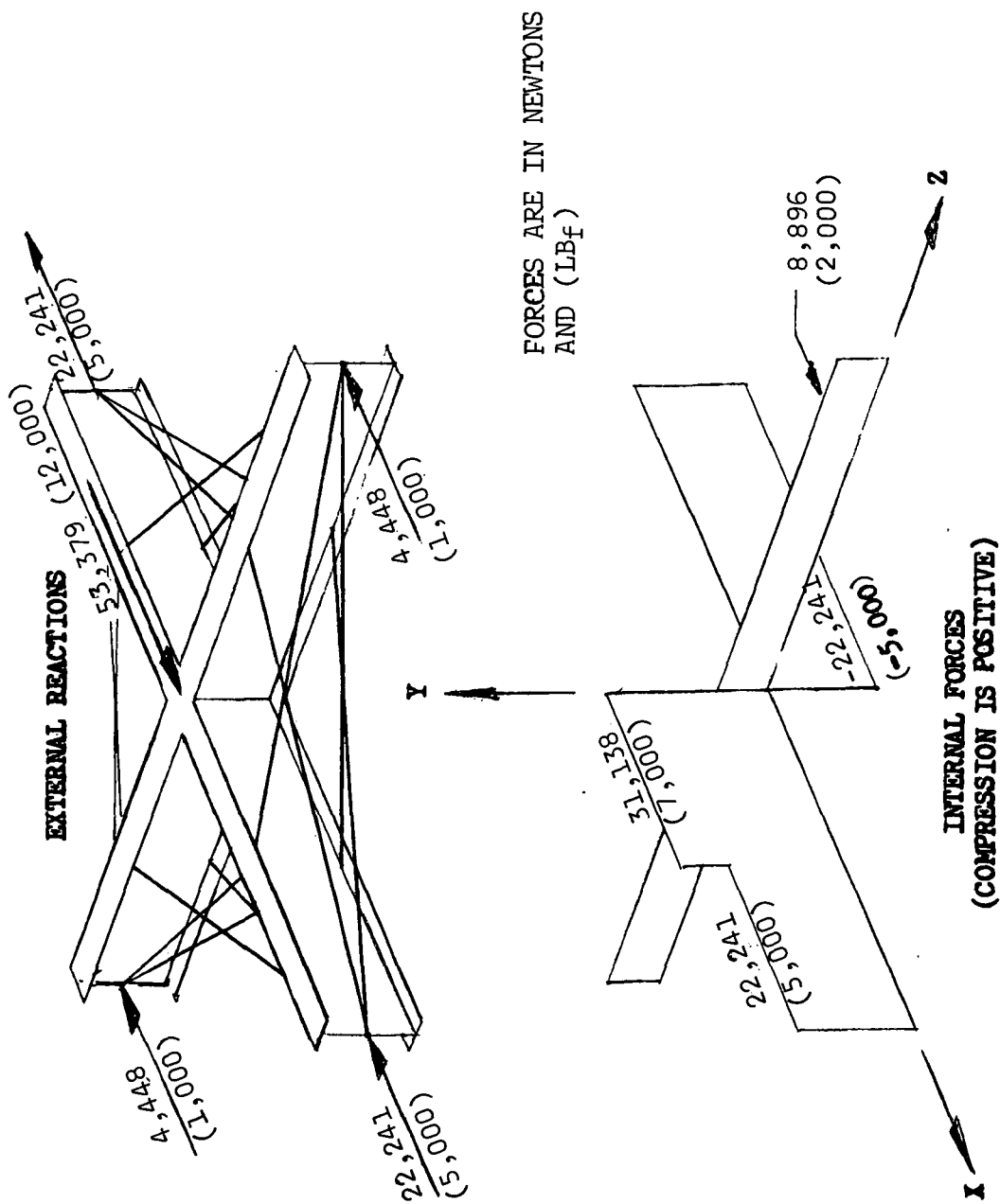


FIGURE 3-28. TENSION ROD LOAD DISTRIBUTION

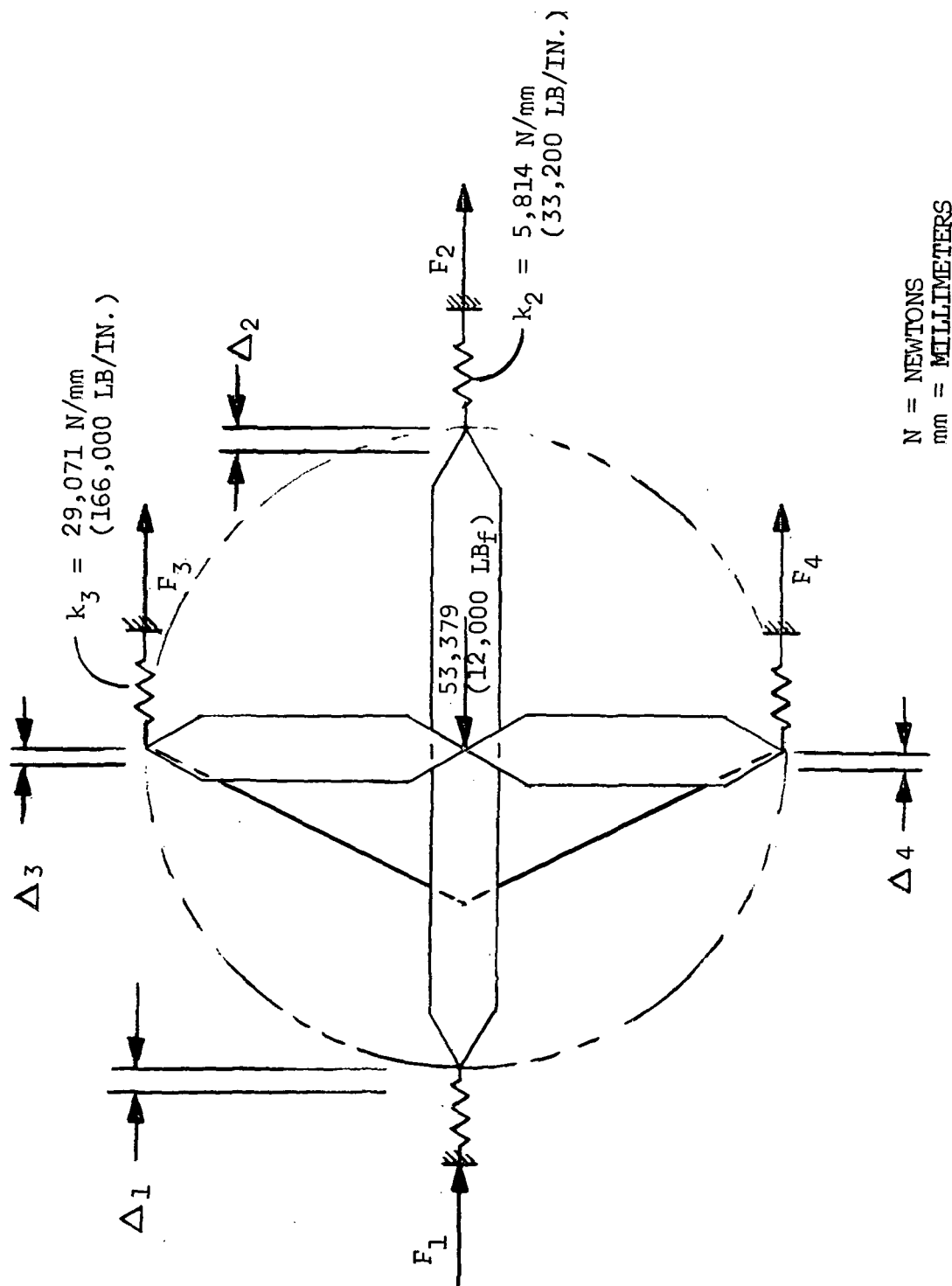


FIGURE 3-29. TENSION ROD SIZING MODEL



of 8,896 Newtons (2,000 lb<sub>f</sub>) and undergoes a change in length of 0.203 mm (0.008 in.). It is apparent from Figure 3-28 that pretensioning the tension rods will increase the compressive loading of the beams and further decrease their lengths. It is also apparent that a reasonable degree of pretensioning will not significantly affect the design. As shown in Figure 3-28, the external SLA forces total 53,379 Newtons. The compression and tension load in the main beam was limited to 22,241 Newtons (5,000 lb<sub>f</sub>) at the SLA attach points. This limit load was established to be safely below the LM attach point limit load imposed on the SLA which is 30 percent higher. The internal forces diagram is drawn with the assumption that tension rods have no pretension load. Tension rods were sized for spring rates to distribute the loads as discussed above, and are aluminum with cross-sectional diameters of 13.2 mm (0.520 in.).

Table 3-7 contains a comparison of LM attach point limit loads and Cannonball attach point limit loads.

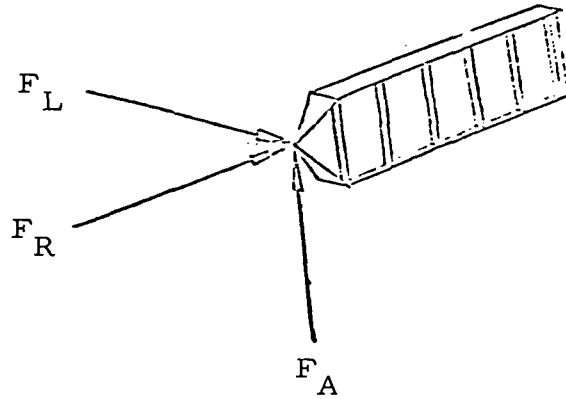
### 3.4.5 FINITE ELEMENT ANALYSIS OF SUPPORT STRUCTURE

#### 3.4.5.1 INTRODUCTION

The finite element analysis of the support structure was conducted utilizing the NASTRAN (NASA Structural Analysis) computer program, and consisted of both a static and a dynamic solution. The static solution was used to verify the stress analysis described in 3.4.4. The dynamic analysis was used to determine the Satellite and support structure dynamic environment and their influence in the vehicle dynamics.

A finite element model of the structure was prepared for the NASTRAN computer program, and consisted of the complete support structure, as shown in Figure 3-30. The model was made up of 114 grid points connected by the appropriate structural members such as bars, rods, and shear panels, as shown in Figure 3-31. The hold-down arms were also modeled as an integral part of the cross beam structure. The model was used first to obtain the static solution cases with the load conditions described in 3.4.1. Then the same model was used to obtain modal deformation, and lastly the model was used to obtain the frequency response of the structure and Satellite.

TABLE 3-7. LM - SEPS ATTACH POINT  
LIMIT LOAD COMPARISON



	LM Attach Point Limit Load <u>Newton (Pounds)</u>	SEPS Attach Point Limit Load <u>Newton (Pounds)</u>
$F_A$ Compression	185,193 (41,633)	57,497 (12,926)
Tension	64,868 (14,583)	38,468 ( 8,648)
$F_R$ Compression	35,230 ( 7,920)	22,241 ( 5,000)
Tension	28,927 ( 6,503)	22,241 ( 5,000)
$F_L$	$\pm 49,193$ ( $\pm 11,059$ )	$\pm 4,448$ ( $\pm 1,000$ )

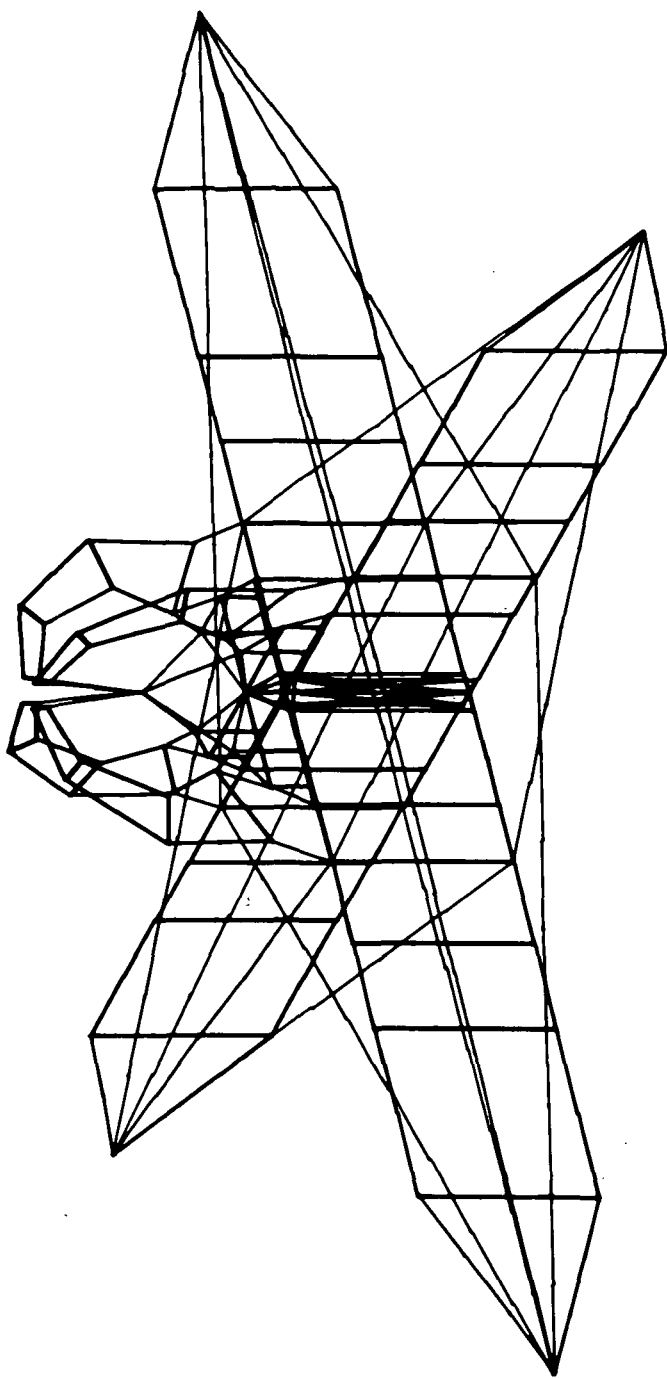


FIGURE 3-30. FINITE ELEMENT MODEL

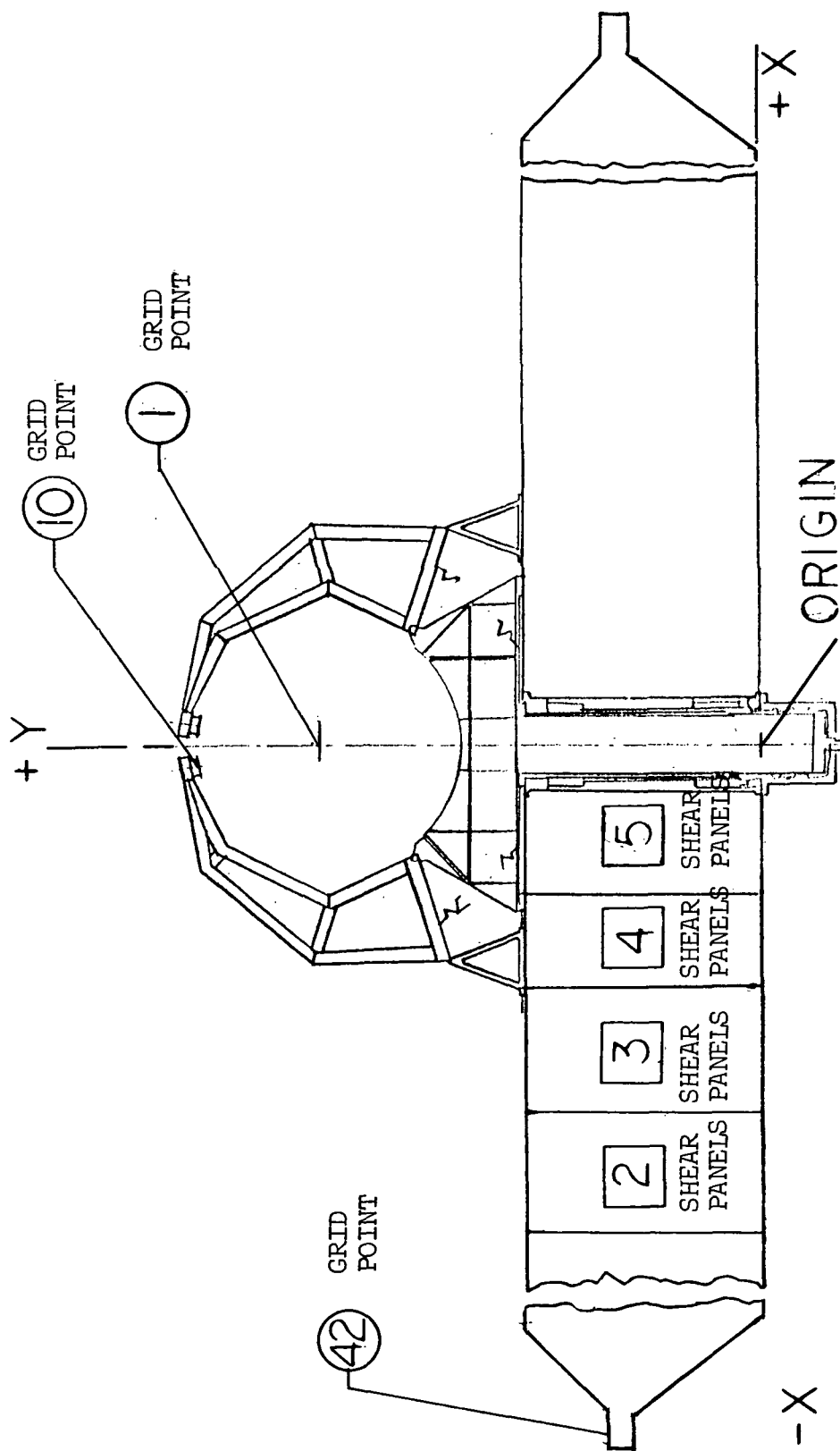


FIGURE 3-31. TYPICAL GRID POINTS AND STRUCTURAL ELEMENTS

#### 3.4.5.2 DESCRIPTION OF THE MODEL

The finite element model of the cross beam and the payload holddown arms was developed in a rectangular coordinate system with its origin placed at the center line of the vehicle and at the bottom of the cross beam, as shown in Figure 3-31. The nodes or grid points were selected in such manner to best represent the structure. The support attach points in the SLA were modeled as simple supports in each of the three major planes, as indicated in Figure 3-32. The geometry and material of each component were selected as determined in 3.4.4 and assigned to each component accordingly.

The static loads were applied at discrete selected grid points to simulate the Satellite mass, and the longitudinal, and the lateral acceleration for the two critical loading conditions.

#### 3.4.5.3 STATIC ANALYSIS FINITE ELEMENT MODEL

A static analysis was conducted using the finite element model to verify the stress analysis and member sizing described in 3.4.4. The static analysis was first run to determine deflections at each grid point, internal loads, reactions, and stresses in each member.

The results of the static analysis indicated that the static deformations for both load cases were small and in agreement with the stress analysis section of this report. The internal forces, reactions, and stresses of each member were also calculated, and compared with the stress analysis section. It was concluded that the member sizes established in 3.4.4 were generally appropriate, although, with additional iterations, the support structure could be improved by redistributing stress, and redistributing the cross sectional areas to obtain optimum load distribution and deflections.

#### 3.4.5.4 NATURAL FREQUENCIES AND MODE SHAPES

The finite element model was used to obtain the normal modes of the structure for a selected frequency range. The modal analysis was performed to better understand and evaluate the support structure design, to study coupling probability with vehicle modes, and to provide information to obtain vehicle loads, and vibration response.

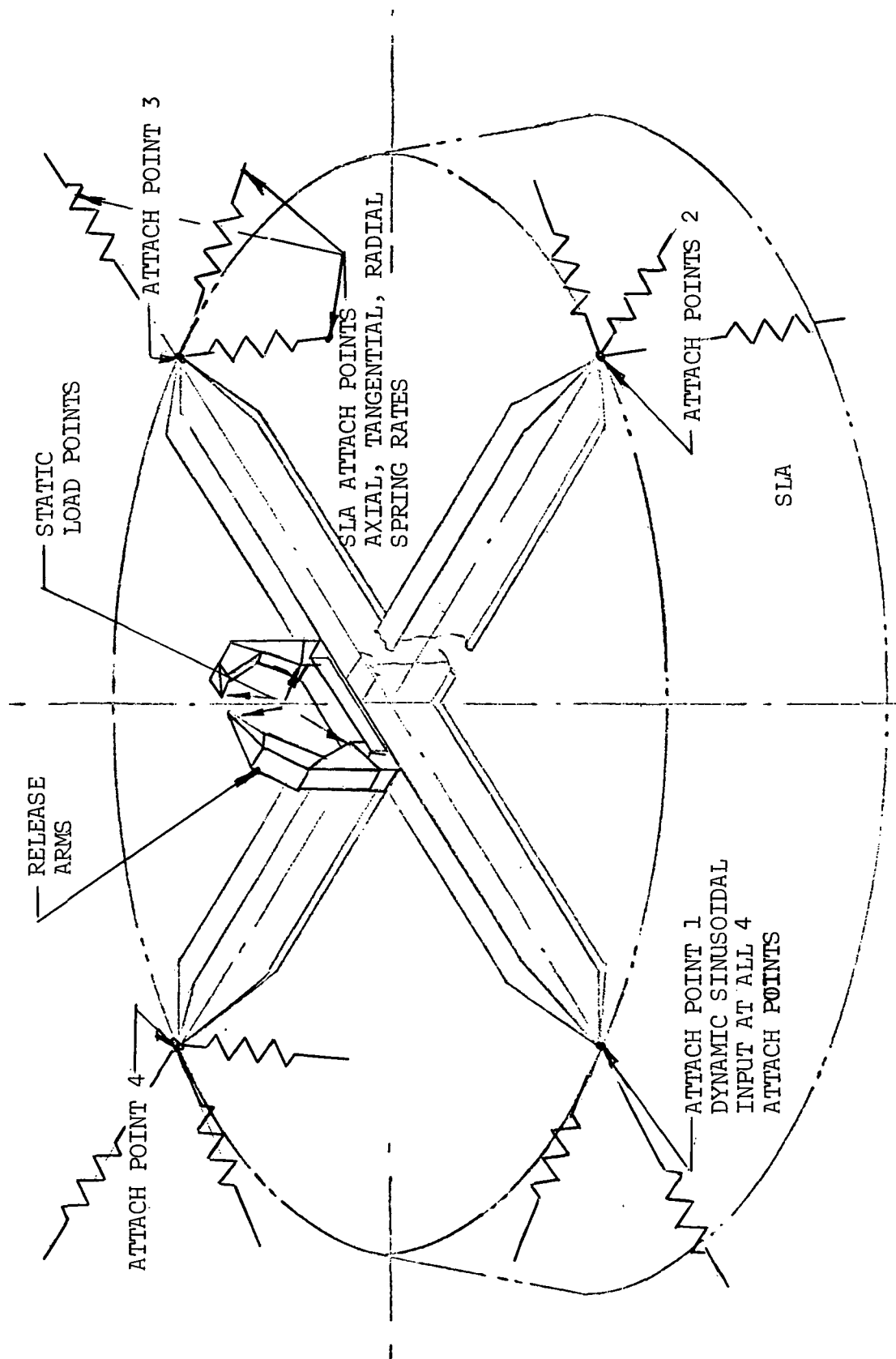


FIGURE 3-32. SLA ATTACH POINT MODEL

TABLE 3-8. SUPPORT STRUCTURE NATURAL FREQUENCIES

MODE NO.	EXTRACTION ORDER	EIGENVALUE	R E A L   E I G E N V A L U E S		GENERALIZED MASS	GENERALIZED STIFFNESS
			RADIANS	CYCLES		
1	9	4.807764+03	6.933804+01	1.103549+01	2.201755+01	1.058552+05
2	7	1.045133+04	1.022318+02	1.627069+01	1.319044+01	1.378577+05
3	6	1.044976+04	1.024683+02	1.630834+01	1.327158+01	1.393484+05
4	8	1.145348+04	1.070209+02	1.703291+01	6.637909+00	7.602714+04
5	2	1.417138+05	3.764490+02	5.991372+01	2.310164+00	3.273822+05
6	1	1.423557+05	3.773005+02	6.004924+01	2.225642+00	3.168327+05
7	3	1.557304+05	3.946269+02	6.280683+01	2.324321+00	3.619675+05
8	4	1.806297+05	4.250055+02	6.764173+01	2.262706+00	4.087120+05
9	5	1.814960+05	4.260235+02	6.780374+01	2.360753+00	4.284672+05
10	10	2.381020+05	4.879570+02	7.766077+01	1.386053+00	3.300221+05
11	11	1.487163+06	1.219493+03	1.940883+02	6.047034+01	8.992925+05

The results of the modal analysis are shown in Table 3-8, from the first mode at a frequency of 11 Hz, to the eleventh mode at a frequency of 194 Hz. In the second, third, and fourth modes there is an interaction between the longitudinal and lateral modes and all occur between 16 to 17 Hz. All the mode shapes for these natural frequencies are shown as plotted by the computer in Figures 3-33 through 3-38.

#### 3.4.5.5 VIBRATION ANALYSIS

The same model used for the modal analysis was utilized to obtain the frequency response of the support structure and Satellite. One thing added to the model was a mass to simulate the Satellite. The model was excited by a sinusoidal forcing function applied at the SLA attach points in both the longitudinal (Y) and lateral (X) axes, independently from each other.

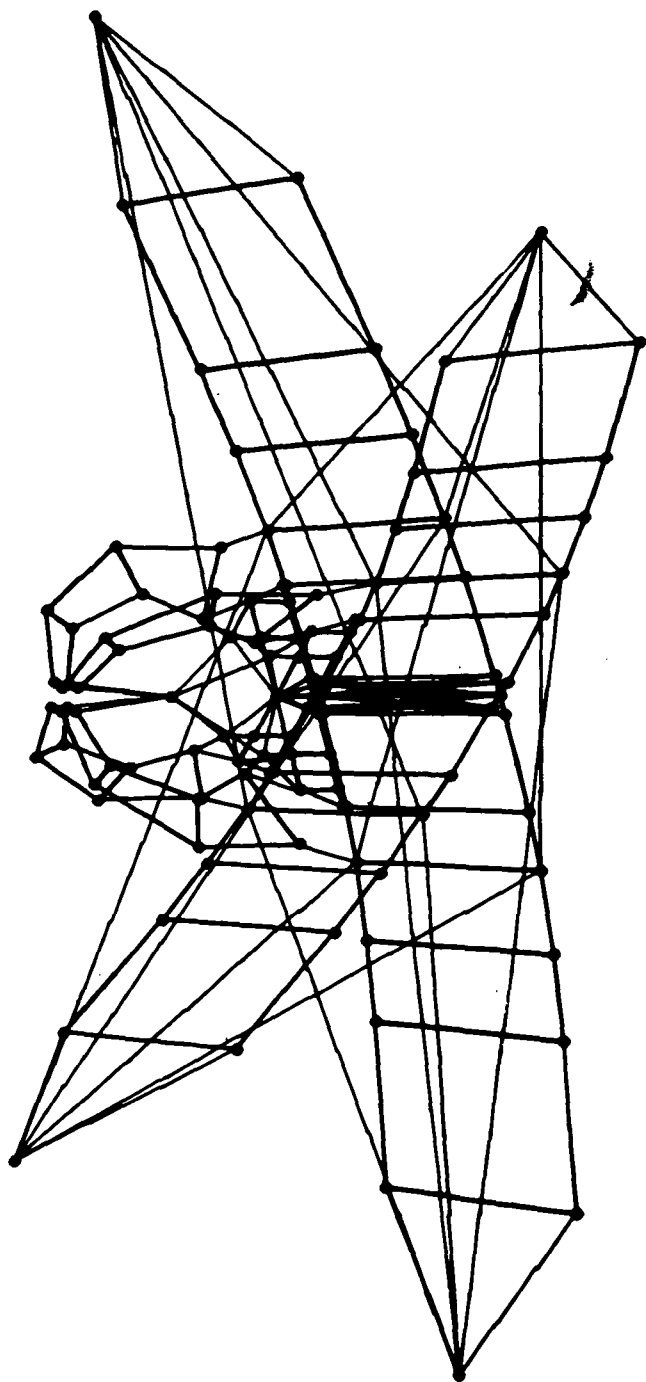
The forcing function used to excite the support structure was based on previously developed Saturn IB/ATM data as presented in Table 3-9.

TABLE 3-9. DESIGN SPECIFICATION FOR SINUSOIDAL VIBRATION FOR SATURN S-IB/S-IVB/ATM AT THE SLA OUTRIGGER

- o FLIGHT AXIS (3-50 Hz at 3 Octave/Minute)
  - 3 to 7 Hz at 0.044 inches double amplitude displacement
  - 7 to 21 Hz at 0.051 g's peak
  - 21 to 50 Hz at 0.20 g's peak
- o LATERAL AXIS (1.7 - 20 Hz at 3 Octave/Minute)
  - 1.7 to 4.3 Hz at 0.84 inches double amplitude displacement
  - 4.3 to 10.0 Hz at 0.40 g's peak
  - 10.0 to 20.0 Hz at 0.168 inches double amplitude displacement

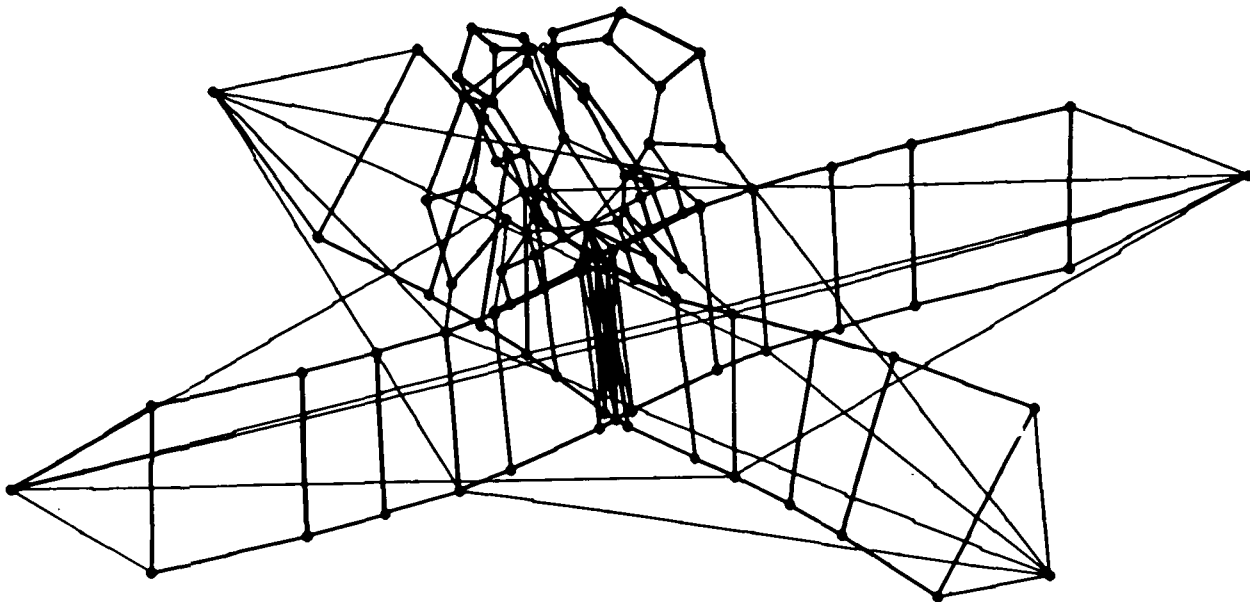
The results of the analysis indicate that the Satellite (grid point 1) has a maximum amplification factor (ratio of response acceleration to input acceleration) of 8.427 in the lateral axis at a frequency of 18.9 Hertz and for the longitudinal axis the maximum amplification



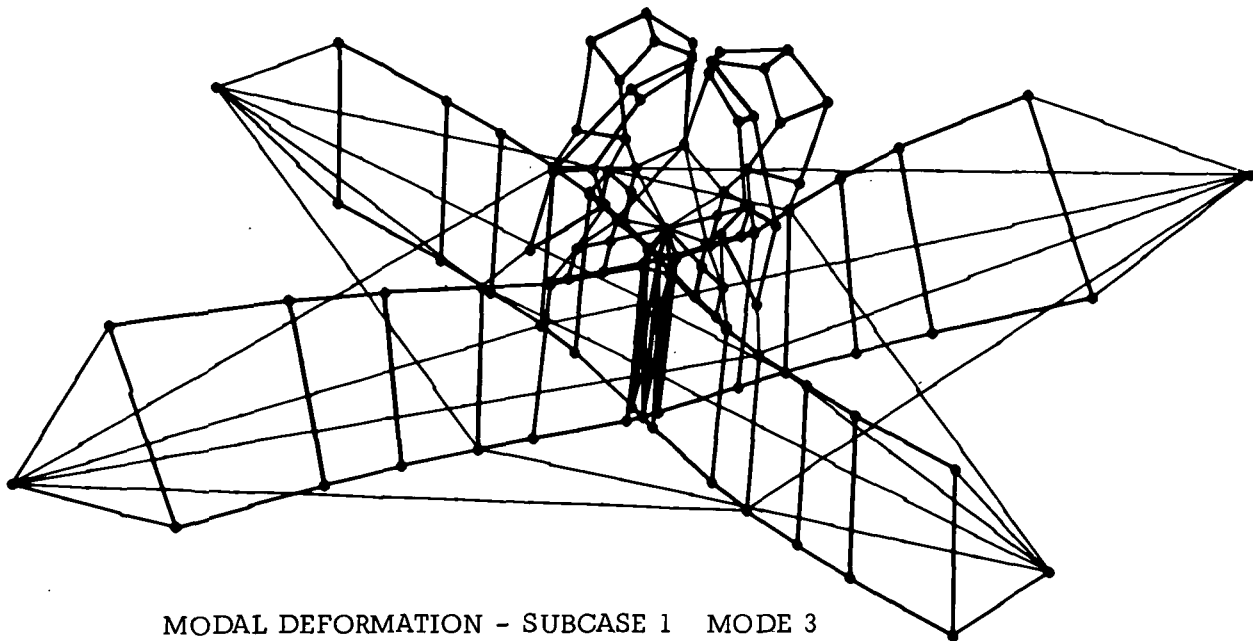


MODAL DEFORMATION 1 - SUBCASE 1 MODE 1  
EIGENVALUE = 4807.7637000 FREQ. 11.0 HZ

FIGURE 3-33. MODE SHAPE, MODE 1

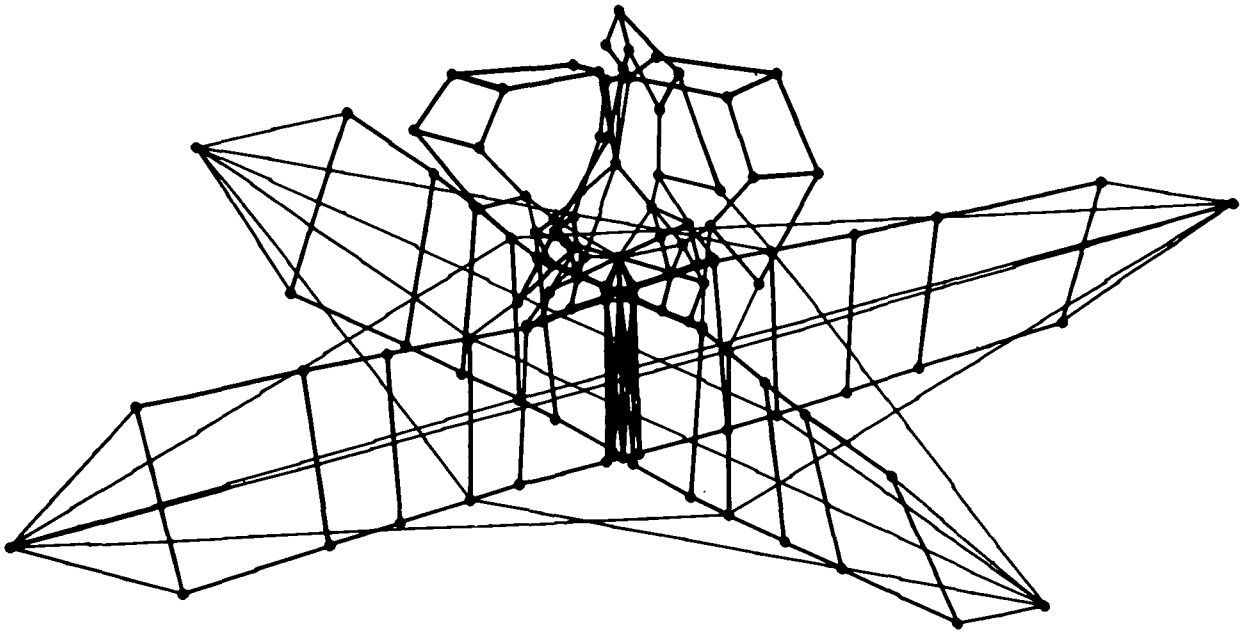


MODAL DEFORMATION - SUBCASE 1    MODE 2  
 EIGENVALUE = 10451.333000    FREQ. 16.27 HZ

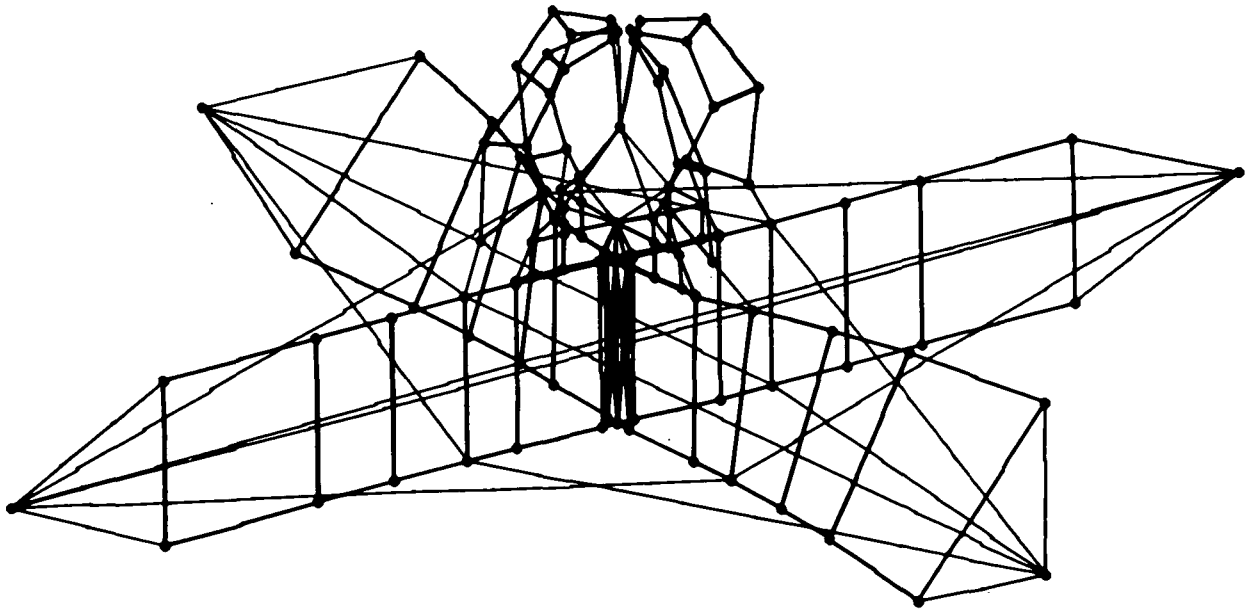


MODAL DEFORMATION - SUBCASE 1    MODE 3  
 EIGENVALUE = 10499.758000    FREQ. 16.3 HZ

FIGURE 3-34. MODE SHAPE, MODES 2 AND 3

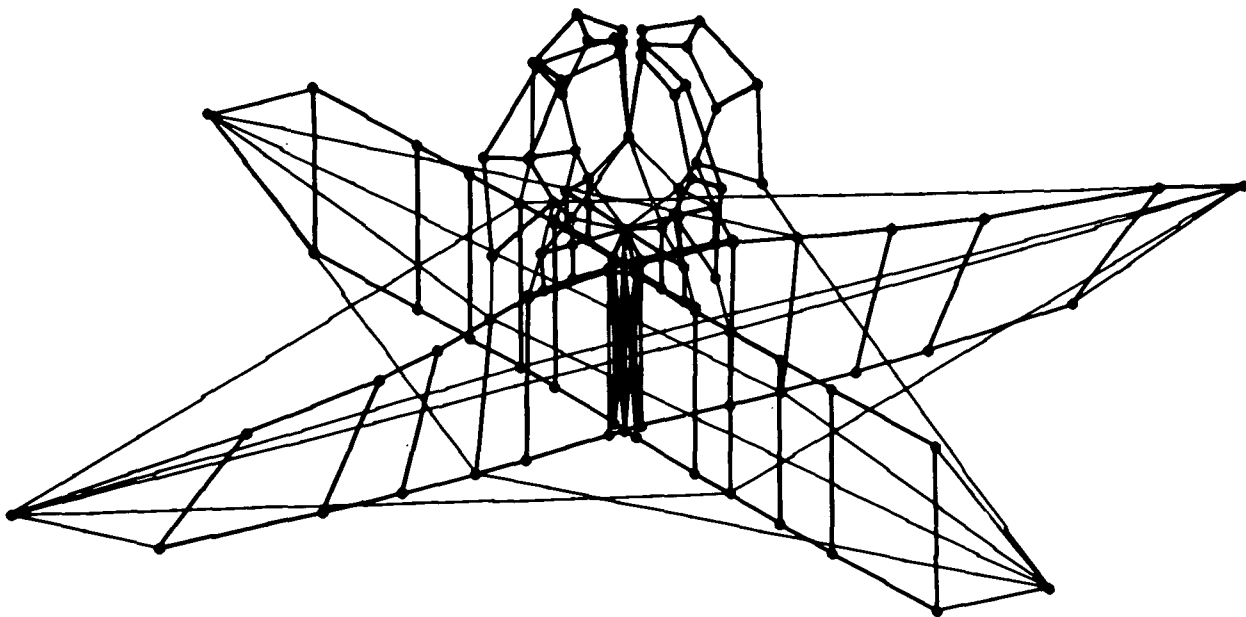


MODAL DEFORMATION - SUBCASE 1    MODE 4  
EIGENVALUE = 11453.477000    FREQ. 17.0 HZ

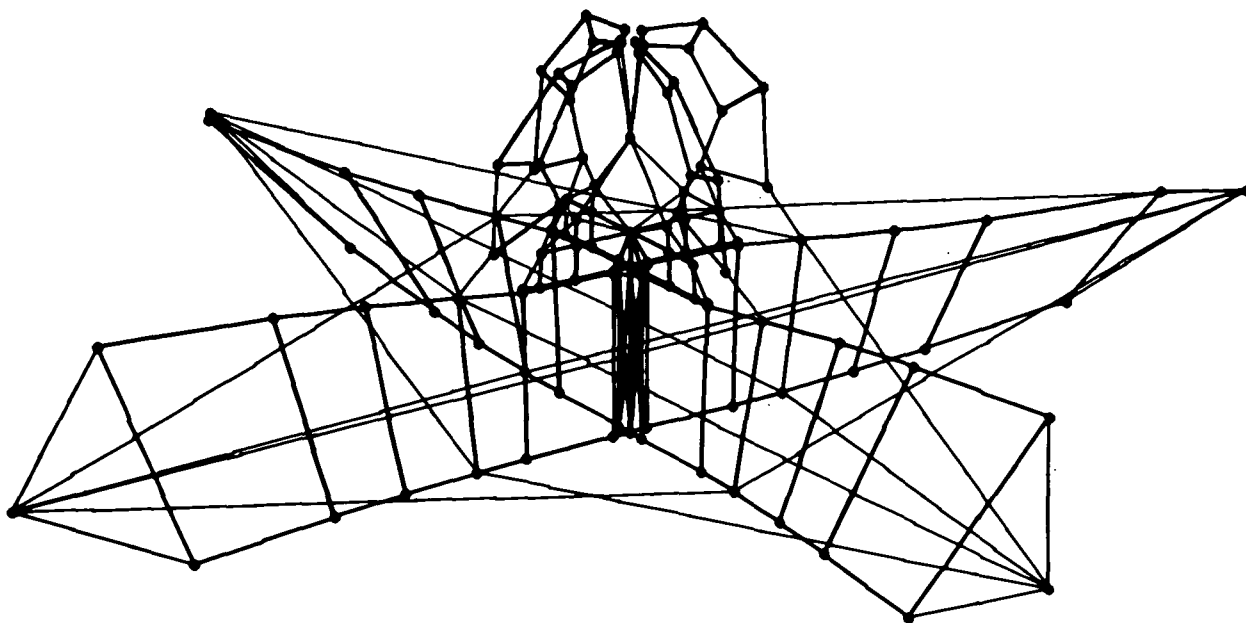


MODAL DEFORMATION - SUBCASE 1    MODE 5  
EIGENVALUE = 141713.83000    FREQ. 59.9 HZ

FIGURE 3-35. MODE SHAPE, MODES 4 AND 5

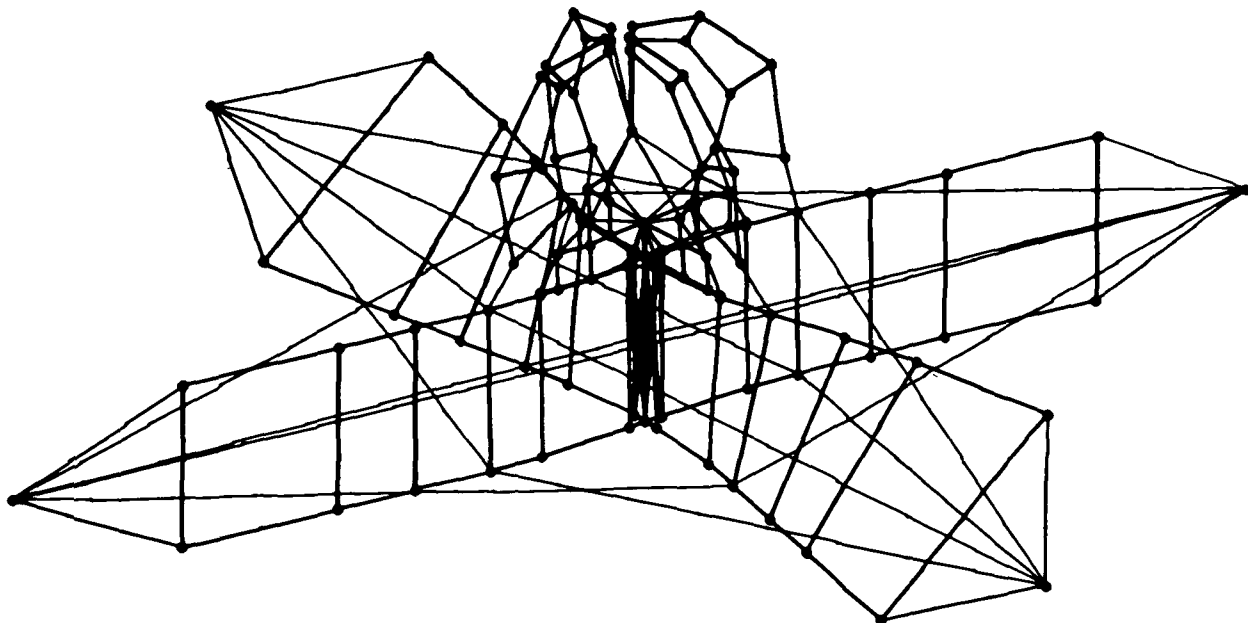


MODAL DEFORMATION - SUBCASE 1 MODE 6  
EIGENVALUE = 142355.65000 FREQ. 60.0 HZ

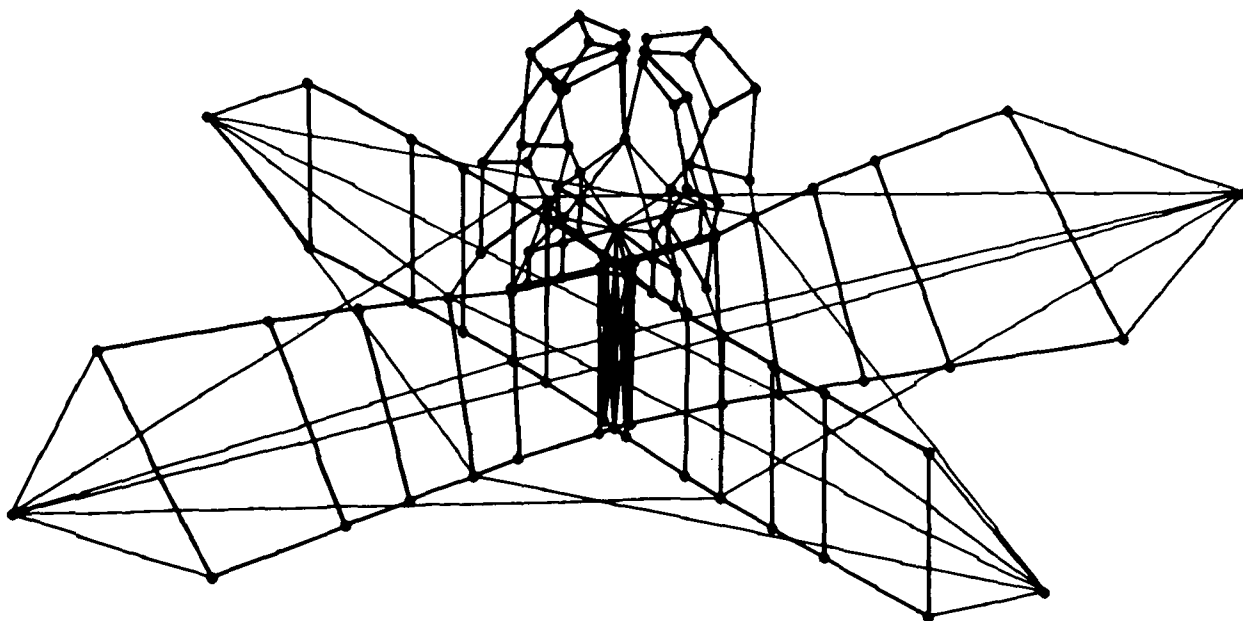


MODAL DEFORMATION - SUBCASE 1 MODE 7  
EIGENVALUE = 155730.41000 FREQ. 62.8 HZ

FIGURE 3-36. MODE SHAPE, MODES 6 AND 7

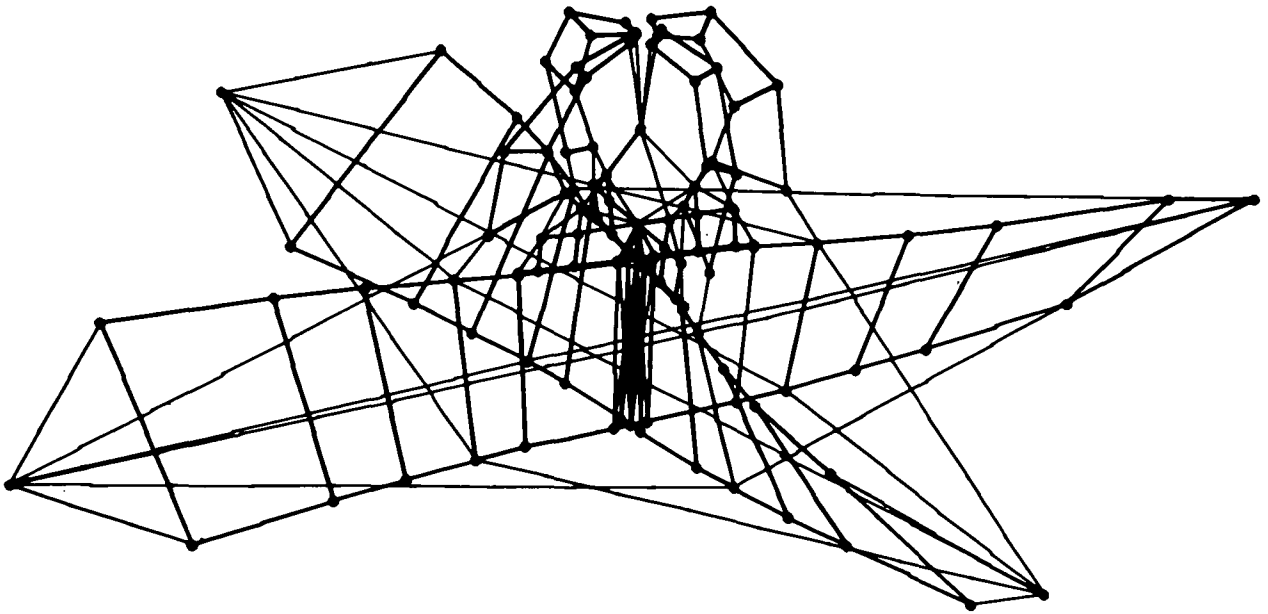


MODAL DEFORMATION - SUBCASE 1 MODE 8  
 EIGENVALUE = 181495.98000 FREQ. 67.8 HZ

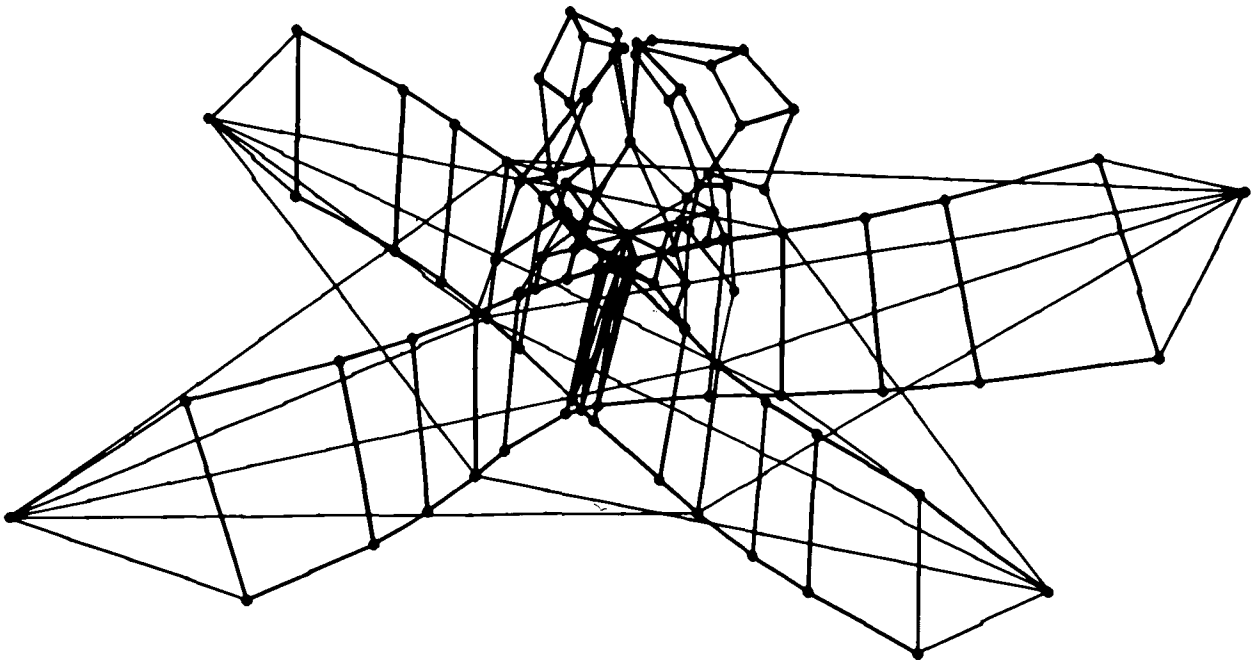


MODAL DEFORMATION - SUBCASE 1 MODE 9  
 EIGENVALUE = 180629.69000 FREQ. 67.6 HZ

FIGURE 3-37. MODE SHAPE, MODES 8 AND 9



MODAL DEFORMATION - SUBCASE 1    MODE 10  
EIGENVALUE = 238102.00000    FREQ. 77.7 HZ



MODAL DEFORMATION - SUBCASE 1    MODE 11  
EIGENVALUE = 1487162.90000    FREQ. 194.0 HZ

FIGURE 3-38. MODE SHAPE, MODES 10 AND 11

factor is 6.8 at a frequency of 13 Hertz. Figures 3-39 and 3-40 present the structural response amplification factor for the center of mass of the Satellite for the lateral and longitudinal axes, respectively, as a function of frequency. Also shown on these figures is the input accelerations which correspond to the specification presented in Table 3-9. The response of the Satellite to the excitation acceleration is the product of the excitation acceleration and the amplification factor at a given frequency. Tables 3-10, 3-11, 3-12, and 3-13 present the printouts of the NASTRAN program of the structural response characteristics of the Satellite center of mass for the longitudinal and lateral axes. The values presented in these tables represent amplification factors, having been obtained using a constant 1-g acceleration input. Tables 3-10 and 3-12 give the acceleration response of the Satellite, where  $T_1$ ,  $T_2$ , and  $T_3$  are the acceleration vectors in the X, Y, and Z directions, respectively, and presented in inches/second/second.  $R_1$ ,  $R_2$  and  $R_3$  are the angular acceleration values about the X, Y, and Z axes, respectively, and are presented in radians/second/second. Tables 3-11 and 3-13 give the displacement response of the Satellite, where  $T_1$ ,  $T_2$  and  $T_3$  are the displacements, in inches, in the X, Y, and Z directions, respectively.  $R_1$ ,  $R_2$ , and  $R_3$  are the angular displacements, in radians, about the X, Y, and Z axes, respectively.

From the dynamic analysis results of the support structure it is apparent that the longitudinal response (Y axis) is not excessive; however, the transverse, or lateral (X or Z axis), response produces accelerations of 25.8 g's peak at 18.9 Hz, which is excessive, and indicates that some modification to the support structure is needed to improve its lateral response characteristics. Although sufficient analysis has not been conducted to fully determine the most appropriate changes, it is believed that one modification needed is to reduce the eccentricity between the center of mass of the Satellite and the neutral axis of the main cross beams, which is the main cause for the high lateral frequency response of the support structure. Other possible modifications are to increase the stiffness of the holddown arms and to improve the torsional stiffness of the cross beams.

#### 3.4.6 ACOUSTIC ENVIRONMENT

The acoustical environment for the Satellite and its support structure was based upon previously developed Saturn IB/ATM data and is shown in Figure 3-41. There was no analysis of the support structure conducted for the acoustical environment because it is

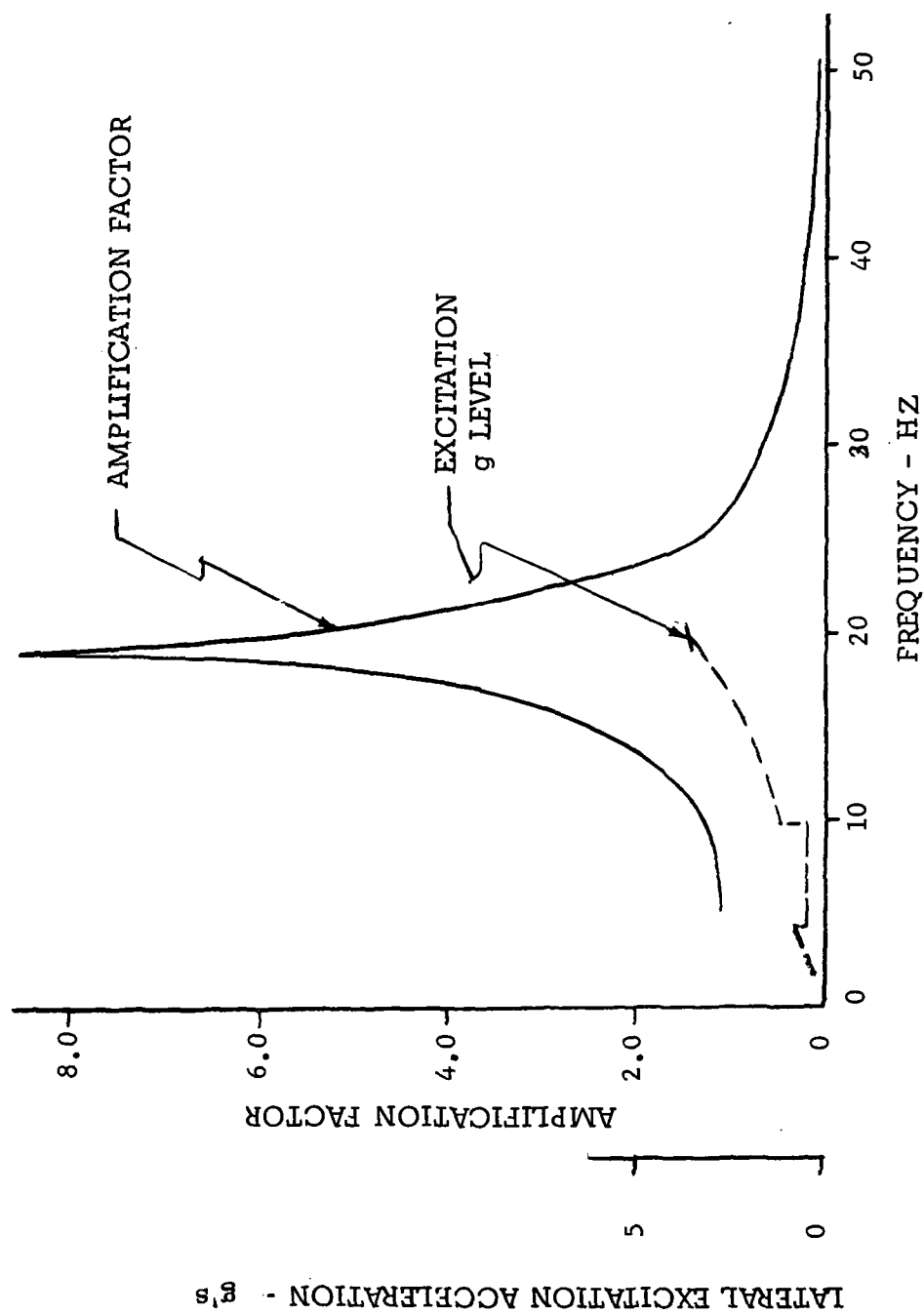


FIGURE 3-39. LATERAL AMPLIFICATION FACTOR VERSUS FREQUENCY



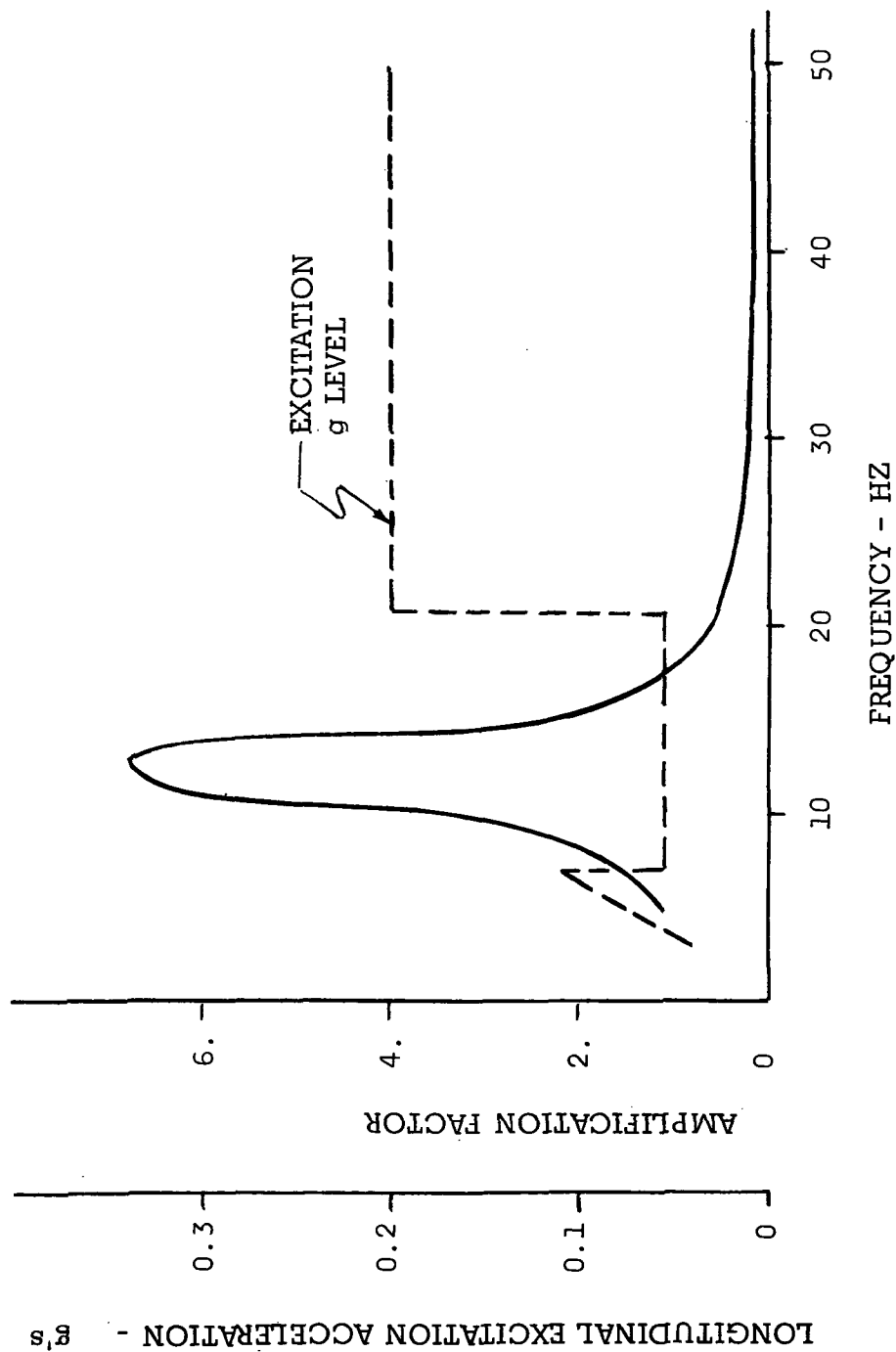


FIGURE 3-40. LONGITUDINAL AMPLIFICATION FACTOR VERSUS FREQUENCY

TABLE 3-10. LONGITUDINAL AXIS ACCELERATION RESPONSE

Y-AXIS EXCITATION POINT-ID =		C.O.M.P.L.E.X. A.C.C.E.L.E.R.A.T.I.O.N. V.E.C.T.O.R. (MAGNITUDE/PHASE)										SUBCASE 1	
FREQUENCY	TYPE	T1	T2	T3	M1	R2	M3						
5.02500000	6	4.999371-03 172.7541	4.595551+02 358.9166	3.747340-12 359.8336	6.981264-14 357.4158	8.440406-13 14.0685	4.481845-04 353.0735						
5.64418900	6	4.866195-03 172.2479	4.846176+02 358.5451	5.043525-12 355.9443	1.195475-13 356.6660	3.193326-13 36.3209	6.061579-04 352.6592						
6.37137500	6	9.672277-03 171.5336	5.207412+02 358.0395	5.457216-12 353.5915	1.811010-13 354.4259	2.234888-12 176.7278	8.371287-04 352.0654						
7.19224900	6	1.412999-02 175.4857	5.752376+02 357.2009	1.542027-11 354.3715	1.842275-13 354.9346	1.149376-12 156.0191	1.191950-03 351.1760						
8.11688300	6	2.180488-02 168.6489	6.633384+02 355.8911	4.266308-12 163.4152	4.238330-14 145.6925	3.347317-12 162.3097	1.777891-03 349.7509						
9.16490300	6	3.678754-02 166.0101	8.227540+02 353.5098	1.765938-11 345.9631	4.106826-13 345.5914	6.593652-13 115.9314	2.872530-03 347.1985						
1.03456901	6	7.328238-02 159.9727	1.177311+03 348.1347	1.083986-11 347.7998	2.217401-13 346.2170	1.231050-12 57.1453	5.399521-03 341.5564						
1.16766101	6	2.151277-01 138.6720	2.398898+03 327.8440	4.770835-12 116.5326	1.072707-13 120.3503	1.033958-11 108.9810	1.466271-02 320.8177						
1.31832501	6	3.592449-01 37.0507	2.634477+03 227.8938	4.966167-11 224.1388	1.196819-12 221.3445	1.209251-11 223.4760	2.201098-02 220.0299						
1.48617801	6	2.099463-01 5.1764	9.211972+02 199.2039	9.216839-12 196.4814	3.186806-13 193.9058	3.993593-11 302.3354	1.106691-02 189.4759						
1.67990901	6	2.261856-01 350.6189	4.873111+02 192.7284	2.938987-11 173.6997	6.999730-13 172.3680	1.786713-12 111.4947	9.536677-03 177.2513						
1.89634501	6	4.529715-01 305.1916	3.042075+02 190.0125	3.065078-11 129.1141	7.685132-13 128.0645	1.321361-12 31.2259	1.331200-02 136.8773						
2.14066601	6	1.916651-01 212.8475	2.061334+02 168.5455	1.780111-11 36.7714	9.615938-13 36.3686	2.310908-13 48.3954	2.821827-03 62.1330						
2.41646501	6	7.684373-02 196.8868	1.465569+02 187.0365	2.672592-12 28.1845	7.214401-14 29.1655	3.099321-14 149.0357	8.210052-04 143.2287						
2.72779701	6	4.316788-02 191.4621	1.075194+02 187.0191	7.228507-13 25.2897	2.190609-14 28.6095	7.066183-14 51.8498	1.329569-03 172.2520						

TABLE 3-11. LONGITUDINAL AXIS DISPLACEMENT RESPONSE

Y-AXIS EXCITATION POINT-10		COMPLEX DISPLACEMENT VECTOR (MAGNITUDE/PHASE)							SUBCASE 1	
FREQUENCY	TYPE	T1	T2	T3	R1	R2	R3			
5.00000000	G	5.065422-06 352.7591	4.656267-01 178.9166	3.796546-15 179.8336	7.073500-17 177.4130	8.596136-16 194.0685	4.541058-07 173.0735			
5.04410000	G	5.459505-06 352.2474	3.853331-01 178.5451	4.010249-15 175.9443	9.505562-17 176.6659	2.539103-16 216.3209	4.819732-07 172.6592			
6.37137500	G	6.035353-06 351.5338	3.2449345-01 178.3095	3.405219-15 173.5914	1.136042-16 174.4259	1.394536-15 356.7278	5.223556-07 172.0654			
7.19224900	G	6.919150-06 353.4857	2.816814-01 177.2009	5.132578-15 174.3715	9.021222-17 174.9345	5.628243-16 336.3191	5.836722-07 171.1760			
8.11888300	G	8.379177-06 348.8489	2.549076-01 175.8911	1.640225-15 343.4152	1.628705-17 325.6925	1.286337-15 342.3097	6.835997-07 169.7509			
9.16449300	G	1.109392-05 346.3101	2.481159-01 173.5098	5.325493-15 165.9631	1.230485-16 165.5914	1.988431-16 295.9314	8.662617-07 167.1985			
1.03456900	G	1.734287-05 339.9727	2.786203-01 168.1347	2.565342-15 167.7998	5.247658-17 166.2170	2.913380-16 237.1453	1.277840-06 161.5564			
1.16786100	G	3.995348-05 318.6720	4.455229-01 147.8440	8.860385-16 296.5326	1.992229-17 300.3503	1.864549-15 288.9810	2.723156-06 140.8177			
1.31832500	G	5.236560-05 217.0527	3.839660-01 47.8938	7.237963-15 44.1388	1.744309-16 41.3444	1.762428-15 43.9763	3.208001-06 40.0499			
1.40817600	G	2.401837-05 195.1764	1.053621-01 19.2034	1.054178-15 16.4814	3.645030-17 13.9058	4.564249-15 122.3354	1.265780-06 9.4759			
1.67990900	G	2.034176-05 17.66189	4.373963-02 12.7284	2.637949-15 353.6997	6.282754-17 352.3880	1.603732-16 291.4997	8.559844-07 357.2513			
1.89634500	G	3.190635-05 125.1918	2.142770-02 10.0125	2.158972-15 309.1141	5.413235-17 308.0645	9.307374-17 211.2255	9.376673-07 316.8773			
2.14066600	G	1.059464-05 32.8475	1.139438-02 8.5455	9.839873-16 216.7714	2.551540-17 216.3686	1.277395-17 228.3954	1.559814-07 242.1330			
2.41646500	G	3.333272-06 16.8868	6.357489-03 7.8365	1.159343-16 208.1845	3.129533-18 259.1655	1.344454-18 329.0357	3.561436-08 323.2287			
2.72779700	G	1.469324-06 11.4621	3.660182-03 7.0191	2.460734-17 205.2698	7.457288-19 208.6095	2.405476-18 231.8498	4.526133-08 352.2520			

TABLE 3-12. LATERAL AXIS ACCELERATION RESPONSE

X-AXIS EXCITATION		COMPLEX LATERAL ACCELERATION VECTOR (MAGNITUDE/PHASE)										SUBCASE 2	
POINT-10 =		T1	T2	T3	R1	R2	R3						
FREQUENCY	TYPE												
5.000000+00	G	4.116245+02 359.6234	5.093486+03 172.8033	3.171658+12 172.4136	1.030079+13 170.0099	3.125541+12 181.5525	5.901616+01 173.8544						
5.644189+00	G	4.191731+02 359.5136	6.974910+03 172.3103	3.544206+12 178.2214	1.012986+13 176.1284	2.659343+12 186.5921	7.679473+01 173.7273						
6.371375+00	G	4.292264+02 359.3599	7.796237+03 171.6125	1.994056+12 352.7476	4.324108+14 352.2963	8.123045+12 177.0179	1.005517+00 173.5579						
7.192249+00	G	4.427984+02 359.1554	1.425765+02 170.5843	7.225830+13 184.6289	2.906539+14 173.8411	8.216950+12 178.3411	1.327586+00 173.3293						
8.118883+00	G	4.614622+02 358.8730	2.189926+02 168.9717	1.966207+12 348.0012	5.318717+14 348.1746	2.941272+12 195.8219	1.772763+00 173.0156						
9.164903+00	G	4.877785+02 358.4725	3.673313+02 166.1616	5.134543+12 346.7635	1.584049+13 348.3884	5.235931+12 184.9904	2.404672+00 172.5745						
1.034569+01	G	5.262477+02 357.8830	7.265455+02 160.1583	2.652385+12 347.2232	7.458014+14 346.8226	1.662547+11 173.4208	3.335746+00 171.9321						
1.167661+01	G	5.855140+02 356.9665	2.114497+01 138.8948	4.335596+13 320.4013	2.224412+14 195.5805	2.243812+11 168.1759	4.784332+00 170.4468						
1.318325+01	G	6.684501+02 355.4156	3.495357+01 37.3129	5.225580+12 343.8137	8.516554+14 345.2134	2.713943+11 162.0428	7.234909+00 169.3359						
1.488176+01	G	6.746544+02 352.3865	2.318673+01 5.4750	1.245176+11 157.7920	4.081394+13 157.7990	1.289145+10 111.2466	1.200504+01 166.1581						
1.679939+01	G	1.351095+03 344.5063	2.145570+01 350.9417	9.372794+12 144.5818	2.390391+13 144.5836	4.522661+11 15.6699	2.423637+01 158.1198						
1.896345+01	G	3.256347+03 342.0596	4.237765+01 305.5396	4.331989+10 234.4626	1.093244+11 234.4436	8.527566+11 318.4277	7.691832+01 115.4600						
2.146660+01	G	1.508119+03 211.5338	1.770692+01 213.1024	2.421812+11 36.7893	7.169317+13 35.4004	3.117861+12 271.7065	4.744620+01 24.6415						
2.416465+01	G	6.196812+02 196.9592	7.041650+02 196.9754	8.460806+12 18.0277	2.479864+13 14.9584	3.945863+12 211.6993	2.631297+01 9.6551						
2.727747+01	G	3.378732+02 192.8238	3.964334+02 191.2146	3.289462+12 12.1674	4.049653+14 27.6045	5.381717+13 237.0299	1.977772+01 4.9166						

TABLE 3-13. LATERAL AXIS DISPLACEMENT RESPONSE

X-AXIS EXCITATION		COMPLEXP L A C E M E N T V E C T O R										SUBCASE 2	
POINT-10 "		(MAGNITUDE/PHASE)											
FREQUENCY	TYPE	T1	T2	T3	R1	R2	R3						
5.00000000	6	4.170628-01 179.6239	5.157741-06 352.8033	3.213561-15 352.4136	1.043668-16 350.0049	3.166836-15 1.5525	5.979587-04 353.8544						
5.64418900	6	3.332964-01 179.5108	5.545947-06 352.3163	2.818098-15 358.2214	8.054535-17 356.1284	2.074762-15 8.5921	6.106165-04 353.7273						
6.37137500	6	2.678307-01 179.3599	6.112703-06 351.6125	1.244260-15 172.7476	2.698178-17 172.2963	5.666789-15 357.0179	6.274272-04 353.5579						
7.19224900	6	2.168287-01 179.1554	6.981660-06 350.5843	3.538332-16 4.6289	1.423269-17 353.8411	4.223662-15 358.3411	6.650399-04 353.3293						
8.11868300	6	1.773294-01 176.8730	8.415444-06 346.4717	7.555737-16 168.0012	2.043876-17 168.1746	1.130272-15 15.8219	6.812372-04 353.0156						
9.16490300	6	1.470961-01 178.4725	1.167752-05 346.1618	1.546411-15 166.7605	4.776978-17 168.3084	1.578986-15 4.9903	7.251709-04 352.5745						
1.03456901	6	1.245408-01 177.8830	1.719429-05 340.1580	6.276375-16 167.2232	1.753166-17 166.8226	3.934552-15 350.4208	7.894312-04 351.9322						
1.16786101	6	1.087415-01 176.9605	3.927039-05 318.8948	8.068900-17 140.9013	4.136746-18 5.5805	4.167203-15 348.1759	8.885396-04 350.9468						
1.31832501	6	9.977471-02 175.5156	5.394325-05 217.3129	7.616346-16 163.8107	1.241176-17 165.2104	3.955449-15 342.8428	1.054455-03 342.3059						
1.48817601	6	1.000368-01 172.3865	2.308862-05 185.4750	1.424172-15 337.7920	4.668103-17 337.7990	1.474463-14 291.2466	1.373423-03 346.1581						
1.67990901	6	1.212703-01 164.5063	1.925801-05 170.9917	8.412747-16 324.5618	2.143545-17 324.5636	4.059408-15 195.6709	2.175366-03 338.1198						
1.89634501	6	2.293698-01 122.0596	2.965001-05 125.5096	3.051356-14 54.4626	7.700564-16 54.4936	6.006627-15 138.4277	5.417954-03 295.4603						
2.14060601	6	6.336366-02 31.5338	9.787806-06 33.1024	1.338698-15 216.7893	3.962965-17 215.4004	1.723452-16 91.7065	2.622460-03 204.6415						
2.41642501	6	2.688961-02 16.4592	3.054595-06 16.9753	3.670211-16 198.0277	1.075739-17 194.9564	1.711675-16 31.6993	1.141429-03 189.6551						
2.72779701	6	1.150191-02 12.8208	1.349542-06 11.2146	1.119801-16 192.1674	1.378586-18 247.6095	1.832049-17 57.3299	6.732597-04 184.9166						

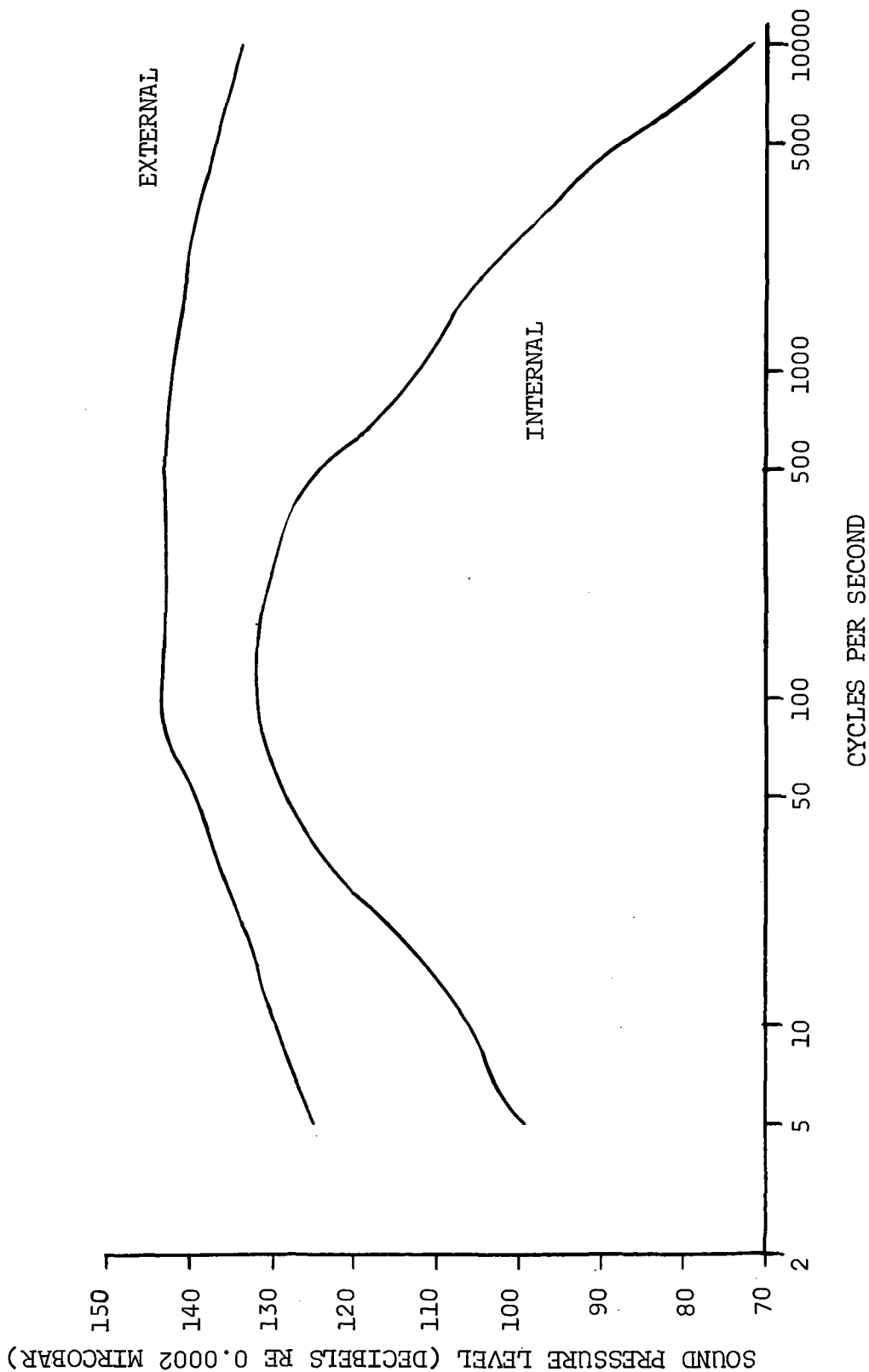


FIGURE 3-41. SOUND PRESSURE LEVEL VERSUS FREQUENCY  
SATURN S-IB/S-IVB/ATM-SLA

expected that the acoustical environment would not be as severe as the sinusoidal vibration cases. The acoustical specification given shows the internal and external environment. The maximum levels for both internal and external cases are in a frequency range of 100 to 200 Hz and since this is far above significant sinusoidal disturbances, it was assumed that no coupling would occur.

### 3.5 PAYLOAD SYSTEMS MASS SUMMARY

The total mass above the Instrument Unit was computed to be 2658.1 kg (5,778 lb). Table 3-14 is a summary table listing primary hardware elements and their associated weights. The payload support structure consisting of main cross beams, payload mount, holddown arms, and purge cover assembly has a mass of 366.9 kg (809 lb). Power supply and ordnance weight is 9.1 kg (20 lb), and the purge supply system mass is 6.4 kg (14 lb). Both the SLA and nose cone are developed hardware items with masses of 1791.7 kg (3,868 lb) and 484 kg (1,067 lb), respectively. Structural masses presented in Table 3-14 were determined with a minimum design safety factor of 1.4. These masses do not necessarily agree with those presented in Section 4.0 since they are the results of later analysis and were not considered in the mission planning. The additional requirement can be met by the proposed payload improvement consideration.

TABLE 3-14. PAYLOAD SYSTEMS MASS SUMMARY

<u>Item</u>	<u>Mass - kg and (lbm)</u>
Payload Support Structure	366.9 (809)
Main Cross Beams	263.5 (581)
Upper Flanges	42.2 ( 93)
Lower Flanges	31.3 ( 69)
Webs	71.2 (157)
Transverse Stiffeners	21.3 ( 47)
Longitudinal Stiffeners	18.6 ( 41)
End Fittings	27.2 ( 60)
External Cylinder	10.0 ( 22)
Gussets	8.6 ( 19)
Tierods and Attachments	26.3 ( 58)
Miscellaneous Fittings	6.8 ( 15)
Payload Mount	56.7 (125)
Frame Assembly	18.6 ( 41)
Internal Cylinder	3.6 ( 8)
Ejection Spring	22.7 ( 50)
Release Mechanism	11.8 ( 26)
Holddown Arms	36.7 ( 81)
Purge Cover Assembly	10.0 ( 22)
Power Supply and Ordnance	9.1 ( 20)
Purge Supply System	6.4 ( 14)
SLA	1791.7 (3868)
Nose Cone	<u>484.0 (1067)</u>
TOTAL	2658.1 (5778)



## SECTION 4. LAUNCH VEHICLE CONFIGURATION DEFINITION

### 4.1 CONFIGURATION SUMMARY

This study considers only the Saturn IB configuration for the SEPS launch vehicle. This launch vehicle consists of an S-IB for the first stage, a Saturn V or Saturn IB/S-IVB as the second stage and a Saturn IB Instrument Unit. The payload (everything above the Instrument Unit) consists of a SLA/Nosecone external similar to AS-204 configuration with the 3628 kilograms (8000 lb) SEPS enclosed within the SLA.

The desired SEPS orbit requires an S-IVB capable of re-starting to circularize the orbit at the proper altitude. A Saturn IB/S-IVB may be modified to obtain this restart capability or a Saturn V/S-IVB with this capability already existing may be modified to mate with the S-IB stage.

The launch vehicle recommended based upon availability, performance characteristics and cost consists of S-IB stage SA-212, S-IVB stage SA-513 and Instrument Unit S-IU-212. The estimated mass data for this vehicle is tabulated in Table 4-1.

### 4.2 S-IB STAGE MODIFICATION DEFINITION AND INTERFACES

#### 4.2.1 S-IB STAGE MODIFICATIONS

No modifications are required to adapt the S-IB Stage for the SEPS mission. Functionally the S-IB Stage is adequate as the first stage is boosting the 3628 kilograms (8000 lb) SEPS into the 3719 kilometer (2008 NM) orbit. Studies performed on the S-IB stage for this configuration have revealed no mechanical or functional problems that would prevent the accomplishment of this mission. Areas of investigation were structural capability, structural dynamics and interface; the results of these analyses can be found in references 3 through 6.

#### 4.2.2 S-IB STAGE SELECTION FOR SEPS

The present S-IB stage availability status has nine S-IB stages in some state of readiness from which a selection can be made for the SEPS mission. Stages 206 through 212 are complete stages, and stages 213 and 214 are complete with the exception of fins. S-IB stages 206

TABLE 4-1. EARTH PHYSICS SATELLITE - PHASE B STUDIES  
VEHICLE MASS BREAKDOWN

	MASS	
	<u>kilograms</u>	<u>(lbm)</u>
PAYLOAD (SEPS)	3636.8	(8018)
Payload Attach.	338.8	(747)
SLA (Fixed)	598.7	(1320)
Instrument Unit	2041.1	(4500)
S-IVB Sep. (Dry & Residuals)	12550.8	(27670)
Flight Performance Reserve	1011.5	(2230)
Weight In Orbit Less Payload	16541.0	(36467)
S-IVB Thrust Decay Prpt. (2nd Burn)	35.4	(78)
S-IVB Mainstage Propt. (2nd Burn)	3266.7	(7202)
S-IVB Build Up & Start Prpt. (2nd Burn)	212.7	(469)
Losses in Orbit (LOX, LH <sub>2</sub> , APS)	400.1	(882)
SLA/NC Jettison	1639.7	(3615)
S-IVB Consumed & Jettisoned (2nd Burn)	5554.7	(12246)
S-IVB Thrust Decay Prpt. (1st Burn)	37.6	(83)
S-IVB Mainstage Prpt. (1st Burn)	101058.9	(222798)
Ullage Cases	59.9	(132)
S-IVB Consumed & Jettisoned (1st Burn)	101156.5	(223013)
S-IVB STAGE IGNITION MASS	123342.9	(271926)
Misc. Sep. Sys. Comp.	23.1	(51)
Ullage Propellant	53.5	(118)
S-IVB Build Up & Start Prpt.	187.3	(413)
Interstage	3084.4	(6800)
S-IB Sep. (Dry & Residuals)	43030.7	(94867)
S-IB Stage Jettison Mass	46379.1	(102249)
S-IB/S-IVB Frost	498.9	(1100)
Gear Box Fuel Consumed & Ser. Items	333.4	(735)
Outboard Engine T.D. Prpt. to Sep.	755.2	(1665)
Inboard Engine T.D. Prpt.	984.3	(2170)
Mainstage Propellant Consumed	401123.7	(884331)
S-IB Consumed Weight at Separation	403695.6	(890001)
S-IB STAGE IGNITION MASS	450074.7	(992250)
LIFTOFF MASS	577054.5	(1272194)

through 209 are presently committed to the Skylab program. Stages 210 through 214 have no firm commitment; however, several options are being considered to utilize these stages. All completed S-IB stages (206 through 212) have an assigned S-IVB stage with the exception of S-IB-212. The S-IVB stage for S-IB-212 was modified to accommodate the Saturn Work Shop (SWS) and is presently scheduled as part of the SA-513 mission. The S-IB-212 presently has no assigned S-IVB stage and would not interfere with other planning if selected for the SEPS Mission.

The S-IB-212 stage was static fired on July 25, 1968 and placed in storage at MAF on June 30, 1969. The stage was relocated to MSFC and re-entered into storage on August 20, 1970. No SEPS peculiar modifications are required for this stage, assuming that all electrical interfaces will be made compatible on the selected S-IVB stage.

#### 4.3 S-IVB STAGE

##### 4.3.1 S-IVB STAGE MODIFICATIONS (References 7 and 8)

This SEPS mission imposes on the second stage of the Saturn IB launch vehicle two unique requirements: additional auxiliary propulsion requirements and a J-2 engine restart requirement.

##### 4.3.1.1 AUXILIARY PROPULSION SYSTEM REQUIREMENTS

Table 4-2 presents the required Auxiliary Propulsion System (APS) impulse usage for the baseline vehicle of the SEPS mission. Maneuvering rates used in the analyses are assumed to be 0.3 deg/sec in the steering planes and 0.5 deg/sec in the roll plane. Main engine thrust misalignment and CG offsets are taken to be 1.0 degree and 7.62 cm (3.0 inches) respectively.

Disturbances during first and second burn consist of:

1. Separation transients (first burn only)
2. J-2 engine exhaust swirl torques during both burns
3. Cutoff transients (first burn only)
4. J-2 engine fuel lead prior to second restart

The S-IVB/IB stage APS does not have axial thrusters for propellant settling (ullaging) or evasive maneuver capability. The

TABLE 4-2. SMITHSONIAN SATELLITE MISSION  
SEPS MISSION APS USAGE

	IMPULSE	
	<u>Newton-Sec</u>	<u>(Lbf-Sec.)</u>
FIRST BURN		
Disturbance Control	16458	(3, 700)
COAST - 1 HOUR		
P/L Shroud release - local horizontal maneuver	6672	(1, 500)
Limit cycle operation	3425	(770)
CVS disturbance	3603	(810)
SECOND BURN		
Propellant settling & O <sub>2</sub> H <sub>2</sub> Burner disturbances	147325	(33, 120)
Disturbance control	979	(220)
COAST - 2 HOUR		
P/L Jettison Maneuvers	2135	(480)
Evasive Maneuver	102309	(23, 000)
Limit cycle operation	<u>6850</u>	<u>(1, 540)</u>
	294204	(65, 140)
TOTAL AVAILABLE: S-IVB/IB - 122771 Newton-sec (27, 600 lbf-sec.)		
TOTAL AVAILABLE: S-IVB/V - 327389 Newton-sec (73, 600 lbf-sec.)		
(50 percent loading)		

Saturn V APS has this capability. If a Saturn V APS is used, the ullage thrusters on the system will be used for propellant settling and will increase the nominal APS impulse requirement by 140653 Newton-seconds (31,620 lb-sec). In addition, disturbances, caused by the  $O_2H_2$  burner on the S-IVB/V will add another 6672 Newton-seconds (1,500 lb-sec). The total requirements for propellant settling and  $O_2H_2$  burner disturbance is 147325 Newton-sec (33,120 lb-sec) over the nominal requirements. If the S-IVB/IB APS is used, provisions are required for propellant settling and evasive maneuver capabilities. For either case, the impulse requirement for the S-IVB/IB vehicle or S-IVB/V vehicle will be respectively only 33 percent or 57.5 percent (based on an APS loading of 50 percent) of the total impulse available per vehicle, excluding the evasive maneuver.

The S-IVB/V APS is being recommended for the SEPS mission and will be offloaded by the maximum test verified amount of 50 percent to increase payload capability. Based on a 20 percent flight performance reserve and 8.2 kilograms (18 pounds) of unusable propellant, 45.4 kilograms (100 pounds) of APS propellant is available for the evasive maneuver.

In low earth orbit, the evasive maneuver requires a single maneuver involving an impulse from the auxiliary propulsion system (APS) or a LOX dump. Either would be sufficient to lower the perigee of the spent S-IVB stage, allowing its orbit to rapidly decay. Due to the altitude involved in the SEPS mission, the decay cannot be relied upon to provide adequate separation between payload and stage. Therefore, the evasive maneuver would involve two impulses, the first to lower the stage perigee and the second, at the new perigee, to lower the apogee so that it will not coincide with the SEPS altitude.

The  $\Delta V$  capability of the APS is plotted in Figure 4-1 as a function of S-IVB/APS propellant consumption. If the APS was fully loaded at liftoff about 190.5 kilograms (420 pounds) of propellant would remain for the evasive maneuver. This propellant quantity allows for all ullaging and attitude requirements, including attitude requirements during the coast between first and second evasive burns. The maximum evasive maneuver  $\Delta V$  capability for the APS is then on the order of 25.9 meters/sec (85 ft/sec). Added to this an estimated LOX dump capability of 6.1 meters/sec (20 ft/sec) makes the total maximum  $\Delta V$  capability for the evasive maneuver of 32 meters/sec (105 ft/sec). If all of this  $\Delta V$  capability is utilized, the S-IVB stage orbit can be dropped below the SEPS Satellite orbit by as much as 101.8 kilometers (55 nautical miles), assuming the stage is put in a circular orbit. As currently foreseen, the APS will be loaded halfway, leaving only 45.4

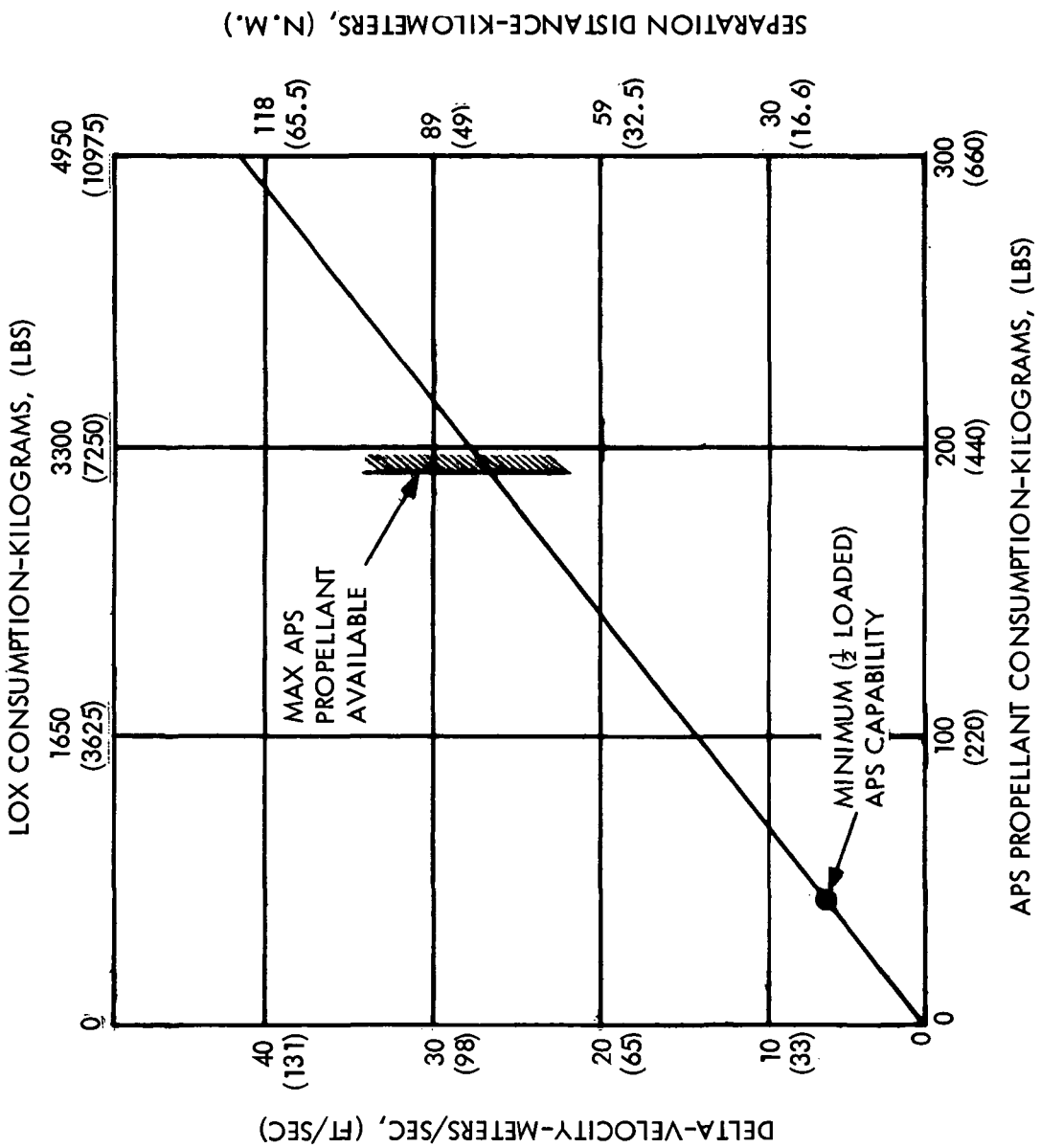


FIGURE 4-1. APS PERFORMANCE CAPABILITY

kilograms (100 pounds) for the evasive maneuver. This corresponds to a total  $\Delta V$  capability, excluding LOX dump, of 6.1 meters/sec (20 ft/sec). The resulting orbit would be 18.5 kilometers (10 nautical miles) below the SEPS orbit.

#### 4.3.1.2 ENGINE SYSTEM REQUIREMENTS

In order to meet the requirements of the SEPS mission, restart is required after a 1/2 orbit coast period. The 1/2 orbit (one hour) restart violates Rocketdyne's present constraint of a minimum coast period of 80 minutes prior to restart. Rocketdyne recommends reducing the Start Tank energy by lowering the vent relief setting and retiming the Main Oxidizer Valve to obtain acceptable restart conditions. New Start Tank restart requirements will be  $792.9 \pm 33.47$  Newton/cm<sup>2</sup> ( $1150 \pm 50$  psi) and  $133 \pm 16^{\circ}\text{K}$  ( $240 \pm 30^{\circ}\text{R}$ ).

Rocketdyne recommends (Table 4-3) a five second fuel lead for restart after a one hour orbital coast as compared to Apollo's eight seconds. This change compensates for the lower thrust chamber jacket temperature. A five second fuel lead is contingent upon installation of insulation on the engine nozzle.

TABLE 4-3 J-2 ENGINE SEPS MODIFICATIONS

Modification requirements for 60 minute coast:

- a. Five second fuel lead
- b. Reduce Start Tank vent/relief setting to  $792.9 \pm 33.47$  Newtons/cm<sup>2</sup> ( $1150 \pm 50$  psia)
- c. Change Start Tank refill orifice
- d. Retime Main Oxidizer Valve
- e. Add J-2 Bell insulation (S-IVB/IB only)

5.5/4.8 MRCV selection based on start restraints of:

- a.  $5.0 \pm .2$  required for start
- b.  $4.5 \pm .2$  required for restart
- c. 4.8 acceptable for start and restart with lower start tank pressurization energy
- d. 5.5/4.5 MRCV range not available with present valve.

The Start Tank vent relief change will also affect first burn start and thus the Start Tank liftoff box. The allowable liftoff box will be defined during the flight-planning phase, and the associated chill-down sequence will be established during CDDT Test Verification.

Use of the 5.5/4.5 Mixture Ratio Control Valve (MRCV) results in increased performance over the 5.5/4.8 MRCV, but these valve settings miss the start requirement by 0.3. The 5.5/4.8 MRCV meets the first start requirement and deviates only 0.1 from the required restart range. Therefore, the 5.5/4.8 valve settings was selected for the SEPS mission with a lower start tank energy to compensate for this small deviation.

#### 4.3.2 SATURN IB/S-IVB STAGE

The Saturn IB versions of S-IVB require hardware modifications and/or additions (Figure 4-2) to meet the mission coast and restart conditions. These changes, which affect the LOX chilldown system, feed system, outlets, stage pneumatic system, slosh control baffles, repressurization, ullage (Sat V APS), electrical and LH<sub>2</sub> tank vent systems, are described below.

##### 4.3.2.1 LOX CHILLDOWN SYSTEM

The Saturn V LOX chilldown system feed line check valve can be installed directly by replacing a nut and a strainer. Installation of the check valve will prevent chill pump damage in the event of LOX backflow. The Saturn V LOX Diffuser will be installed on the existing return line by adding four bolts and a gasket. Addition of the diffuser minimizes disturbances to the LOX due to LOX chilldown return flow.

##### 4.3.2.2 ANTI-VORTEX SCREENS AND FLIPTOP SCREENS

The Saturn V LH<sub>2</sub> Tank Anti-vortex Screen and Fliptop Screen Assembly replaces the Anti-vortex Screen on the Saturn IB vehicle. The Saturn V LOX Tank Fliptop Screen can be installed directly on the Saturn IB outlet. Addition of the fliptop screens allows vapors, collected under the screens, to be rejected, thus preventing vapor ingestion into the feed lines.

##### 4.3.2.3 CONTINUOUS VENT SYSTEM

The Saturn V Continuous Vent System (CVS) will be added to the Saturn IB Vehicle. This system can be installed with minimal difficulty as was done in AS-203. The CVS addition will provide propellant settling during vehicle coast.



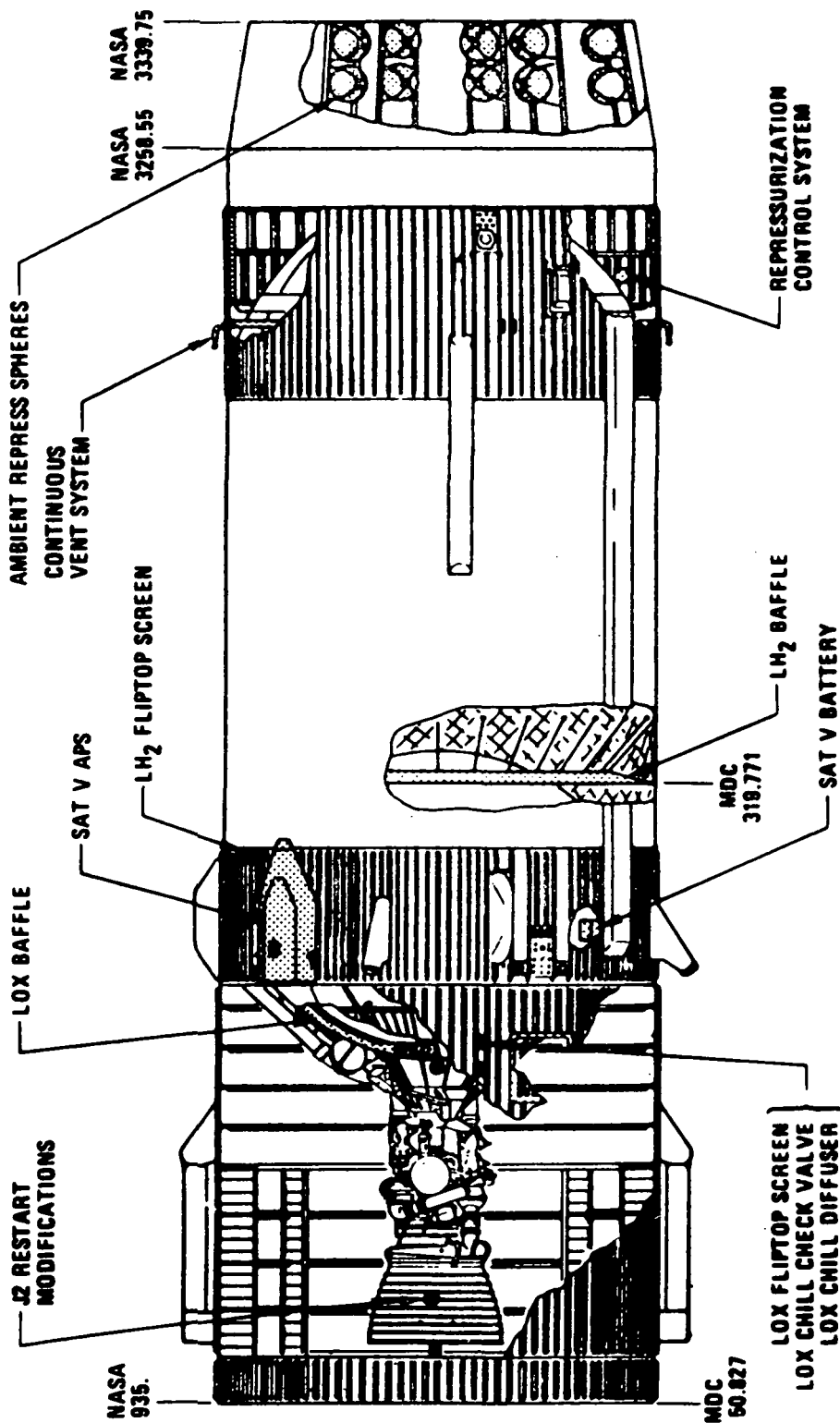


FIGURE 4.2 S-IVB/IB/SEPS MODIFICATIONS

#### 4.3.2.4 PNEUMATIC SYSTEM

The pneumatic system modifications consist of the addition of the Saturn V CVS Actuation Control Module and the addition of a purge bag around the pneumatic sphere with a GN<sub>2</sub> Purge Line from the Environmental Control System (ECS) to the purge bag.

#### 4.3.2.5 SLOSH CONTROL

The new nylon fabricated LH<sub>2</sub> Ring Baffle (Figure 4-3) is .558 meters (22 inches) long and is oriented at 15 degrees from the horizontal. The base of the Baffle is attached at station 319.771 to minimize slosh amplitudes at S-IVB cutoff and to provide adequate propellant damping during coast to ensure positive restart.

The new metallic LOX Baffle is cruciform in shape. Each leg of the cruciform is .152 meters (6. inches) high and placed 90 degrees apart. The upper end of the baffle legs are attached to the thrust cone structure-LOX tank interface. The base of the cruciform segments are attached to a 1.24 meters (49 inch) diameter metallic support ring. LOX slosh control is provided to ensure that propellant sloshing will not impair restart capability.

#### 4.3.2.6 REPRESSURIZATION SYSTEMS

The selection of candidate systems for propellant tanks repressurization was limited to the ambient and cryo repressurization systems used on the S-IVB/V, and cold helium blowdown through the LOX pressurization module (for LOX repressurization), because it is an available means on the S-IB. Cryo repressurization, which involves use of the O<sub>2</sub>H<sub>2</sub> burner, was eliminated because of the difficulty of installing a new line from the LH<sub>2</sub> tank to the burner (tank sealing problem). This left four candidates for consideration: (1) and (2) a forward (SLA) or aft (thrust structure) mounted ambient helium system; or (3) and (4), a combination of cold helium residual with either systems (1) or (2). Systems (1) and (2) require ten .127 cubic meter (4.5 ft<sup>3</sup>) storage spheres, seven for LH<sub>2</sub> tank repressurization and three for LOX tank repressurization. Systems (3) and (4) do not require any ambient helium spheres for LOX repressurization as there is enough cold helium residual available.

The ambient helium repressurization system for each propellant tank consists of high pressure storage spheres manifolded together, a repressurization module made up of two parallel shutoff valves, a dump valve and a filter, a flow controlling orifice, and the necessary

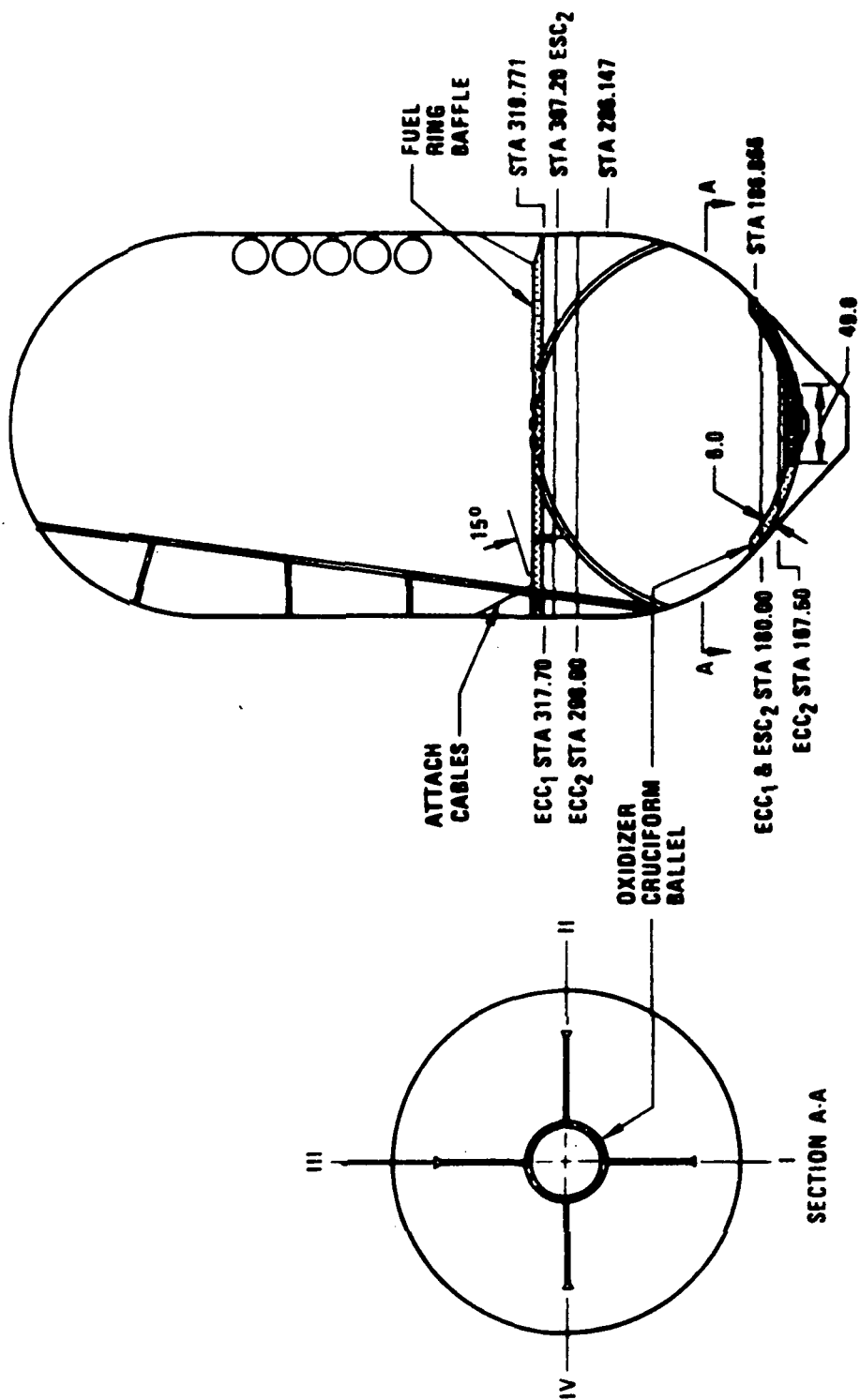


FIGURE 4.3 S-IVB SLOSH BAFFLE INSTALLATIONS

pipe assemblies. These items are included in the various S-IVB engineering drawings. The installation of the forward mounted system requires rework and additions to the SLA. This system is the same as designed for the AS-206 restart study. Aft mounting of the storage spheres requires a structural beefup of the thrust structure. This beefup consists of removing the forward intermediate frame (1A67839) and installing the heavier S-IVB/V thrust structure frame (1B52893).

The cold helium residual can be provided for LOX tank repressurization by using the LOX tank pressurization system as is. No mods are required.

The factors influencing the selection of one of the four candidate systems are cost, weight, reliability and demonstrated performance. The two candidates which incorporate aft-mounted storage spheres are more expensive than the corresponding forward mounted systems. The combination of LH<sub>2</sub> ambient repressurization and cold helium residual for LOX repressurization is more advantageous cost-wise, except that the repressurization performance of cold helium gas in flight has not yet been demonstrated. Therefore, based on a combination of cost and proven performance, the forward mounted system of LOX and LH<sub>2</sub> ambient repressurization is chosen.

The electrical circuits for all configurations are of comparable complexity. The engineering effort for the aft ambient installation is approximately 60 percent more than the forward installation, but the number of hours under consideration are not significant. The main difference in cost between forward and aft mounted systems is caused by the beefup requirement on the thrust structure.

#### 4.3.2.7 AUXILIARY PROPULSION SYSTEM

The Saturn V/S-IVB Auxiliary Propulsion System (APS) is recommended for installation on the Saturn IB/S-IVB Aft Skirt as the ullaging system used at first engine cutoff and just prior to engine restart and for altitude control and evasive maneuvers. The installation is a retrofit operation and will entail the following structural rework to the Aft Skirt.

- a. Remove the Saturn IB/IVB APS, the attach fittings, the environmental seal structures, and the Aft fitting internal support fittings and intercostals.
- b. Relocate the APS centerline .0365 meters (1.437 inches) toward stringer numbers 56 and 112.

- c. Install new attach fittings, internal support fittings and intercostals, environmental seal structure, and fairing attach channels and fittings.
- d. Strengthen the intermediate frame located at station 220.750 by the addition of a 1.61 square cm (0.250 square inch) strap to the inboard cap extending from the APS centerline to 1.02 meters (40 inches) on either side.

This installation can be made with a mated Saturn IB/S-IVB Aft Skirt.

#### 4.3.2.8 ELECTRICAL SYSTEM

The existing aft number 2 battery has a rating of 82800 coulombs (23 ampere-hours). The requirements for the restart mission amount to 111600 coulombs (31 ampere-hours). It is recommended that the qualified battery presently used on Saturn V, which has a capacity of  $27 \times 10^4$  coulombs (75 ampere-hours), be installed. This battery is made up of two boxes instead of one and requires a new installation. However, the electrical and structural design effort, prepared as part of the 206 restart study, are still applicable and can be released with minimum effort. The battery will be installed between stringers 102 and 105 and between stringers 2 and 3. Saturn V/S-IVB battery support intercostals are installed at the four noted stringer locations and the battery units are located on each side of panel position number 17. This arrangement requires no modification to the Saturn IB/S-IVB battery support structure.

The forward battery number 2 has a rating of 11520 coulombs (3.2 ampere-hours). The load demanded from this battery consists of the PU system which draws approximately four amperes and range safety system number 2 which draws approximately 0.3 amperes.

The PU electronics is used primarily for loading propellant and monitoring propellant status during flight. The battery will provide power for 45 minutes of flight. To eliminate the need for increasing the capacity of forward battery number 2, it is recommended that the PU System be shut off by a programmed command after first engine burn. It is turned on again prior to second engine start as it is not mandatory that the data be received during coasting flight for mission success.

#### 4.3.3 SATURN V/S-IVB STAGE

The basic Saturn S-IVB/V Stage is designed for a restart mission; therefore, modifications for the SEPS Mission are not extensive.

There are, however, certain modifications required due to the SEPS Mission peculiarities (i. e., low propellant residual restart).

The basic stage modifications include (Figure 4-4):

- Removal of present baffles.
- Installation of low residual baffles.
- Modification of existing repressurization system.
- Modification of S-IB Interstage.

#### 4.3.3.1 SLOSH CONTROL

To control fuel sloshing and to prevent venting of liquid hydrogen during orbital coast, the Saturn V/S-IVB stage employs a baffle and deflector assembly located in the forward end of the fuel tank. The inner tubular ring of the deflector and the supporting struts are aluminum parts and therefore represents a significant weight penalty. Due to the low fuel level of the SEPS Mission these items are removed, thereby providing a mass saving of 89.8 kilograms (190 pounds) and improving access to the fuel tank for subsequent rework. The propellant tank wall studs are left in place.

As described previously for the S-IVB/IB, a new fuel baffle is installed at station 319.771 for slosh control after engine cutoff and prior to engine restart. The LOX slosh baffle has a cruciform shape and extends from the thrust structure/aft dome intersection to 1.24 meter (49 inch) diameter support ring in the bottom of the tank.

#### 4.3.3.2 REPRESSURIZATION

The selection of candidate systems for propellant tank repressurization was limited to the cryo and ambient repressurization systems already installed on S-IVB/V and combinations of these systems involving modifications, additions and/or deletions (for weight savings). Also considered in these combinations was the direct use of cold helium residual supplied through the LOX pressurization module, instead of routing it through the O<sub>2</sub>H<sub>2</sub> burner as is done in cryo repressurization.

The ambient repressurization and cold helium residual systems are the same as described for S-IVB/IB. The cryo repressurization system uses cold helium stored in .099 cubic meter (3.5 cubic feet) high pressure spheres and supplied by the regulator in the LOX pressurization module to the LOX and LH<sub>2</sub> cryo repressurization modules. Each of these modules consists of a pair of parallel shutoff valves, a plenum

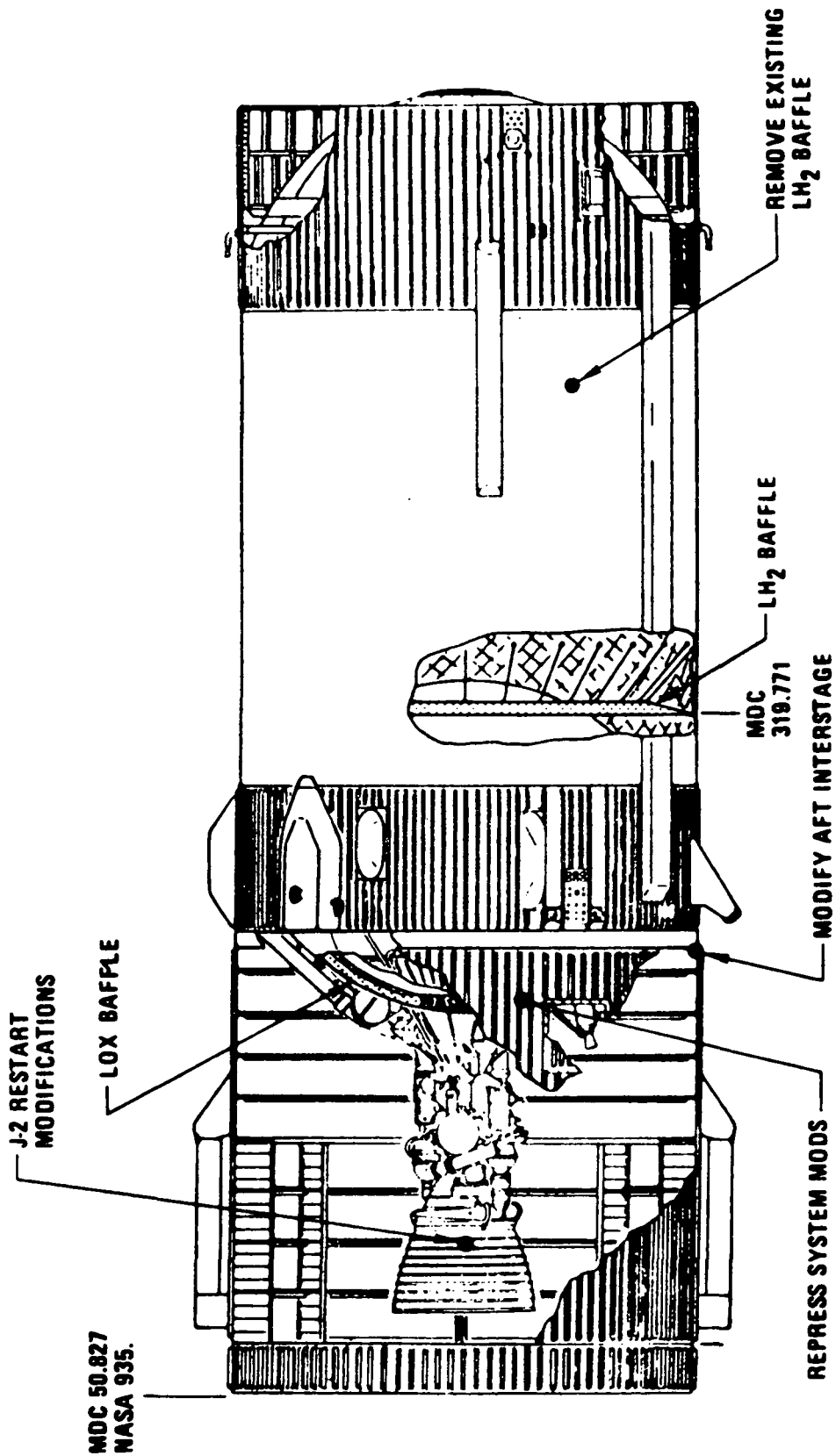


FIGURE 4.4 S-IVB/V/SEPS MODIFICATIONS

chamber and associated plumbing. From these modules the helium is routed through the heat exchanger coils in the  $O_2H_2$  burner to increase its energy level and through the flow controlling orifices to the propellant tanks. It should be noted that burner operation in the SEPS Mission requires an extension of the LOX feed lines inside the tank to get below the liquid level in the tank.

Six candidate systems were considered. The first system is the combination of ambient plus cryo repressurization available on the present configuration. The LOX and  $LH_2$  ambient systems here contain two and five storage spheres respectively. Note, however, that one of the LOX spheres is also connected with the  $LH_2$  system. The second system consists of the same elements as the first, but in this system all seven storage spheres are manifolded together to supply the  $LH_2$  tank, while in the  $O_2H_2$  burner the  $LH_2$  repressurization coils are tied into the LOX repressurization system. The third system consists of cryo repressurization only. The ambient repressurization systems are removed to save weight. The fourth and fifth systems provide ambient repressurization only. One is a forward, the other is an aft mounted system as described for the S-IVB/IB. The sixth candidate is a combination of ambient repressurization for the  $LH_2$  tank and cold helium residual feed directly to the LOX tank. This system uses the same principle as the second candidate, except that it operates without the  $O_2H_2$  burner.

The recommended system (ambient fuel and cryo LOX) consists of the same elements as the present system. The same factors (cost, weight, reliability, and proven performance) as applied to the S-IVB/IB trade study influence the selection of the S-IVB/V repressurization system candidate. Only the third candidate burner was not entered in the costing study because its performance was determined to be marginal. Of the remaining candidates, the first two systems, i.e., the present configuration and the slightly modified one, using burner for LOX repressurization only, are the most cost effective. The latter, although obviously requiring some expense, is chosen because cryo repressurization of the LOX tank is not nearly as critical as that of the  $LH_2$  tank. The effect of sensible heating of the liquid in the tank on NPSH is much greater for  $LH_2$  than for LOX. Also, in case of a burner failure it is still possible to repressurize the LOX tank with cold helium directly supplied through the LOX pressure system by a simple change of time base, comparable to TB6A in the Apollo flights. The burner voting circuit can supply the trigger activating this alternate time base. The electrical complexity of all the circuits is approximately equal. More effort is required to remove the  $O_2H_2$  burner and install a complete ambient system, but the variation in engineering effort is not of



such a magnitude to influence system selection. The major cost item in the other candidate systems is the cost of fabrication and installation of the ambient helium storage spheres.

#### 4.3.3.3 INTERFACE

Mating the Saturn V/S-IVB Stage to a Saturn IB Interstage requires modification to the prime structure of the Saturn IB/S-IVB interstage to distribute the discontinuity in loading resulting from the unequal number of stringers at the interface plane and to accept the bolt hole pattern of the Saturn V/S-IVB.

A new outer frame cap of the interface frame (Figure 4-5), having the same shape as the existing cap but with a revised trim (to attach new stiffeners) and the Saturn V/S-IVB bolt hole pattern, is installed in the Interstage. Tee stiffeners are attached between interstage stringers and extend from the frame cap .33 meters (13.5 inches) aft to the first interstage intermediate frame. These tee stiffeners pick up part of the discontinuous load and shear this load to the adjacent interstage stringers.

Structural revisions in the interstage area will require changes in the wiring installations. If an existing cable is long enough to reach the revised interface it will be installed; for those cables which will not reach, an adapter cable will be fabricated to compensate for the difference in length.

There are seven measurements and commands peculiar to S-IVB/IB that are spares on the comparable S-IVB/V pins, and there are two pins which have a conflict between the S-IVB/IB and S-IVB/V. These differences will require minimal wiring changes.

The electrical interface with the IU consists of functions which interconnect the S-IVB/V and IU, and the IU with the stage(s) below the S-IVB/V. The interstage interface consists of functions interconnecting the S-IVB/V and S-IB and the S-IB with the IU. It is recommended to tie back 31 wires, some of which carry signals from the S-IB telemetry from the S-IVB. Other changes include five wiring revisions and the addition of two wires. These changes do not cause a significant impact.

#### 4.3.4 S-IVB STAGE SELECTION FOR SEPS

The present S-IVB stage status reveals six complete Saturn IB/S-IVB stages and five complete Saturn V/S-IVB stages available for consideration for the SEPS Mission. S-IVB-212 and S-IVB-515 were

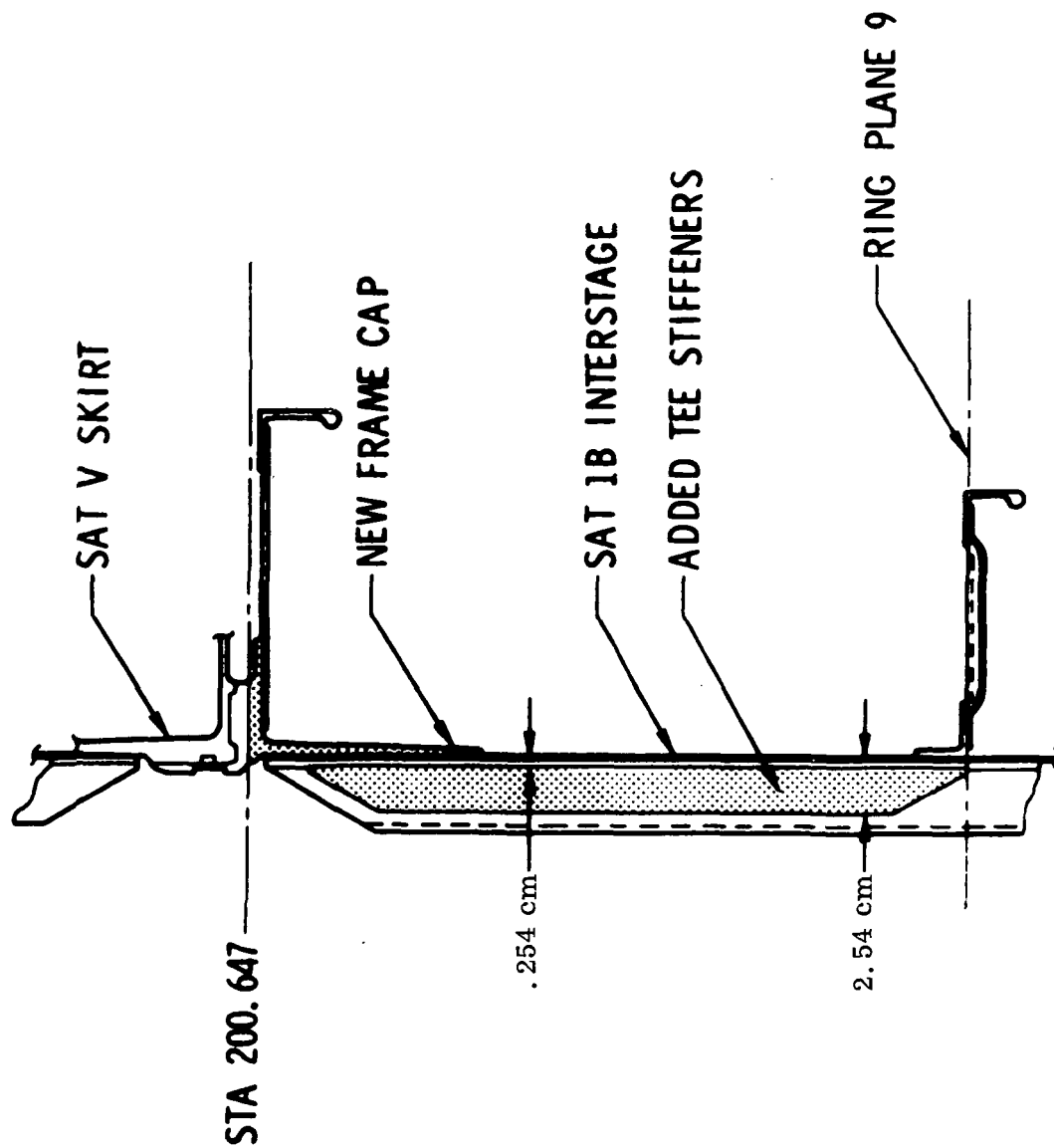


FIGURE 4.5 SAT IB/S-IVB INTERSTAGE MODIFICATIONS

reworked for Saturn workshops. Of the six Saturn IB/S-IVB stages available, four have firm mission plans and the other two are being considered for missions in the second Skylab. Of the five Saturn V/S-IVB stages available, three are assigned to Apollo missions and two have no present assignment. One of the two unassigned Saturn V/S-IVB stages completes the stack for a complete Saturn V launch vehicle, available for future mission applications. The other Saturn V/S-IVB stage would be available for SEPS consideration.

The S-IVB stage to be utilized for the SEPS mission must be capable of restarting to circularize the orbit at the proper altitude. The Saturn IB/S-IVB would require extensive modification while the Saturn V/S-IVB has this capability. The Saturn V/S-IVB stage does, however, require modification to mate with the S-IB stage. A Saturn V/S-IVB stage is recommended for SEPS based upon availability without interference to present planning or breaking up a stacked vehicle in either program and lower modification cost as the restart package is present on the Saturn V/S-IVB stage.

Present planning does not assign missions to Saturn V/S-IVB stages 513 and 514. S-IVB-513 is presently stacked with the SA-514 launch vehicle; however, a performance comparison of the two S-IVB stages reveals the S-IVB-514 to be the higher performer. As the performance of S-IVB-513 is adequate to meet the requirements for SEPS, this stage was selected leaving the higher performing stage for a more sophisticated Apollo type mission.

#### 4.4 S-IU STAGE (Reference 9 )

##### 4.4.1 S-IU STAGE MODIFICATION

Based on the preliminary data for the SEPS mission, there appears to be no significant structural problems associated with the IU. However, the preliminary stress data does indicate that an increase in vent area and/or a structural modification, similar to the bonded washers for Skylab, may be required if the standard SLA and nosecone (AS-204 configuration) is used.

The SEPS design tension loads are considerably greater than those for other IU missions, with the exception of Skylab, and results in negative margins of safety in yield at the lower IU interface flange. The relatively light payload, in combination with the large projected area of the shroud above the IU, causes excessive tension loads at the lower IU interface.

The use of a smaller volume shroud or a lower compartment delta pressure, via an increase in S-IVB vent area, should reduce the IU tension loads. Another method would be to move the SEPS support attach points closer to the IU. Finally, the addition of bonded washers at the lower interface, similar to those on Skylab, would increase the IU tension capability.

A brief investigation was conducted to assess the capability of the existing IU Environmental Control System (ECS) in meeting the SEPS mission requirements. Further, structural temperature predictions indicate that the addition of exterior surface insulation to the IU structure is not required.

Contamination of the satellite is not considered a potential problem as the satellite will be enclosed by a protective cover and the cavity will be purged with GN<sub>2</sub>.

The following network changes have been identified:

#### EDS and IU/Payload Changes

Remove the EDS engine cutoff wiring to the S-IB and S-IVB stages.

Delete the EDS/Apollo busses +6D91, +6D92 and +6D93.

Delete the S-IVB stage fuel tank pressure indication wiring to the spacecraft.

Delete the spacecraft control of Saturn Vehicle circuitry (+6D31).

Add SLA/Nosecone deployment circuitry.

Add to new payload interface cable to the measuring distributor to accommodate added SLA/Payload measurements.

#### IU/S-IVB Changes

Add IU circuitry for S-IVB measurement O<sub>2</sub>/H<sub>2</sub> burner malfunction.

The majority of these network changes can be accomplished by modifications to the EDS distributor, the control distributor 603A2, and the measuring distributor 602A3. These three distributors shall be

provided from existing government inventory and can be modified for installation on AS-209 at KSC. If AS-209 is used as the Skylab Rescue Vehicle, these distributors will be reworked for another vehicle.

The attitude control system should be capable of performing all phases of the SEPS mission. Certain hardware modifications must be made to the Flight Control Computer (FCC), such as filters and optimum gains; however, these modifications must be performed for each FCC, regardless of the launch vehicle mission.

It is desired to roll the S-IVB/IU at a rate such that when the payload is ejected, it will have a spin greater than 0.6 degrees/second. Roll rates of this magnitude cannot be sustained with the present attitude control system since the rate ledge for roll is 0.5 degrees/second. However, this can be corrected by a software change to the LVDC flight program.

#### 4.4.2 S-IU STAGE SELECTION FOR SEPS

The present S-IU stage status indicates that 7 Saturn IB IU's and 5 Saturn V IU's are available. All Saturn V IU's are assigned to a completely stacked launch vehicle; three of these vehicles have firm mission assignments; one is the Skylab backup launch vehicle; and the remaining vehicle is unassigned. All Saturn V launch vehicles with an assigned mission require an IU and any future plans for the unassigned Saturn V will require an IU. All Saturn IB IU's are assigned to a complete launch vehicle with the exception of S-IU-212. No S-IVB stage exists in the Saturn IB-212 stack. Of the Saturn IB launch vehicles, four have firm missions and the two remaining complete vehicles are tentatively planned for manned missions associated with Skylab B or with other manned missions presently being considered. The IU stage for Saturn IB-212 is presently being assembled. This IU, when complete, will not be a part of any present mission since the Saturn IB-212 is not a complete launch vehicle. S-IU-212 will meet all the requirements for this mission with very few modifications. The S-IU software is scheduled far enough in advance to allow development without significant additional cost.

#### 4.5 GROUND SUPPORT EQUIPMENT MODIFICATION DEFINITION (Reference 10)

The basic ground support equipment modification effort will be to provide a reconfiguration modification kit to update LC-39 (which includes FR-3, ML-3, Pad B, High Bay 1 and the Low Bay) and the Saturn IB System Development Facility from a manned AS-209 configuration to an unmanned S-IB-212/S-IVB-513/S-IU-212 configuration.

The LVGSE update will primarily effect the electrical support equipment. Some effort will also be necessary for the Saturn ground computer system, operational display system and the mechanical ground support equipment.

The principal hardware impact that has been identified beyond the normal LVGSE impact includes:

- a. Reactivation of the S-IVB  $O_2H_2$  burner system.
- b. Minor modification to the S-IVB stage pressurization system.
- c. Minor modification to the S-IVB engine preparation system.
- d. Addition of payload pneumatics and ordnance systems.
- e. Deletion of EDS, Q-Ball and Apollo Spacecraft simulator interfaces.

## SECTION 5. MISSION ANALYSIS

### 5.1 MISSION PROFILE

#### 5.1.1 LAUNCH SEQUENCE

The SEPS mission requires insertion of the payload into a 3720 km (2008.6 nm) circular orbit, inclined at 55 degrees to the equatorial plane. Figure 5-1 illustrates the launch sequence which consists of three phases: boost, coast, and final burn into the operational orbit. The boost phase begins with a northerly launch from Pad 39B at Kennedy Space Center. A flight azimuth of 37.94 degrees east of north provides a planar boost flight for the 55 degree inclination requirement. Completion of the S-IVB first burn inserts the vehicle into a 150 x 3720 km (81 x 2008.6 nm) elliptical orbit.

The coast mission phase requires approximately 63 minutes and consists of the Hohmann transfer from 150 km (81 nm) to the operational orbit altitude of 3720 km (2008.6 nm). Early in the coast the payload shroud, consisting of the SLA and nosecone, is jettisoned in a retrograde direction. The vehicle is then oriented and maintained in a local horizontal attitude for the remainder of the coast.

The final phase of the launch sequence consists of the S-IVB stage second burn at first apogee passage in the elliptical orbit. This circularization burn establishes the operational orbit required by the SEPS satellite. Just prior to engine start the IU will command a local horizontal attitude hold mode which will be maintained throughout the burn.

#### 5.1.2 PAYLOAD SEPARATION

Following insertion into the operational orbit, the vehicle will be maneuvered to the payload separation attitude. This attitude is defined by the requirement that the satellite spin axis be orientated normal to the ecliptic plane. The satellite will then be released as the vehicle crosses the equatorial plane at the first ascending node in the operational orbit. For thermal heating control, the satellite is required to have a spin rate of approximately 0.6 deg/second. This will be provided by rolling the S-IVB stage with the Auxiliary Propulsion System prior to payload separation.

#### 5.1.3 S-IVB EVASIVE MANEUVERS

To decrease the possibility of recontact with the satellite, two S-IVB APS retroburns will be used to lower the S-IVB/IU orbit. The first retroburn will occur at the first descending node after payload separation (approximately 84 minutes) and will provide a perigee of the S-IVB/IU orbit below the satellite

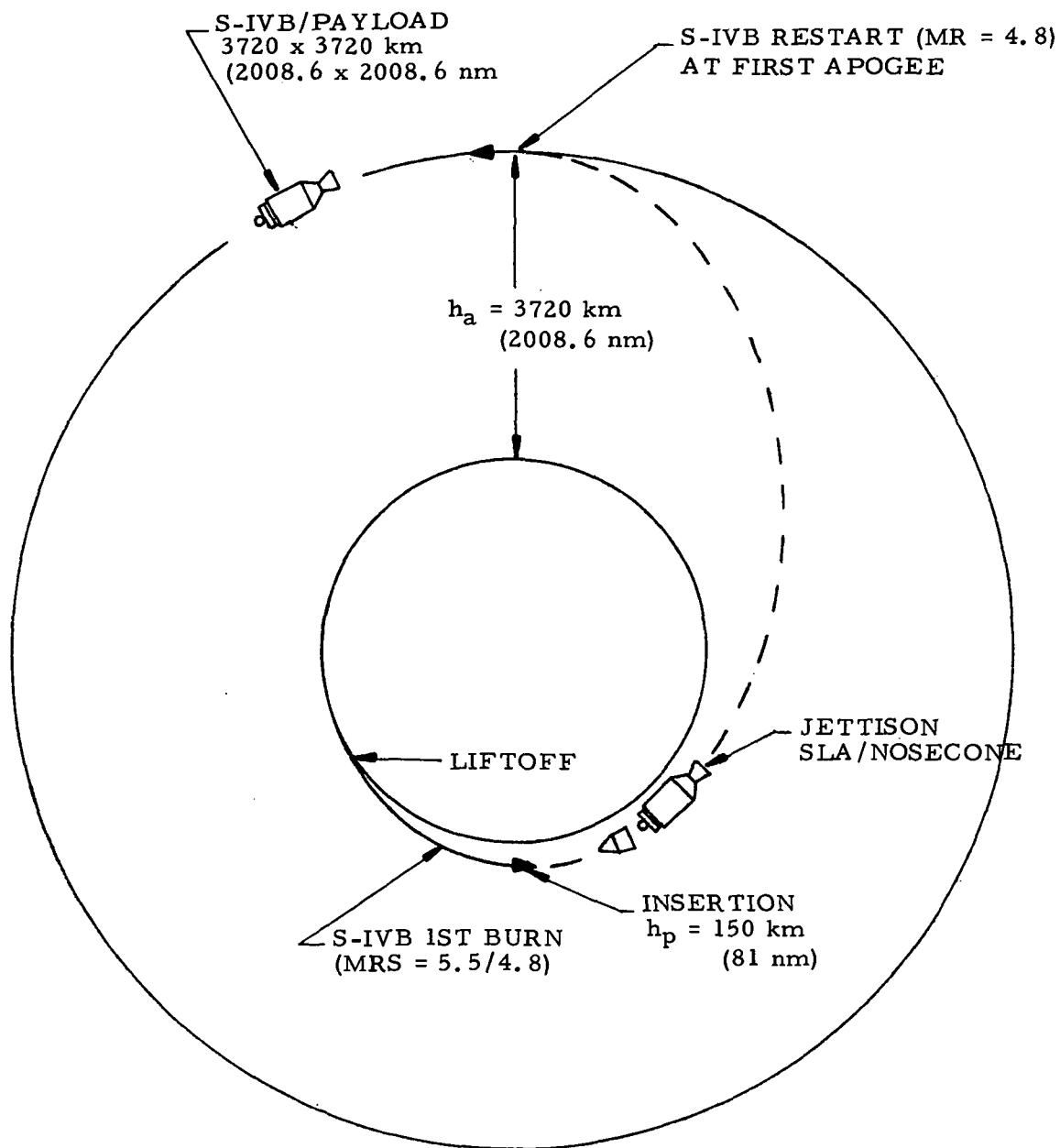


FIGURE 5-1. LAUNCH VEHICLE FLIGHT PROFILE



orbit. The second retroburn will occur at the first ascending node after payload separation (approximately 168 minutes) and will lower the apogee of the S-IVB/IU orbit. These evasive maneuvers will completely separate the orbits of the S-IVB/IU and satellite and will provide a near zero probability of re-contact.

## 5.2 MISSION TIME LINE

Table 5-1 contains approximate values of the flight sequence of event times for the SEPS mission based on the Saturn launch vehicle defined as a result of the Phase B study.

## 5.3 PERFORMANCE ANALYSIS

### 5.3.1 LAUNCH VEHICLE BOOST TRAJECTORY

A modified Saturn IB launch vehicle, defined as a result of the Phase B studies of the proposed Smithsonian Earth Physics Satellite (SEPS) mission, can insert a satellite of approximately 3637 kg (8018 lb) into the required orbit, i. e. , circular at an altitude of 3720 km (2008.6 n mi) and an inclination of 55 degrees. In addition to the satellite, weight above the IU at insertion includes 599 kg (1320 lb) of fixed payload enclosure and a 339 kg (747 lb) payload adapter.

There are several possibilities for increasing the launch vehicle payload capability if necessary. In addition to the payload capability trade-off data presented in Section 5.3.3, a payload increase of approximately 347 kg (lbm) can be realized by reducing the FPR requirements from 3-sigma to 2-sigma values.

As a result of the Phase B study, the Saturn launch vehicle stages recommended for the SEPS mission are S-IB-212, S-IVB-513, and S-IU-212. The S-IVB stage engine mixture ratio settings will be 5.5:1.0 and 4.8:1.0. Trajectory parameters presented below are indicative of those expected for the launch vehicle defined as a result of the Phase B study.

Time history plots of significant trajectory parameters through S-IVB first burn are shown in Figures 5-2 through 5-10. Additional trajectory data are presented in Reference 11. The flight environment is expected to be more severe than that predicted for the Saturn IB flights of the Skylab Program. However, the Saturn IB/SEPS flight environment is significantly less severe than that experienced during the flight of the SA-203 launch vehicle. A comparison of the flight environment parameters for these three vehicles is shown in Table 5.2.

TABLE 5-1  
MISSION TIMELINE

EVENT	FLIGHT TIME - SECONDS
Liftoff	0
Initiate Tilt	10.0
Tilt Arrest	131.5
IECO	138.3
OECO	141.3
S-IB/S-IVB Separation	142.7
J-2 Ignition Signal	144.0
J-2 90% Thrust	147.5
Ullage Case Jettison	154.6
Initiate IGM	166.9
Mixture Ratio Shift	434.0
S-IVB 1st Burn Cutoff (GCS)	577.7
Orbit Insertion (Maneuver to Retro Attitude for SLA/Nosecone Jettison; Begin LH <sub>2</sub> Boil-Off and Venting)	587.7
Jettison SLA/Nosecone (Maneuver to and Maintain Local Horizontal Hold - Nose Forward)	1247.7
Termination of LH <sub>2</sub> Boil-Off	4192.7
Begin Inertial Attitude Hold	4332.7
S-IVB Restart Sequence Command	4342.7
J-2 Ignition	4347.7
J-2 90% Thrust	4351.2

TABLE 5-1 (Concluded)  
MISSION TIMELINE

EVENT	FLIGHT TIME - SECONDS
S-IVB 2nd Burn Cutoff (GCS)	4368.9
Orbit Insertion (Termination of Interial Attitude Hold; Maneuver to and Maintain Local Horizontal Hold - Nose Forward; Begin Vent of S-IVB Propellant Tanks	4378.9
Termination of S-IVB Vent	5278.9
Payload Separation (Maneuver to and Maintain S-IVB/IU in Retro Attitude)	7068.9
S-IVB APS 1st Retro Burn	12109.0
S-IVB APS 2nd Retro Burn	17149.0

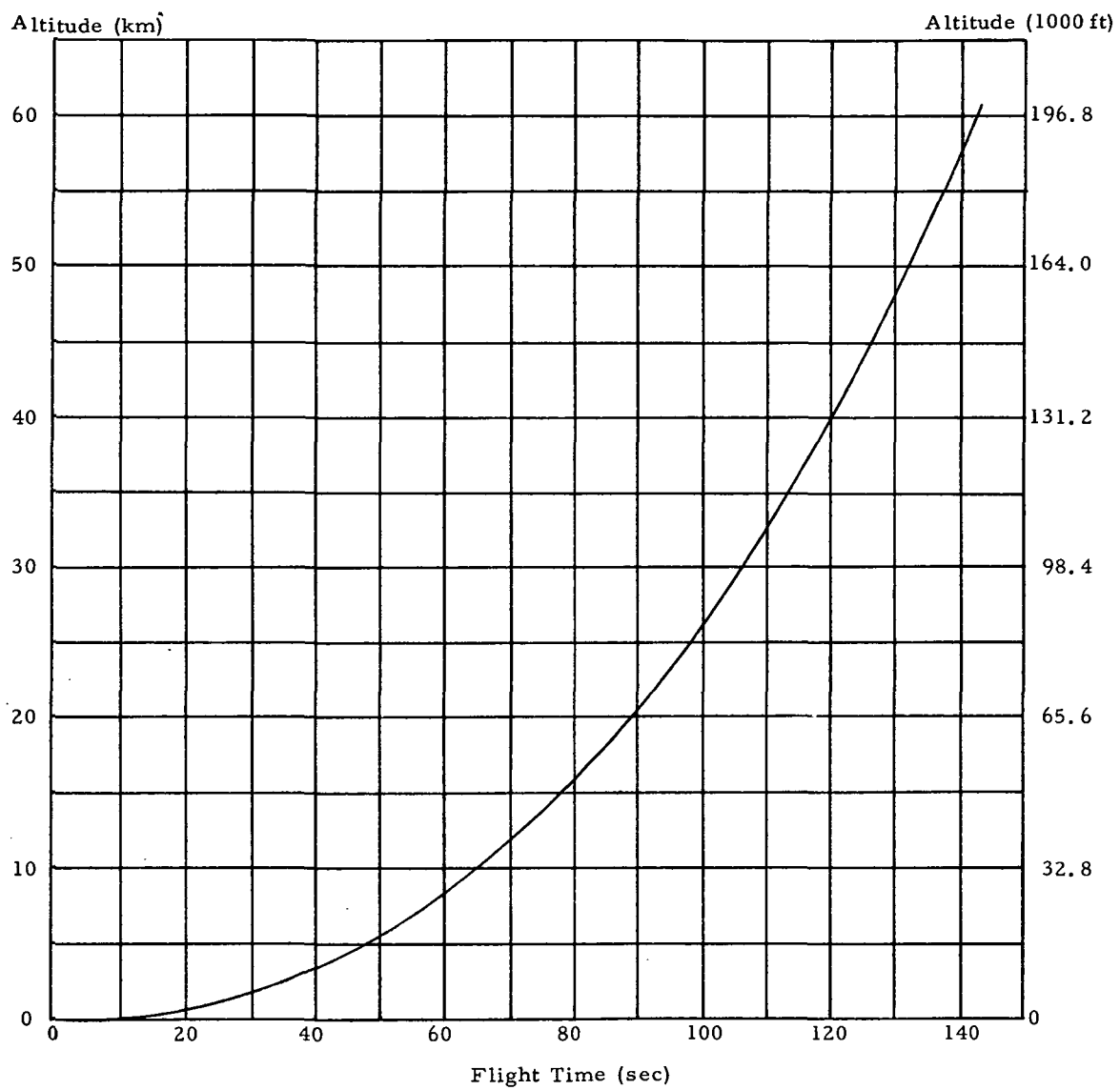


FIGURE 5-2. ALTITUDE VS. TIME - S-IB STAGE FLIGHT

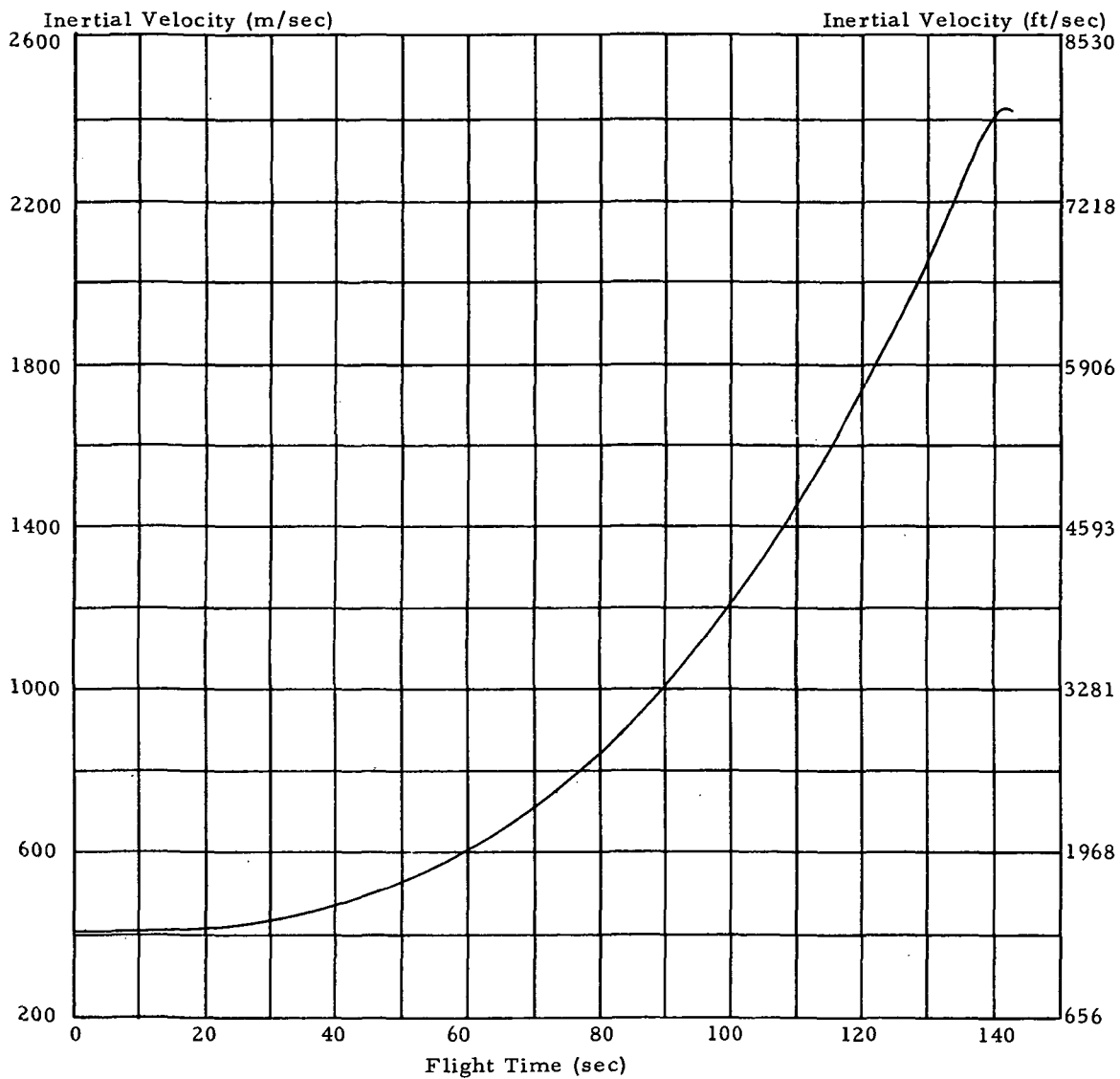


FIGURE 5-3. VELOCITY VS. TIME - S-IB STAGE FLIGHT

Inertial Pitch Attitude (deg)

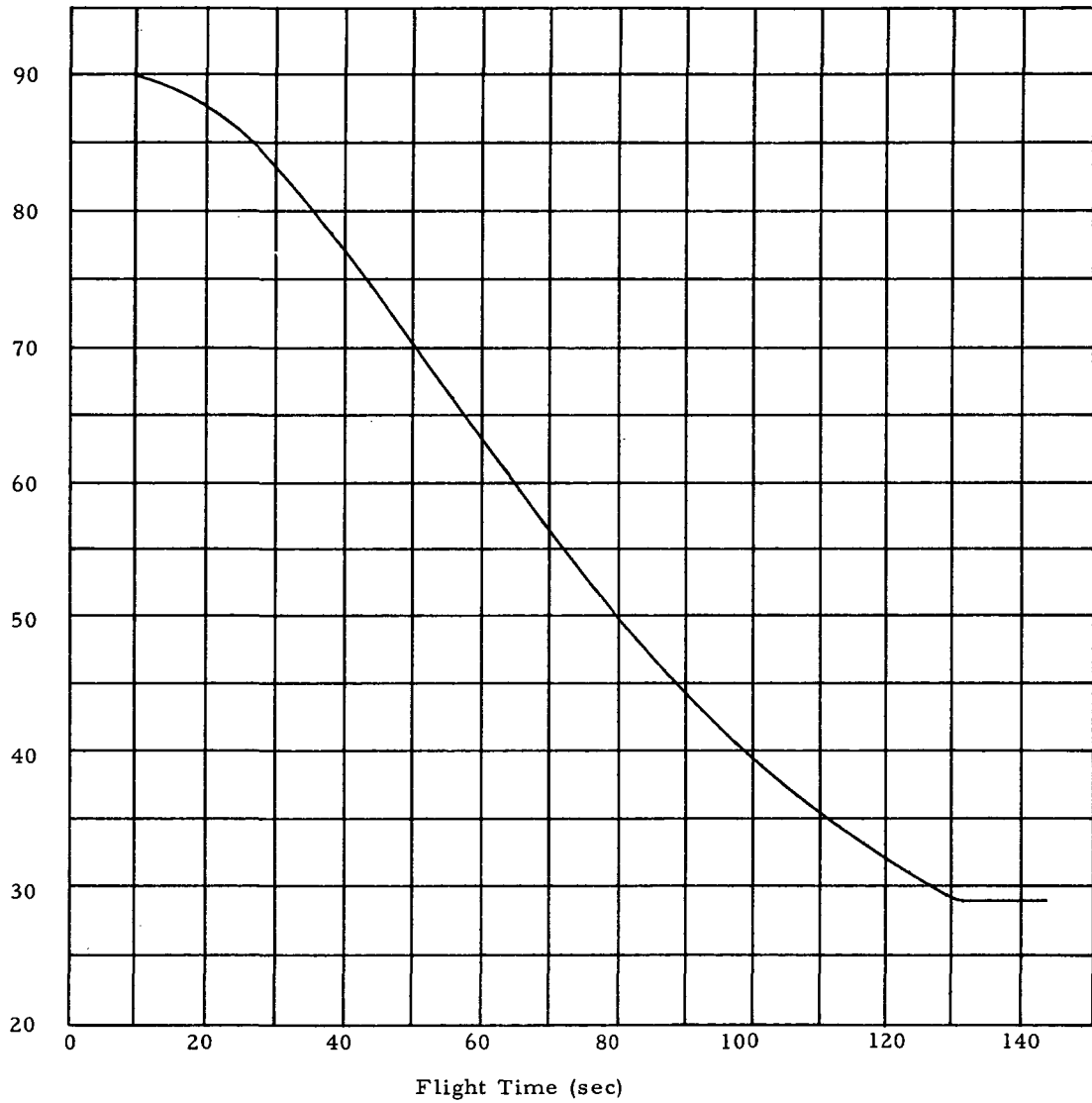


FIGURE 5-4. PITCH ATTITUDE VS. TIME - S-IB STAGE FLIGHT

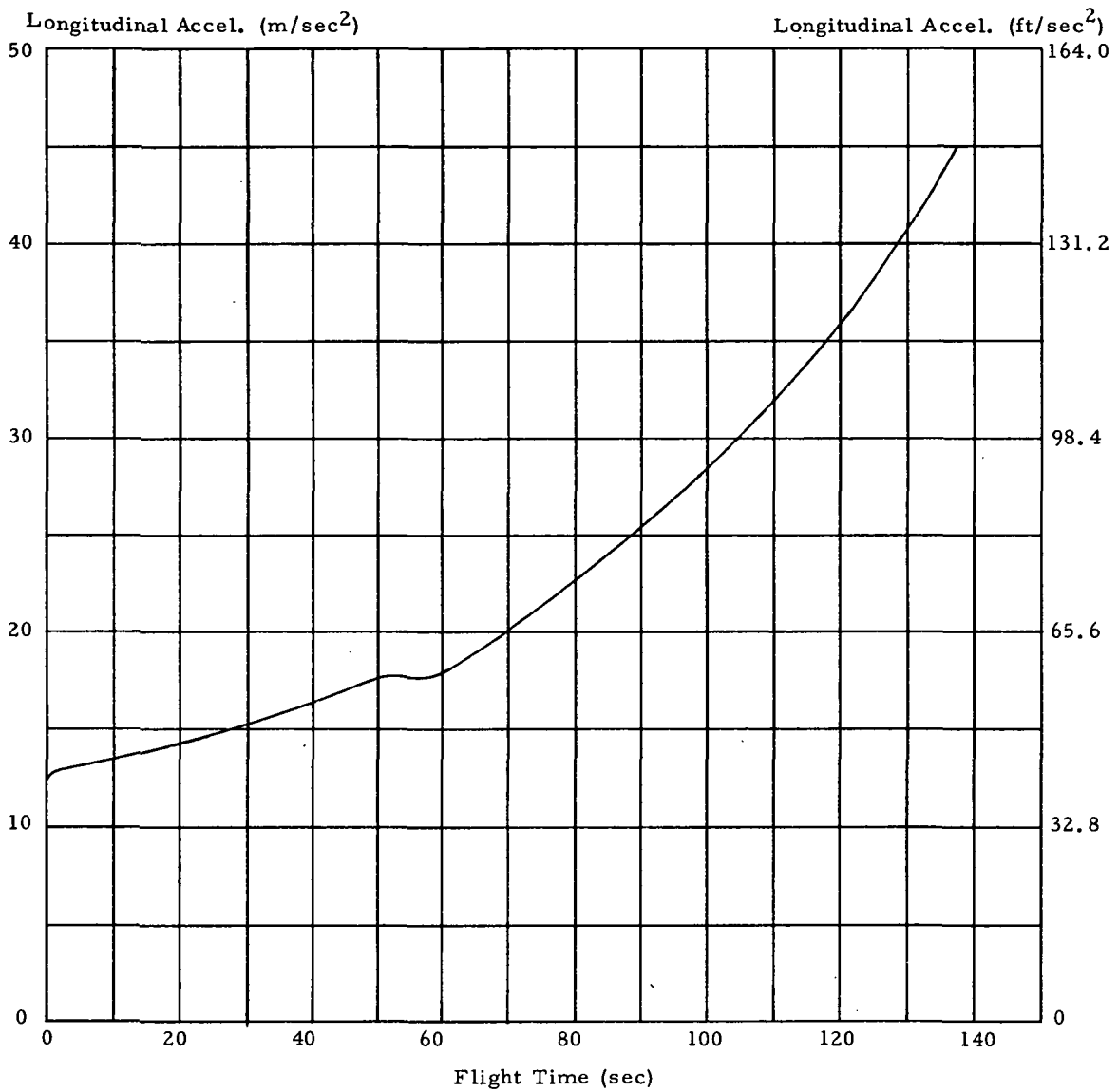


FIGURE 5-5. ACCELERATION VS. TIME - S-IB STAGE FLIGHT

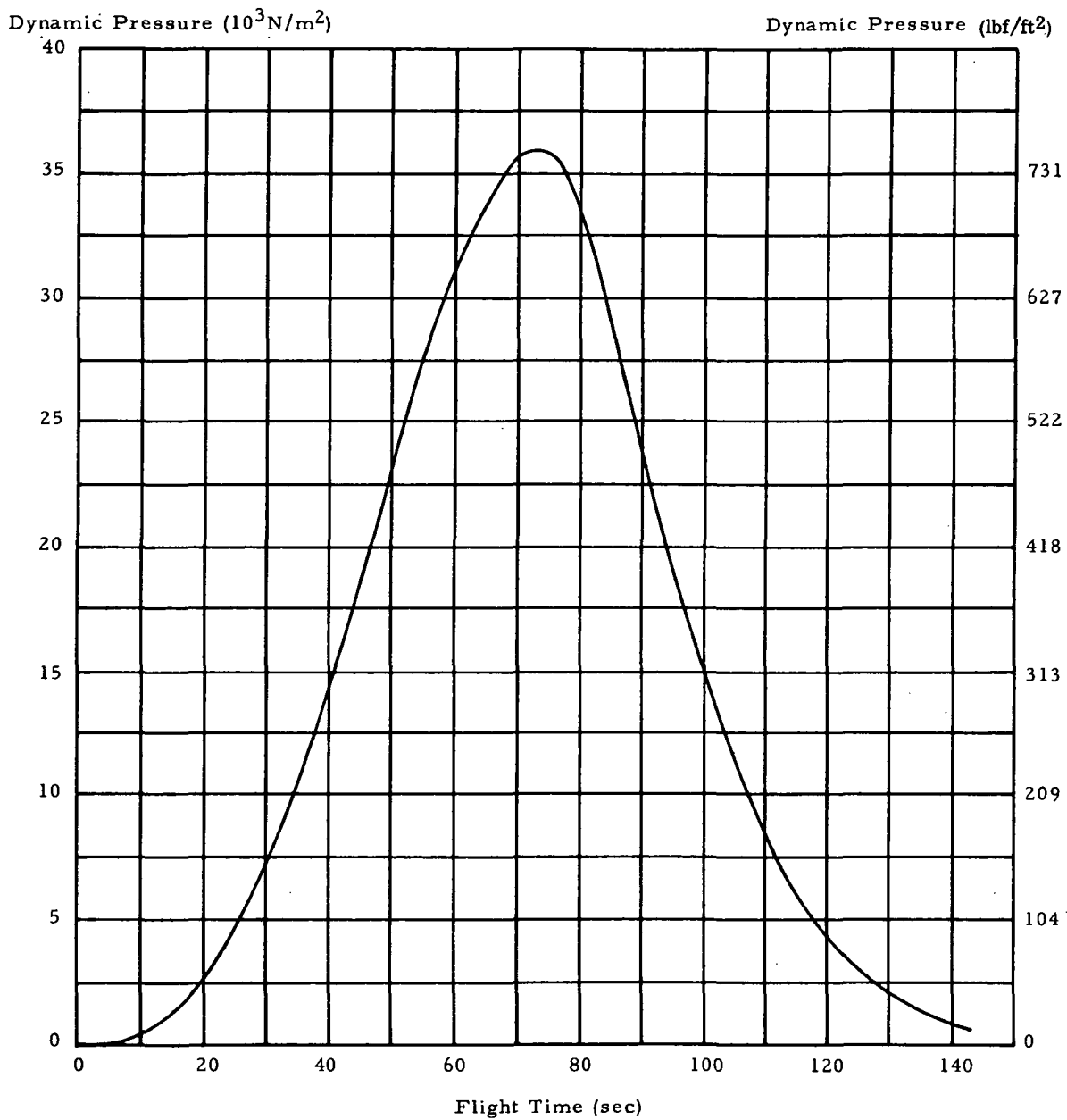


FIGURE 5-6. DYNAMIC PRESSURE VS. TIME - S-IB STAGE FLIGHT



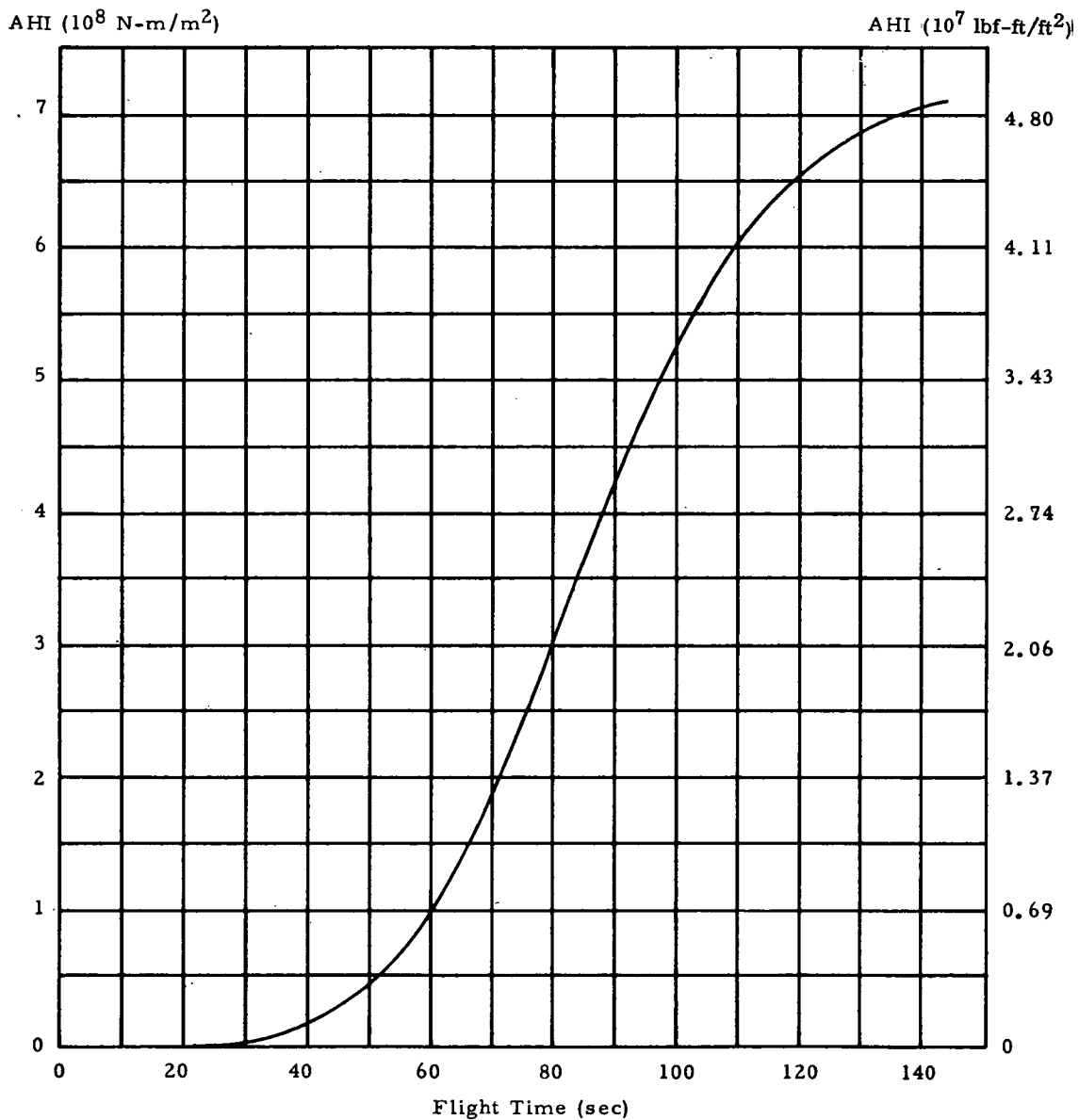


FIGURE 5-7. AERO-HEATING INDICATOR VS. TIME - S-IB STAGE FLIGHT

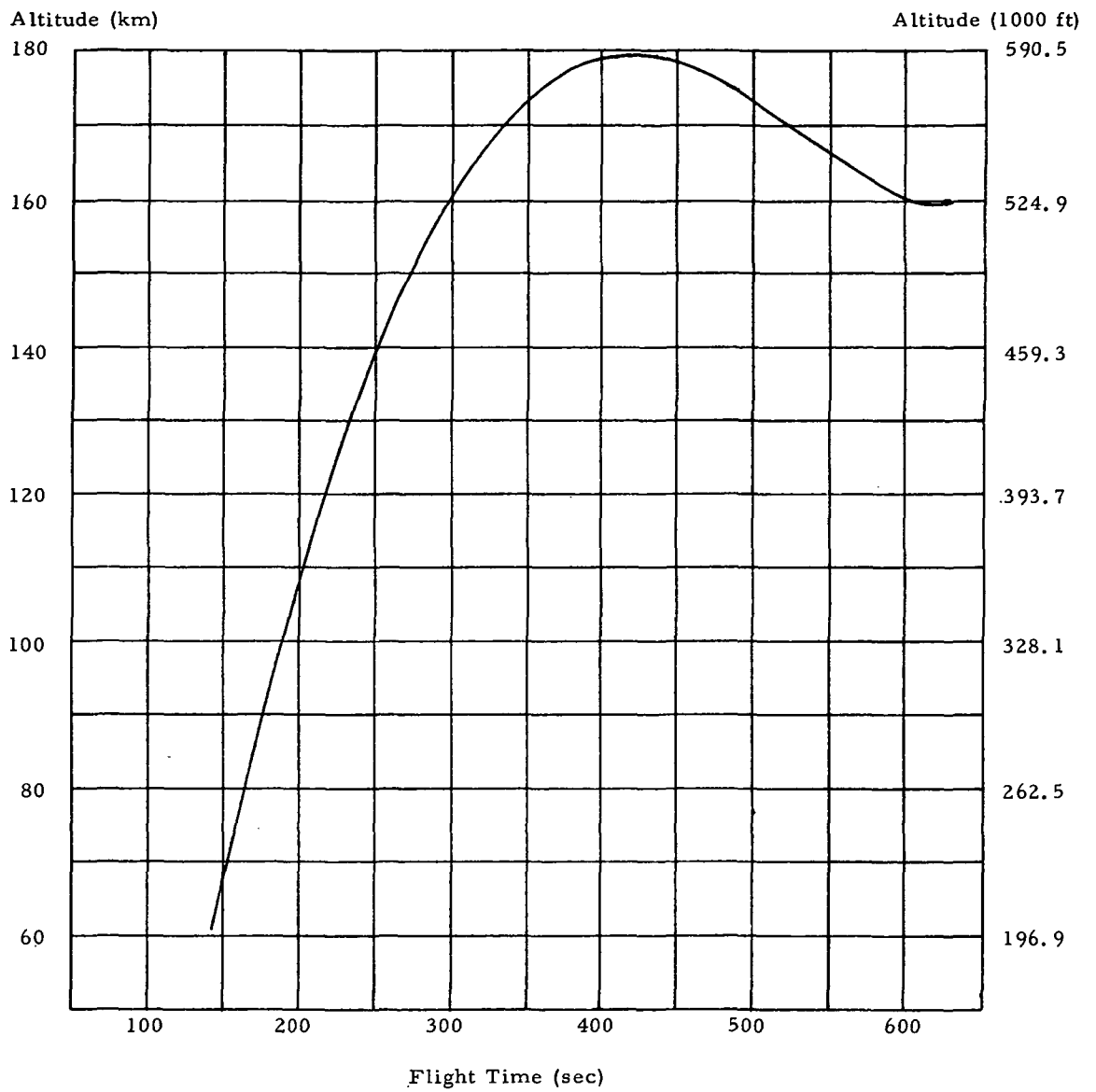


FIGURE 5-8. ALTITUDE VS. TIME - S-IVB FIRST BURN

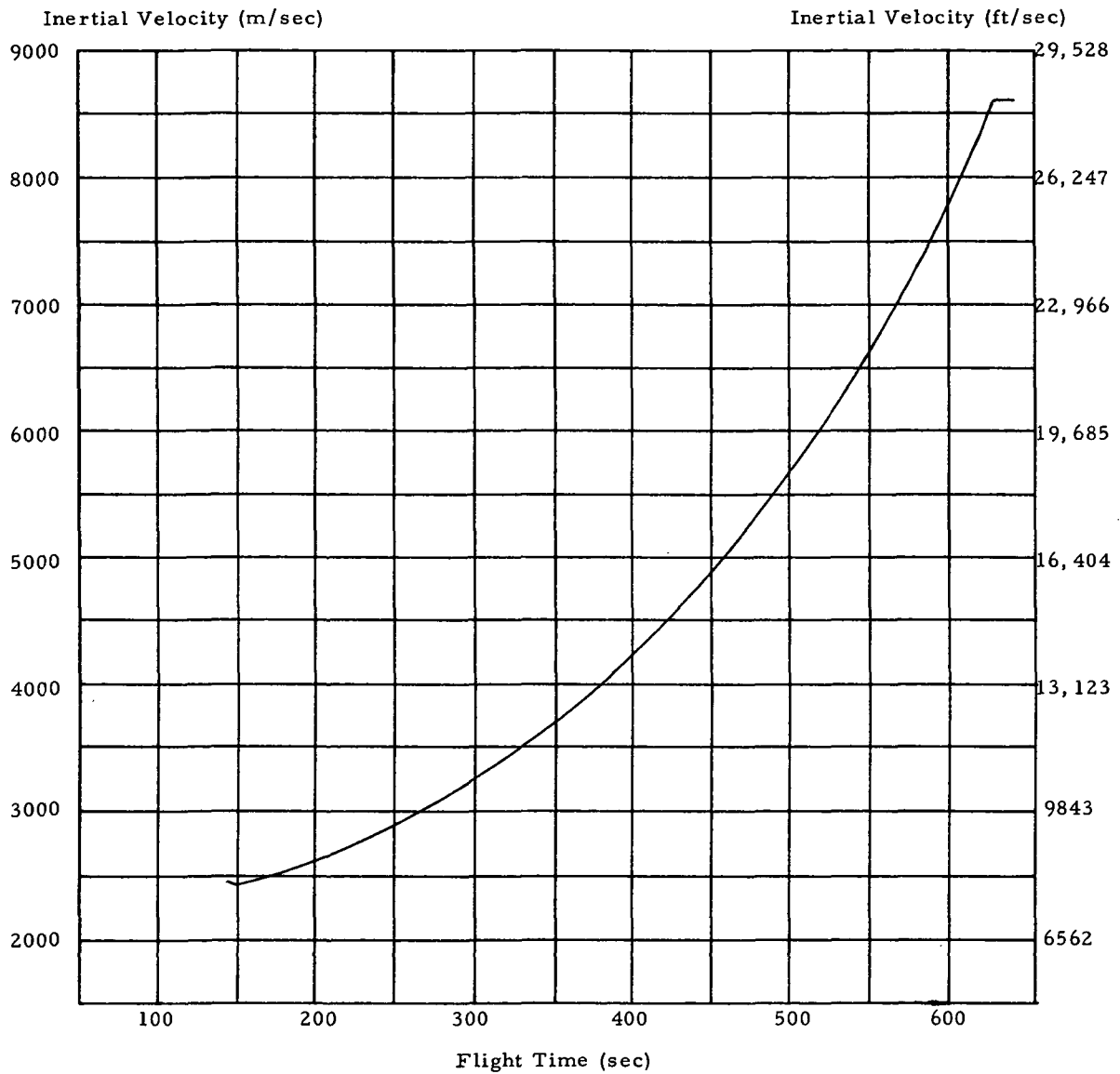


FIGURE 5-9. VELOCITY VS. TIME - S-IVB FIRST BURN

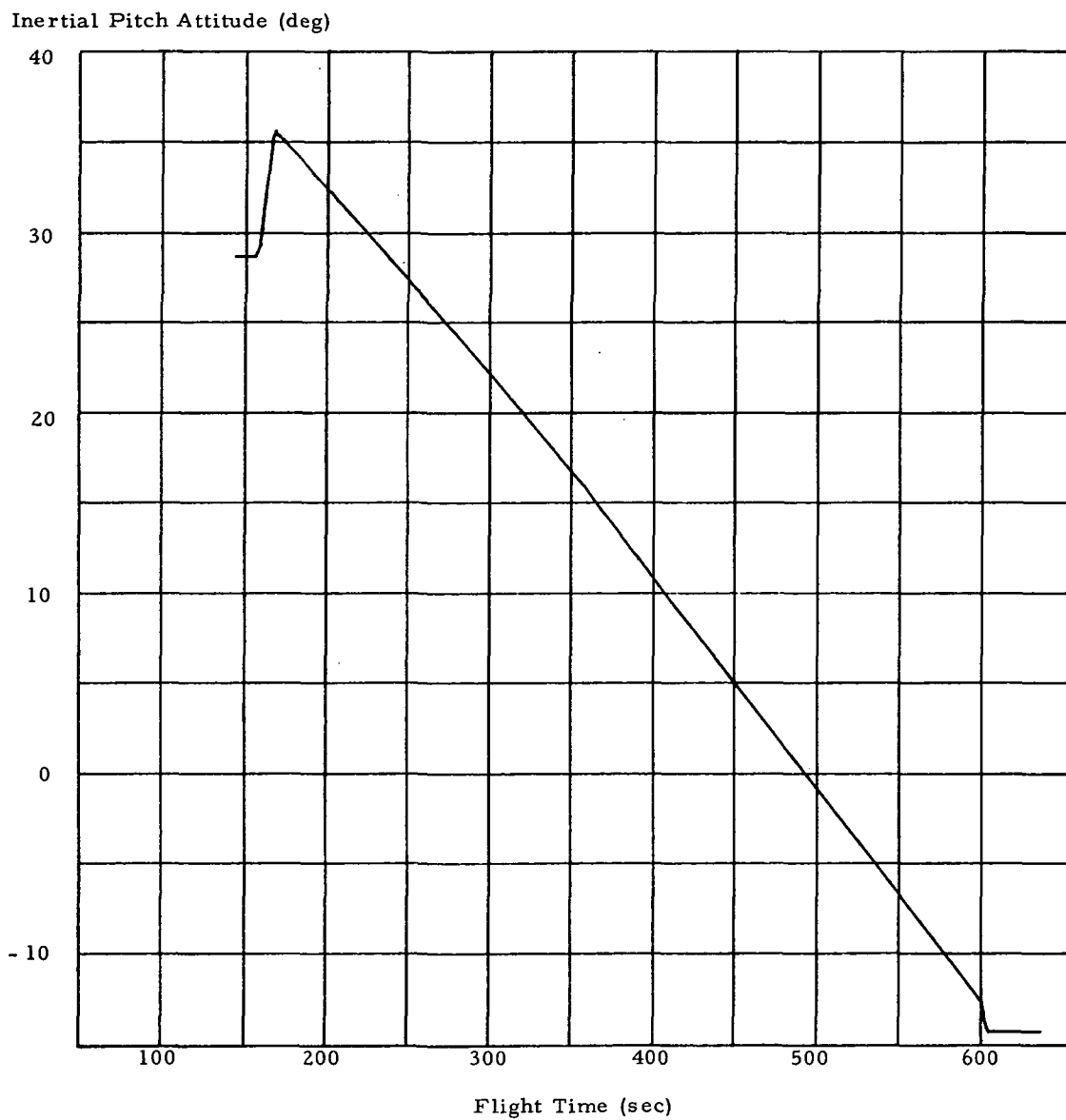


FIGURE 5-10. PITCH ATTITUDE VS. TIME - S-IVB FIRST BURN

TABLE 5.2 FLIGHT ENVIRONMENT

Vehicle	Max. Dynamic Press		Max. S-IB Accel. g's	AHI @ S-IB Sep.	
	N/m <sup>2</sup>	(lb/ft <sup>2</sup> )		N-m/m <sup>2</sup>	(lbf-ft/ft <sup>2</sup> )
SA-203	40,374	(843)	5.78	88.06 x 10 <sup>7</sup>	(60.34 x 10 <sup>6</sup> )
SEPS	35,990	(752)	4.61	70.80 x 10 <sup>7</sup>	(48.52 x 10 <sup>6</sup> )
SL-2	33,666	(703)	4.34	63.67 x 10 <sup>7</sup>	(43.63 x 10 <sup>6</sup> )

### 5.3.2 LAUNCH VEHICLE DISPERSION ANALYSIS

Early in the Phase B study, a launch vehicle dispersion analysis was conducted based on a Preliminary Reference Trajectory. This preliminary trajectory was generated for a launch vehicle consisting of the S-IB-210 and S-IVB-514 stages. The results of the dispersion analysis are presented in terms of the Flight Performance Reserve (FPR) requirement and effects on the design trajectory parameters of acceleration, dynamic pressure, and an aerodynamic heating indicator (AHI). Additional details of the dispersion analysis are presented in Reference 12.

#### 5.3.2.1 FLIGHT PERFORMANCE RESERVE

The individual contribution of each error source to the Saturn IB/SEPS vehicle FPR is shown in Table 5-3. These data reflect 3-sigma tolerances to the error sources considered, and, when combined by the root-sum-square method show that 593 kg (1307 lb) of LOX and 448 kg (987 lb) of LH<sub>2</sub> are required for FPR; a total propellant loading of 1041 kg (2294 lb).

An identification of the significant contributors to the FPR is provided by Table 5-4. As indicated by these data, 70% of the LOX FPR is required to compensate for S-IVB stage error sources. Two S-IVB stage error sources, the LOX residual case and stage inert weight, account for nearly 97% of the LH<sub>2</sub> FPR.

Since there is some consideration of reducing the Saturn IB/SEPS vehicle FPR to that required to compensate for error source tolerances at the 2-sigma level, the LOX and LH<sub>2</sub> required for this case have been determined. Under this assumption (i.e., 2-sigma FPR), the LOX and LH<sub>2</sub> requirements are reduced to 395 kg (871 lb) and 298 kg (658 lb), respectively.

#### 5.3.2.2 DESIGN TRAJECTORY PARAMETERS

Tables 5-5, 5-6, and 5-7 show the prime contributors to the maximum envelopes of the design trajectory parameters.

TABLE 5 -3  
SATURN IB LAUNCH VEHICLE DISPERSION ANALYSIS

PROPELLANT RESERVES REQUIRED TO OFFSET ERROR SOURCE  
EFFECTS ON PERFORMANCE

<u>STAGE</u> ERROR SOURCE	PROPELLANT REQUIREMENT			
	LOX		LH <sub>2</sub>	
3 $\sigma$ TOLERANCE	kg	(lbm)	kg	(lbm)
<u>S-IB Stage -Non Prop.</u>				
Non Propellant Mass				
+140.6 kg (+310 lb)	+12.2	(+27)	+2.7	(+6)
-140.6 kg (-310 lb)	-12.2	(-27)	-2.7	(-6)
Thrust Misalignment				
+ .62 DEG PITCH	-10.9	(-24)	-2.3	(-5)
- .62 DEG PITCH	+14.1	(+31)	+3.2	(+7)
+ .62 DEG YAW	+3.2	(+7)	+0.5	(+1)
- .62 DEG YAW	+1.4	(+3)	+0.5	(+1)
Axial Force Coefficient				
+15%	+112.5	(+248)	+24.9	(+55)
-15%	-111.1	(-245)	-24.9	(-55)
<u>S-IB Stage Propulsion</u>				
Propellant Density				
High LOX	+13.2	(+29)	+3.2	(+7)
Low LOX	+11.3	(+25)	+2.3	(+5)
High Fuel	+219.5	(+484)	+49.4	(+109)
Low Fuel	-50.8	(-112)	-11.3	(-25)
Propellant Loading				
+0.35% LOX	-71.7	(-158)	-15.9	(-35)
-0.35% LOX	+71.7	(+158)	+15.9	(+35)
+0.35% Fuel	+39.0	(+86)	+8.6	(+19)
-0.35% Fuel	-39.5	(-87)	-8.6	(-19)
Thrust & Flow Rate				
+1.5%	-107.5	(-237)	-24.0	(-53)
-1.5%	+129.3	(+285)	+28.6	(+63)

TABLE 5-3 (CONT'D)  
SATURN IB LAUNCH VEHICLE DISPERSION ANALYSIS

PROPELLANT RESERVES REQUIRED TO OFFSET ERROR SOURCE  
EFFECTS ON PERFORMANCE

STAGE ERROR SOURCE	PROPELLANT REQUIREMENT			
	3 $\sigma$ TOLERANCE	LOX kg (lbm)	LH <sub>2</sub> kg (lbm)	
Isp & Flow Rate				
+0.9 SEC	-64.0	(-141)	-14.1	(-31)
-0.9 SEC	+63.5	(+140)	+14.1	(+31)
Engine Mixture Ratio				
LOX Residual	+96.2	(+212)	+21.3	(+47)
Simultaneous Depl.	-93.4	(-206)	-20.9	(-46)
<u>S-IB Stage-Environment</u>				
Winds				
Head	+74.4	(+164)	+16.3	(+36)
Tail	-174.6	(-385)	-39.0	(-86)
Right Cross	+3.2	(+7)	+0.9	(+2)
Left Cross	+11.3	(+25)	+2.3	(+5)
Atmosphere				
Maximum Profile	+31.8	(+70)	+6.8	(+15)
Minimum Profile	-54.0	(-119)	-11.8	(-26)
<u>S-IVB Stage-Non Prop.</u>				
Stage Inert Mass				
+408.2 kg (+900 lb)	+325.2	(+717)	+72.1	(+159)
-408.2 kg (-900 lb)	-324.3	(-715)	-72.1	(-159)
<u>S-IVB Stage-Propulsion</u>				
Propellant Loading				
+768.4 kg (+1694 lb)	-15.9	(-35)	-3.6	(-8)
-768.4 kg (-1694 lb)	+19.1	(+42)	+4.1	(+9)
Thrust & Flow Rate				
+1.98%	-118.4	(-261)	-26.3	(-58)
-1.98%	+131.5	(+290)	+29.0	(+64)

TABLE 5-3, (Concluded)  
SATURN IB LAUNCH VEHICLE DISPERSION ANALYSIS

PROPELLANT RESERVES REQUIRED TO OFFSET ERROR SOURCE  
EFFECTS ON PERFORMANCE

<u>STAGE</u> ERROR SOURCE	PROPELLANT REQUIREMENT			
	3 $\sigma$ TOLERANCE	LOX kg (lbm)	LH <sub>2</sub> kg (lbm)	
Isp & Flow Rate				
+2.40 SEC	-174.2	(-384)	-38.6	(-85)
-2.21 SEC	+160.6	(+354)	+35.8	(+79)
LOX & Fuel Residual				
$\Delta$ EMR = -2.96%	-433.6	(-956)	+433.6	(+956)
$\Delta$ EMR = +2.22%	+312.1	(+688)	-312.1	(-688)
FPR	592.8	(1307)	447.7*	(987)

\* INCLUDES FUEL BIAS



TABLE 5-4  
SATURN IB LAUNCH VEHICLE DISPERSION ANALYSIS  
ERROR SOURCE CONTRIBUTION TO FLIGHT PERFORMANCE RESERVES

ERROR SOURCE	PERCENT CONTRIBUTION	
	LOX	LH <sub>2</sub>
S-IVB Stage Inert Mass	30.1	2.6
S-IVB Fuel Residual	27.7	*
S-IVB LOX Residual	*	93.8
S-IB Fuel Density	13.7	*
S-IVB Isp & Flow Rate	7.3	*
S-IVB Thrust & Flow Rate	4.9	*
S-IB Thrust & Flow Rate	4.8	*
Axial Force Coefficient	3.6	*
S-IB LOX Residual	2.6	*
All Others	5.3	3.6

\*Less than 1.0% Contribution

TABLE 5-5  
SATURN IB LAUNCH VEHICLE DISPERSION ANALYSIS  
AXIAL ACCELERATION COMPARISONS

ERROR SOURCE	THREE SIGMA TOLERANCE	AXIAL ACCELERATION DISPERSIONS @ 135 SECONDS m/sec <sup>2</sup> (ft/sec <sup>2</sup> )
S-IB Thrust (Constant Isp)	+1.5%	2.159 (7.083)
S-IB RP-1 Density	+3 $\sigma$ Surface Temp.	1.545 (5.069)
S-IB LOX Density	-3 $\sigma$ Surface Winds	0.820 (2.690)
S-IB Isp (Constant Thrust)	-0.9 sec	0.292 (0.958)
S-IVB Propellant Loading	-768.4 kg (-1694 lbm)	0.280 (0.919)
S-IB LOX Loading	-0.35%	0.245 (0.804)
All Others		0.158 (0.518)
ROOT SUM SQUARE		2.823 (9.262)

NOMINAL +RSS AXIAL ACCELERATION = 47.426 m/sec<sup>2</sup> (155.597 ft/sec<sup>2</sup>)

NOTE:

1. Estimated acceleration at IECO event is 48.132 m/sec<sup>2</sup> (157.913 ft/sec<sup>2</sup>)

TABLE 5-6  
SATURN IB LAUNCH VEHICLE DISPERSION ANALYSIS  
DYNAMIC PRESSURE COMPARISONS

ERROR SOURCE	THREE-SIGMA TOLERANCE	Q DISPERSIONS @ 72 SECONDS	
		N/m <sup>2</sup>	(lbf/ft <sup>2</sup> )
Headwinds	3 $\sigma$ Profile	1304	(27.2)
Atmospheric Density (Std. Temp. and Press.)	Max. Density (+ $\rho = f(h)$ )	628	(13.1)
Axial Force Coefficient	-15%	530	(11.1)
S-IB Thrust Misalignment (In Pitch Plane)	-0.62 deg	383	( 8.0)
Left Crosswind	3 $\sigma$ Profile	167	(3.5)
S-IB Isp (Constant Thrust)	-0.9 sec	49	(1.0)
All Others		59	(1.2)
ROOT-SUM-SQUARE		1598	(33.4)
NOMINAL +RSS Q = 36,736 N/m <sup>2</sup> (767 lbf/ft <sup>2</sup> )			

TABLE 5 -7  
SATURN IB LAUNCH VEHICLE DISPERSION ANALYSIS  
AERO-HEATING INDICATOR COMPARISONS

ERROR SOURCE	THREE-SIGMA TOLERANCE	AHI DISPERSIONS @ 140 SECONDS	
		$10^7 \text{ N-m/m}^2$	$(10^6 \text{ lbf-ft/ft}^2)$
Atmospheric Density (Std. Temp. and Press.)	Max. Density ( $+p = f(h)$ )	3.206	(2.197)
S-IB RP-1 Density	$-3\sigma$ Surface Temp.	2.562	(1.756)
Left Crosswind	$3\sigma$ Profile	2.227	(1.526)
Headwind	$3\sigma$ Profile	2.156	(1.477)
S-IB Thrust	-1.5%	2.056	(1.409)
S-IB Thrust Misalignment (In Pitch Plane)	-.62 deg	1.570	(1.076)
S-IB LOX Density	$+3\sigma$ Surface Winds	0.918	(0.629)
S-IB Thrust Misalignment (In Yaw Plane)	-.62 deg	0.450	(0.308)
All Others		0.229	(0.157)
ROOT-SUM-SQUARE		5.852	(4.010)
NOMINAL +RSS AHI = $73.280 \times 10^7 \text{ N-m/m}^2$ ( $50.213 \times 10^6 \text{ lbf-ft/ft}^2$ )			

NOTE:

1. Estimated AHI at S-IB separation event is  $73.321 \times 10^7 \text{ N-m/m}^2$   
( $50.241 \times 10^6 \text{ lbf-ft/ft}^2$ ).

In order to provide a measure of the "severity" of the flight environment being predicted for the Saturn IB/SEPS vehicle, the following provides a comparison of the design trajectory parameters with those experienced by SA-203.

TABLE 5-8 TRAJECTORY PARAMETERS

Vehicle	Trajectory	Max. Dyn. Press.	Max. Accel.	AHI @ S-IB Sep.
		$\text{N/m}^2$ (lb/ft <sup>2</sup> )	g's	$\text{N-m/m}^2$ (lbf-ft/ft <sup>2</sup> )
SA-203	Nom. Flight	40,374 (843)	5.78	$88.06 \times 10^7$ ( $60.34 \times 10^6$ )
SEPS	Nom. Flight	35,137 (734)	4.76	$66.64 \times 10^7$ ( $45.66 \times 10^6$ )
SEPS	Nom. +3 $\sigma$ RSS	36,736 (767)	4.91	$73.32 \times 10^7$ ( $50.24 \times 10^6$ )

The above comparison shows that the 3-sigma maximum design trajectory parameters predicted for the Saturn IB/SEPS vehicle are well below those experienced during the flight of SA-203.

### 5.3.3 TRADE STUDIES

The following results show the changes in vehicle performance which can be effected by variations in the baselined mission requirements and launch vehicle weights. These results were obtained from References 7, 11, and 13.

#### 5.3.3.1 FLIGHT PROFILE

The ground rules for the Phase B Studies of the proposed SEPS mission specified a circular orbit at 3720 km (2008.6 nm) with an inclination of 55 degrees. Since the Smithsonian proposal indicated that an orbit altitude above 3000 km (1619.9 nm) is considered adequate for the mission, this analysis was performed to determine what payload gains could be effected by lowering altitude below the 3720 km (2008.6 nm) ground ruled for the study. In addition, the effects of decreasing orbit inclination, and of variations in the perigee insertion altitude were examined.

Altitude and Inclination. The following figure shows the effects on payload when altitude and/or inclination of the final orbit is varied from 3720 km (2008.6 nm) and 55 degrees.

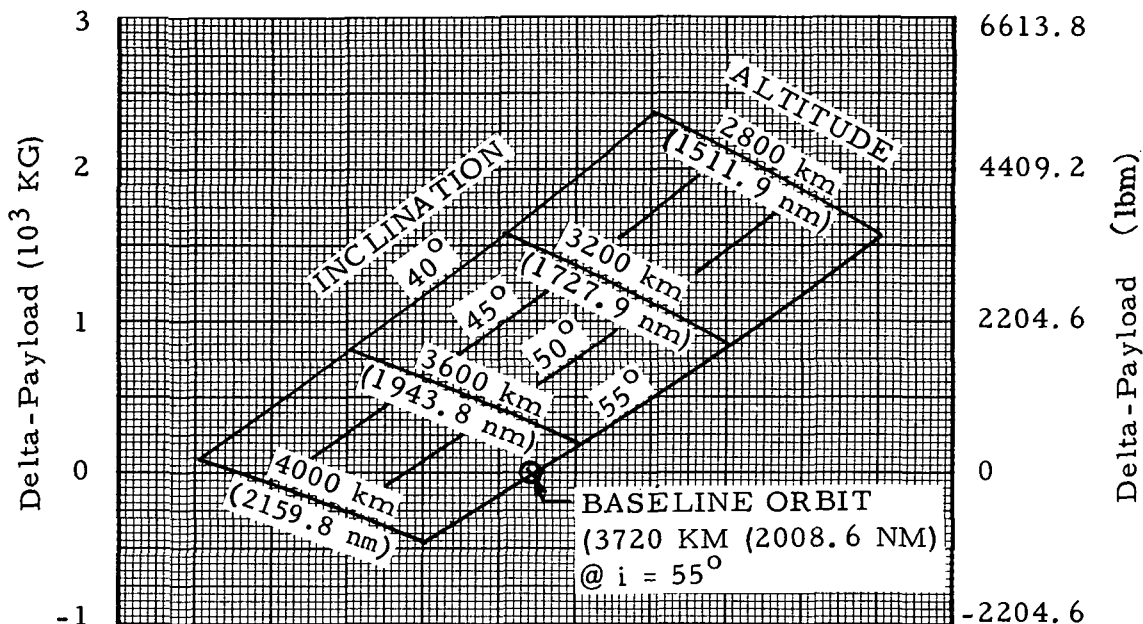


FIGURE 5-11. DELTA-PAYLOAD VS ALTITUDE & INCLINATION

Figure 5-11 indicates that approximately 1224.7 kg (2700 lb) of payload can be gained by decreasing the operational orbit altitude from 3720 km (2008.6 nm) to 3000 km (1619.9 nm), while maintaining a 55 degree inclination.

**Perigee Insertion.** A perigee insertion altitude of 150 km (81 nm) has been baselined for the SEPS mission. Figure 5-12 indicates the effect on payload capability and flight environment for variations in perigee insertion altitude. As shown, a payload gain of approximately 294.8 kg (650 lb) can be achieved by lowering the perigee insertion altitude from 150 km (81 nm) to 92.6 km (50 nm). For the resulting flight profile, the flight environment parameters (evaluated at S-IB stage separation) of maximum dynamic pressure, maximum acceleration, and aerodynamic heating indicator are all still well below the maximums experienced during the flight of the SA-203 vehicle.

#### 5.3.3.2 RANGE SAFETY

The following results represent the performance and range safety trade-offs associated with selected trajectories for the SEPS mission. Specific trajectories examined are: 1) the baseline 55 degree inclination planar flight profile, 2) a 55 degree inclination orbit achieved through boost flight yaw-steering, and 3) a 50 degree inclination planar flight profile. A lateral cross-range impact corridor of 52 km (28.1 nm) on either side of the nominal Instantaneous Impact Prediction (IIP) trace has been considered in this analysis.

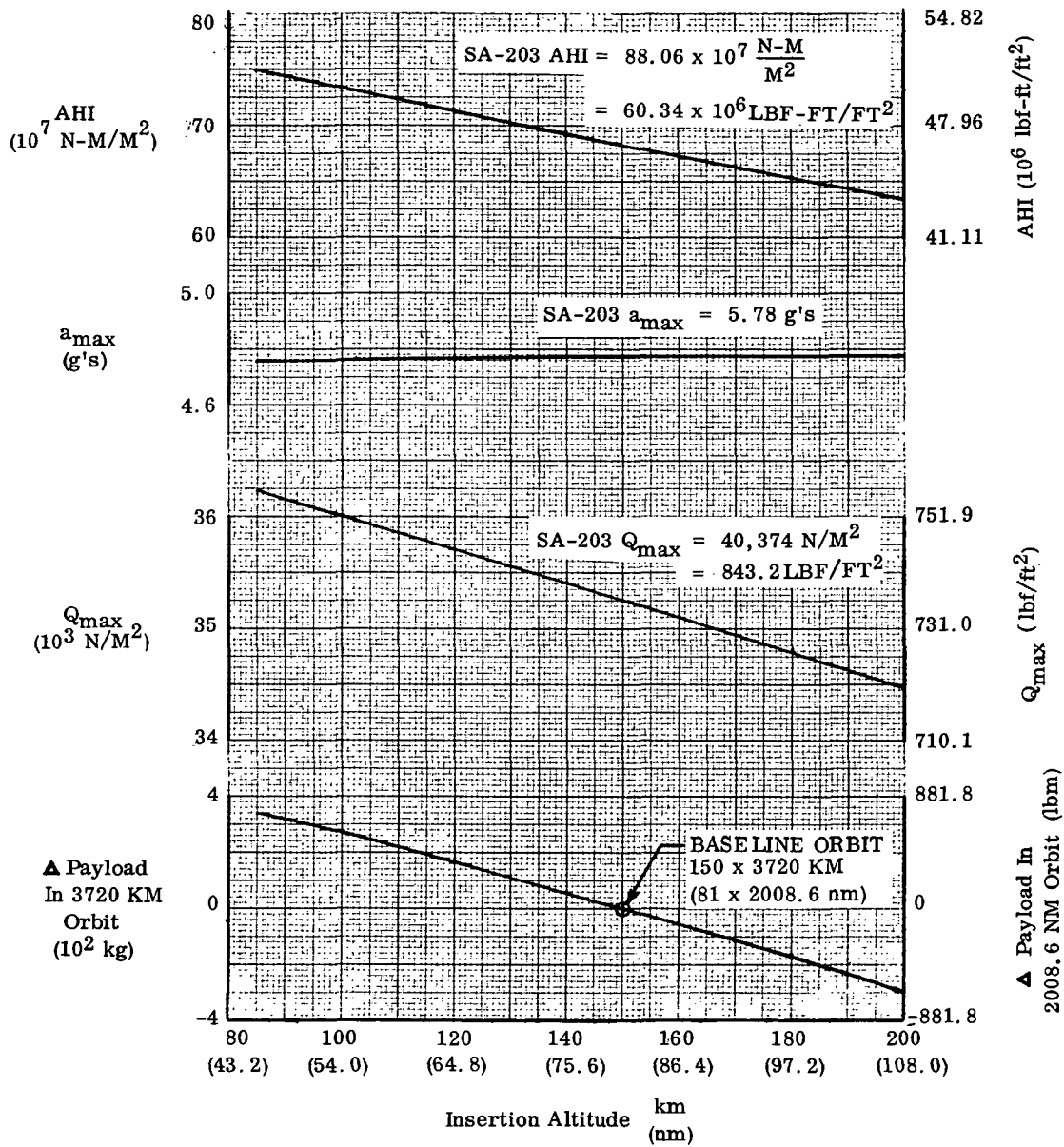


FIGURE 5-12. DELTA-PAYLOAD & FLIGHT ENVIRONMENT VS. INSERTION ALTITUDE

Baseline Flight Profile. The IIP trace and crossrange impact corridor for a 55 degree inclination planar launch are illustrated in Figures 5-13 and 5-14. A 55 degree inclination causes the planar IIP trace to traverse Newfoundland and Eurasia including the Balkan States.

Total landmass impact probability is the same order of magnitude as in the planned Skylab/Saturn IB flights. However, the higher inclination proposed for the SEPS mission results in a number of additional countries within the range safety lateral corridor limits.

Launch Azimuth/Inclination Effects. Figures 5-13 and 5-14 also contain the IIP traces for the 50 degree inclination planar launch and the 55 degree inclination non-planar launch. In Figure 5-14, the IIP trace for the latter trajectory is shown as coincident with the IIP trace for a planar launch to the same inclination. The two IIP traces are very similar, but not coincident; thus the equivalence implied in Figure 5-14 is for clarity only.

For the baseline flight profile and the two alternate trajectories, the impact probability over Eurasia is approximately the same. Differences in the total landmass impact probability for each IIP trace are almost totally attributable to differences in the impact probabilities for Newfoundland. An overfly of Newfoundland is significant because it occurs during an interval when the rate of change in the IIP trace is small compared to the rate of change during an overfly of Eurasia. The result is a much higher dwell time and impact probability for Newfoundland than for a landmass of comparable size in Eurasia. Thus, total landmass impact probability can be reduced if a Newfoundland overfly is avoided.

It is apparent from Figure 5-13 that the dwell time for Newfoundland is highest for a 55 degree inclination planar flight. A slight reduction in dwell time can be achieved by utilizing a non-planar launch to a 55 degree inclination, but the required "dog-leg" maneuver results in a reduced payload capability. The payload loss which will be incurred with boost flight yaw-steering to a 55 degree inclination orbit is shown in Figure 5-15.

Based on a previous range safety analysis of Saturn IB flight to a 55 degree inclination orbit, it was determined that a launch azimuth of about 55 degrees is required to reduce, by an order of magnitude, the Newfoundland impact probability. As illustrated in Figure 5-15, this would reduce the payload capability for the SEPS mission by approximately 952.5 kg (2100 lb).



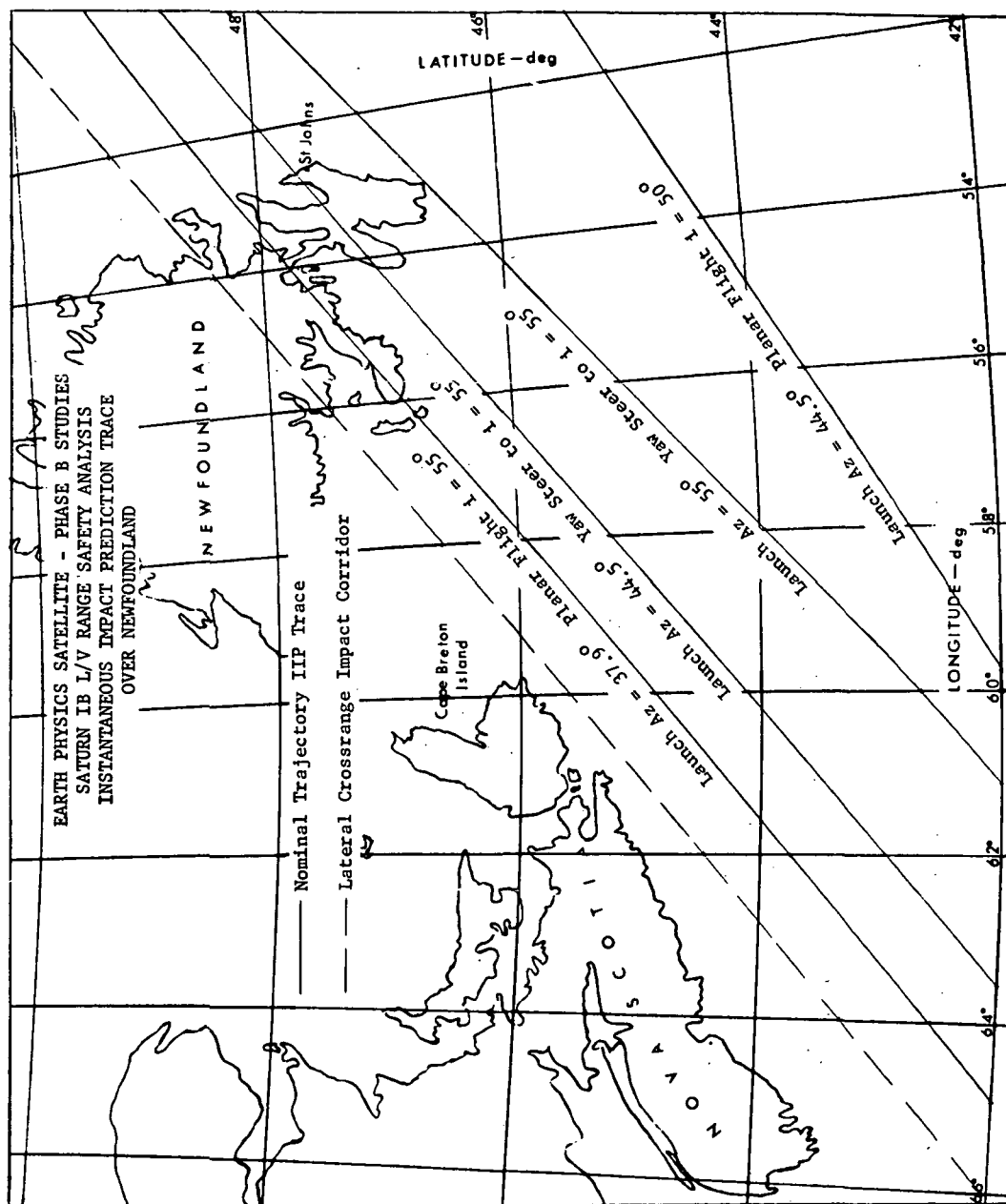


FIGURE 5-13. INSTANTANEOUS IMPACT PREDICTION TRACE OVER NEWFOUNDLAND



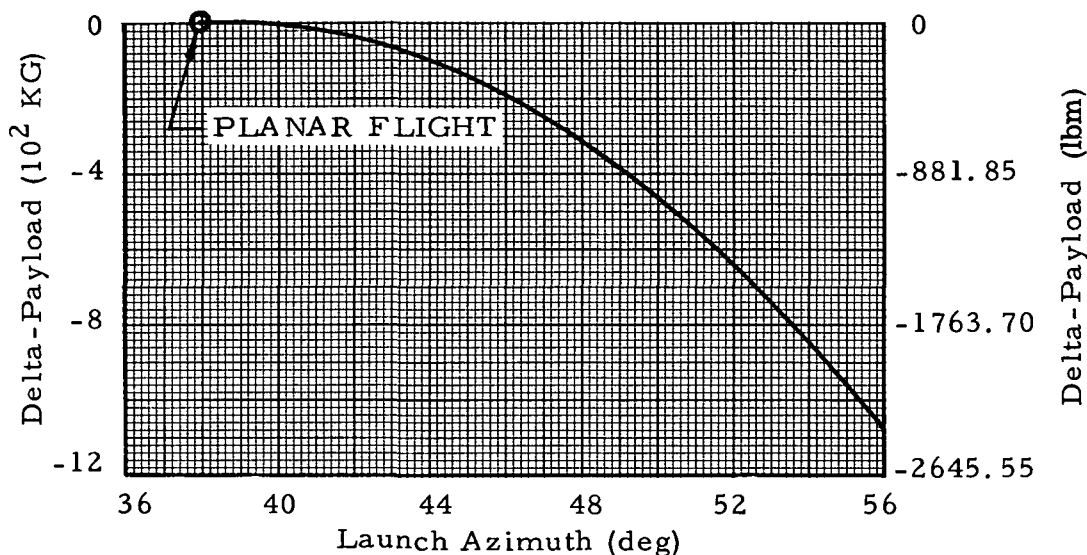


FIGURE 5-15. PAYLOAD PENALTY FOR BOOST FLIGHT  
YAW-STEERING TO 55 DEGREE INCLINATION

A Newfoundland overfly can be completely avoided by reducing the orbit inclination to 50 degrees. This flight plan has the additional advantage of reducing the number of Eurasia countries overflown. The total Eurasian impact probability however, is approximately the same as that for a 55 degree inclination. Reducing the SEPS mission orbit to 50 degrees inclination would increase the Saturn IB payload capability by approximately 226.8 kg (500 lb), as previously presented in Section 5.3.3.1.

#### 5.3.3.3 SLA/NOSECONE JETTISON SEQUENCE

A jettison of the SLA/Nosecone during boost flight can provide a significant payload increase for the SEPS mission. If the jettisonable portion of the SLA/nosecone is separated just prior to active guidance initiation, via a small solid rocket motor (SRM), additional "useful payload" can be carried to orbit. Such a mode of operation was planned for the Saturn IB launch of the AAP "Wet Workshop."

The potential payload increase for the SEPS mission by utilization of the boost flight SLA/nosecone jettison scheme is presented as Figure 5-16. This figure shows the payload to be gained, over that obtainable with the baseline

SLA/nosecone separation sequence, as a function of jettisonable weight. The baseline sequence considers jettison of the SLA/nosecone during the 150 x 3720 km (81 x 2008.6 nm) transfer orbit.

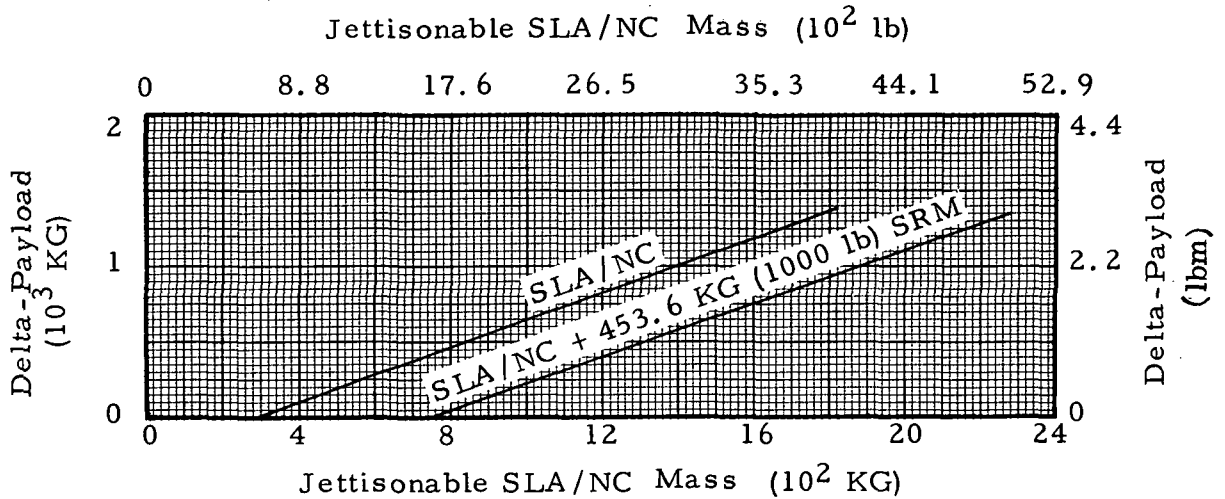


FIGURE 5-16. PAYLOAD INCREASE BY JETTISONING SLA/NOSECONE DURING BOOST FLIGHT

Note that two curves are displayed in Figure 5-16; the one labeled "SLA/NC" represents an idealized case where no additional systems weight is required to effect the jettison. The lower curve reflects the addition of a SRM in order to show the sensitivity of payload to changes in jettisoned weight. For an example of the payload improvement possible with this mode of operation, consider the SLA/Nosecone jettisonable weight of 1639.7 kg (3615 lb) from Table 4-1. Referring to the upper curve, the payload gained by jettisoning this weight during flight would be approximately 1230 kg (2712 lb). However, since it is assumed a SRM will be required to separate the SLA/Nosecone, refer to the lower curve for the payload gain when the jettisoned weight is now 2093.3 kg (4615 lb). Note that the payload increase has been reduced to approximately 1185 kg (2612 lb).

#### 5.3.3.4 LAUNCH VEHICLE WEIGHTS

As shown in Table 4-1, the jettison weight of the SLA/Nosecone is approximately 1639.7 kg (3615 lb) for the Saturn IB/SEPS launch vehicle defined as a result of the Phase B study. A liftoff weight reduction of the jettisonable SLA/Nosecone would permit an increase in payload weight. With the SLA/Nosecone jettisoned in the 150 x 3720 km (81 x 2008.6 nm) elliptical orbit, the payload weight gain is 84% of the SLA/Nosecone weight reduction.

The effect of the S-IVB stage weight is a one-to-one trade with the payload. If the S-IVB stage inert weight (dry plus residuals) is reduced the payload weight can be increased by an equal amount.

#### 5.3.4 ORBITAL STUDIES

##### 5.3.4.1 PRELIMINARY ERROR ANALYSIS

The SEPS mission requires that the eccentricity of the operational orbit be less than 0.01. Therefore, a preliminary orbit error analysis (Reference 13) has been conducted to determine what dispersions in the payload orbit could be expected, due to launch vehicle performance and hardware error sources. This analysis is based on a nominal circular orbit at 3720 km (2008.6 nm) altitude achieved by the S-IVB stage second burn. An inertial hold steering mode is assumed for the S-IVB restart, and all error sources identified as possible contributors to the orbit dispersion are examined to ascertain their individual and combined effects.

The nominal S-IVB restart sequence of events was assumed to be referenced to a timebase established at 5 degree elevation acquisition by the tracking station at Carnarvon, Australia. During the orbit coast prior to restart, the vehicle attitude is maintained nose forward in a local horizontal hold mode. At 40 seconds prior to the J-2 restart ignition, an inertial hold mode is commanded and maintained throughout the S-IVB second burn.

The nominal steering mode described above for orbital flight was selected for its simplicity and correspondence to orbital attitude maneuvers which have been performed during S-IVB/IU flights during the Apollo program. Performance during the S-IVB apogee burn was not a determining factor in selecting this flight sequence; using alternate steering modes, i.e., attitude programmed to provide thrust colinear with the inertial velocity vector, etc., does not reduce the propellant requirement.

Presented in Figure 5-17 are the effects on orbit eccentricity due to the error sources identified as contributors to orbit dispersion, when utilizing the simplified guidance scheme assumed for the S-IVB stage apogee burn.

The first source of error examined was that associated with an off-nominal establishment of the timebase at tracking station acquisition, caused by dispersions in apogee of the transfer orbit at S-IVB stage first burn cutoff. The apogee dispersions are a combination of the effects due to guidance hardware errors and the expected deviations in J-2 engine thrust decay impulse following

RESTART SEQUENCE TIME BASE INITIATED AT CARNARVON ACQUISITION (elev. = 5°)

VEHICLE ATTITUDE MAINTAINED NOSE FORWARD IN LOCAL HORIZONTAL DURING COAST

INERTIAL ATTITUDE MAINTAINED DURING SECOND S-IVB BURN

NOMINAL ORBIT ECCENTRICITY = .0001

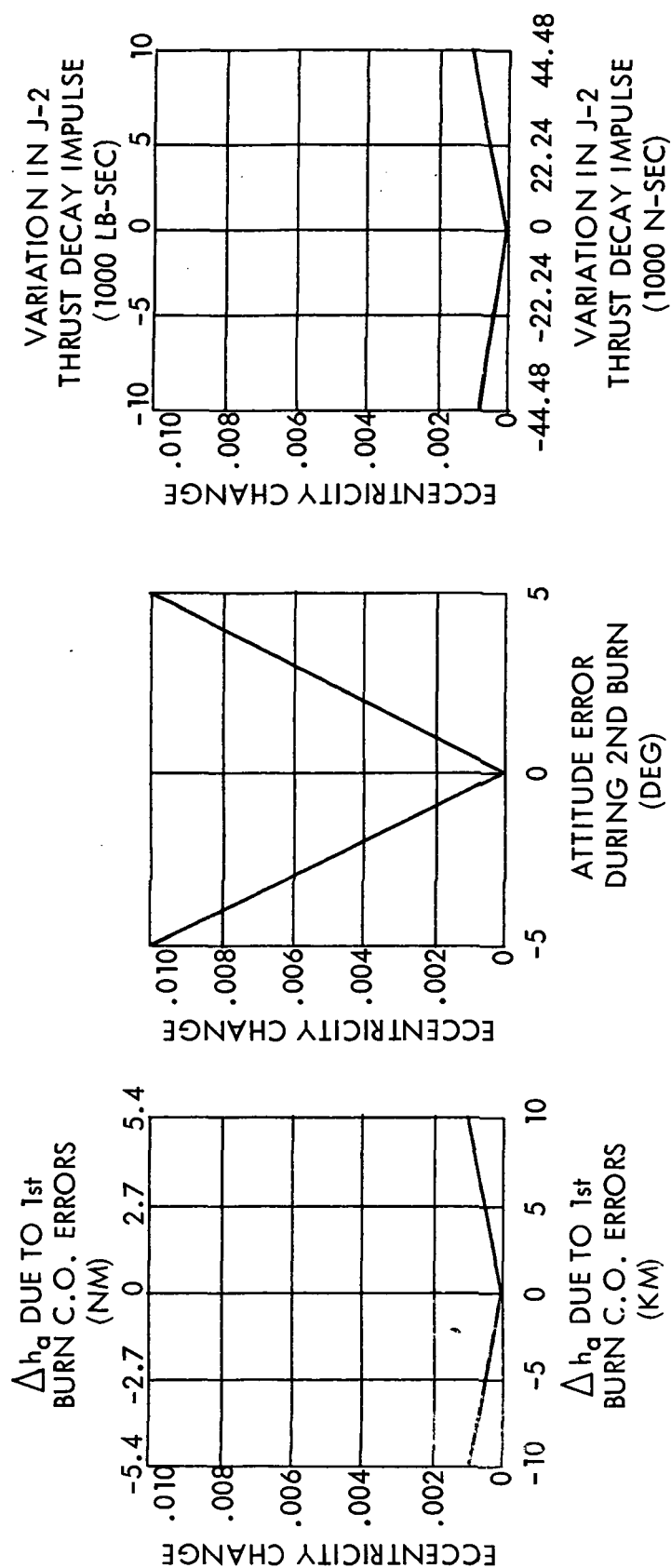


FIGURE 5-17. PRELIMINARY ORBIT ERROR ANALYSIS

the first burn cutoff. The expected dispersions in apogee were found to be approximately  $\pm 8.5$  km ( $\pm 4.6$  nm). To be conservative, trajectory simulations were then made in which the first burn cutoff yielded orbits having  $\pm 10$  km ( $\pm 5.4$  nm) dispersion in apogee. Using these dispersed trajectories, and again establishing the sequence of events at Carnarvon acquisition, the S-IVB stage restart was resimulated. The resultant dispersion in orbit eccentricity is as shown by the first plot of the figure, a dispersion of 0.001 from nominal.

The next error source considered was that of an attitude error during the apogee burn. Since it was uncertain what error magnitude might be associated with the proposed steering scheme, attitude errors up to  $\pm 5$  degrees were considered. These results are shown by the center plot. If the nominal attitude "deadband" of 1 degree (normally considered for orbital attitude hold modes) is assumed as representative for the inertial hold mode during the S-IVB burn, then the resultant orbit eccentricity dispersion is about 0.001.

The final plot of Figure 5-17 shows the effects on orbit eccentricity due to variations in J-2 thrust decay impulse following the apogee burn. Using the  $\pm 26,422$  N-sec ( $\pm 5940$  lb-sec) dispersion in thrust decay impulse provided for the launch vehicle dispersion analysis, a dispersion of 0.0005 in orbit eccentricity was obtained.

Based on the preliminary orbit error analysis described in the preceding paragraphs, it appears that holding orbit eccentricity dispersions to less than  $\pm 0.005$  should be within the capability of the launch vehicle identified for the SEPS mission.

#### 5.3.4.2 ORIENTATION OF SATELLITE SPIN AXIS

Presented below are results of an analysis performed (Reference 14) to determine the launch window resulting from the geometric orientation requirement of the SEPS spin axis.

In order to control the orbital thermal heating, the SEPS will have a spin rate at separation of approximately 0.6 degree per second. The most effective orientation of the satellite spin axis is perpendicular to the ecliptic plane, providing a constant sun direction relative to the spin axis. In order to minimize the out-of-plane yaw maneuver of the S-IVB to provide the desired spin axis orientation, the orbital node should have an initial alignment of 180 degrees from the vernal equinox direction for orbit and ecliptic plane relative orientation. Initial orientation of the orbit plane is a function of time of year and time of day the ground launch occurs. The time to launch from Kennedy Space Center into

the 55-degree-inclination orbit in order to effect the desired 180-degree orientation of the orbit plane is given in Figure 5-18 as a function of time of year. Launch time is given both for a northerly and a southerly launch azimuth although only northerly launches are being considered for the mission. Referring to the figure, launch dates between February 1 and July 1 would require a nighttime launch, where the scheduled launch time would be between 7 p. m. and 5 a. m. at KSC.

The minimum yaw maneuver required of the S-IVB stage is 11.5 degrees (90 degrees minus the ecliptic plane inclination of 23.5 degrees and the orbit plane inclination of 55 degrees). If the yaw maneuver was constrained to 11.5 degrees, this would allow only an on-time launch and would not permit any launch delay. Figure 5-19 depicts the ground launch window duration versus S-IVB stage yaw maneuver required to give the satellite the desired spin-axis orientation. A 30-degree yaw maneuver limit would provide a 5.7-hour ground launch window once every 24 hours, considering only one launch azimuth; in either a northerly or a southerly direction.

Separation of the satellite and the S-IVB stage would be scheduled to occur at the orbital line of nodes for the nominal launch-on-time conditions. This is the optimum point in orbit for separation which would require the minimum 11.5-degree yaw maneuver to orient the satellite spin-axis perpendicular to the ecliptic plane.

The yaw maneuver requirement sensitivity for a separation point other than at the ascending or descending nodes is given in Figure 5-20. Considering a 30-degree limit on the S-IVB yaw maneuver, separation of the S-IVB stage and satellite could take place between southern and northern latitudes of 22.5 degrees.

#### 5.3.4.3 RELATIVE MOTION DUE TO SEPARATION

Separation of the SEPS from the S-IVB stage will be performed by a spring system. As a result, a positive velocity increment is imparted to the satellite causing the separation point to be perigee of the satellite orbit while a negative velocity increment is imparted to the S-IVB stage causing the separation point to be apogee of the S-IVB orbit.

As discussed in the previous section, to achieve the desired orientation of the satellite spin axis requires a minimum S-IVB out-of-plane angle at separation of 11.5 degrees. Since an off-nominal launch time would increase the required orientation angle, a maximum out-of-plane angle of 30 degrees was considered in the separation analysis (Reference 14).



o Orbit Inclination of 55 Degrees

Time of Day  
at Cape - Hrs

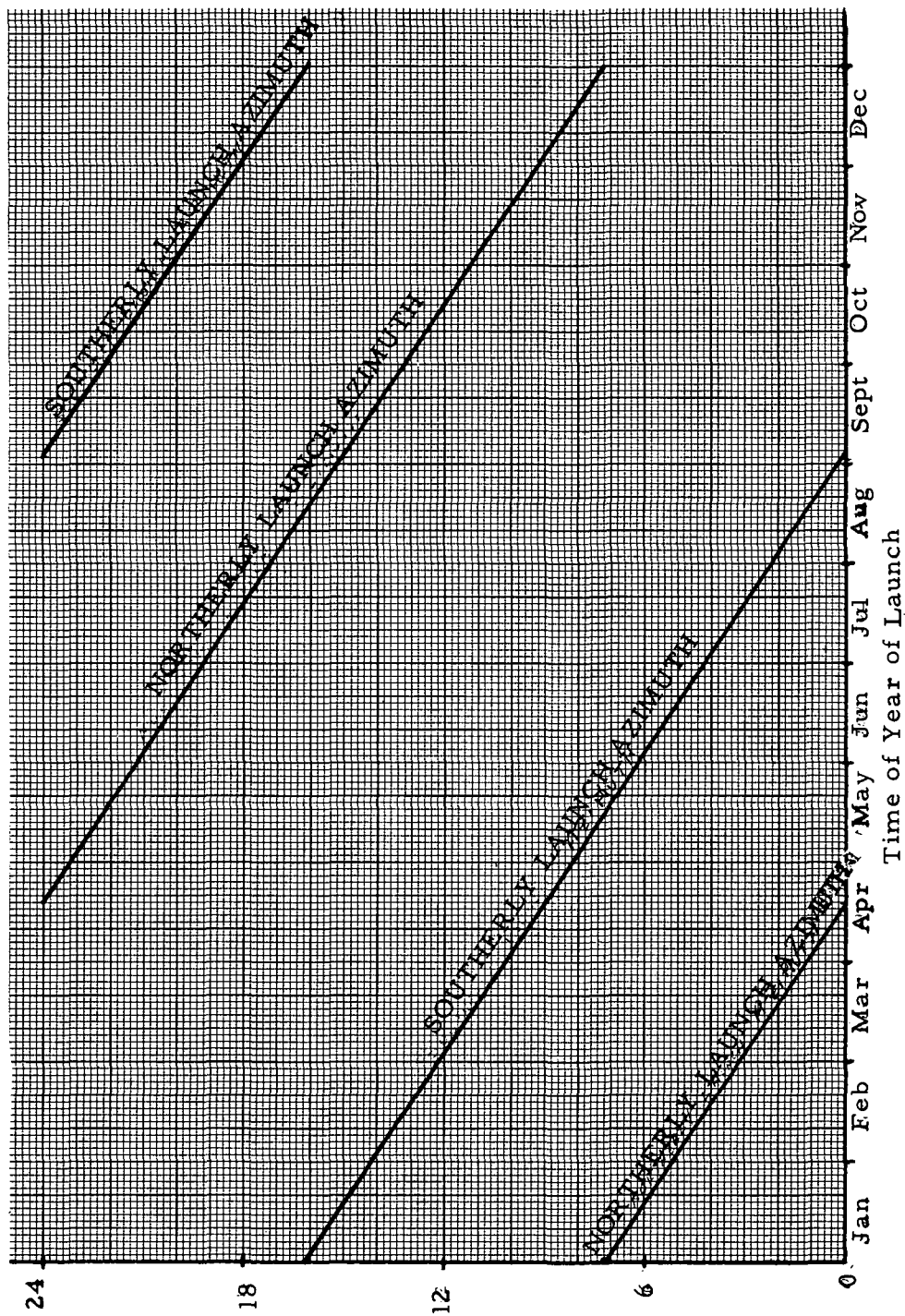


FIGURE 5-18. TIME OF LAUNCH FOR ORBITAL NODE OF 180 DEGREES

° ORBIT INCLINATION OF 55 DEGREES

X<sub>Y</sub> (DEG)

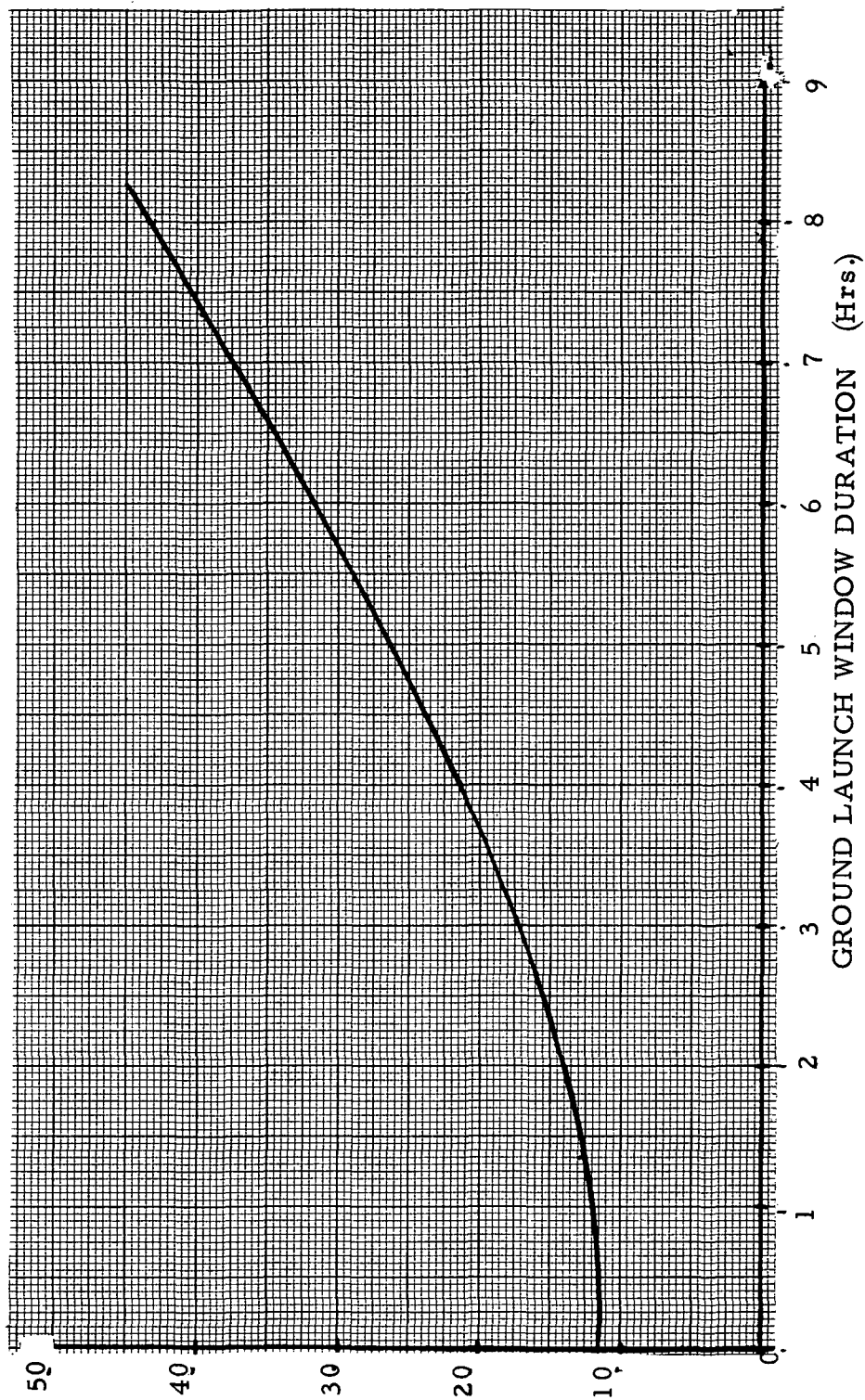


FIGURE 5-19. LAUNCH WINDOW VS. YAW MANEUVER

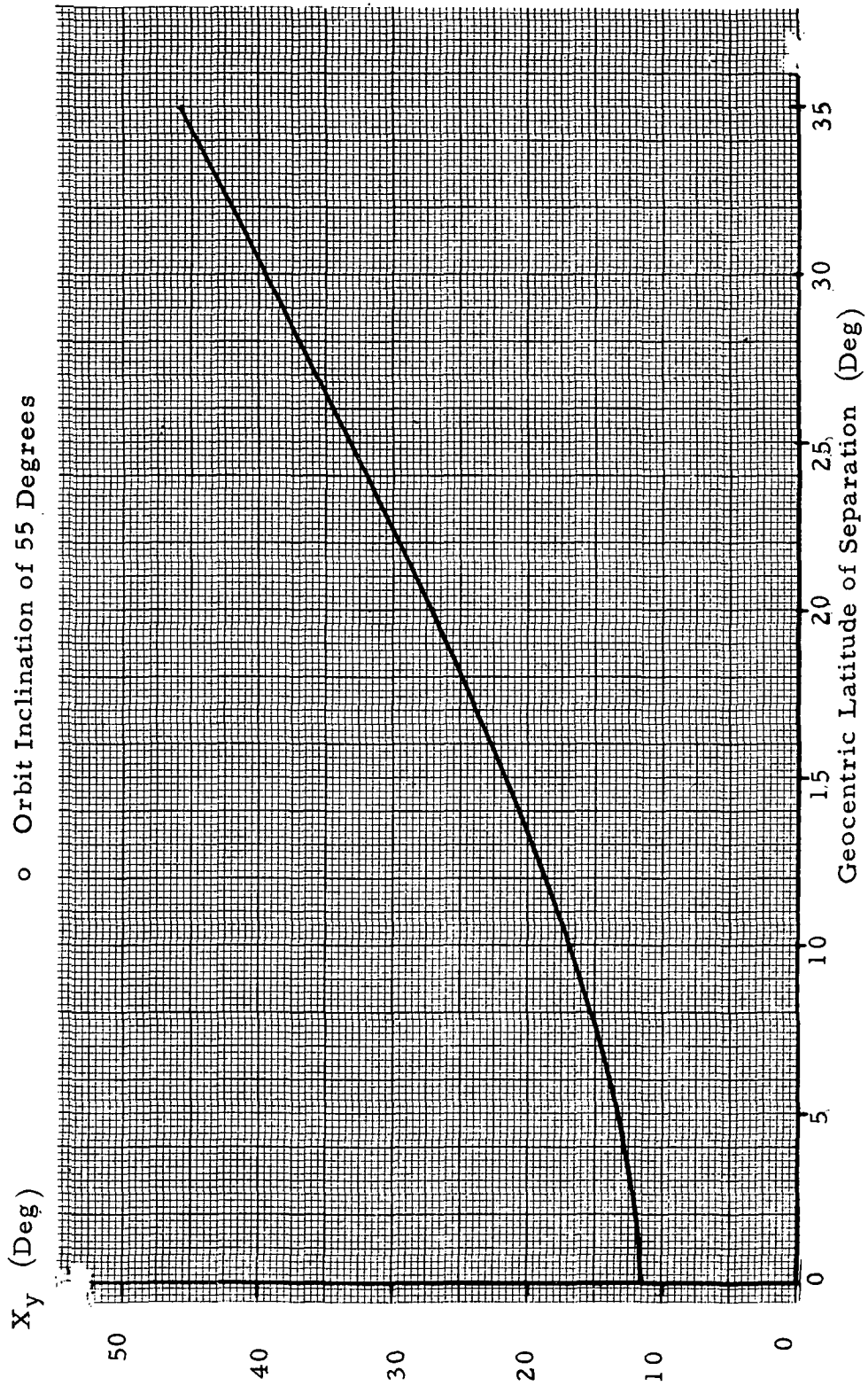


FIGURE 5-20. LATITUDE AT SEPARATION VS. YAW MANEUVER

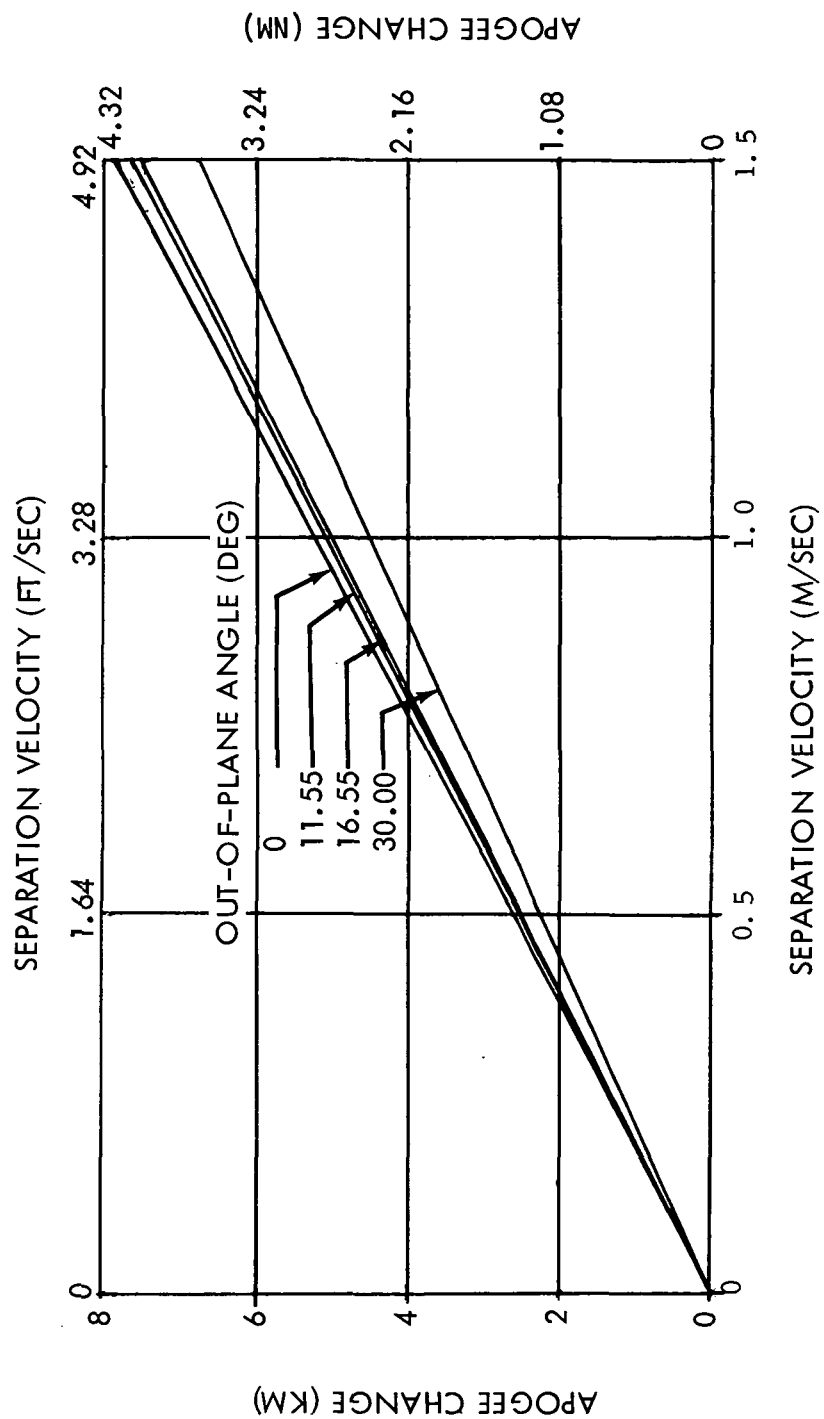


FIGURE 5-21. APOGEE CHANGE DUE TO SEPARATION VELOCITY

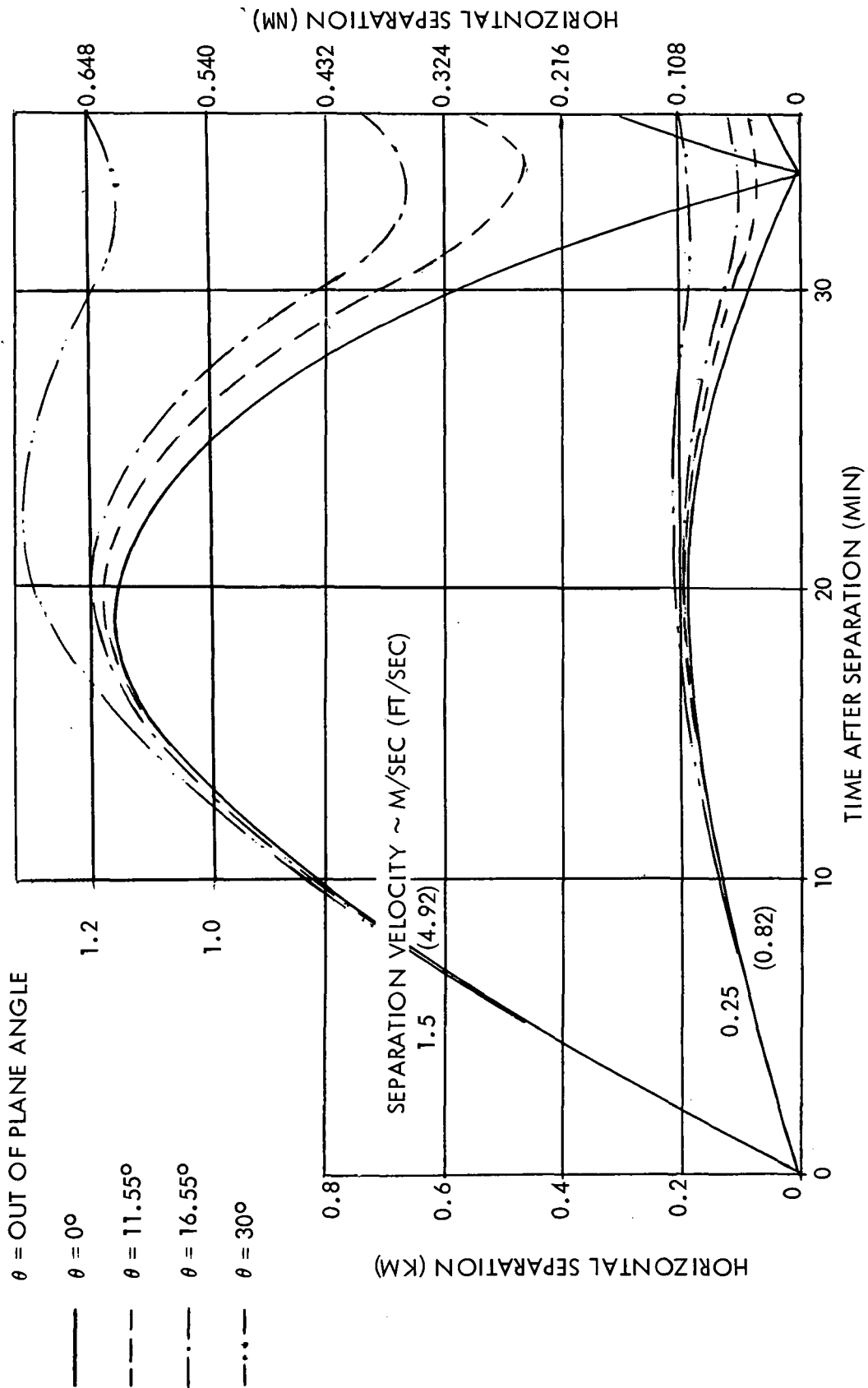


FIGURE 5-22. HORIZONTAL SEPARATION TIME HISTORY

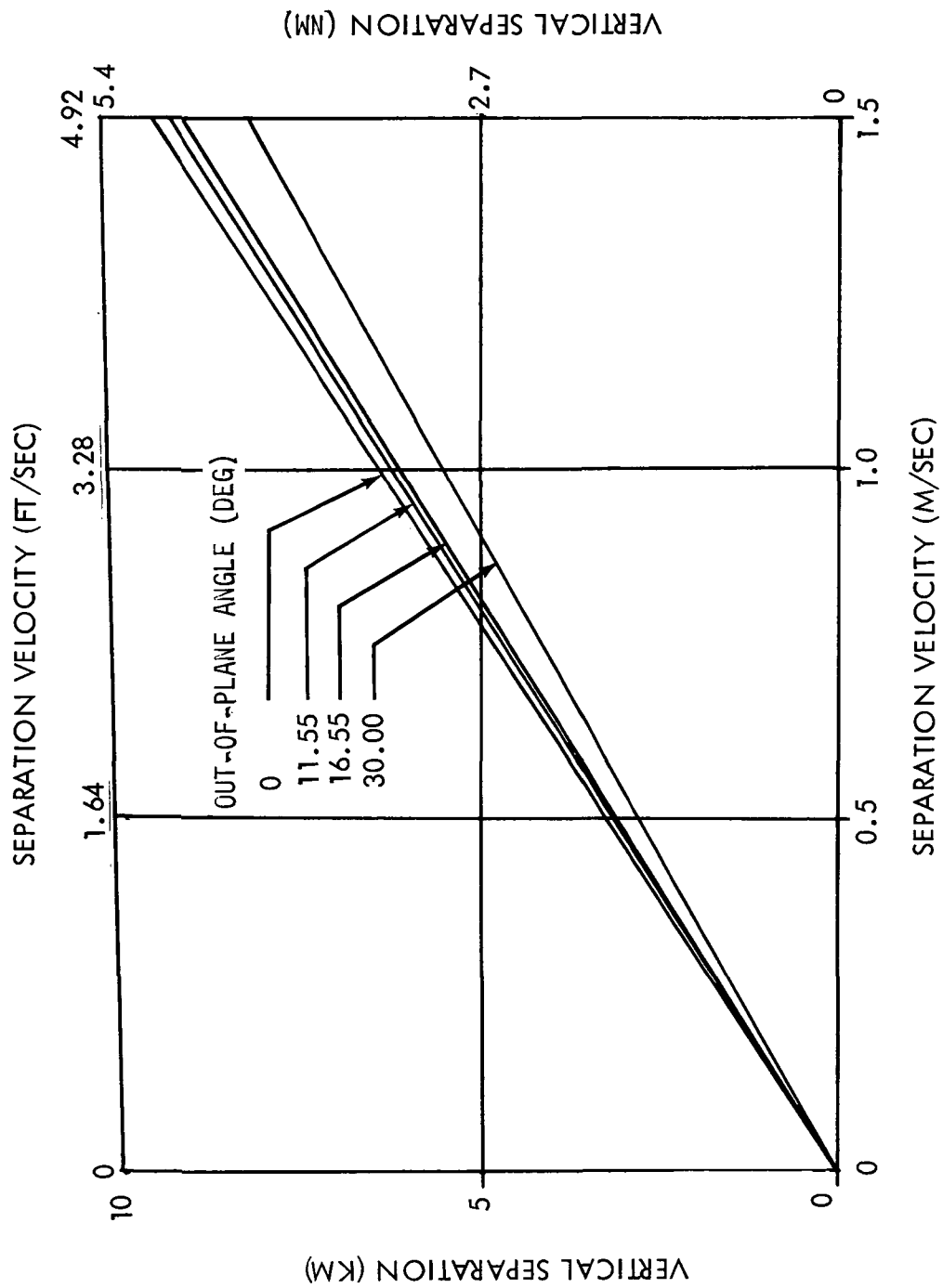


FIGURE 5-23. MAXIMUM VERTICAL SEPARATION

Figure 5-21 presents the change in apogee of the SEPS orbit as a function of separation velocity. A time history of the horizontal separation distance is shown in Figure 5-22 while Figure 5-23 shows the maximum vertical separation between the SEPS and the S-IVB as a function of separation velocity. The maximum vertical separation distance occurs at 84 minutes after separation and is the point at which the first retroburn for the evasive maneuver would occur.

#### 5.3.4.4 S-IVB/SATELLITE RECONTACT ANALYSIS

The following present results of an analysis of the S-IVB evasive maneuver which will be performed in order to minimize the possibility of a recontact with the payload. Additional information on the evasive maneuver is presented in References 7, 13, and 14.

Figure 5-24 shows the impulsive  $\Delta V$  required to achieve a desired change in S-IVB/IU orbit altitude. The total  $\Delta V$  requirement is shown for several attitude angles during the first burn of a two impulse maneuver, required to establish a circular orbit below the initial orbit altitude. The S-IVB stage attitude for the second burn, at perigee of the transfer orbit, is assumed to be 180 degrees in all cases.

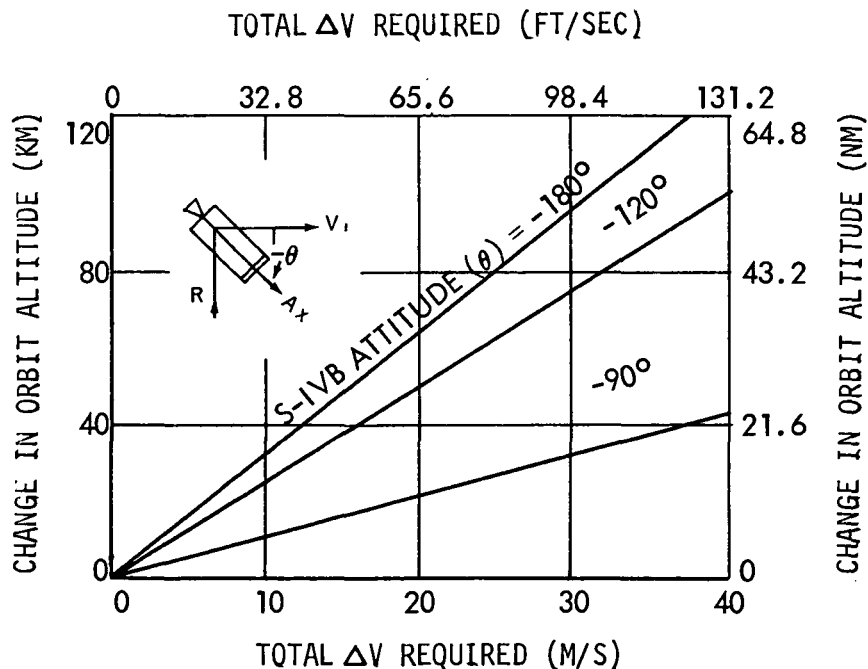


FIGURE 5-24. S-IVB DELTA-VELOCITY REQUIRED TO ESTABLISH ORBIT BELOW PAYLOAD

The velocity increments required for the evasive maneuver could be provided by: 1) the APS system, 2) a propellant dump producing thrust as the residual LOX and LH<sub>2</sub> are dumped through the J-2 engine, or 3) a combination of these. It is anticipated that the APS system will be used to perform the SEPS mission evasive maneuver. Figure 5-25 provides an indication of the total velocity increment available as a function of S-IVB APS propellant.

Present plans, for the SEPS mission, are to off-load the S-IVB/V APS modules by 50 percent. As shown in Section 4.2.1.1, it is estimated that 45.4 kg (100 lb) of APS propellant will be available for the two S-IVB evasive maneuver burns. From Figure 5-25, this will provide a velocity increment of 6.3 m/s (20.7 ft/sec) and a maximum altitude change of 20 km (10.8 nm) as shown in Figure 5-24.

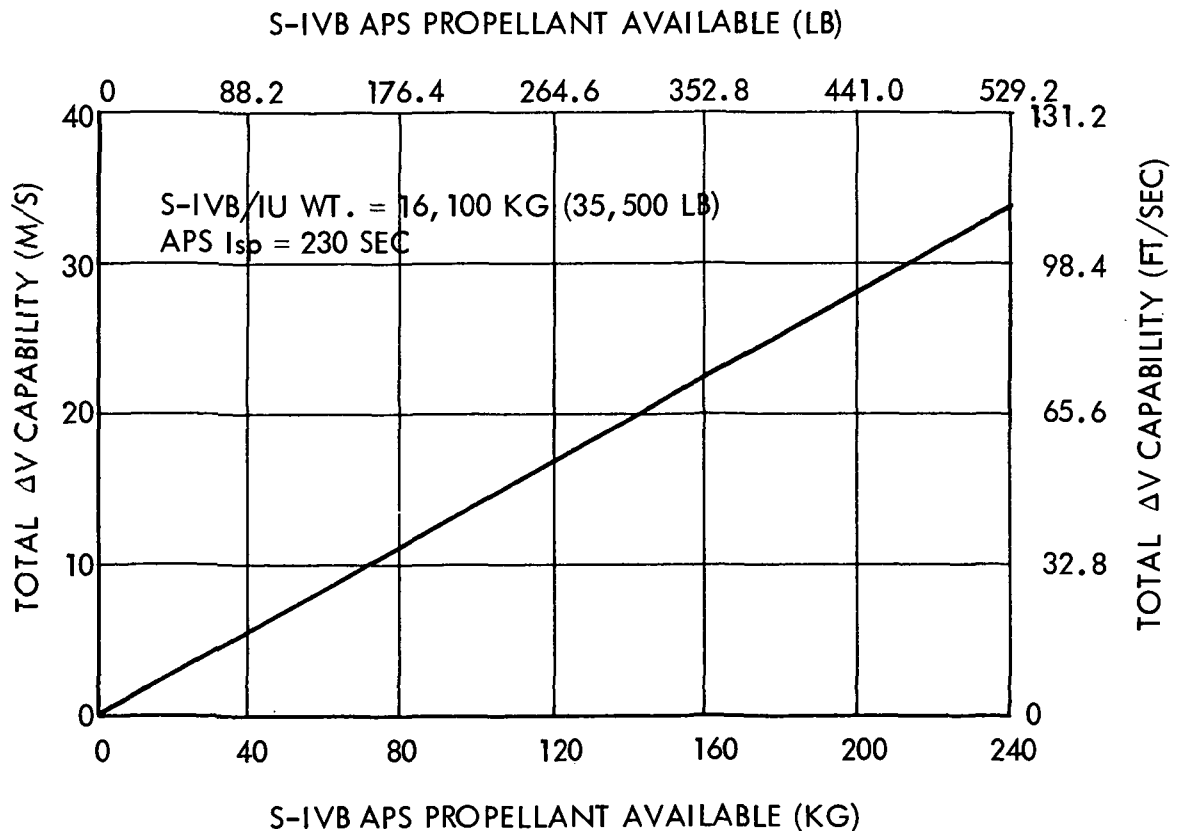


FIGURE 5-25. TOTAL DELTA-VELOCITY CAPABILITY OF S-IVB APS SYSTEM



The first retro impulse should be applied at the point of maximum vertical separation; i. e. , 84 minutes after separation, corresponding to the first nodal crossing after separation. The second retro impulse should be applied at 168 minutes after separation, corresponding to the second nodal crossing after separation. Figures 5-26 and 5-27 present time histories of the relative separation distances between the SEPS and S-IVB stage for several retro velocities.

#### 5.3.4.5 SATELLITE LIGHTING

The amount of time the satellite is in sunlight is determined from the orbit altitude and the solar look angle which is a function of the orbit inclination and relative alignment of the earth-sun line with respect to the orbit plane. The magnitude of the solar look angle has a range of  $\pm 78.5$  degrees for an orbit inclination of 55 degrees. The minimum time the satellite spends in sun light in the operational orbit is 132 minutes per orbit, the amount of earth occultation being 36 minutes per orbit. This condition occurs when the solar look angle is zero. There will be periods of time when the solar look angle is greater than 39 degrees and the satellite will have 100 percent illumination per orbit. A time history of the solar look angle is given in Figure 5-28 for a launch date of March 21. There will be three times during a one-year mission when there is no earth occultation. Maximum duration with 100 percent sun illumination is 50 days. The total time the satellite will spend in 100 percent sun light will be approximately 120 days per year.

#### 5.3.4.6 SATELLITE DESPIN

A magnetic damping torque resulting from the interaction of the earth's magnetic field with the rotating solid spherical mass of the satellite will generate eddy currents causing the satellite to despin. The magnitude of the eddy current is a function of orbital altitude, inclination, and the parameters characterizing the satellite configuration.

As shown in Reference 14, the estimated time for the SEPS to despin to 0.1 of its initial spin rate is 3-years for a worst case orientation with the spin axis perpendicular to the magnetic field. For parallel alignment there would be no eddy current set up and no despin torque.

If this rate of despin presents a problem for controlling the orbital thermal condition of the satellite, lamination of the core and caps (which make up the satellite sphere) with several thin sheets of an insulator perpendicular to the spin axis would avoid or reduce the despin rate. Installing the insulation would increase the time required to despin, to 0.1 of the initial spin rate, to more than 10 years.

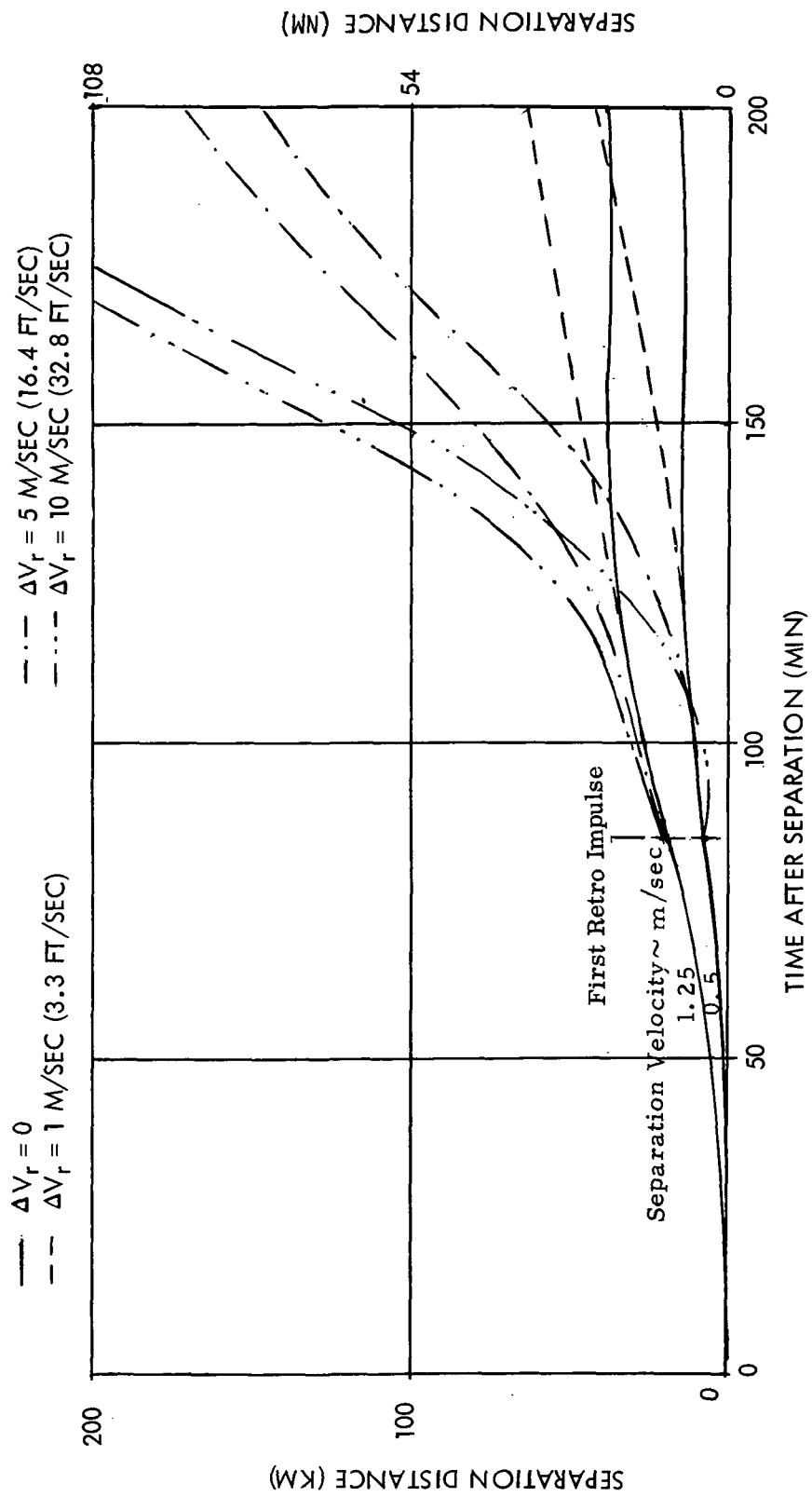


FIGURE 5-26. EFFECT OF ONE S-IVB RETRO IMPULSE

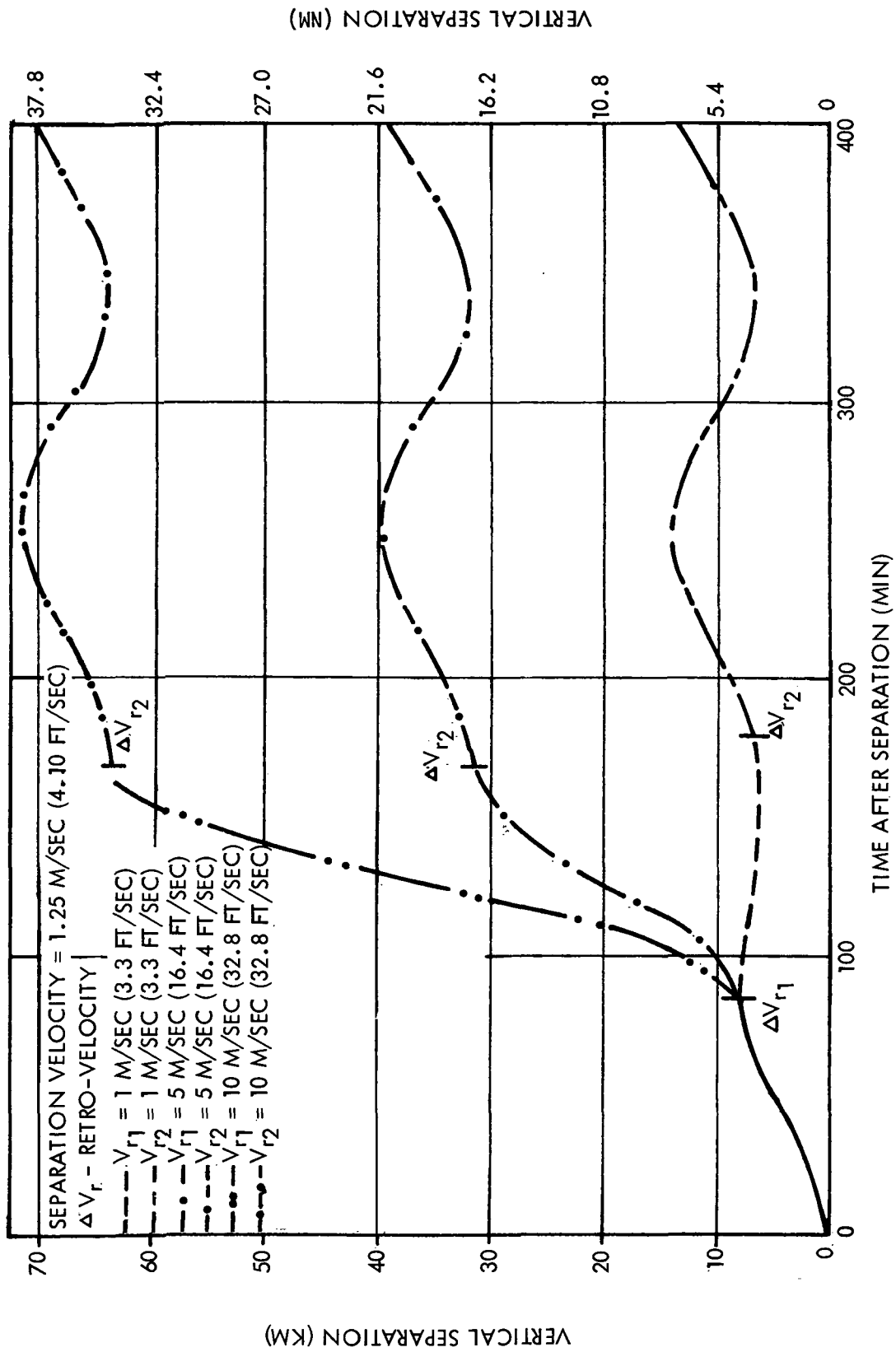


FIGURE 5-27. EFFECT OF TWO S-IVB RETRO IMPULSES

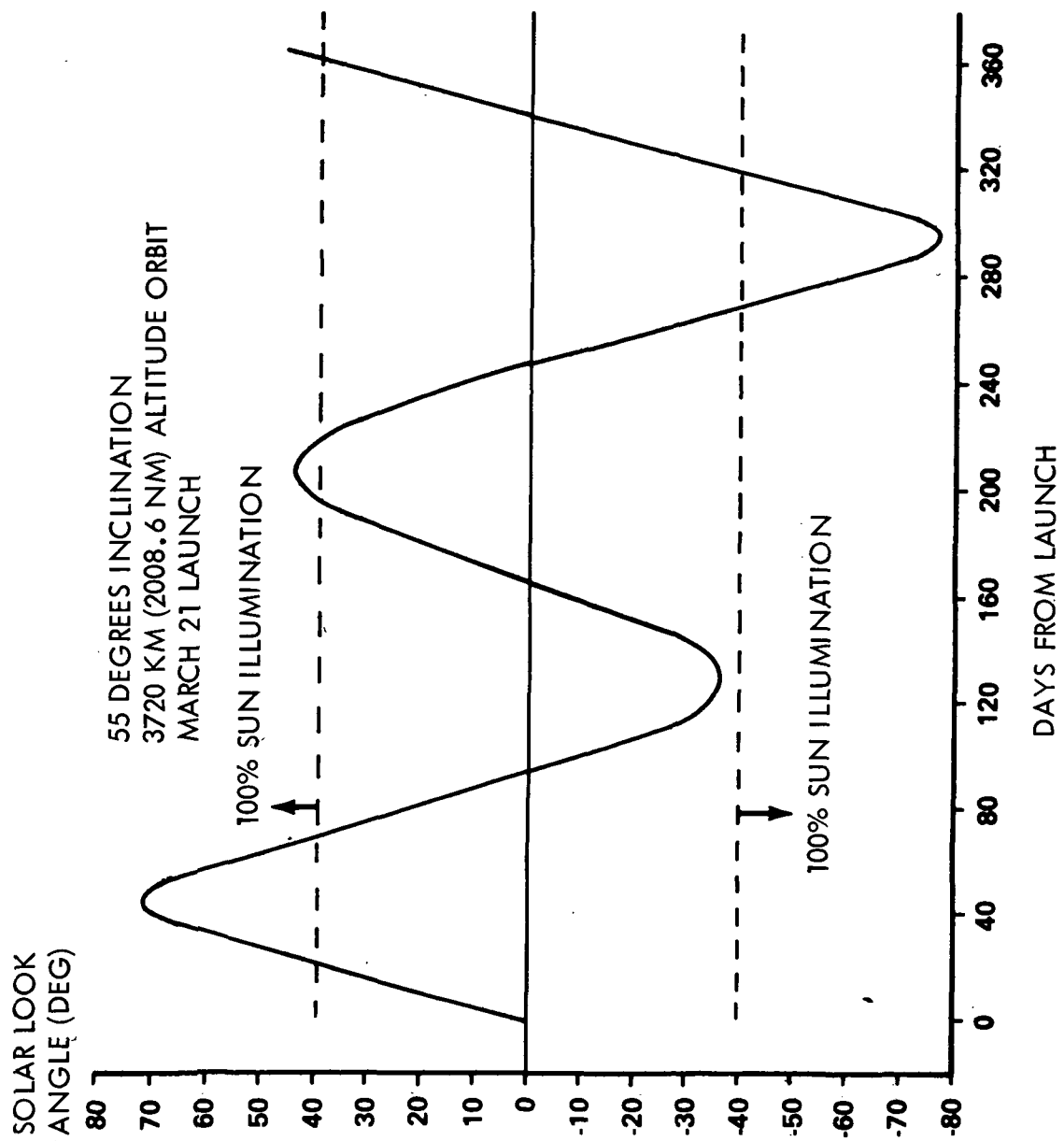


FIGURE 5-28. TIME HISTORY OF SOLAR LOOK ANGLE

## 5.4 TRACKING AND COMMUNICATIONS

Because the SEPS mission involves an unmanned launch with a passive payload, an original groundrule imposed on the Phase B study states that no downrange tracking installations are required. However, if the downrange facilities are maintained in an operational status for future Skylab missions, it is anticipated that they would be used for the SEPS mission. Consequently, the tracking and communications analysis results are presented in this section in two parts: coverage with the Skylab network and minimum requirements for assurance of mission objectives. Additional tracking and communications results are presented in References 15 and 16.

### 5.4.1 COVERAGE WITH SKYLAB NETWORK

The Skylab tracking, telemetry, and command communications system network consists of twelve stations shown in Table 5-9. Also described are the systems available at each station along with station symbol designations and coordinates.

A tracking coverage summary of the SEPS launch vehicle from liftoff through 8 hours of flight is displayed on the world maps presented as Figures 5-29 and 5-30. A detailed communications timeline, based on coverage above zero elevation angle, is shown in Figure 5-31. Continuous tracking coverage of the launch phase to insertion in the 150 x 3720 km (81 x 2008.6 nm) orbit is provided by MILA, Bermuda, and the Insertion Ship. Jettison of the SLA/Nose-cone occurs during coverage by Madrid. Tracking of the S-IVB stage restart sequence is covered by the Australian stations at Carnarvon and Honeysuckle. Separation of the payload occurs within view of Hawaii. The first of the two APS retroburns performed by the S-IVB stage is covered by Ascension Island and Canary Island, while the second is under surveillance of Guam and Honeysuckle.

The previous results, based on coverage above zero elevation angle, show that adequate tracking coverage should be available for all critical events during launch vehicle flight. However, an analysis of anticipated signal levels at Carnarvon, Australia, during S-IVB engine restart shows that only marginal telemetry and command data links are anticipated. The slant range from the Carnarvon station to the launch vehicle at S-IVB restart will be approximately 4845 km (2616 nm). The tracking radar signal will be 20 dB above the threshold level. The present VHF telemetry will have a greater than nominal bit error rate with only 10 dB above receiver threshold signal. The command transmitter will provide only 2 dB above the threshold signal and a solid locked command link cannot be assured until after the burn has occurred.

TABLE 5-9  
TRACKING AND COMMUNICATIONS NETWORK

STATION	TYPE (1)	SYMBOL	GEODETIC LATITUDE(2) (DEG NORTH)	LONGITUDE(2) (DEG EAST)
MILA	CCS, T, C	MIL	28.508272	-80.693417
Bermuda	CCS, T, C	BDA	32.351286	-64.658181
Insertion Ship	CCS, T, C	INS	46.000000	-55.000000
Canary Island	CCS, T	CYI	27.764536	-15.634814
Ascension	CCS, T	ACN	-7.955056	-14.327578
Madrid	CCS	MAD	40.455358	- 4.167394
Carnarvon	CCS, T, C	CRO	-24.907592	113.724247
Honeysuckle	CCS	HSK	-35.597222	148.979167
Guam	CCS, T	GWM	13.309244	144.734414
Hawaii	CCS, T	HAW	22.124897	-159.664989
Goldstone	CCS	GDS	35.341694	-116.873289
Corpus Christi	CCS, T	TEX	27.653750	-97.378469

NOTES:

- (1) CCS denotes command and communications systems; T denotes telemetry stations; and C denotes C-band radar stations.
- (2) All coordinates are referenced to Fischer Ellipsoid of 1960.

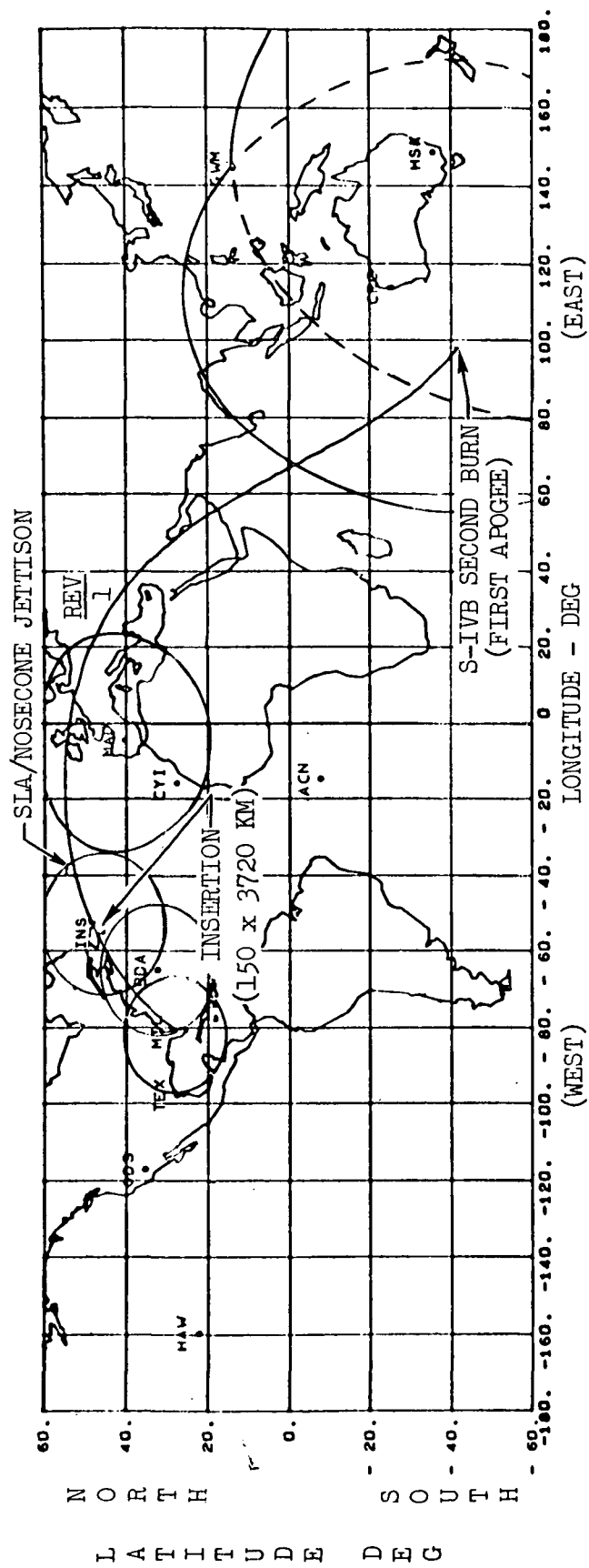


FIGURE 5-29. TRACKING COVERAGE - LIFTOFF THROUGH S-IVB RESTART

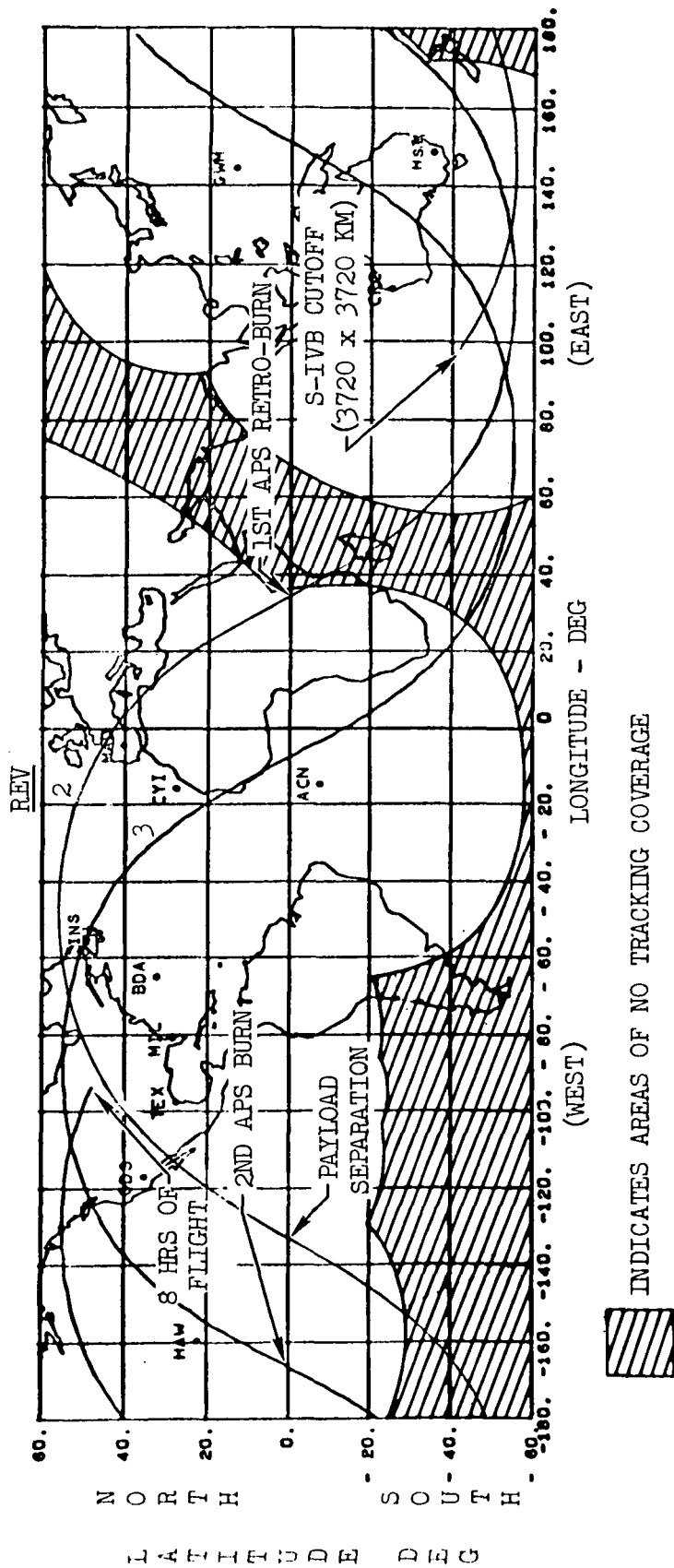


FIGURE 5-30. TRACKING COVERAGE FOLLOWING S-IVB RESTART



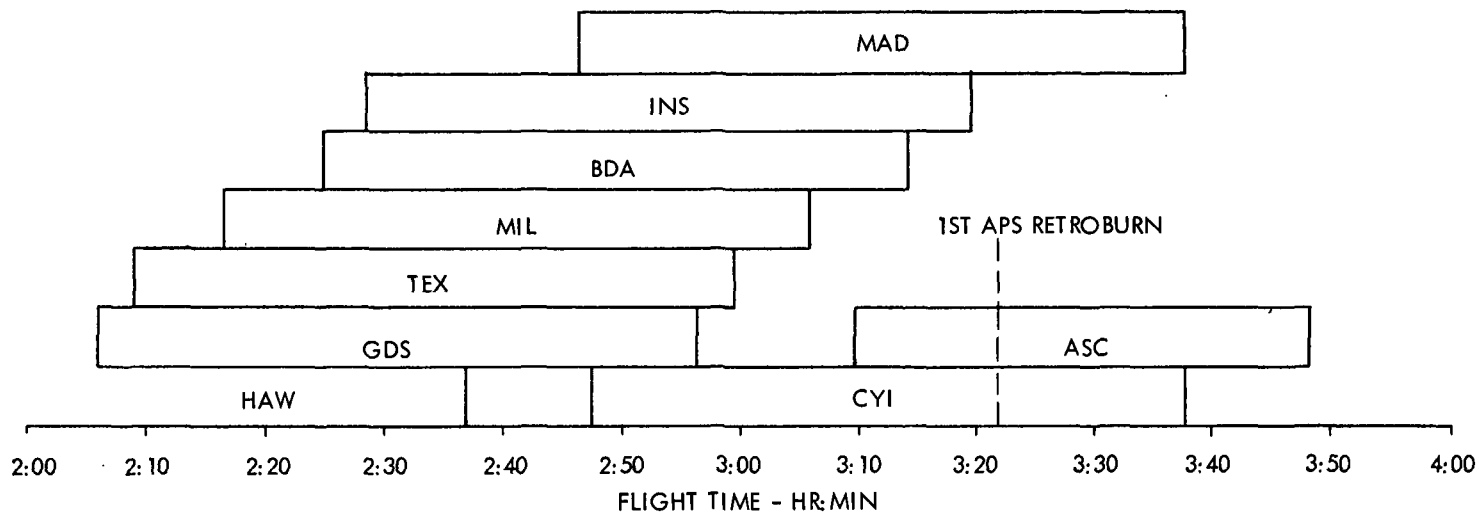
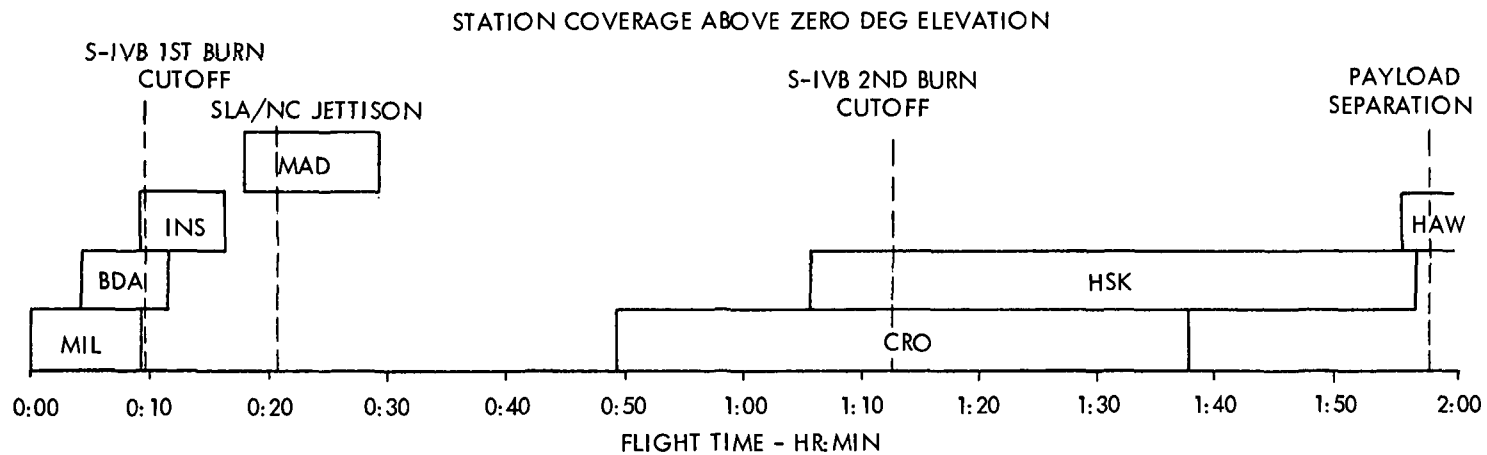


FIGURE 5-31. COMMUNICATION TIME LINES

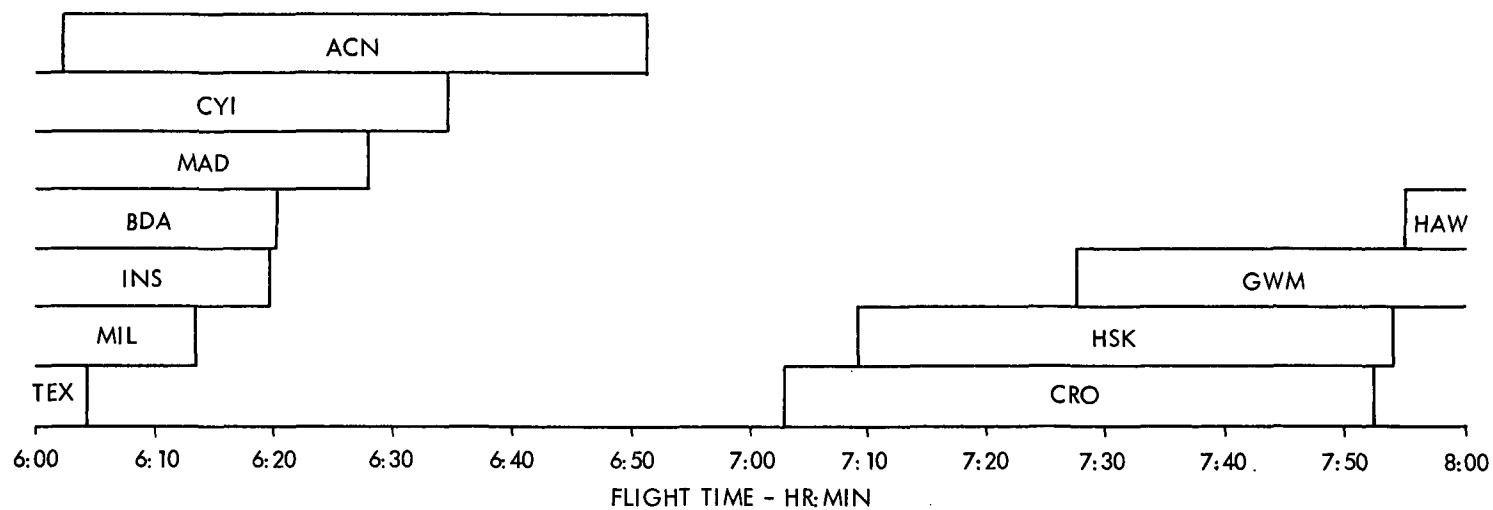
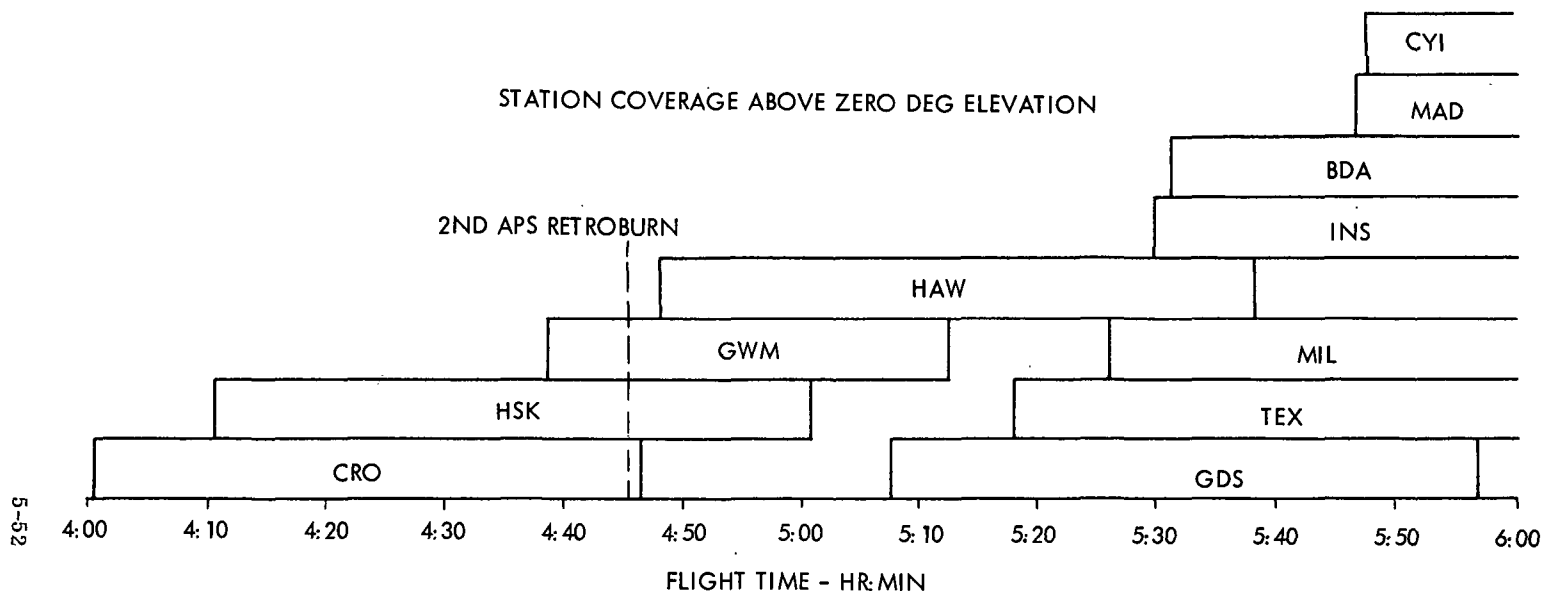


FIGURE 5-31(CONT), COMMUNICATION TIME LINES

Although telemetry and command data links are not a requirement at this time, the S-IVB restart sequence can be covered by placing an instrumentation ship near latitude  $45^{\circ}$  South and longitude  $90^{\circ}$  East. This location would cover the planned S-IVB restart at first apogee in the  $150 \times 3720$  km ( $81 \times 2008.6$  nm) orbit, as well as second apogee should the planned restart be delayed. The ship will be south of apogee at both opportunities with a slant range to the launch vehicle of 3969 km (2143 nm) and an average TM signal level of 15 dB above threshold at first opportunity. At second apogee, the slant range to the launch vehicle will be 4709 km (2543 nm) with an average TM signal level 13 dB above threshold.

#### 5.4.2 MINIMUM COVERAGE FOR ASSURANCE OF MISSION OBJECTIVES

The absolute minimum number of stations required to verify mission success is the radar and telemetry facilities at the Merritt Island Launch Area (MILA). Complete tracking and performance telemetry data are available until approximately 540 seconds after liftoff when the minimum elevation angle of zero is reached at a slant range of 1448 km (782 nm) to the launch vehicle. At that time, the signal level of the tracking radar will be 32 dB above receiver threshold. The vehicle telemetry signal level at the VHF station and the command link signal level will be 22 dB and 13 dB, respectively, above receiver threshold.

With only the MILA station, initial orbit attainment is not known immediately and second burn cannot be verified until the end of the first revolution, some 168 minutes later. At the end of the first revolution the vehicle will be at a slant range of approximately 6200 km (3348 nm) from MILA. The radar will have a signal above threshold margin of 20 dB and the telemetry will have a margin of 10 dB above threshold.

For verification that first orbital insertion is attained, a tracking ship with radar, telemetry, and command capabilities should be located at  $-60^{\circ}$  East,  $40^{\circ}$  North. The station at Bermuda was considered for verifying insertion but the low insertion altitude and the range at insertion from Bermuda limit the effectiveness of data from that station for this launch. Should assignment of a North Atlantic ship not be feasible, a ship located as proposed for second burn coverage would serve to verify initial orbital entry at the half-way point in the revolution.

The instrumentation ship, located at  $90^{\circ}$  East,  $45^{\circ}$  South as proposed, would have approximately 18 minutes of tracking at sufficient elevation angles to obtain high resolution data for coverage of the S-IVB second burn. Later in the

orbit, MILA will have approximately 15 minutes of tracking time at sufficient elevation angles to obtain high resolution data. With a ship to cover the second burn of the S-IVB and MILA to verify orbital circularization, the mission objectives can be verified.

## 5.5 SUBSYSTEMS

### 5.5.1 THRUST VECTOR CONTROL SYSTEM

This section summarizes the results of S-IB stage and S-IVB stage pitch/yaw bending stability analyses, S-IVB stage bending/sloshing stability analyses, S-IB stage six degree-of-freedom rigid body wind response analyses, a stability analysis of the coupled vehicle/pedestal/pad configuration on Launch Pad 39, and a controllability analysis to determine inflight wind limits. Detailed results of these analyses are presented in References 17 and 18.

#### 5.5.1.1 STABILITY ANALYSIS

A pitch/yaw stability analysis was conducted during S-IB and S-IVB stage flight. A roll stability analysis was not conducted because the roll torsion characteristics are very similar for both the CSM and nosecone vehicles. Sloshing stability was not investigated during S-IB stage flight but was investigated at two time points during S-IVB stage flight.

S-IB Stage. Figure 5-32 shows a time history of the aerodynamic disturbance moment coefficient ( $C_1$ ) for the S-IB/SEPS Vehicle. The magnitude of  $C_1$  for other nosecone type vehicles is also shown near the time of maximum dynamic pressure for comparison purposes. These results show that the S-IB/SEPS aerodynamic characteristics are not as severe as the AS-204 vehicle but are more severe than the AS-206 vehicle. Control system designs for the AS-204, -206, and -208 vehicles were chosen as candidates for the S-IB/SEPS configuration.

The results of the pitch/yaw stability analysis for the three control systems show that although the AS-206 and AS-208 control filters provide satisfactory bending stability characteristics, the low frequency stability margins could be improved by adjusting the control gains. Consequently, the AS-206 control filters were used and control gain interactions were made until satisfactory control gain profiles were determined. Figure 5-33 shows the recommended control gain profiles. Time histories of the rigid body gain and phase margins are summarized in Figure 5-34. The AS-206 control filters and the recommended control gains provide adequate rigid body and bending stability characteristics during S-IB stage flight.

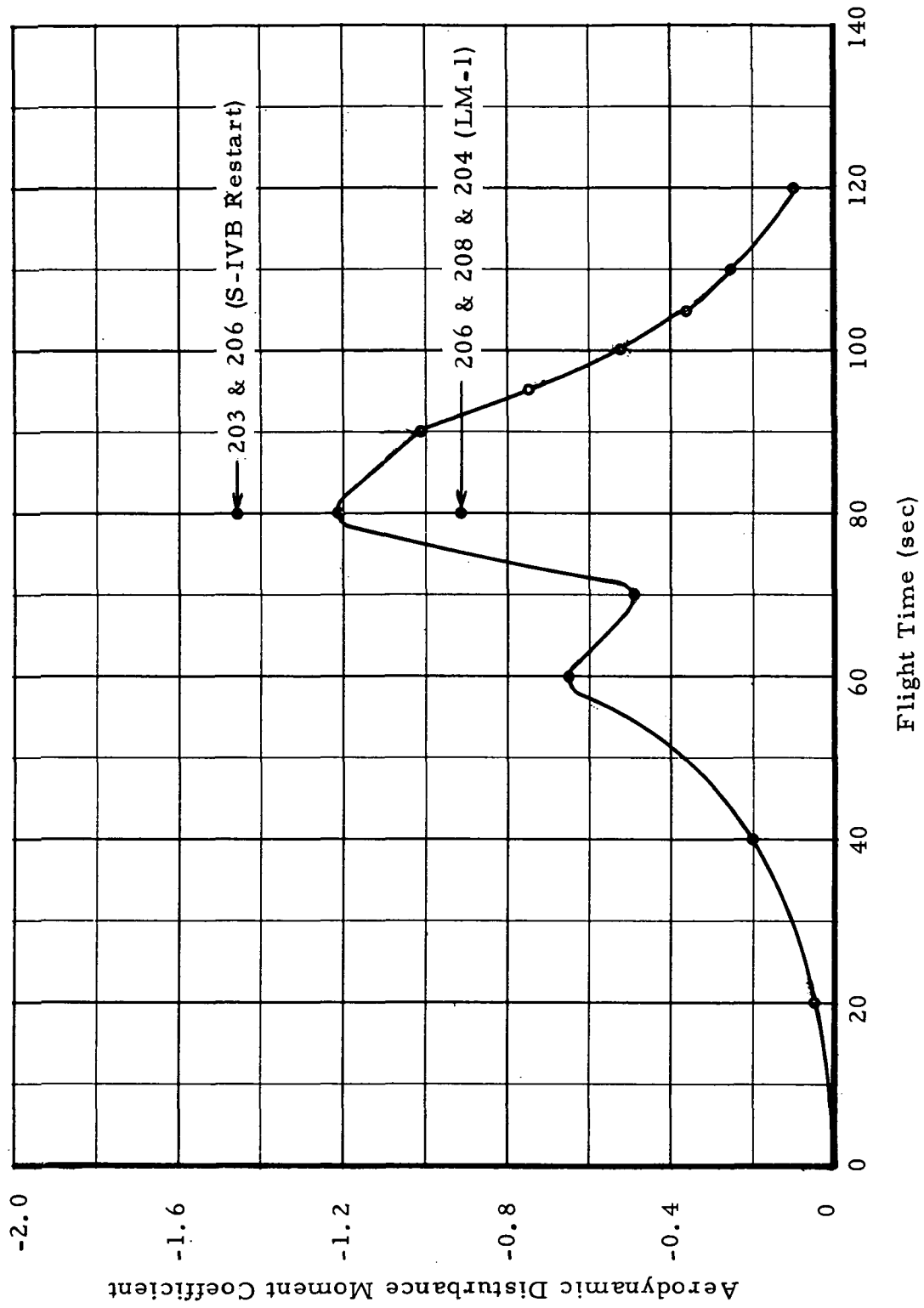


FIGURE 5-32. AERODYNAMIC DISTURBANCE MOMENT COEFFICIENT TIME HISTORY

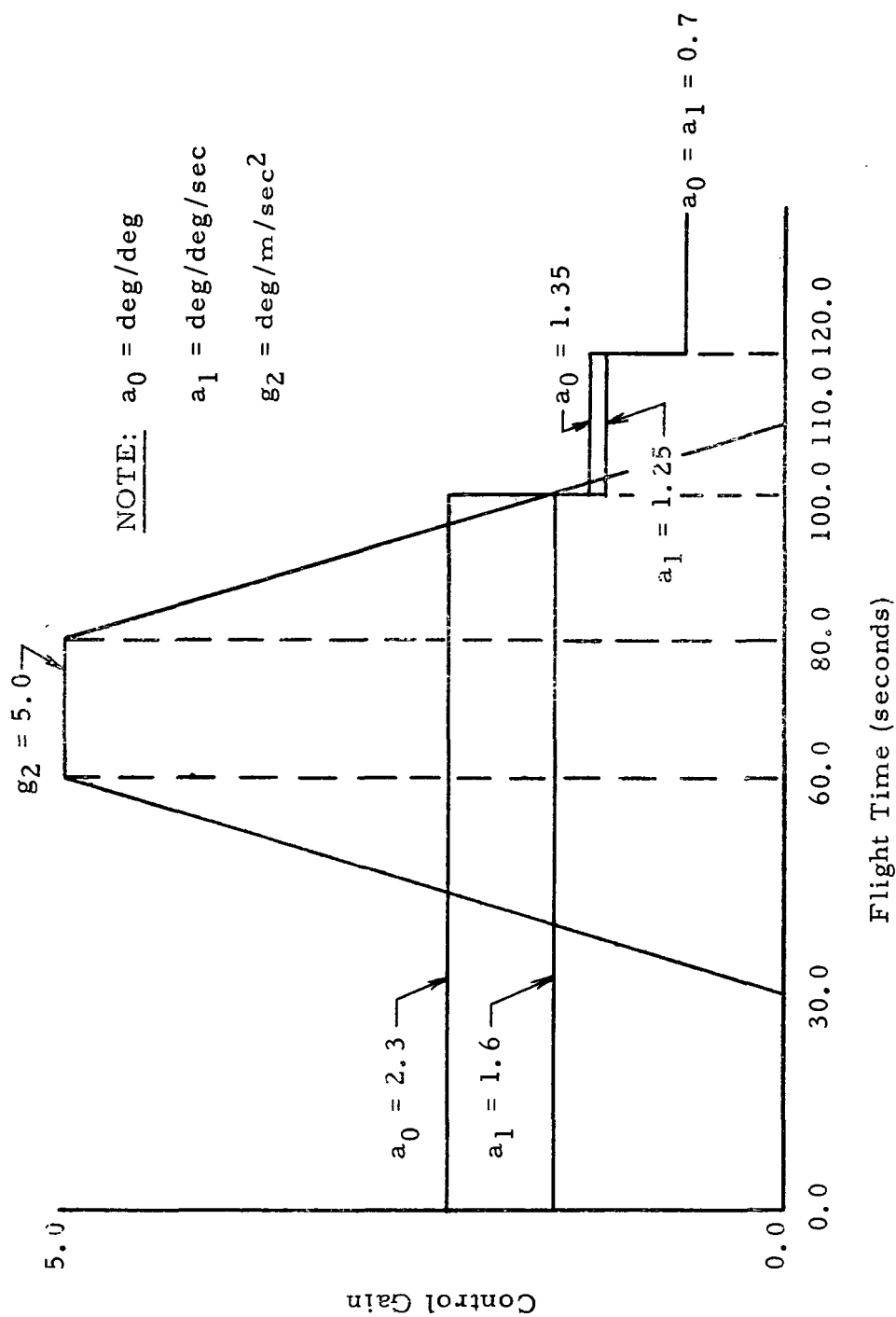


FIGURE 5-33. RECOMMENDED FIRST STAGE PITCH/YAW CONTROL GAINS

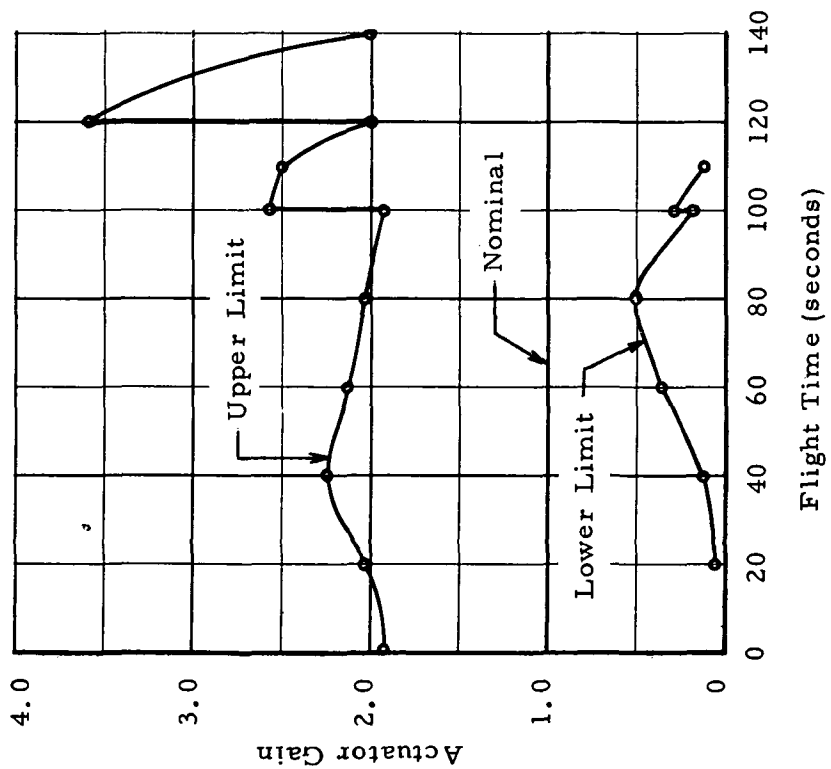
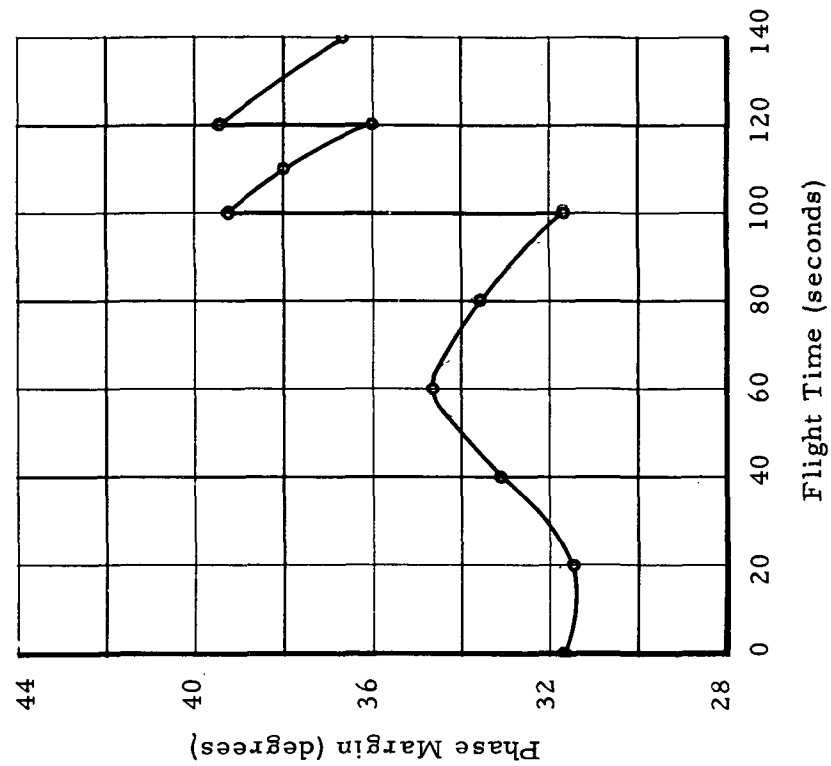


FIGURE 5-34. FIRST STAGE PITCH/YAW STABILITY MARGINS

A cursory stability analysis was performed for the S-IB/SEPS configuration on Launch Pad 39 at ignition. Figure 5-35 shows the root locus plots for the first two coupled vehicle/pedestal/pad modes. The results show that both modes are unstable at nominal gain and that the times to double amplitude are 58.1 seconds for mode 1 and 2.6 seconds for mode 2. As a comparison, the lowest time to double amplitude for the SL-2 vehicle, using the same pedestal/pad spring data, is 100 seconds. These results show a potential problem area for the S-IB/SEPS configuration. More detailed stability and response analyses are necessary to determine the seriousness of the problem.

S-IVB Stage. The S-IVB stability analysis was performed using the AS-206 and AS-208 S-IVB control systems. The two control systems are nearly identical, the major difference being that the AS-208 networks are balanced while the AS-206 networks are not. The pitch/yaw stability analysis shows that no rigid body or bending stability problems exist for the S-IVB/SEPS configuration using the AS-206/208 S-IVB control system.

S-IVB sloshing stability was investigated at two flight times (146 and 400 seconds). Root locus plots for the LOX and hydrogen sloshing modes are presented in Figure 5-36. The results show that the sloshing modes are stable and possess adequate stability margins at the time points investigated. No unusual problems were uncovered by this cursory investigation and it is expected that sloshing stability will be no worse on this vehicle than on any of the previous vehicles.

#### 5.5.1.2 RESPONSE ANALYSIS

A wind response analysis was conducted for the S-IB/SEPS configuration during first stage flight using the AS-206 control system. The vehicle was subjected to a spectrum of 95% Apollo design winds which peak at 9, 10, 12 and 14 km (29.5, 32.8, 39.4, and 45.9 ft x 10<sup>3</sup>) in both pitch tailwind and yaw wind directions. The results show that the vehicle displays satisfactory response characteristics. The structural loading on the vehicle was assessed by monitoring the time histories of the bending moments at Stations 941 and 1186. Station 941 is the bottom of the S-IB spider beam while Station 1186 is the bottom of the S-IVB aft skirt. The results show that the structural loads are well below the structural limits for all cases investigated.

A comparison of the vehicle responses using the AS-203, AS-206 and AS-208 control systems was made by subjecting the vehicle to a 95% design wind which peaks at 9 km (29.5 ft x 10<sup>3</sup>). The results show that the vehicle response using the AS-206 and AS-208 control systems are almost identical. The angle of attack is slightly larger using the AS-203 control system; however, the engine gimbal angles are about the same for all three control systems.



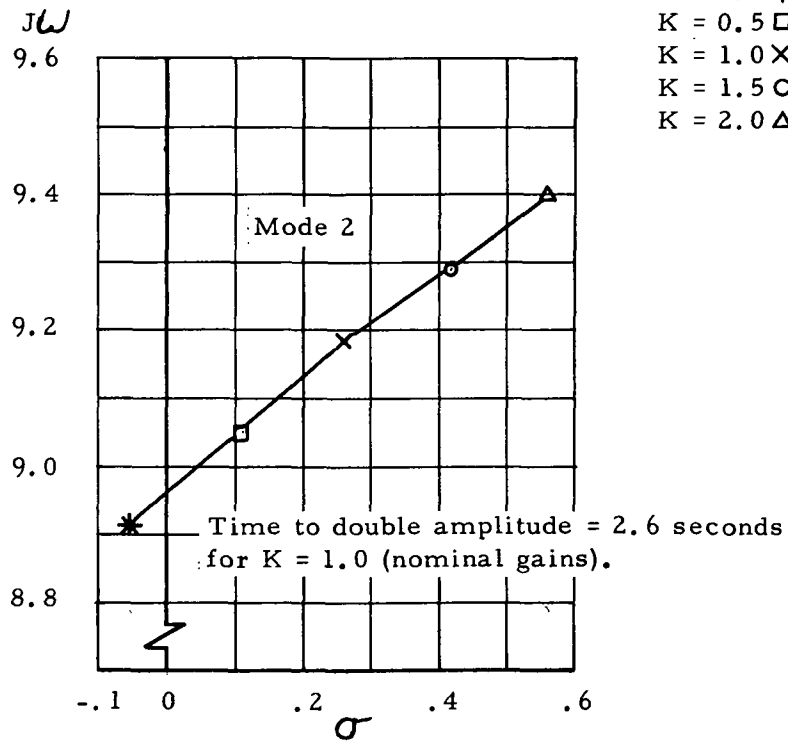
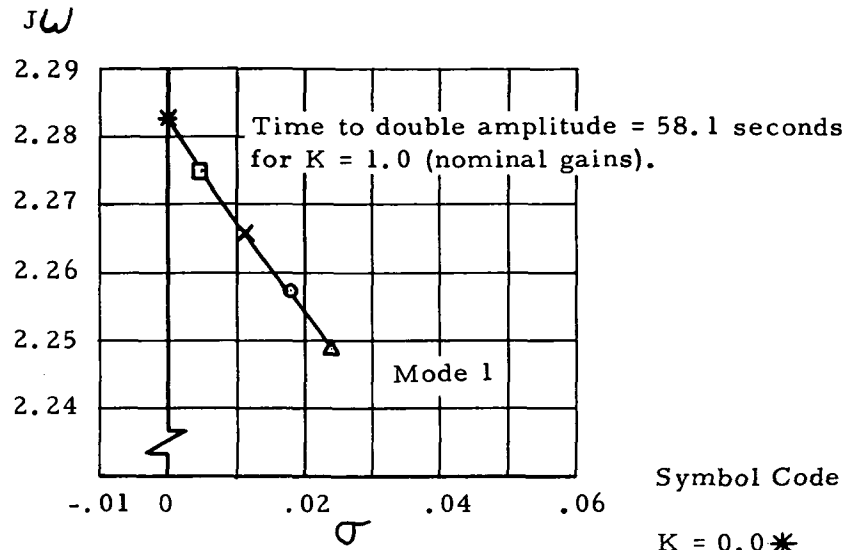
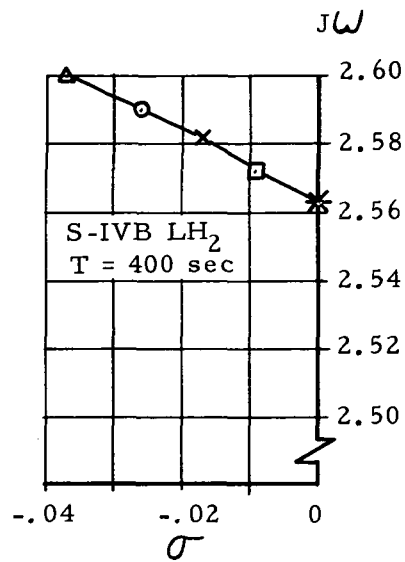


FIGURE 5-35. ROOT LOCI FOR FIRST AND SECOND  
COUPLED VEHICLE/PEDESTAL/PAD  
MODES



Symbol Code

K = 0.0 \*  
K = 0.5 □  
K = 1.0 ×  
K = 1.5 ○  
K = 2.0 △

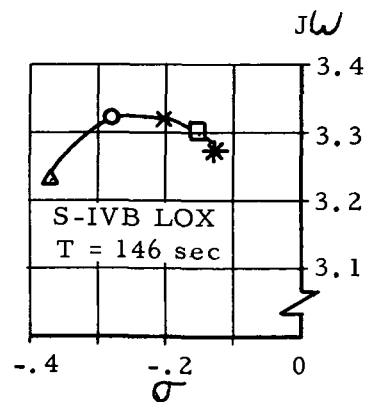
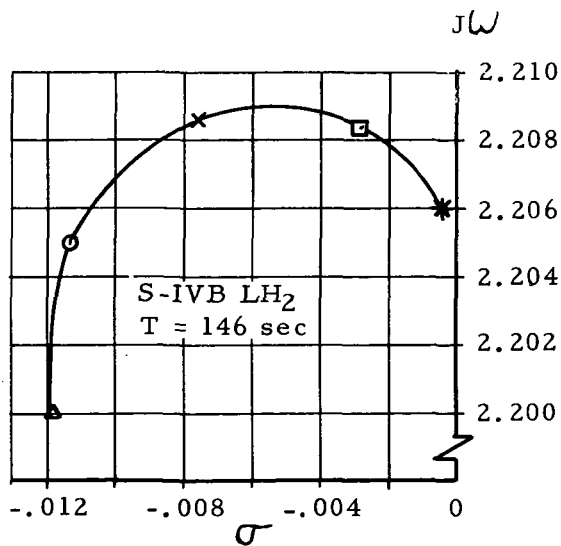
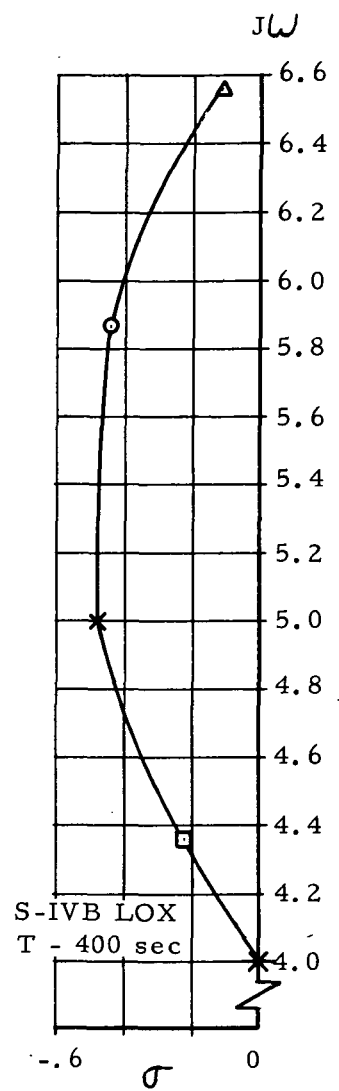


FIGURE 5-36. SECOND STAGE PITCH/YAW SLOSHING ROOT LOCI

A comparison of the vehicle responses using the AS-206 and the recommended control system was made using a 95% design wind which peaks at 9 km ( $29.5 \text{ ft} \times 10^3$ ). The vehicle responses are nearly identical using the two control systems.

Variations in the accelerometer control gain profile were considered using the recommended control system. The recommended accelerometer control gain profile peaks at  $5 \text{ deg/m/sec}^2$ . Accelerometer control gain profiles which peak at 4.5, 5.5 and  $6 \text{ deg/m/sec}^2$  were considered using the recommended control system and a 95% full shear wind which peaks at 9 km ( $29.5 \text{ ft} \times 10^3$ ). The results show that the angles of attack and engine gimbal angles are reduced as the accelerometer gain is increased. The reductions are rather small and the nominal accelerometer control gain profile, which peaks at  $5 \text{ deg/m/sec}^2$ , is adequate for the S-IB/SEPS configuration.

#### 5.5.1.3 WIND LIMITS

A launch vehicle controllability analysis was performed to determine the inflight wind limits for controllability. A comparison of the limits with the three sigma statistical winds at the Eastern Test Range is also presented. The off-nominal conditions considered are a three sigma variation of the center of pressure location ( $C_1/C_2$ ) and a spectrum of synthetic wind profiles, comprised of a 95% quasi-steady-state wind envelope, a wind shear buildup, and a superimposed gust. The results presented are applicable to the previously recommended AS-206 control system.

The wind limit results, based upon vehicle controllability, for the Saturn IB/SEPS trajectory are displayed in Figures 5-37 and 5-38. Figure 5-37 depicts the wind limit versus altitude determined for the headwind and tailwind directions, while Figure 5-38 shows the results of the left and right crosswind limits. The wind limits are presented for wind only and for wind plus  $3\sigma$   $C_1/C_2$  variations. The inner curves on the two figures represent the maximum  $3\sigma$  monthly wind profile (solid line), which occurs during the month specified, for the indicated wind direction, and the  $3\sigma$  annual wind profile (dashed line).

The minimum predicted controllability wind limits for the Saturn IB/SEPS vehicle with  $3\sigma$   $C_1/C_2$  variation are 84, 98, 77, and 76 m/sec (275.6, 321.5, 252.6, and 249.3 ft/sec) for the head, tail, left cross, and right cross wind directions, respectively. The minimum controllability wind limit for each wind direction occurs at an altitude of 10 km ( $32.8 \text{ ft} \times 10^3$ ).

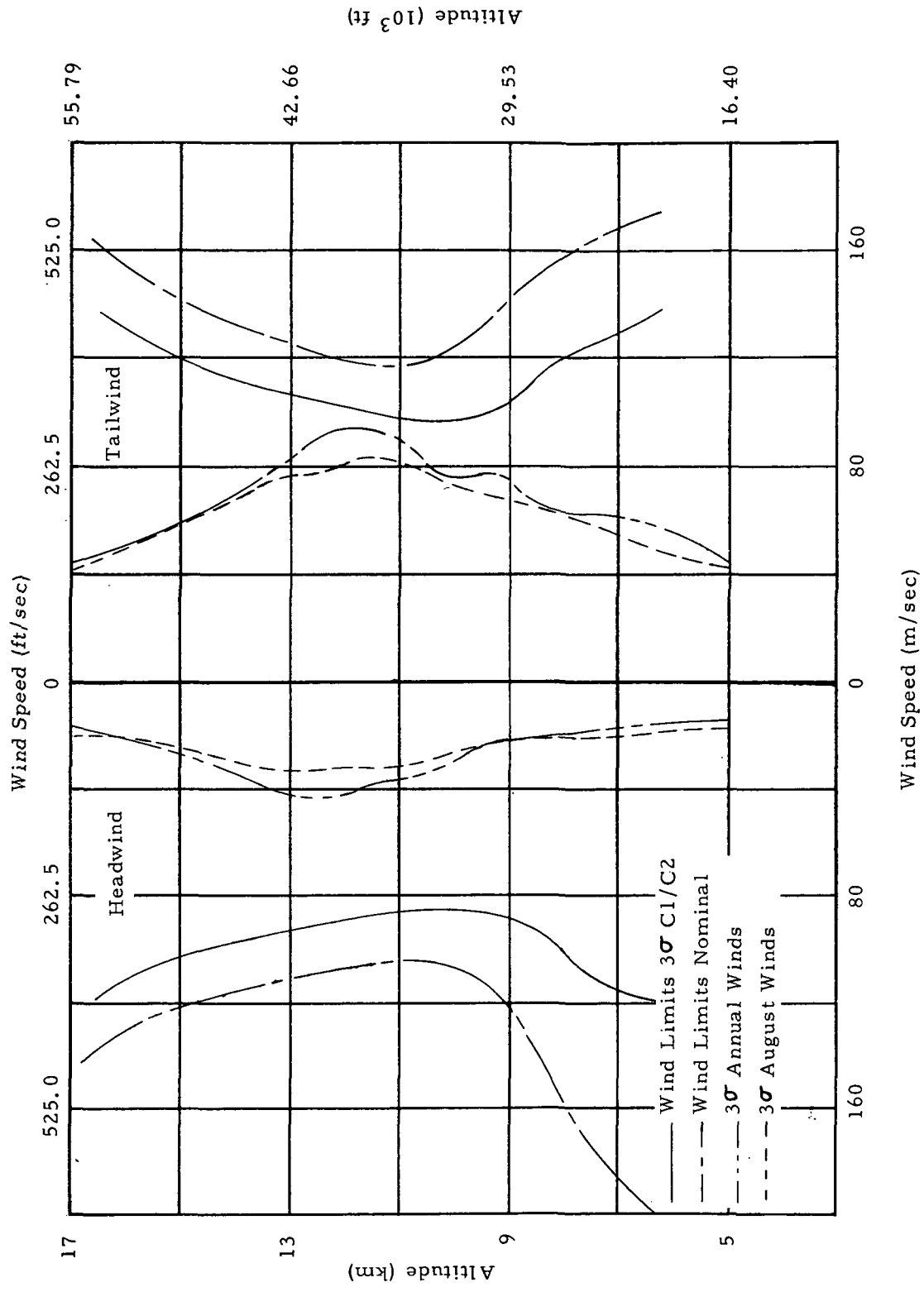


FIGURE 5-37. BOOST FLIGHT HEAD-TAIL WIND SPEED LIMITS

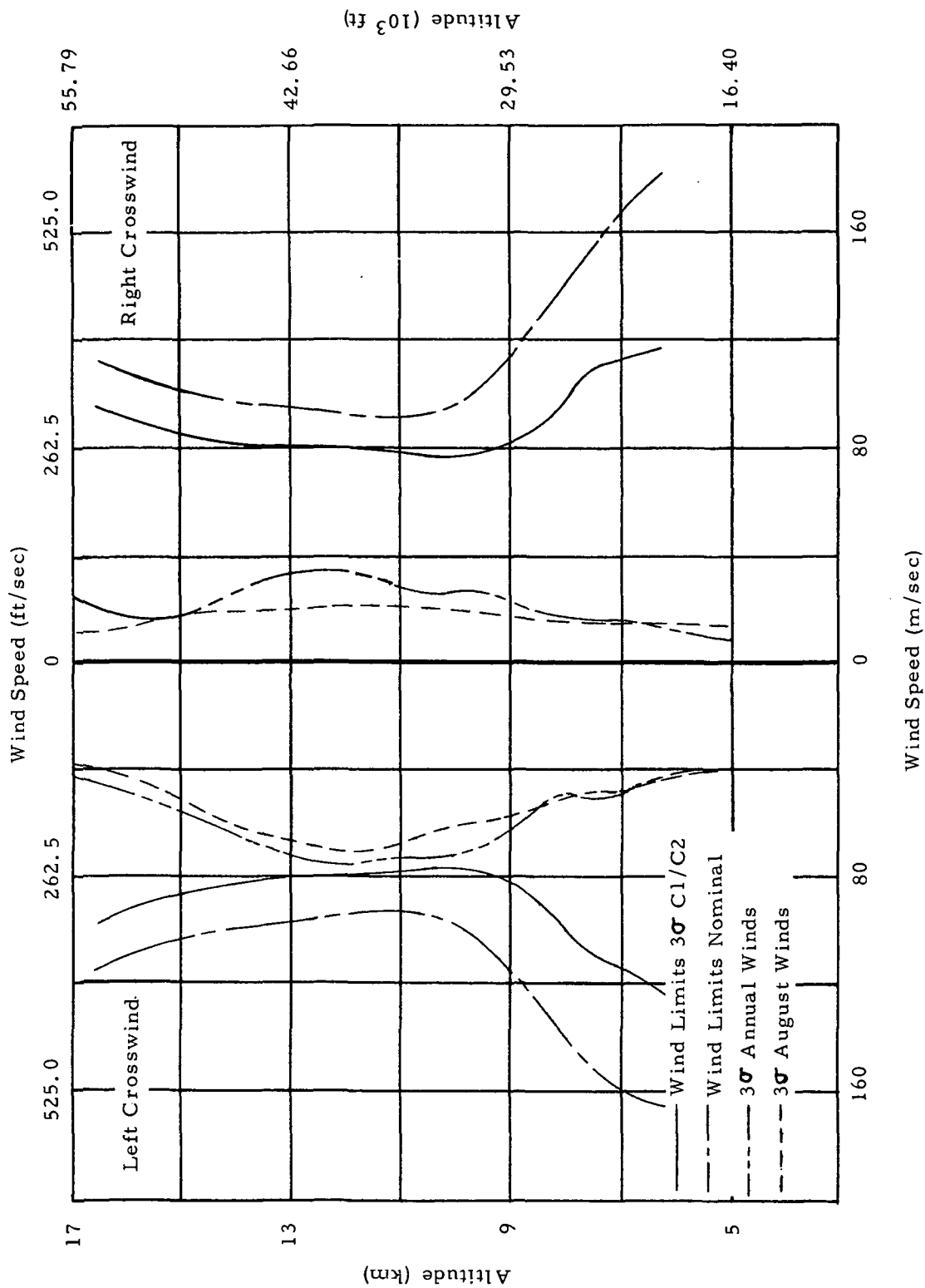


FIGURE 5-38. BOOST FLIGHT LEFT-RIGHT CROSSWIND SPEED LIMITS

It is evident that the Saturn IB/SEPS launch vehicle may be flown through design wind speeds for each wind direction. The wind limits, based upon vehicle controllability, for each wind direction are not exceeded by the maximum  $3\sigma$  monthly profiles for the indicated wind directions. Also, the controllability wind limits are not exceeded by the  $3\sigma$  annual profile. Therefore, the probability that a Saturn IB/SEPS launch will be restricted by inflight winds, based upon vehicle controllability, is less than 0.135 percent for the windiest month for each wind direction.

#### 5.5.2 STRUCTURAL ANALYSIS

Structurally, each stage of the SEPS launch vehicle is sensitive to different loading phenomena. While on the pad the S-IB stage is limited by the maximum wind loading it can withstand. To increase the maximum allowable wind level a damper must be used. Towards the end of first stage flight, the Saturn IB vehicle is most sensitive to the POGO effect. The S-IVB and S-IU stages structural capability is limited by the loading experienced during maximum dynamic pressure.

##### 5.5.2.1 S-IB STAGE

A structural loads evaluation was performed for the anticipated launch and prelaunch conditions (Reference 19). This section presents summaries of this loads evaluation, an investigation of the damper characteristics (Reference 6), and a longitudinal stability analysis (Reference 5).

A comparison of the S-IB Stage CEI criteria loads with those of the proposed SEPS configuration is presented in Tables 5-10 and 5-11. The transient loads during launch are not significantly different.

The base bending moments are compared with CEI criteria in Table 5-10. The results of a preliminary evaluation of the primary structural components under the combined bending and axial loads of Tables 5-10 through 5-12 are presented in Table 5-13 in terms of a stress ratio - the ratio of limit to ultimate stresses. The critical components under freestanding and launch conditions are the 177.8 cm (70 in) LOX tanks or the holddown structure as indicated by the circled numbers.

For a wind of 19.5 m/sec (38 knots) no vehicle status results in a stress ratio that exceeds the limiting value of 0.8 that corresponds to the required unmanned safety factor of 1.25. At 24.7 m/sec (48 knots) only the empty vehicle with pressurized tanks satisfies this requirement, and at 31.9 m/sec (62 knots) the ultimate stresses are exceeded in all the free standing conditions.

TABLE 5-10  
MAXIMUM LONGITUDINAL LOAD FACTORS ON  
S-IB PROPELLANT TANKS DURING LAUNCH

TANK	CEI	SEPS
177.8 cm (70 in) LOX	1.67	1.66
177.8 cm (70 in) FUEL	1.52	1.51
266.7 cm (105 in) LOX	1.44	1.51

TABLE 5-11  
MAXIMUM HOLDDOWN LOADS DURING LAUNCH  
NEWTONS (POUNDS)

	CEI	SEPS
Tension	$2.395 \times 10^6$ (538,396)	$1.730 \times 10^6$ (388,854)
Compression	$7.569 \times 10^6$ (1,701,637)	$7.432 \times 10^6$ (1,670,780)

TABLE 5-12  
BASE BENDING MOMENT  
 $10^6$  NEWTON-METERS ( $10^6$  INCH-POUNDS)

DRAG	LIFT	RESULT	CEI	WIND VELOCITY	TANKS
1.58(14)	4.52(40)	4.75(42)		19.5 m/sec (38 knots)	Empty
2.49(22)	5.65(50)	6.21(55)		24.7 m/sec (48 knots)	
4.18(37)	13.6(120)	14.1(125)	5.20(46)	31.9 m/sec (62 knots)	
1.58(14)	1.69(15)	2.37(21)	2.03(18)	19.5 m/sec (38 knots)	Full
2.49(22)	8.13(72)	8.47(75)		24.7 m/sec (48 knots)	
4.18(37)	9.04(80)	9.94(88)	6.33(56)	31.9 m/sec (62 knots)	

Wind Probability - one hour exposure during worst wind month, referenced to  
161.5 meter (530 ft) level

95 percent-19.5 m/sec (38 knots)  
99 percent-24.7 m/sec (48 knots)  
99.9 percent-31.9 m/sec (62 knots)

TABLE 5-13  
STRESS RATIO SUMMARY FOR PRIMARY STRUCTURE

Status \ Wind Velocity		19.5 m/sec (38 kts) 95%	24.7 m/sec (48 kts) 99%	31.9 m/sec (62 kts) 99.9%
FREESTANDING	Empty	NP	.773 (9)	.989 (9)
		P	.494 (9)	.632 (9)
	Full	NP	.581 (12)	.992 (9)
		P	.581 (12)	.914 (9)
LAUNCH	Holddown		.743 (12)	
	Rebound		.733 (12)	
	Liftoff		.396 (9)	

NP: No Ullage Pressure S-IB Propellant Tanks

P: Ullage Pressure =  $6.89 \times 10^4$  Newtons/Meter<sup>2</sup> (10 psig)

(9) 177.8 cm (70 in) LOX Tank Critical

(12) Holddown Structure Critical

Stress Ratio = Ratio of Limit to Ultimate Stress for Unmanned Safety Factor of 1.25. Stress Ratio  $\leq 0.8$



By interpolation of these data it is estimated that a damper will be required for wind velocities greater than 22.6 m/sec (44 knots) on the full vehicle and 25.7 m/sec (50 knots) on the empty vehicle with pressurized tanks.

Values of the stress ratio at other locations are shown in Table 5-14. As might be expected, the critical structural components are near the base of the vehicle.

To protect the vehicle from excessive stress loadings due to winds while on the launch pad, a damper is required to reduce the vibrational level caused by unsteady drag and vortex shedding. The results of this damper study (Reference 6 ) are:

- a. Because of the configuration, each frequency of the Vehicle/Pedestal/LUT system is close to that frequency of its major components, the Vehicle/Pedestal or the LUT, of which the displacement dominates the system mode shape.
- b. Except for a few modes, each system mode shape of the Vehicle/Pedestal/LUT is essentially one of its major component modes slightly coupled with other component modes.
- c. When a system frequency of the Vehicle/Pedestal/LUT is close to one of the frequencies of its major components, the Vehicle/Pedestal or the LUT, then this system mode shape may show coupling vibration of the major components.
- d. The damper significantly increases the modal damping ratio for the fundamental mode of the Vehicle/Pedestal/LUT system.
- e. The damping force between the damper and the vehicle is proportional to the forcing frequency, the displacement amplitude and the damping coefficient; and it can become very large if the forcing frequency is high and the displacement is large.

A "POGO" analysis of the S-IB stage flight was performed in order to (a) establish the structural models, (b) determine longitudinal dynamic characteristics, and (c) investigate instability gains.

- a. Structural Models: Two structural models of the vehicle were established. The first model (zero through 120 seconds of flight) consisted of 30 masses and 33 stiffnesses. The second model (flight time 120 through 140 seconds) consisted of 24 masses and 27 stiffnesses.

TABLE 5-14 STRESS RATIO SUMMARY - LAUNCH CONDITIONS

STRESS RATIO SUMMARY - LAUNCH CONDITIONS

19.5 m/sec (38 KNOT) (95%) WIND

STATION	FREESTANDING	HOLDDOWN	REBOUND	LIFTOFF
1663	.015	.013	.016	.019
1662	.025	.023	.026	.022
1540	.030	.027	.031	.025
1538	.013	.011	.012	.011
1272	.152	.140	.180	.247
1189	.158	.145	.186	.247
962	.175	.172	.212	.213
SPIDER BEAM	.244	.210	.271	.204
177.8 cm (70 in) LOX TANK	.421	.361	.434	.396
177.8 cm (70 in) FUEL TANK	.334	.387	.385	.394
266.7 cm (105 in) LOX TANK	.316	.371	.402	.364
HOLDDOWN FITTING	.581	.743	.733	-
MAXIMUM	.581	.743	.733	.396

STRESS RATIO = RATIO OF LIMIT TO ULTIMATE STRESS

FOR UNMANNED SAFETY FACTOR OF 1.25

STRESS RATIO  $\leq$  0.8

- b. Dynamic Characteristics: Dynamic characteristics were determined up to the 16th mode. The first ten modes are plotted in Figure 5-39.
- c. Instability Gains: Instability gain factors were determined for excitation frequencies from zero through 30 hertz. These instability gains are expressed in the decibel scale where a decibel number less than zero is stable and one larger than zero is unstable. Figure 5-40 shows the instability gain prior to outboard engine cutoff. At this time the vehicle is most prone to a POGO effect as the instability gain is only -3 decibels at 12 hertz.

#### 5.5.2.2 S-IVB STAGE

Rigid body loads and vibrational analyses were performed (Reference 7) and are summarized below.

Maximum structural loading on the S-IVB stage can occur during maximum dynamic pressure when the vehicle is at maximum angle of attack. The preliminary maximum  $q\alpha$  condition for the SEPS launch is:

Flight Time	=	66.6 seconds
Dynamic Pressure	=	$3.682 \times 10^4 \text{ N/m}^2$ (769 lb/ft <sup>2</sup> )
Angle of Attack	=	8.0 degrees
Engine Deflection	=	5.0 degrees
Axial Load Factor	=	1.92

This condition results from a 95 percentile scalar cross wind of 75 m/sec (246 ft/sec). Maximum tension and compression loads resulting from this condition are shown in Figure 5-41. Discontinuities in the curves result from the effects of an internal pressure of  $1.93 \times 10^5 \text{ N/m}^2$  (28 psi) in the LH<sub>2</sub> tank. An ultimate safety factor of 1.25 was used for this unmanned mission.

Table 5-15 shows a comparison of SEPS loads and S-IVB/IB stage capability. It can be concluded from this table that, from structural considerations, a S-IVB/IB stage can perform the SEPS mission. Applicable differential pressures are specified with the compression capability of the stage. For this

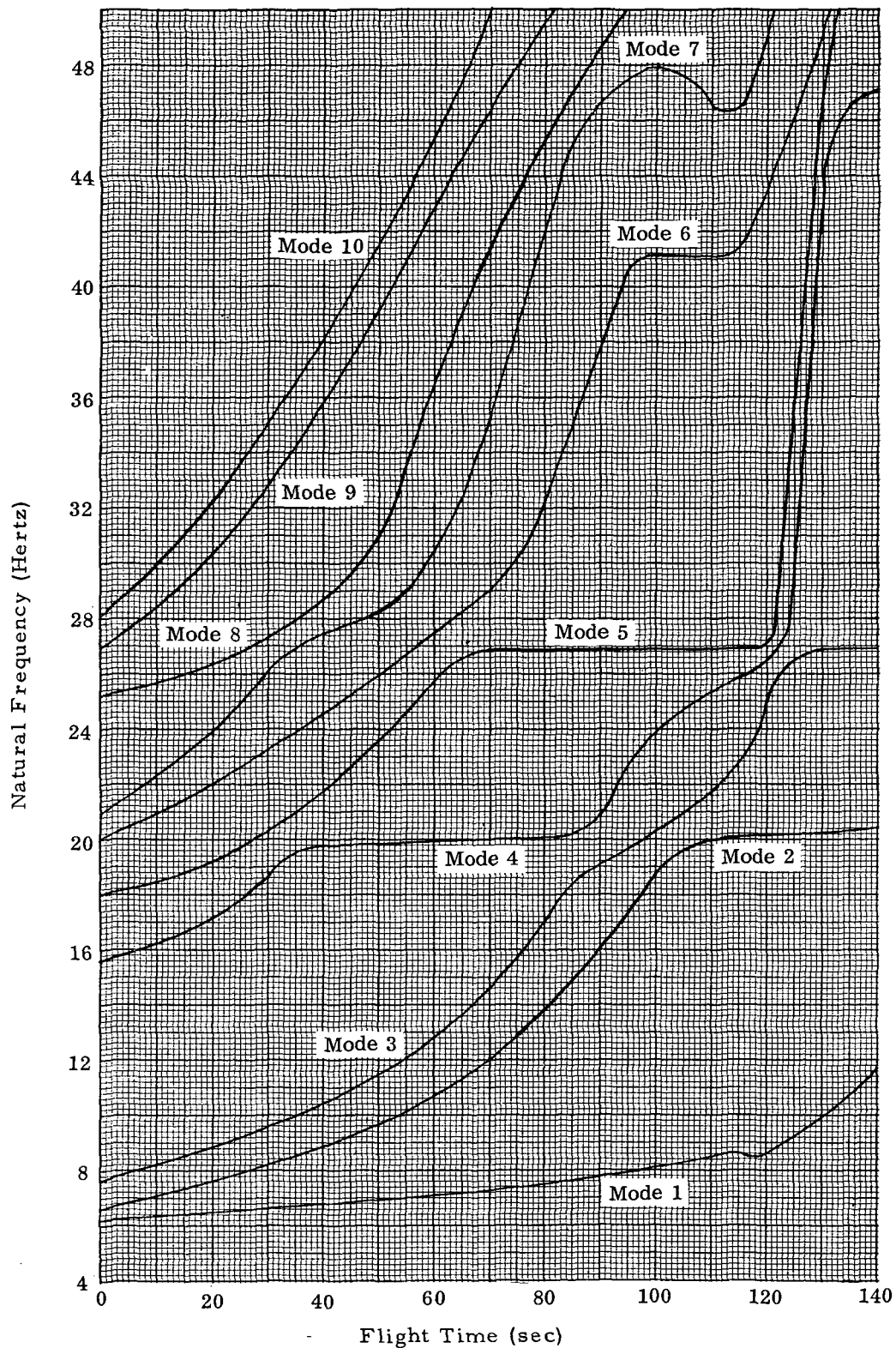


FIGURE 5-39. NATURAL FREQUENCY VERSUS FLIGHT TIME

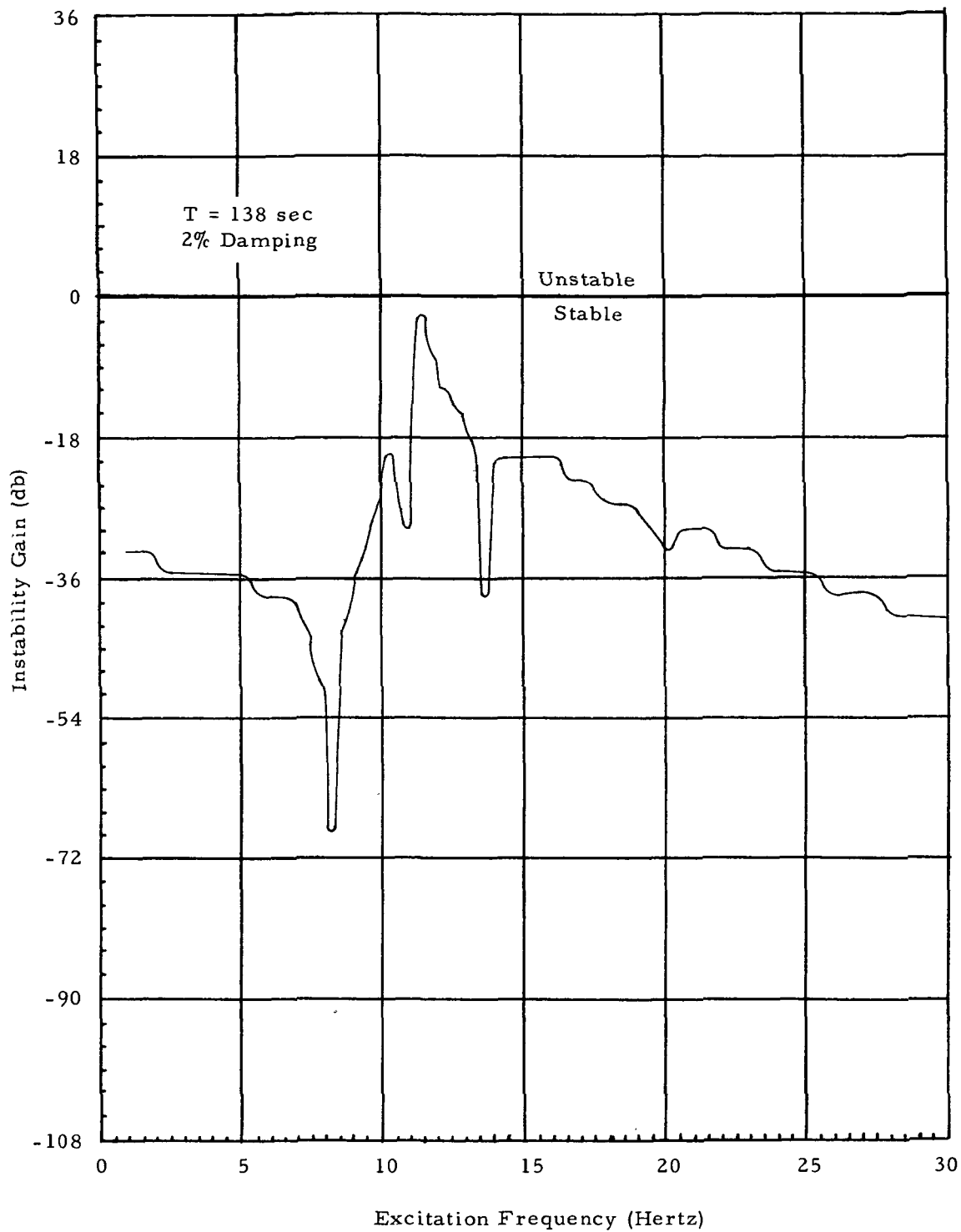


FIGURE 5-40 INSTABILITY GAIN VERSUS EXCITATION FREQUENCY

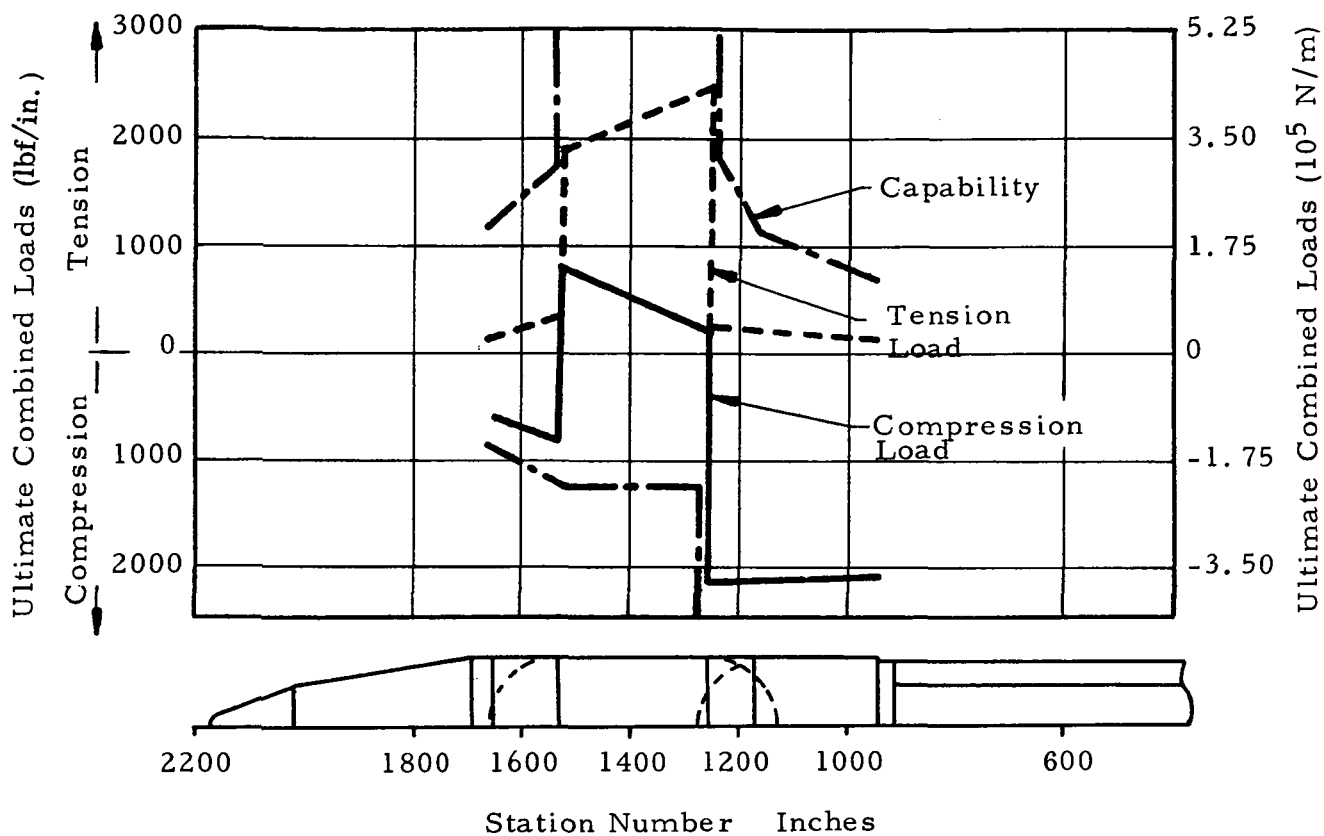


FIGURE 5-41. S-IVB MAXIMUM  $q_{\infty}$  LOADS

Table 5-15  
COMPARISON OF S-IVB LOADS AND S-IVB/IB STRUCTURAL CAPABILITY

STATION	ULTIMATE MAXIMUM LOADS, N/m (lbf/in.)		S-IVB/IB CAPABILITY	
	COMPRESSION	TENSION	COMPRESSION	TENSION
1662	-9.77 x 10 <sup>4</sup> (-558)	2.56 x 10 <sup>4</sup> (+146)	-1.65 x 10 <sup>5</sup> (-945) (1)	2.10 x 10 <sup>5</sup> (+1200)
1540 FWD	-1.42 x 10 <sup>5</sup> (-810)	6.58 x 10 <sup>4</sup> (+376)	-1.96 x 10 <sup>5</sup> (-1119) (2)	3.26 x 10 <sup>5</sup> (+1860)
1540 AFT	1.34 x 10 <sup>5</sup> (+763)	3.41 x 10 <sup>5</sup> (+1949)	-2.20 x 10 <sup>5</sup> (-1256)	1.44 x 10 <sup>6</sup> (+8250)
1272 FWD	4.08 x 10 <sup>4</sup> (+233)	4.30 x 10 <sup>5</sup> (+2453)	-2.20 x 10 <sup>5</sup> (-1256)	1.44 x 10 <sup>6</sup> (+8250)
1272 AFT	-3.77 x 10 <sup>5</sup> (-2150)	4.20 x 10 <sup>4</sup> (+240)	-4.80 x 10 <sup>5</sup> (-2740) (3)	3.01 x 10 <sup>5</sup> (+1719)
1186	-3.75 x 10 <sup>5</sup> (-2140)	3.80 x 10 <sup>4</sup> (+217)	-4.35 x 10 <sup>5</sup> (-2482) (3)	2.10 x 10 <sup>5</sup> (+1200)
962	-3.71 x 10 <sup>5</sup> (-2120)	2.73 x 10 <sup>4</sup> (+156)	-4.48 x 10 <sup>5</sup> (-2560) (3)	1.34 x 10 <sup>5</sup> (+767)

(1) - DIFFERENTIAL PRESSURE = 3.86 x 10<sup>4</sup> N/m<sup>2</sup> (5.6 PSI)

(2) - DIFFERENTIAL PRESSURE = 3.47 x 10<sup>4</sup> N/m<sup>2</sup> (5.04 PSI)

(3) - DIFFERENTIAL PRESSURE = 2.41 x 10<sup>4</sup> N/m<sup>2</sup> (3.5 PSI)

vehicle, the pressures in the aft compartment, between the S-IVB and S-IB, should remain approximately the same as previous Saturn IB pressures. Differential pressures in the forward compartment were estimated to be  $2.41 \times 10^4 \text{ N/m}^2$  (3.5 psi) (limit) or  $3.02 \times 10^4 \text{ N/m}^2$  (4.38 psi) (ultimate), which is less than the  $3.47 \times 10^4 \text{ N/m}^2$  (5.04 psi) used to determine the forward skirt capability.

Stringer temperatures were estimated to be slightly lower for this vehicle than for Saturn IB design values. Since the mass forward of the S-IVB is greatly reduced from previous flights, 20,000 kg to 10,400 kg (44,000 lb to 23,000 lb), and over-all vehicle acceleration is only slightly increased, the S-IVB stage appears adequate for the maximum acceleration condition.

The loads discussed in this section were determined from a preliminary loads trajectory using a rigid body analysis. When authority to proceed is given for this mission a firm loads trajectory will be defined and flexible body loads will be calculated because they result in slightly higher vehicle loads.

The increase in acoustic levels and resulting vibration levels for the SEPS mission is less than a 0.5 db increase over Saturn V levels and less than a 2 db increase over Saturn IB levels. A margin of safety exists between the predicted SEPS mission levels and the current specifications at all frequencies.

A review of the proposed modifications to either a S-IVB/IB or S-IVB/V stage indicates no requirement for qualification or requalification vibration testing. By using designs which are similar to mainline installations, the use of analytical methods will be sufficient to ensure the structural integrity of any modifications.

The following are conclusions on dynamic environments for the SEPS mission:

- a. The vibration, shock, and acoustic criteria for mainline S-IVB is applicable for the SEPS mission.
- b. Basic structure and S-IVB common components are qualified for launch on either Saturn IB or Saturn V vehicle.
- c. S-IVB/V peculiar components, such as the APS,  $\text{H}_2\text{O}_2$  burner, etc., although requiring a separate analysis to compare Saturn IB and Saturn V criteria, should require no requalification testing.
- d. No qualification or requalification testing on any modifications will be required.



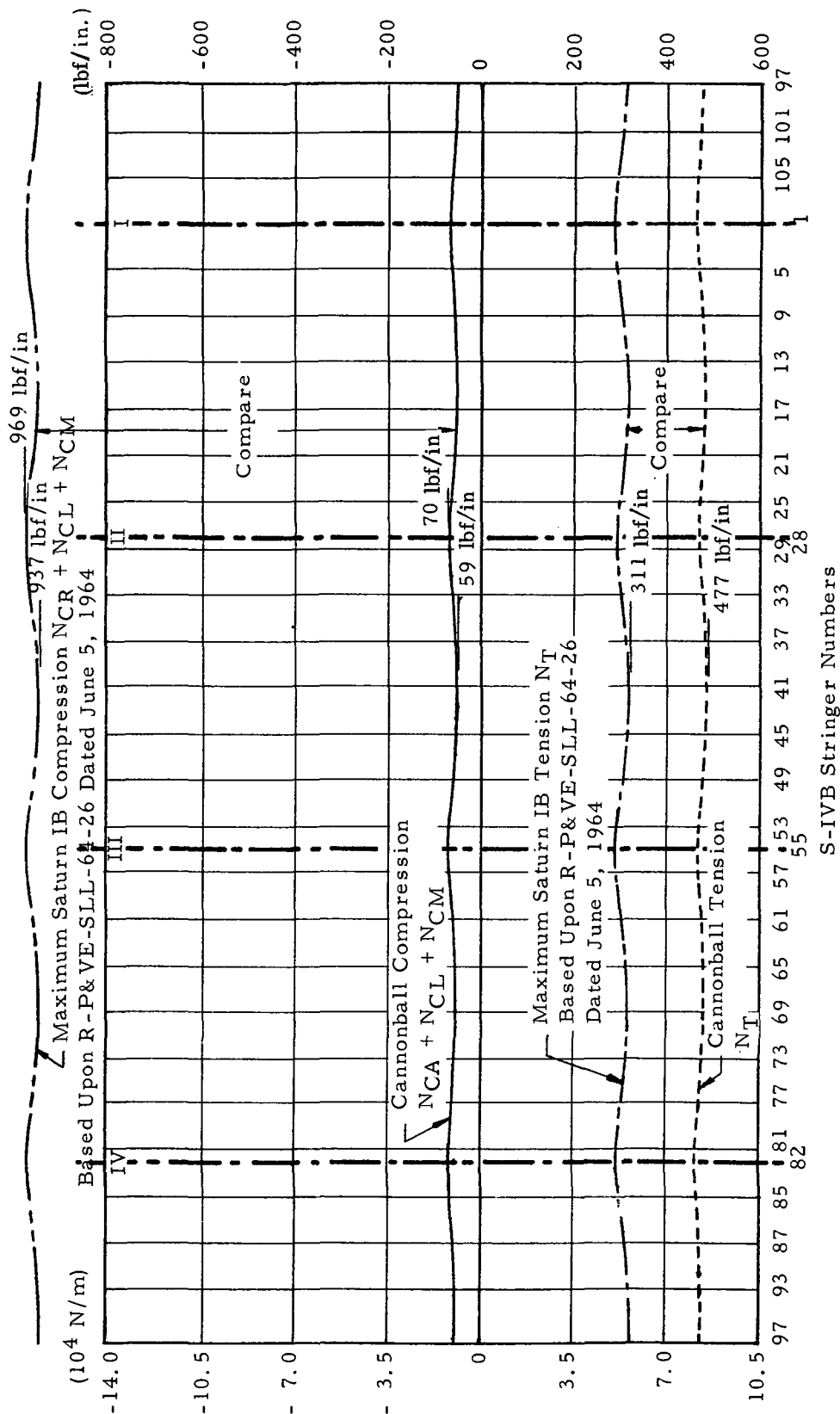
### 5.5.2.3 S-IU STAGE

Several items were considered in the S-IU stress analysis (Reference 9) and are summarized below:

- o Ground wind loads were determined for 95 percent and 99 percent peak winds and are less than on either Saturn V or Saturn IB and have been determined not to be critical.
- o The temperatures of the IU at IECO were compared with previous Saturn V flights which did not have the cork insulation added to the IU. The temperatures were generally equal to or less than the Saturn V temperatures.
- o The SEPS payload mass was compared with previous missions and is considerably lower than any previous payload of the 200 or 500 series, with the exception of the -203 mission. AS-203 was a special mission vehicle, whose primary payload was a 1681 kg (3707 lb) nosecone.
- o The maximum compartment delta pressure was assumed to be equivalent to that previously predicted for the AS-203 flight. This value,  $10.3 \times 10^3 \text{ N/m}^2$  (1.5 psi), was based on an early prediction and may be somewhat high. More refined data should reflect a decrease in this compartment delta pressure, but increased vent area or other modifications still may be required.
- o The MAX  $q$  tension loads were calculated assuming compartment delta pressure of  $1.03 \times 10^4 \text{ N/m}^2$  (1.5 psi),  $G = 1.9$ ,  $M = -2.43 \times 10^6 \text{ N-m}$  ( $-21.500 \times 10^6 \text{ in.-lbs}$ ) (from Saturn IB loads criteria) and longitudinal air loads similar to 200 series flights. The SEPS design tension loads are considerably greater than other flights of the IU (see Figure 5-42), with the exception of Skylab, resulting in negative margins of safety in yield of the lower IU interface flange. The relatively light payload, in combination with the large projected area of the shroud above the IU, causes these excessive tension loads at the lower IU interface.

The use of a smaller volume shroud or lower compartment delta pressure should reduce the IU tension loads. Another method to reduce the IU tension loads would be to move the SEPS support

# LOWER INTERFACE STATION 1633



NOTE: 513 Skylab-I Loads Not Shown

FIGURE 5-42. LIMIT RUNNING LOAD (Max Qα)

attach points closer to the IU. Also, the addition of bonded washers at the lower interface, similar to those on Skylab, would increase the IU tension capability and should eliminate the problem.

Flight vibrations of the SEPS IU should be very similar to the vibrations monitored on AS-201 through -204 for the following reasons:

- o All use the same S-IB boosters.
- o Structures above and below the IU are approximately the same for all.
- o Initial flight trajectories are approximately the same for all.

However, there may be slightly different vibration levels for the following reasons:

- o The total mass above the IU is much less for the SEPS mission than for previous Saturn IB missions.
- o The SEPS and support structure is quite different from that of the LM.

Even though these two differences should cause only slightly higher vibration levels in the SEPS IU, there is a possibility that the vibration levels at a few discrete frequencies could be considerably higher than experienced on the earlier Saturn IB IU's. One point of concern is that with only the SEPS mass in the SLA, there will be less mass damping of the SLA structural vibration. This vibration would be transmitted through the structure to the IU.

Another point of concern is the low frequency responses of the SEPS and its supports. The design natural frequency of the support structure (approximately 8.5 Hz) should not cause a problem; however, higher modes of this vibration could be a problem if they respond near the critical frequencies for the IU. The possibility that these higher modes will coincide with the critical IU frequencies is remote; however, care should be taken during the design and evaluation of the support structure to reduce the amplitude of these higher mode responses.

In conclusion, there may be slightly increased vibrations on the SEPS IU from that of prior IU flights. However, if the previously mentioned two points of concern are considered during final design and evaluation, the SEPS IU vibration environment should not exceed the IU vibration qualification levels.

#### 5.5.2.4 VEHICLE BENDING VIBRATION ANALYSIS

A preliminary bending vibration analysis was performed (Reference 20) in order to obtain the input data required for the control system assessment. Modal data were determined for the vehicle at 40 second intervals of S-IB stage flight, at three time points (90% thrust, midpoint, and cutoff signal) during the S-IVB stage first burn, and at two time points (90% thrust and cutoff signal) during the S-IVB stage second burn. In addition, modal data were determined for the vehicle at ignition while constrained on the LC-39 launch pedestal.

Table 5-16 presents a comparison of the SEPS bending mode frequencies, at three time points during S-IB stage flight, with other nose cone launch vehicles. The SEPS first stage bending characteristics are more similar to the Saturn IB/S-IVB restart vehicle than any of the other nose cone vehicles.

TABLE 5-18 PRELIMINARY BENDING MODE CHARACTERISTICS  
COMPARISON OF FIRST STAGE BENDING MODE  
FREQUENCIES

VEHICLE	1st MODE FREQUENCIES (rad/sec)			
	LIFT-OFF MASS <u>kg</u>	<u>lbm</u>	t = 0	t = 80 t = CO
SEPS	577,158	1,272,416	12.19	17.92 18.39
SA-203	538,295	1,186,738	12.14	21.44 21.56
AS-206/S-IVB RESTART	568,578	1,253,499	12.07	19.32 20.42
AS-208	582,085	1,283,277	10.41	14.99 15.18
VEHICLE	2nd MODE FREQUENCIES (rad/sec)			
			t = 0	t = 80 t = CO
SEPS			30.04	37.71 62.15
SA-203			34.18	40.98 62.16
AS-206/S-IVB RESTART			32.95	39.80 62.31
AS-208			28.84	37.99 58.63

## SECTION 6 CONCLUSIONS AND RECOMMENDATIONS

### 6.1 CONCLUSIONS OF PRESTUDIES

Results of studies have concluded that the Earth Physics Program requires a satellite whose configuration is explicitly designed for the purpose of making possible laser range measurements to accuracies of two centimeters (2 cm) or better. The total range error that the satellite could contribute to the 2 cm total of the laser observations was budgeted at the five millimeter (5 mm) level, and the conclusion was that this accuracy could be obtained through careful design and fabrication.

### 6.2 SATELLITE CONCLUSIONS

A goal of this limited study program was to evolve a complete detail design for the satellite. This design was achieved on the basis of the performance requirements, practical design considerations, and thermal analysis. The presently designed satellite is a completely passive 3628 kg (8000 lbm), 76.2 cm (30.0 in) diameter sphere carrying 864 retroreflectors distributed as evenly as possible over the surface.

The selected orbit does not impose any serious limitations on the design beyond the usual outgassing, long-term radiation exposure, nominal thermal environment, and micrometeoroid considerations. Since the satellite is passive, many of the usual orbital considerations are not applicable or exert only a minimum influence.

#### 6.2.1 CORE

The primary requirements on the core configuration are that the satellite be spherical, compact, rigid, and symmetrical (i.e., the centers of mass and geometry must coincide within an allowable tolerance). Results of an initial thermal analysis overview concluded that there were no critical thermal problems within the core itself that might affect any design decisions.

In the designed satellite, a cubical inner core surrounded by six spherical caps was chosen as the best configuration for fabrication of the satellite core. Depleted uranium, alloyed with a small amount of molybdenum to enhance the machining properties and to increase hardness, was selected as the optimum choice of high-density core material to provide the high mass-to-area ratio. Vacuum deposition (i. e., ion plating) of aluminum was chosen as the optimum process and material for the surface treatment of the uranium core. The allowable overall symmetrical inaccuracy of the satellite (including the positioning of the retroreflectors relative to the center of mass and to each other) was established to be one (1) millimeter or less. Sufficient balancing capability (i. e., the eccentricity of the center of mass and geometry) of approximately 13.6 N-m (10 ft-lb) in any direction is provided by adjustment of three counterweights contained within the cubical inner core oriented along mutually perpendicular axes.

#### 6.2.2 RETROREFLECTOR ARRAY

The primary requirements on the retroreflector array configuration are that the satellite provide a reflected laser return signal strong enough to be measurable and consistent enough so that the variations in the measured range are within the required tolerances. The conclusions of the thermal analysis overview provided the following design guidelines:

1. Temperature gradients within the retroreflectors will degrade their optical performance, but their thermal environment can be properly controlled, with the result that satisfactorily high optical performance can be attained.

2. Proper control of the thermal environment of the retroreflector can be achieved within the operational requirements of the satellite with a reasonably wide range in several of the more critical aspects such as the conductance of the retroreflector mounting and the satellite spin rate and spin-axis orientation.

In the designed satellite, the retroreflector array chosen most suitable for obtaining the desired return signal consists of 864 cylindrical cube corner retroreflectors of high-grade fused silica. The retroreflectors are 3.65 cm (1.438 in) diameter in size with aluminum reflective coating on the cube surfaces. No overcoating is applied to the cube surfaces and no coating is applied to the entrance surface. The design was tailored for conical return beam accuracy within 30 to 40 microradians half angle. The retroreflectors are arranged in a general triangular pattern in each quadrant of each of the six spherical caps. The mount design is similar to that of the lunar retroreflector array.

The total number of retroreflectors, the circular configuration, and the size were chosen by balancing the laser-ranging requirements against practical considerations such as machining complexity, tolerance buildup, handling, and testing. The choice of fused silica as the retroreflector material, besides best meeting all the requirements, has the advantage of a vast amount of directly applicable data accumulated from the fused silica lunar-array retroreflectors. The solid coated retroreflectors are the most desirable in terms of signal strength and were selected mainly because of their well developed state of the art. No protective overcoating will be applied to the cube surfaces in order to provide a low - emissivity surface to minimize radiative coupling between the retroreflector and the surrounding satellite core.

## 6.3 PAYLOAD SYSTEMS CONCLUSIONS

### 6.3.1 INTERFACE

The geometric launch vehicle interface for the satellite was established to be the external spherical surface of the satellite. This requires that the payload support structure and the ejection mechanism be designed to bear only against the outside spherical surface of the satellite and in a manner that does not damage the surface or structure. A limitation that the satellite handling rig cannot encroach on the space below a horizontal plane intersecting the sphere at the equivalent of 35 degree south latitude was imposed to ensure no mechanical interference during mating of the satellite to the launch vehicle.



### 6.3.2 PAYLOAD SHROUD

In the payload systems design, a nose cone similar to the AS-204 configuration and an Apollo Spacecraft Lunar Module Adapter (SLA) were selected for the payload shroud baseline configuration. The SLA provides a suitable structural interface, through the four Lunar Module support points, for the payload support structure. These existing flight-qualified hardware, for which aerodynamic and flight data are available, can be utilized without modification and are compatible with the selected launch vehicle performance capability.

### 6.3.3 SUPPORT SYSTEM

In the selected support system design, the satellite is held in a support frame by four equally spaced support pads which have ball socket joints. The support points are located 45 degrees below the equator of the spherical satellite. A fixture provides the amount of preload necessary to prevent the satellite from lifting from its lower support points under any loading condition. A cover enclosure (consisting of a lower permanently-mounted bowl and an upper deployable shell) surrounding the satellite serves to contain nitrogen purge gas and preclude entrance of contaminants until the satellite is released in orbit. A cruciform beam structure interconnects the support frame and the SLA. The design provides for satellite installation by complete removal of the holddown arms and associated enclosure by removing bolts at the hinge point of the arms.

### 6.3.4 EJECTION SYSTEM

The selected satellite ejection system design incorporates a compressed spring to permit limited travel of the support frame when a release mechanism linkage pin puller is actuated by an ordnance system. Although a single pin puller is utilized, complete redundancy is provided in the ordnance system and the pin puller incorporates dual pressure cartridges for redundant actuation. A second pin puller could be incorporated by providing a

second release point within the release mechanism linkage, but is presently considered to be an unwarranted complication. The EBW firing unit and battery interface with the IU for inflight control and monitoring and with the SLA umbilical for preflight operations.

#### 6.3.5 ANTI-CONTAMINATION SYSTEM

To protect the satellite against contaminating environments, an anti-contamination enclosure and purge system is required. The requirements of the purge system, however, are not well defined; therefore, three purge system concepts were examined to cover the expected range of requirements. The first, a pressure regulated system for constant positive purge pressure. The second, a blow-down system for a small positive purge pressure that decreases as a function of time. The function of both the first and second systems is dependent on the accumulative leakage area of the anti-contamination enclosure. The third, an anti-contamination enclosure pressure release system for purge pressure not required to last until satellite release. In this system, continuous gas flow is not required to maintain purge and the enclosure is sufficiently tight so gas will not be lost readily through leakage.

#### 6.4 LAUNCH VEHICLE CONFIGURATION CONCLUSIONS

The only satellite launch vehicle configuration considered in this study was basically a Saturn IB configuration. Restart capability to circularize the satellite orbit at the proper altitude is required. The selected baseline configuration consists of a Saturn IB S-IB first stage, interstage, and Instrument Unit (IU), and a Saturn V S-IVB second stage.

No modifications are required to the S-IB stage for the mission. The selected S-IVB stage was designed for restart and modifications for the mission are not extensive. The basic stage modifications include removal of the present baffles and installation of low residual baffles, and modification of the existing repressurization system. Structural modifications to the interstage are required at the interface plane of the S-IVB stage. Structural

modification such as bonded washers and/or increased vent area may be required to the IU but present no significant problem. Only basic modifications are required to the ground support equipment.

## 6.5 MISSION PROFILE CONCLUSIONS

The mission requires insertion of the satellite into a 3720 km circular orbit, inclined at 55 degrees to the equatorial plane. An additional requirement, that the satellite have a minimum spin rate of 0.1 RPM and a spin-axis orientation normal to the ecliptic plane within 3 degrees at orbital injection, was imposed for purposes of this study based only on considerations of the short-range thermal environment.

In the selected baseline profile, a flight azimuth of 37.94 degrees E of N provides a planar boost flight for the 55 degree inclination requirement. S-IVB first burn inserts the vehicle into a 150 by 3720 km elliptical orbit. A coast phase of approximately 63 minutes is required to transfer from 150 km to the operational orbit altitude of 3720 km. Early in the coast the payload shroud (the deployable portion of the SLA and the nosecone) is jettisoned in a retrograde direction. The vehicle is then oriented and maintained in a local horizontal attitude for the remainder of the coast. At first apogee passage in the elliptical orbit, the S-IVB stage will perform a second burn to circularize to the operational orbit. The vehicle will maneuver so that the satellite spin axis is oriented normal to the ecliptic plane for release of the satellite as the vehicle crosses the equatorial plane at the first ascending node in the operational orbit. The S-IVB stage Auxiliary Propulsion System (APS) will spin the vehicle at a minimum rate of 0.6 deg/sec prior to release of the satellite. Two S-IVB APS retroburns will be used to lower the S-IVB/IU orbit. These evasive maneuvers will completely separate the orbits of the S-IVB/IU and the satellite and will provide a near zero probability of recontact.

The modified Saturn IB launch vehicle can insert the satellite into the required orbit and several means are available

for increasing the payload capability if necessary. The flight environment is significantly less severe than that experienced during the SA-203 launch vehicle flight and the range safety total landmass impact probability is the same order of magnitude as in the planned Skylab/Saturn IB flights. The absolute minimum number of ground stations required to verify launch mission success is one, the radar and telemetry facilities at the Merritt Island Launch Area (MILA). However, with only the MILA station, initial orbit attainment is not known immediately and second burn cannot be verified until the end of the first revolution.

A potential problem area for the selected satellite launch vehicle configuration was identified by a cursory stability analysis for the ignition condition on Launch Pad 39. The first two coupled vehicle/pedestal/pad modes are unstable at nominal gain. More detailed stability and response analyses are necessary to determine the seriousness of the problem.

## 6.6 RECOMMENDATIONS

Due to the limited scope of this phase-B study insufficient data was available to adequately define some requirements and criteria significant to mission success. Therefore, additional studies, analyses, and tests, as appropriate, are recommended in the areas defined by, but not necessarily limited to, the following:

1. Refinement of the transfer function for predicting the characteristics of the return laser pulse signal (composed of returns from many individual retroreflectors) by taking into account the actual diffraction pattern of the retroreflectors.

2. Specification and verification of a suitable grade of fused silica using criteria based on a complete analysis of the laser-beam transfer function.

3. More accurate prediction of the in-orbit performance of the surface treatment, mount conductance, and thermal/optical performance of the retroreflectors.

4. Determination of the overall optimum orbit-injection motion and any potential passive means for stabilizing or controlling the motion.

5. Definition of the anti-contamination purge system requirements.

6. Determination of the stability and response conditions at ground ignition.

Additional recommendations are made in the following areas:

1. For the scientific purpose of tectonic measurements, ground stations are recommended in the most stable area (the Canadian Shield), reasonably stable regions of North America, and in tectonically active regions such as the eastern Mediterranean, Ethiopia, and Japan.

2. The recommended launch vehicle consists of the S-IB stage S-IB-212, S-IVB stage S-IVB-513 and Instrument Unit S-IU-212 based upon availability, performance characteristics, and cost. This selection does not conflict with current authorized mission planning.

3. The anti-contamination enclosure pressure release system is recommended as the baseline for the satellite anti-contamination purge system. The assumed requirements for this system are expected to be the more realistic of the three systems examined and this system offers advantages in simplicity, light-weight, and low cost.

## REFERENCES

1. Thermal Design Study of the Cannonball Satellite, Arthur D. Little Inc. Rpt. No. C-73510, dated 18 June 1971.
2. "Hazards of Depleted Uranium" by Norman C. Rasmussen, dated April 1971.
3. Saturn IB Launch Vehicle Mission Analysis and Modification Definition - Earth Physics Satellite (Phase B-Studies) Interface, Chrysler Technical Report HSM-R6-71, Task 9, dated 10 May 1971.
4. Cannonball Phase B Study Final Review, Structural Assessment: Task 7, Chrysler Corporation, dated 3 June 1971.
5. Longitudinal Stability Analysis 'POGO' of the First Stage Flight of Saturn IB Vehicle for Smithsonian Earth Physics Satellite (SEPS) Project, Chrysler Technical Report HSM-R6-71, Task 7, dated 10 May 1971.
6. Dynamic Characteristics and Damper Study of Saturn IB Vehicle For Smithsonian Earth Physics Satellite (SEPS) Project - Chrysler Technical Report HSM-R7-71, Task 7, dated 10 May 1971.
7. Saturn S-IVB Stage Modification to Support a Proposed Smithsonian Earth Satellite Mission - Volume II, Detailed Technical Report, MDAC Report MDC G 2397, dated June 1971.
8. Smithsonian Earth Physics Satellite Study Final Report (Saturn Engines Program), Rocketdyne Report SEP-1, dated 10 June 1971.
9. Saturn IB Launch Vehicle IU Modifications, IBM Report Number 71 W-00174, dated 4 June 1971.
10. Smithsonian Earth Physics Satellite, Cannonball Launch Vehicle Phase B Study - LVGSE Assessment, Presentation by Bob Cole, General Electric Company, 3 June 1971.
11. Earth Physics Satellite, Phase B Studies Saturn IB Launch Vehicle Final Reference Trajectory, CCSD TN-AP-71-506, May 1971.
12. Earth Physics Satellite Phase B Studies Saturn IB Launch Vehicle Dispersion Analysis, CCSD TN-AP-71-502, April 1971.

13. Earth Physics Satellite Phase B Studies Saturn IB Launch Vehicle Performance Trade Studies, CCSD TN-AP-71-505, May 1971.
14. Smithsonian Earth Physics Satellite Limited Phase B Study Final Report, PD-DO-DIR-71-84, August 20, 1971.
15. Earth Physics Satellite Phase B Studies Saturn IB Launch Vehicle Tracking Analysis, CCSD TN-AP-71-507, May 1971.
16. Earth Physics Satellite Phase B Studies Saturn IB Launch Vehicle Minimum Telemetry/Communication Capability and Requirements, CCSD HEE-R8-71, dated May 14, 1971.
17. Preliminary Saturn IB/Cannonball Control System Analyses, CCSD TB-AP-71-185, dated May 1971.
18. Earth Physics Satellite Phase B Studies Saturn IB Launch Vehicle Rigid Body Controllability Analysis, CCSD TN-AP-71-512, dated May 1971.
19. Saturn IB/Cannonball: Preliminary Structural Loads (Prelaunch and Launch), CCSD TB-P&VE-71-324, dated May 18, 1971.
20. Preliminary Saturn IB Cannonball Vehicle 1st and 2nd Stage Flight Bending Characteristics, CCSD Memo Report TD-PM-SAT-E-6, Task 11, dated March 25, 1971.

VOLUME III

PROJECT PLANNING DATA



## TABLE OF CONTENTS

	<u>Page</u>
SECTION 1. INTRODUCTION	1-1
1.1 GENERAL	1-1
1.2 PROJECT GUIDELINES AND ASSUMPTIONS	1-1
SECTION 2. MANAGEMENT PLAN	2-1
2.1 GENERAL	2-1
2.2 OFFICE OF SPACE SCIENCES AND APPLICATIONS (OSSA)	2-1
2.3 OFFICE OF MANNED SPACE FLIGHT (OMSF)	2-1
2.4 SMITHSONIAN ASTROPHYSICAL OBSERVATORY (SAO)	2-1
2.5 JOHN F. KENNEDY SPACE CENTER (KSC)	2-2
2.6 MARSHALL SPACE FLIGHT CENTER (MSFC)	2-2
2.7 MSFC EARTH PHYSICS SATELLITE PROJECT OFFICE	2-2
2.7.1 OFFICE OF THE MANAGER	2-2
2.7.2 PLANNING AND CONTROL	2-3
2.7.3 INTEGRATION	2-3
2.7.4 PRODUCT ASSURANCE	2-3
2.7.5 MISSION SUPPORT HARDWARE	2-3
SECTION 3. DESIGN DEVELOPMENT	3-1
3.1 GENERAL	3-1
3.2 LAUNCH VEHICLE	3-1
3.2.1 S-IB STAGE	3-1
3.2.2 S-IVB STAGE	3-1
3.3 PAYLOAD	3-1
3.3.1 SHROUD	3-2
3.3.2 PAYLOAD SUPPORT STRUCTURE AND EJECTION MECHANISM	3-2
3.3.3 SATELLITE AND RETROREFLECTORS	3-2
3.4 ASSEMBLY AND HANDLING EQUIPMENT	3-2

SECTION 4.	MANUFACTURING PROGRAM PLAN	4-1
4.1	INTRODUCTION	4-1
4.2	MANUFACTURING REQUIREMENTS	4-1
4.2.1	LAUNCH VEHICLE	4-2
4.2.2	PAYLOAD	4-2
4.2.2.1	SHROUD	4-2
4.2.2.2	PAYLOAD SUPPORT STRUCTURE AND EJECTION MECHANISM	4-2
4.2.2.3	SATELLITE	4-3
4.2.3	SATELLITE ASSEMBLY AND HANDLING EQUIPMENT	4-4
4.3	DOCUMENTATION	4-4
4.3.1	MANUFACTURING PROGRAM PLAN	4-4
4.3.2	HARDWARE REQUIREMENTS AND SPECIFICATIONS	4-5
4.3.3	MANUFACTURING PROCEDURES	4-5
4.3.4	MANUFACTURING REPORTS	4-5
SECTION 5.	TEST PROGRAM PLAN	5-1
5.1	INTRODUCTION	5-1
5.1.1	PURPOSE	5-1
5.1.2	SCOPE	5-1
5.2	APPLICABLE DOCUMENTS	5-1
5.3	TEST AND VERIFICATION PROGRAM	5-2
5.3.1	TESTING PHILOSOPHY	5-2
5.3.2	DEVELOPMENT AND QUALIFICATION TESTS	5-2
5.3.2.1	LAUNCH VEHICLE	5-3
5.3.2.2	DUMMY SATELLITE	5-3
5.3.2.3	PAYLOAD SHROUD, SUPPORT STRUCTURE AND EJECTION MECHANISM	5-4
5.3.2.4	RETROREFLECTORS	5-5
5.3.2.5	GROUND HANDLING AND SUPPORT EQUIPMENT	5-6
5.3.3	FLIGHT ASSURANCE TESTS	5-6
5.4	DOCUMENTATION	5-7
5.4.1	TEST PROGRAM PLAN	5-7
5.4.2	TEST REQUIREMENTS AND SPECIFICATIONS	5-7
5.4.3	TEST PROCEDURES	5-7
5.4.4	TEST REPORTS	5-7

SECTION 6.	RELIABILITY AND QUALITY ASSURANCE PLAN	6-1
6.1	INTRODUCTION	6-1
6.1.1	PURPOSE	6-1
6.1.2	SCOPE	6-1
6.2	APPLICABLE DOCUMENTS	6-1
6.3	RELIABILITY AND QUALITY ASSURANCE PROGRAM	6-2
6.3.1	R&QA PROGRAM REQUIREMENTS AND PHILOSOPHY	6-2
6.3.2	R&QA PROGRAM MANAGEMENT	6-2
6.3.3	R&QA ELEMENTS	6-4
SECTION 7.	FACILITIES UTILIZATION PLAN	7-1
7.1	PURPOSE AND SCOPE	7-1
7.2	FACILITIES REQUIREMENTS	7-1
7.2.1	MANUFACTURING FACILITIES	7-1
7.2.1.1	LAUNCH VEHICLE	7-1
7.2.1.2	PAYLOAD	7-1
7.2.1.2.1	DEPLETED URANIUM SATELLITE	7-1
7.2.1.2.2	RETROREFLECTORS	7-2
7.2.1.2.3	SHROUD	7-2
7.2.1.2.4	PAYLOAD SUPPORT STRUCTURE AND EJECTION MECHANISM	7-2
7.2.1.3	ASSEMBLY AND HANDLING EQUIPMENT	7-2
7.2.2	TESTING FACILITIES	7-3
7.2.2.1	LAUNCH VEHICLE	7-3
7.2.2.2	PAYLOAD	7-3
7.2.2.2.1	ASSEMBLY, TEST AND CHECKOUT	7-3
7.2.2.2.2	ENVIRONMENTAL AND QUALIFICATION TESTING	7-3
7.2.3	LAUNCH SITE FACILITIES	7-4
SECTION 8.	SCHEDULE	8-1
8.1	GENERAL	8-1
8.2	PAYLOAD	8-1
8.3	LAUNCH VEHICLE	8-1

## LIST OF FIGURES

<u>Figure</u>	<u>Title</u>	<u>Page</u>
2-1	Organization Chart -- Office of Manned Space Flight . . . . .	2-2
2-2	Organization Chart -- Marshall Space Flight Center . . . . .	2-4
2-3	Organization Chart -- Earth Physics Satellite Project Office . . . . .	2-5
8-1	SEPS Development and Production Schedule . . . .	8-2

## SECTION 1. INTRODUCTION

### 1.1 GENERAL

The Smithsonian Earth Physics Satellite project has been proposed by the Smithsonian Astrophysical Observatory through the Office of Space Science and Applications to the Office of Manned Space Flight. The Marshall Space Flight Center has performed a Phase B conceptual and preliminary design study based upon the use of a Saturn IB launch vehicle. The project development, management, and support activities necessary for execution of the project are detailed in the following sections of this volume.

### 1.2 PROJECT GUIDELINES AND ASSUMPTIONS

The Smithsonian Earth Physics Satellite project will support Smithsonian Astrophysical Observatory activity in the Earth Physics Program. A high density, low drag, passive satellite is required in a circular orbit at 3700 km (2000 n.m.) altitude and 55° inclination. The desired mass is approximately 3620 kg (8000 lb). The proposed satellite is a 76-cm (30-in.) diameter sphere of depleted uranium which will have an orbital lifetime in excess of 50 years. Optical (laser) tracking will be enhanced by the use of 864 fused silica retro-reflectors imbedded in the surface of the satellite.

The launch vehicle will be a modified Saturn IB composed of hardware that presently exists. The first stage booster will be an S-IB stage, and the second stage will be a modified S-IVB. If an S-IVB-IB is used, a second burn capability must be added. If an S-IVB-V, which has the second burn capability, is selected, then minor modifications peculiar to the Smithsonian Earth Physics Satellite mission must be made.

The payload structure will consist of existing nose cone and shroud hardware, with a new payload support structure to cradle the 3620-kg (8000-lb) satellite.

The assembly tool and handling fixture will be newly designed hardware.

## SECTION 2. MANAGEMENT PLAN

### 2.1 GENERAL

The management planning for implementing the Smithsonian Earth Physics Satellite Project is in accordance with applicable NASA documents. The NASA Office of Space Science will have overall responsibility for the project. The Smithsonian Astrophysical Observatory will be responsible for the payload and establishing project objectives and requirements. The NASA Marshall Space Flight Center, working through the NASA Office of Manned Space Flight, will be responsible for project management and implementation. The John F. Kennedy Space Center will be responsible for launch and launch operations of the Earth Physics space vehicle.

### 2.2 OFFICE OF SPACE SCIENCE AND APPLICATIONS (OSSA)

The Office of Space Science and Applications will have overall project responsibility including establishment of payload technical requirements and standards to accomplish the goals and objectives. The method to be employed by OSSA to exercise overall project management will be determined and established prior to project approval.

### 2.3 OFFICE OF MANNED SPACE FLIGHT (OMSF)

The Office of Manned Space Flight will have responsibility for establishing the overall project management and implementation policies. A project office will be established within OMSF reporting to the Associate Administrator/Manned Space Flight to direct the project within OMSF (Figure 2-1).

### 2.4 SMITHSONIAN ASTROPHYSICAL OBSERVATORY (SAO)

The Smithsonian Astrophysical Observatory will be assigned responsibility by OSSA to develop and deliver the payload for this project. This assignment will include establishing the scientific, engineering and mission requirements for the payload; also, the requirements for tracking and data management and analysis.

# OFFICE OF MANNED SPACE FLIGHT

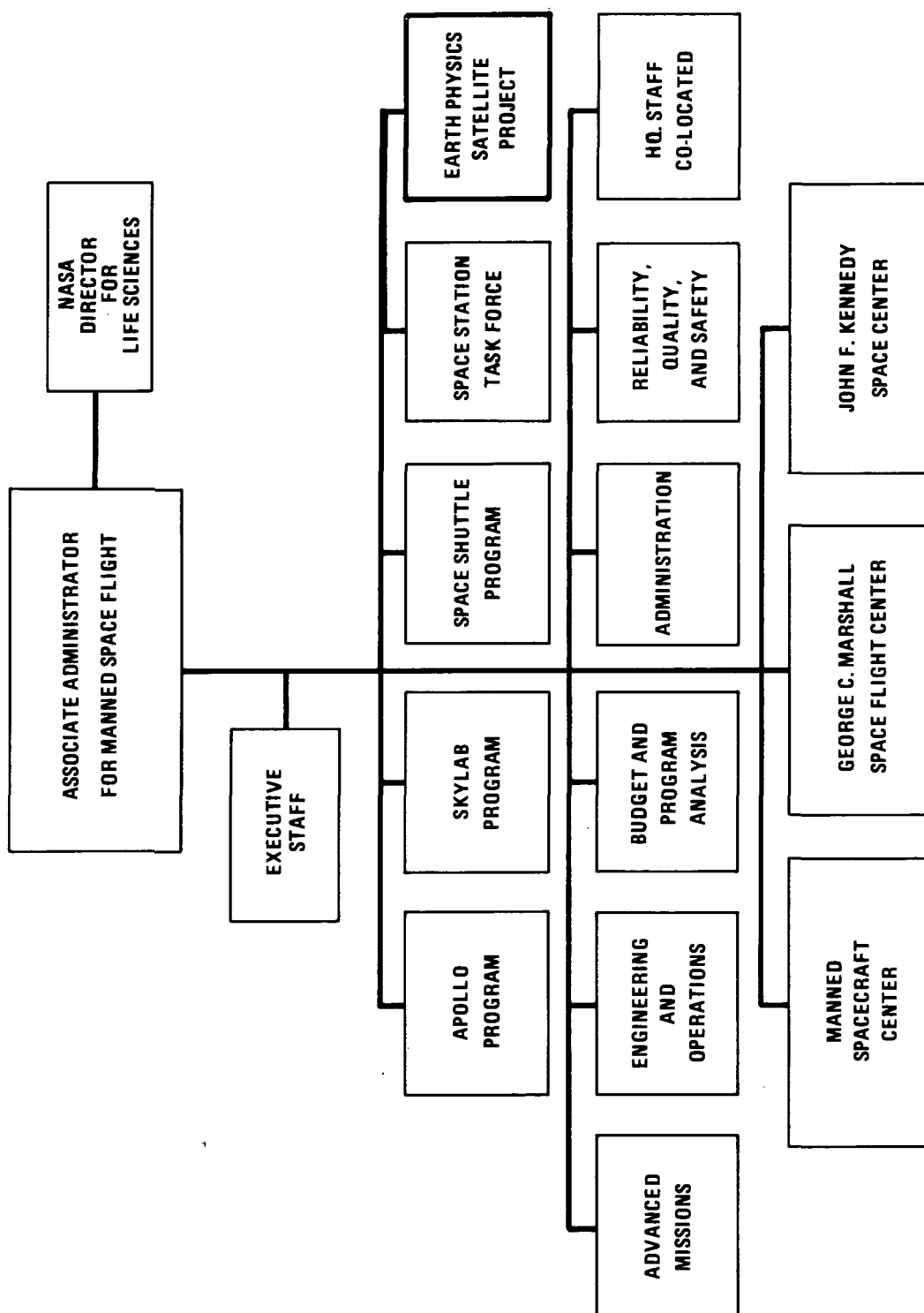


FIGURE 2-1. Organization Chart -- Office of Manned Space Flight

## 2.5 JOHN F. KENNEDY SPACE CENTER (KSC)

This Center reports to the NASA Headquarters Office of Manned Space Flight and is responsible for both manned and unmanned NASA space launches. Consequently, KSC will be responsible for launch operations. Within KSC, the Unmanned Launch Operations Directorate will be responsible to the MSFC Earth Physics Satellite Project Manager for overall launch operations including manpower, equipment, and facilities necessary for launch activities.

## 2.6 MARSHALL SPACE FLIGHT CENTER (MSFC)

MSFC (Figure 2-2) will be named the management center for implementing the Earth Physics Satellite project. The management responsibility within MSFC will be assigned to Program Management, where a project office will be established. This project office will be responsible for direction of MSFC in-house activities, the NASA contractors, and for interfacing with SAO and KSC.

The Marshall Space Flight Center will be responsible for establishing and meeting performance, schedule and cost objectives of the project.

## 2.7 MSFC EARTH PHYSICS SATELLITE PROJECT OFFICE

The Earth Physics Satellite Project Office (Figure 2-3) will be the focal point within MSFC for management of all activities pertaining to the project. Responsibilities will include contracting for and directing the design, development, and procurement of the project hardware; defining launch vehicle requirements, systems integration, payload integration, and overall space vehicle systems integration; and providing technical support to launch operations and mission operations. The project office will consist of four organizational elements as described below:

### 2.7.1 OFFICE OF THE MANAGER

The Manager and his staff will direct the execution of all Earth Physics Project activities. This will include establishing policies and requirements; determining priorities; effecting a system of scheduling and status analysis; reviewing and approving design, production, qualification, and test schedules; reviewing and approving technical baselines and exercising control over technical progress; and providing visibility of major technical problems to higher authority and recommending solutions.



# MARSHALL SPACE FLIGHT CENTER

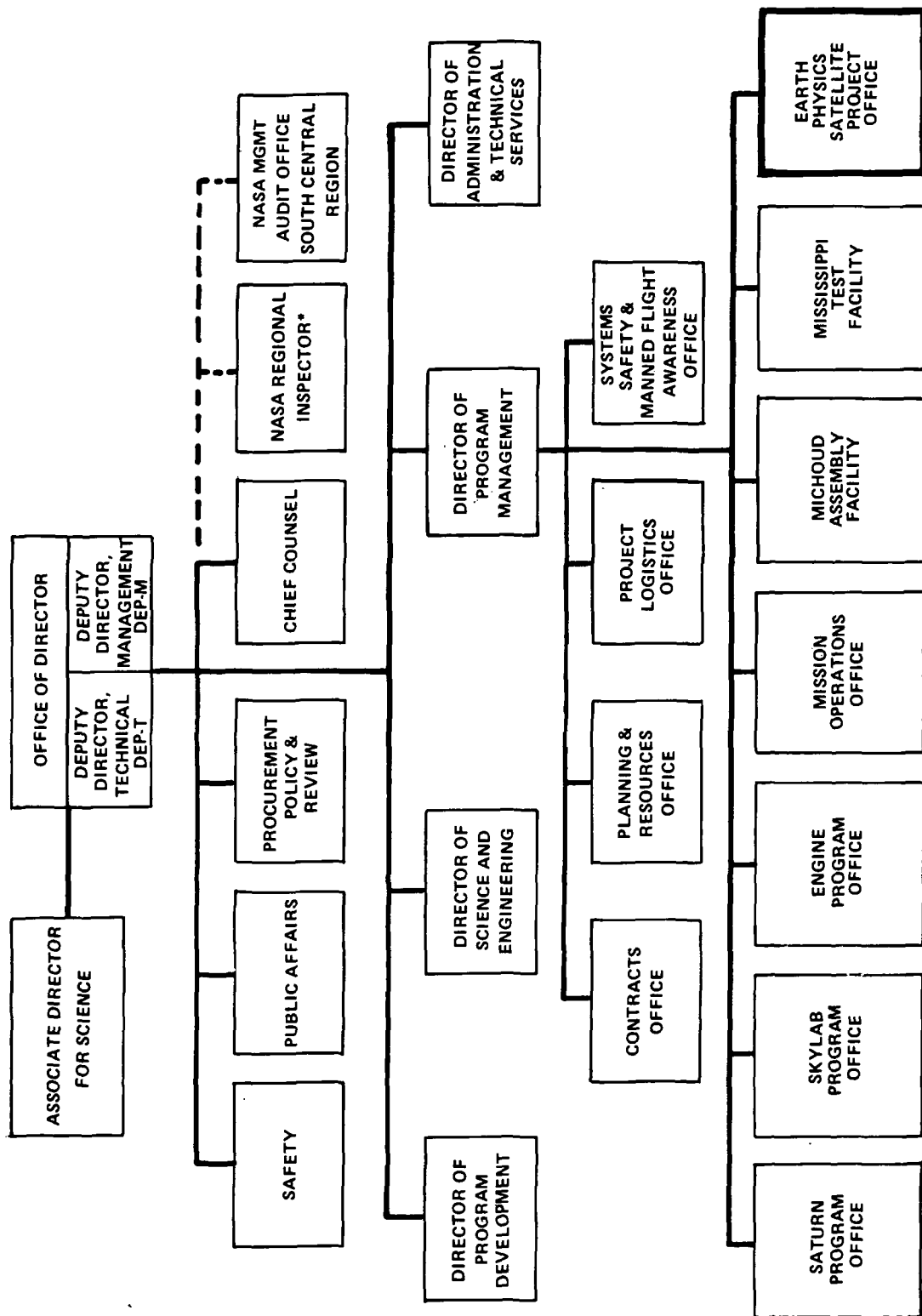


FIGURE 2-2. Organization Chart -- Marshall Space Flight Center

## EARTH PHYSICS SATELLITE PROJECT OFFICE

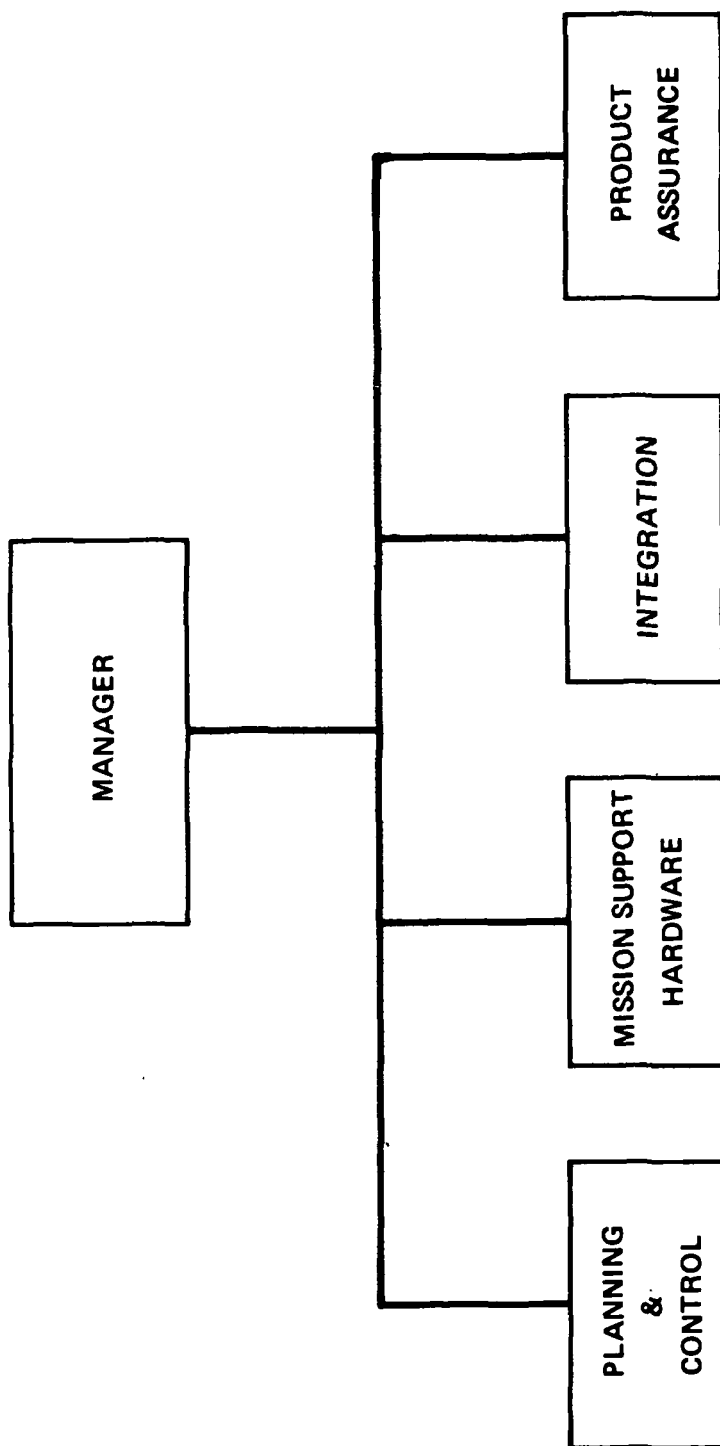


FIGURE 2-3. Organization Chart -- Earth Physics Satellite Project Office

#### 2.7.2 PLANNING AND CONTROL

This element will be responsible for planning and controlling all programmatic aspects of the project. This includes establishing resources requirements and allocations; recommending project priorities and directing a system of scheduling and status analysis; providing management with periodic status reports; directing the preparation and revision of project plans; and analyzing, projecting and controlling project costs.

#### 2.7.3 INTEGRATION

This element will manage the systems engineering and integration activities for the project including mission analyses, interface definition, configuration and change control, design, development and systems testing required to assure compatibility of all project elements. These responsibilities apply to NASA/SAO/industry activities that are necessary to integrate properly all project elements for the overall space vehicle for the mission.

#### 2.7.4 PRODUCT ASSURANCE

This element will be responsible for managing the quality and reliability, safety, test and checkout, and logistics support activities necessary to assure successful mission accomplishment. This will include planning, coordinating, establishing, analyzing, evaluating, assessing, and reporting on these NASA/industry activities.

#### 2.7.5 MISSION SUPPORT HARDWARE

This element will manage the activities required to modify, test, operate, and maintain the launch vehicle, shroud, booster adapter, and associated GSE required for the mission. This includes definition of hardware requirements and direction of the NASA/industry efforts in the areas of development, modification, test, prelaunch checkout, and launch and orbit insertion of the mission payload.

## SECTION 3. DESIGN DEVELOPMENT

### 3.1 GENERAL

The management of the Smithsonian Earth Physics Satellite Project will be the responsibility of Marshall Space Flight Center (MSFC). The design of the depleted uranium ball and the retroreflectors will be the responsibility of the Smithsonian Astrophysical Observatory (SAO). The design of the modification of the launch vehicle and the payload structure will be the responsibility of MSFC, Program Management, and will be delegated to Science and Engineering.

### 3.2 LAUNCH VEHICLE

The design development of the launch vehicle modifications will be accomplished under the direction of MSFC, Program Management, and will be accomplished by the technical laboratories of Science and Engineering and the launch vehicle stage contractors. The work will be accomplished within the scope of existing Saturn contracts.

#### 3.2.1 S-IB STAGE

No design modifications are required for the S-IB stage. Review of the interface connections will be accomplished by the S-IB/IC Stage Project Office, PM-SAT-S-IB/IC. The work will be accomplished within the scope of the existing S-IB stage contract.

#### 3.2.2 S-IVB STAGE

The design modifications for the S-IVB stage vary depending on whether an S-IVB-IB or an S-IVB-V stage is selected for use. The design will be the responsibility of the S-IVB Stage Project Manager, PM-SAT-S-IVB, and will be accomplished by the stage contractor under the technical direction of Science and Engineering laboratories, S&E-CSE, S&E-ASTN, and S&E-ASTR.

### 3.3 PAYLOAD

The design development of the payload will be accomplished under the direction of MSFC, Program Management. The shroud and the payload support structure/ejection mechanism will be the

responsibility of Science and Engineering. The depleted uranium satellite and the retroreflectors will be the responsibility of Smithsonian Astrophysical Observatory (SAO).

#### 3.3.1 SHROUD

The shroud will consist of the Spacecraft/Lunar Module Adapter and the nose cone, which are existing hardware. Any design modifications will be developed by the Astronautics Laboratory, S&E-ASTN.

#### 3.3.2 PAYLOAD SUPPORT STRUCTURE AND EJECTION MECHANISM

The PSS/EM will be new hardware. Design responsibility will be assigned to the Astronautics Laboratory, S&E-ASTN.

#### 3.3.3 SATELLITE AND RETROREFLECTORS

The satellite and retroreflector design will be the responsibility of SAO. Technical development will be accomplished in-house at SAO. Two satellite configurations will be developed. The first is the complete depleted uranium satellite with internal balancing weights, and with externally mounted retroreflectors. The second is a test unit, but without the retroreflectors, to be used in the qualification test program.

#### 3.4 ASSEMBLY AND HANDLING EQUIPMENT

The design development of the assembly and handling equipment will be the responsibility of the Product Engineering and Process Technology Laboratory, S&E-PT. This equipment in its various configurations will be used for the assembly of the satellite, balancing and calibration of the complete satellite assembly, transportation and handling, and installation of the satellite into the launch vehicle.

## SECTION 4. MANUFACTURING PROGRAM PLAN

### 4.1 INTRODUCTION

This plan establishes the basic Manufacturing Program policies, procedures, and responsibilities for the Smithsonian Earth Physics Satellite. The following is developed on the assumption that the launch vehicle will be a Saturn IB, using existing hardware with modifications.

This Manufacturing Plan encompasses the manufacturing activities necessary for the production and/or delivery of the launch vehicle, flight payload including shroud, and qualification hardware. Policies contained in this plan shall be utilized to establish manufacturing implementation procedures. Detailed manufacturing planning shall be accomplished in conjunction with the reliability and quality assurance planning.

This plan covers the activities of Marshall Space Flight Center (MSFC), Smithsonian Astrophysical Observatory (SAO), other government agencies (DCAS), contractors, and suppliers. Any additional manufacturing requirements will be implemented through a revision to this plan and shall be approved by the NASA/MSFC Project Manager.

### 4.2 MANUFACTURING REQUIREMENTS

The manufacturing requirements are developed under the guidelines that the launch vehicle will consist of existing hardware with minimum modifications, and that the payload and related hardware (except shroud) will be newly designed hardware.

Manufacturing management responsibility is assigned to NASA/MSFC, Program Management, Program Engineering Office, PM-SAT-E. Procurement and fabrication responsibilities will be as outlined in the following sections. Reliability and quality assurance will be the responsibility of Program Assurance Office, PM-SAT-A, with support from Quality and Reliability Assurance Laboratory, S&E-QUAL.

#### 4.2.1 LAUNCH VEHICLE

The launch vehicle consists of a Saturn IB, which includes the S-IB Booster, a modified S-IVB second stage, and the Instrument Unit. The units are comprised of existing hardware and will require minimum modification and requalification.

The launch vehicle modifications will be the responsibility of the Saturn Program Office, working through the S-IB/IC Stage Project Office, PM-SAT-S-IB/IC, the S-IVB Stage Project Office, PM-SAT-S-IVB, and the Instrument Unit Project Office, PM-SAT-IU. The work will be accomplished within the scope of the existing Saturn contracts.

No requirements for new resources or facilities are anticipated.

#### 4.2.2 PAYLOAD

The payload consists of the satellite proper, the payload support structure and ejection mechanism (PSS/EM), and the shroud. The satellite and the PSS/EM are newly designed hardware. The shroud includes the nose cone and the Spacecraft/Lunar Module Adapter (SLA), and several variations of hardware presently exist. No new resources or facilities requirements, other than a temporary clean room at SAO, are expected.

##### 4.2.2.1 SHROUD

The shroud consists of the SLA and the nose cone which are existing hardware. Any design modifications and the installation of the related payload hardware will be the responsibility of the Product Engineering and Process Technology Laboratory, S&E-PT. Quality Assurance support will be provided by Quality and Reliability Assurance Laboratory, S&E-QUAL. Existing facilities and resources will be used.

##### 4.2.2.2 PAYLOAD SUPPORT STRUCTURE AND EJECTION MECHANISM

The payload support structure and ejection mechanism (PSS/EM) consists of a pair of crossed beams, 574 cm (226 in.) in length, supporting the ejection mechanism and pressurized satellite

enclosure at the center. The PSS/EM will be fabricated either in-house by NASA/MSFC or by local contractors. Detail design responsibility will be assigned to the Astronautics Laboratory, S&E-ASTN, and manufacturing responsibility to Product Engineering and Process Technology Laboratory, S&E-PT. Existing resources and facilities will be used.

#### 4.2.2.3 SATELLITE

The satellite design and fabrication will be the responsibility of SAO. The design will be done in-house by SAO, and the fabrication will be contracted to a firm which has an AEC license for handling depleted uranium materials. The retroreflector design will be done in-house by SAO, and the fabrication will be contracted to one of several firms qualified in optical glass technology. Quality Assurance support will be provided by NASA/MSFC in the documentation, qualification, testing, and acceptance functions.

The flight satellite will consist of a center cube core weighing approximately 908 kg (2000 lb) with three orthogonally-adjusted counter weights and six spherical caps weighing 454 kg (1000 lb) each in which the 864 retroreflectors are recessed. SAO will be responsible for the design specifications, detail drawings, and the balancing and checkout procedure. The satellite will be fabricated by an outside contractor responsive to the technical direction of the SAO technical representative. Quality assurance control of material composition and packaging and handling are of particular importance. Acceptance testing will be monitored by SAO technical representatives with support from NASA/MSFC quality assurance personnel. After fabrication, assembly, balance and checkout of the satellite (less the retroreflectors), the flight item will be shipped to SAO for installation of retroreflectors and final checkout. Adequate resources and facilities are known to exist at the plants of two contractors who are qualified to fabricate the depleted uranium under AEC licensing. A portable type clean room rated to class 100,000 will be required at SAO.

The dummy unit will be of the same design as the flight satellite except that the mounting holes for the retroreflectors will be omitted. After fabrication, assembly, balance and checkout under the technical direction of the SAO representative, the dummy unit will be shipped to NASA/MSFC to be used in the qualification test program.



The flight type qualification sector will be designed by SAO and fabricated by the outside contractor. The sector will represent a portion of one of the flight sectors. It will consist of a 15.24-cm (6-inch) cube with the top surface rounded to the 38.10-cm (15-inch) radius of the satellite, and a suitable number of retroreflectors installed. It will weigh approximately 56.75 kg (125 lb). The sector will be shipped to SAO for installation of the retroreflectors, and then to NASA/MSFC for qualification tests.

The retroreflector design will be the responsibility of SAO. The fabrication will be by outside contractors qualified in optical glass technology. Quality assurance control of material composition and packaging and handling are of particular importance. Final acceptance testing will be monitored by SAO technical representatives with support from NASA/MSFC quality assurance personnel. The completed units will be shipped to SAO for installation in the satellite flight and qualification test hardware.

#### 4.2.3 SATELLITE ASSEMBLY AND HANDLING EQUIPMENT

The design of the assembly and handling equipment will be the responsibility of NASA/MSFC. The design will be made available to SAO and satellite manufacturer as required. Fabrication will be done by local sub-contractors. NASA/MSFC will develop design specifications and test and checkout procedures and will provide necessary quality assurance support. Existing resources and facilities appear to be adequate for this work.

#### 4.3 DOCUMENTATION

Manufacturing documentation will be developed in the form of hardware requirements and specifications, manufacturing plans and procedures, and quality assurance and inspection requirements and procedures. All documentation will be subject to the approval of the NASA/MSFC Project Manager.

##### 4.3.1 MANUFACTURING PROGRAM PLAN

The manufacturing program plan will be the responsibility of NASA/MSFC. The SAO technical representative will concur on the portions pertaining to the satellite.

#### 4.3.2            HARDWARE REQUIREMENTS AND SPECIFICATIONS

The hardware requirements and specifications for the retroreflectors and the satellite will be the responsibility of the SAO; those of the ground handling equipment and all other launch vehicle related items (i.e., shroud, support structure, ejection mechanism, etc.) will be the responsibility of NASA/MSFC.

#### 4.3.3            MANUFACTURING PROCEDURES

The detail manufacturing procedures for the retroreflectors and the satellite will be the responsibility of SAO; all others will be the responsibility of NASA/MSFC.

#### 4.3.4            MANUFACTURING REPORTS

Any final reports pertaining to the manufacturing activity will be the responsibility of NASA/MSFC, with appropriate input from the SAO technical representative.

## SECTION 5. TEST PROGRAM PLAN

### 5.1 INTRODUCTION

#### 5.1.1 PURPOSE

The purpose of this Test Program Plan is to present a plan for the implementation of the test program required to assure the successful launch and operation of the Smithsonian Earth Physics Satellite. The requirements are developed on the basis that the launch vehicle will be a Saturn IB, using an S-IVB-IB or S-IVB-V second stage with a Spacecraft/Lunar Module Adapter.

#### 5.1.2 SCOPE

This Test Program Plan encompasses the Development Test Program, Qualification Test Program, and the Flight Awareness documentation for these test programs. This plan also identifies the test methods necessary to assess and correlate the data. In addition, this plan identifies the preparation of test procedures and specifications necessary for test, checkout, and preflight acceptance of the parts, assemblies, and complete satellite. Any additional testing required will be implemented through a revision to this plan and shall be approved by the NASA/MSFC Project Manager.

### 5.2 APPLICABLE DOCUMENTS

The following documents form a part of this plan to the extent specified herein. In case of conflict between the requirements of this plan and any referenced document, the requirements of this plan shall govern.

#### NASA Specifications

NHB 5300.4 (IA)	Reliability Program Provisions for Aeronautical & Space System Contractors
NHB 5300.4 (IB)	Quality Program Provisions for Aeronautical & Space System Contractors

### 5.3 TEST AND VERIFICATION PROGRAM

#### 5.3.1 TESTING PHILOSOPHY

The testing and verification will be effected as a minimum program. Only those tests necessary to prove new hardware or overcome more stressing environments will be implemented. Hardware that has prior flight history in equal or greater environments than those of the SEPS project will be qualified on an analysis basis.

Prior to any fabrication or procurement of flight items, a program of design and prototype qualification testing will be undertaken. This qualification testing program will consist of several individual testing projects, each subjecting representative designs and/or prototype hardware items to environmental rigors somewhat greater than those expected for the actual flight items. The extent of tests will encompass (a) mechanical shock, acceleration, and vibration; (b) thermal vacuum and solar radiation; (c) beta, gamma, and UV radiation of retroreflector materials; and (d) optical tests of retroreflectors. The prototype hardware items used in the above-described tests will be fabricated and/or procured per the applicable detail drawings and specifications for the appropriate flight items.

The testing program will be developed based upon the requirements outlined in NHB 5300.4 (IA), Chapter 4, and in NHB 5300.4 (IB), Chapter 7. Testing levels will be in accordance with those experienced on prior Saturn IB flights. The overall activity will be in accordance with the program outlined in Reliability and Quality Assurance Program Plan for Smithsonian Earth Physics Satellite (Section 6 of this report).

#### 5.3.2 DEVELOPMENT AND QUALIFICATION TESTS

This program is based on use of a Saturn IB launch vehicle which is man-rated and has been qualified in a flight program. The shroud has been qualified on earlier programs, but if it must be shortened to reduce weight, additional tests may be required. The payload (satellite), and the support structure and ejection mechanism (PSS/EM) are new hardware and will require complete qualification.

#### 5.3.2.1

#### LAUNCH VEHICLE

The Saturn IB launch vehicle has a prior man-rated flight history and will be qualified by analysis. The first stage S-IB is presently qualified. A second burn restart capability is required on the S-IVB stage. Two possibilities exist for this stage. If an S-IVB-V stage (which has restart capability) is used, the necessary changes will consist of (1) modification of the S-IVB interstage and (2) minor modifications peculiar to the SEPS mission. If an S-IVB-IB stage is used, it will be necessary to add the restart capability. Prior flight experience will allow the qualification of either system by an analysis method.

#### 5.3.2.2

#### DUMMY SATELLITE

Design qualification and prototype testing of less critical and more straight-forward aspects of the satellite will be undertaken in conjunction with other phases of the test program. It is planned that the bolted assembly of the satellite core pieces (cube core, spherical caps and shear pins) and the locking of the adjustable counterweights will be qualified during the qualification testing of the payload support structure and ejection mechanism (PSS/EM) by NASA/MSFC.

A near-mass and geometrically equivalent dummy satellite assembly will be fabricated by SAO prior to the flight assembly and supplied to NASA/MSFC for use in the mass loading for the PSS/EM qualification testing. The dummy satellite assembly will consist of fabricated parts and standard hardware identical to those to be used in the flight satellite assembly except that no retroreflector cavities will be machined into the spherical surface, and hence, no retroreflectors will be installed. It will, however, be representative of the flight assembly insofar as it will consist of a bolted assembly of all core pieces, will contain adjustable and lockable counterweights, will be approximately the same mass and will have identical overall geometry. The satellite will be a 76-cm (30 - in.) sphere of depleted uranium and will weigh approximately 3620 kg (8,000 lb).

The dummy satellite assembly described above will be utilized in several additional capacities. It and its components will be considered as flight spare or backup items; it will be utilized to verify the satellite balancing fixture and balancing techniques; it will be used to proof test the handling fixtures and prove the handling techniques and assembly plan; and it will, by its successful assembly, verify the design geometry, detail drawings and fabrication techniques for the items involved.

### 5.3.2.3 PAYLOAD SHROUD, SUPPORT STRUCTURE AND EJECTION MECHANISM

The payload shroud will consist of a Spacecraft/Lunar Module Adapter (SLA) and a suitable nose cone. The payload support structure and ejection mechanism (PSS/EM) will be designed and fabricated in-house at NASA/MSFC for use with the satellite. The PSS/EM cross-beam structure will mount on the existing "hard points" designed for carrying the Lunar Module loads.

The shroud consisting of an SLA and nose cone has prior flight history and will be qualified by analysis.

The PSS/EM with the dummy satellite will be subjected to a series of tests to qualify the mechanical design. The cross-beam structure consists of two cross arms approximately 574 cm (226 in) in length. The ends of the cross arms will be designed to mate with the hard points on the SLA base ring. These are the same hard points used by the Lunar Module. The support structure includes a partial-sphere mounting cup in which the satellite rests. The spring loaded ejection mechanism is attached beneath the mounting cup, and four holddown arms will be preloaded to approximately 59,994 N (13,500 lbf) each, or 239,976 N (54,000 lbf) total, to restrain the satellite during periods of negative G and lateral acceleration. Enclosure panels will be mounted on the holddown arms to contain a pressurant gas (dry nitrogen) used to preclude contamination of the reflective surfaces.

The qualification tests will include static load tests, structural and acoustical vibration, and mechanical operation of the ejection mechanism. Testing levels will be equivalent to those imposed by the launch vehicle with safety factors as may be appropriate. Items of particular importance during the vibration tests are (1) vibration levels on the panels of the pressurized enclosure, and (2) differential pressures and leakage rates of the pressurant gas. Test hardware models of the SLA are presently being used in the ATM Program and will be made available to this test program. All testing will be conducted in existing facilities at NASA/MSFC.

#### 5.3.2.4 RETROREFLECTORS

The retroreflectors, made of high grade fused silica, are of cylindrical design with corner reflector on one end. The cylinder is approximately 3.65 cm (1.44 in.) in diameter and 3.17 cm (1.25 in.) long. The entrance surface is not coated, but the reflective corner cube will have metallic coating on the surfaces to increase the reflectivity. Contamination and deterioration of these surfaces is a major concern throughout the program.

The retroreflector qualification will consist of a series of tests. As appropriate, the retroreflector will be mounted in a uranium fixture which represents a portion of one of the spherical caps of the satellite. The fixture is envisioned as a 15.24 cm (6 in) cube with the top surface rounded to the 38 cm (15 in) radius of the satellite. The fixture will weigh approximately 56.75 kg (125 lbm).

The retroreflector tests will include, but not necessarily be limited to, the following:

(1) Vibration, acoustic, shock and acceleration exposure to qualify the mechanical design of the mounting of a retroreflector in a cavity machined into a uranium mass.

(2) Thermal vacuum and simulated solar radiation exposure to qualify the thermal design of a mounted retroreflector/surface treated uranium mass system.

(3) Beta, Gamma and UV radiation exposure to qualify the choice and specification of retroreflector material and metallic coating.

(4) Optical testing of mounted and thermally conditioned retroreflectors to verify the retroreflector performance parameters and specified testing technique.

The prototype hardware items used in the above described testing projects will be fabricated and/or procured per the applicable detail drawings and specifications for the appropriate flight items. The ranges and limits of the environmental exposures utilized in the above described testing projects will be established after due consideration of the actual environmental conditions predicted for the flight satellite within a range of possible operational modes and expected useful lifetimes.

The testing will be conducted at NASA/MSFC in existing facilities and equipment. The SAO technical representative will approve and monitor these tests.

#### 5.3.2.5 GROUND HANDLING AND SUPPORT EQUIPMENT

The ground handling and support equipment is an integrated multifunction equipment. It will be capable of use during the assembly and disassembly of the 3620-kg (8000-lbm) satellite. It will be used as an airbearing holding fixture during the balancing and calibration activity. It will be used as part of the transportation equipment during shipping; it will also be used as the transfer equipment to place the satellite into the launch vehicle.

The environmental and qualification testing will consist of static loading tests and the dynamic operational tests to prove the assembly, transportation, and transfer operations. These tests will be performed in existing facilities at NASA/MSFC and possibly at the site of manufacture of the equipment.

#### 5.3.3. FLIGHT ASSURANCE TESTS

Flight assurance testing of the flight satellite assembly will take place while it is supported by and integrated with the PSS/EM or at least the central portion of the PSS/EM. It is planned that the flight satellite assembly and the PSS/EM, or its central portion, be subjected to flight assurance testing simultaneously as this minimizes the requirement for special test fixtures and hence reduces program costs without serious schedule impacts.

Flight assurance testing will consist of exposure to sinusoidal, random and/or acoustic vibration and thermal vacuum at levels expected for the actual launch, flight and subsequent orbit injection. Successful completion of flight assurance testing will be established by visual inspection and by a final balance verification after the flight satellite assembly is removed from the PSS/EM and prior to being packaged for final shipment to the launch site.

NASA/MSFC will be responsible for all aspects of the flight assurance test program including establishing testing levels, plans and procedures; all satellite assembly handling; conducting



actual testing; and reporting test results. Existing NASA/MSFC facilities will be used. The SAO technical representative will concur in all plans and procedures and will be present for all tests and handling of the flight assembly.

#### 5.4 DOCUMENTATION

Test documentation will be developed in the form of test requirements and specifications, test procedures, test plans, and test reports. All documents will be subject to the approval of the NASA/MSFC Project Manager.

##### 5.4.1 TEST PROGRAM PLAN

The test program plan will be the responsibility of NASA/MSFC. The SAO technical representative will concur on the portions pertaining to the satellite.

##### 5.4.2 TEST REQUIREMENTS AND SPECIFICATIONS

The test requirements and specifications for the retroreflectors and the satellite will be the responsibility of SAO; those for the ground handling equipment and all other launch vehicle related items (i.e., shroud, support structure, ejection mechanism) will be the responsibility of NASA/MSFC.

##### 5.4.3 TEST PROCEDURES

The detail test procedures for the retroreflectors and the satellite will be the responsibility of SAO; all others will be the responsibility of NASA/MSFC.

##### 5.4.4 TEST REPORTS

The final test reports will be the responsibility of NASA/MSFC, with appropriate input from the SAO technical representative.

## SECTION 6. RELIABILITY AND QUALITY ASSURANCE PROGRAM PLAN

### 6.1 INTRODUCTION

#### 6.1.1 PURPOSE

This plan establishes the basic Reliability and Quality Assurance (R&QA) policies, procedures, and responsibilities for the Smithsonian Earth Physics Satellite.

#### 6.1.2 SCOPE

This R&QA plan encompasses the R&QA activities associated with the design, development, manufacturing, qualification, testing, and flight assurance of the satellite, the launch vehicle, and the backup hardware. Policies contained in this plan shall be utilized for establishing basic reliability and quality implementation procedures. Detailed inspection and test planning shall be accomplished in conjunction with the manufacturing planning. Qualification testing requirements are outlined in Test Program Plan for Smithsonian Earth Physics Satellite.

This plan covers the activities of Marshall Space Flight Center (MSFC), Smithsonian Astrophysical Observatory (SAO), other government agencies (DCAS), contractors, and suppliers. Any additional R&QA required will be implemented through a revision to this plan and shall be approved by the NASA/MSFC Project Manager.

### 6.2 APPLICABLE DOCUMENTS

The following documents form a part of this plan to the extent specified herein. In case of conflict between the requirements of this plan and any referenced document, the requirements of this plan shall govern.

#### NASA Documents:

NHB 5300.4 (1A)	Reliability Program Provisions for Aeronautical and Space Systems Contractors
-----------------	---

### 6.3 RELIABILITY AND QUALITY ASSURANCE PROGRAM

The Reliability and Quality Assurance Program will be developed using applicable portions of NHB 5300.4(1A) and NHB 5300.4 (1B). The overall activity and the control thereof will be developed in accordance with the requirements detailed herein.

#### 6.3.1 R&QA PROGRAM REQUIREMENTS AND PHILOSOPHY

The R&QA activities will be developed to include the engineering and testing necessary to accomplish an unmanned launch of the satellite. The redundancy of tests and the wider safety and test margins usual in a manned program will be reduced to the minimum acceptable to stay within the bounds of a low cost program. The various environmental qualification tests will be combined where possible, and hardware with prior flight experience will be qualified by similarity or analysis .

#### 6.3.2 R&QA PROGRAM MANAGEMENT

The overall program management is assigned to NASA/MSFC, Program Management, Program Engineering Office, PM-SAT-E. Reliability and quality assurance is the responsibility of Program Assurance Office, PM-SAT-A, with support from the Quality and Reliability Assurance Laboratory, S&E-QUAL.

The reliability and quality assurance of the launch vehicle will be the responsibility of the Program Assurance Office, PM-SAT-A, working through the S-IB/IC Stage Project Office, PM-SAT-S-IB/IC, the S-IVB Stage Project Office, PM-SAT-SIVB, and the Instrument Unit Project Office, PM-SAT-IU. The work will be accomplished within the scope of the existing Saturn contracts.

The payload consists of the satellite proper, the payload support structure and ejection mechanism (PSS/EM), and the shroud. The satellite and the PSS/EM are newly designed hardware. The shroud includes the nose cone and the Spacecraft Lunar Module Adapter (SLA), and several variations of hardware presently exist.

The design development of the shroud and the PSS/EM will be the responsibility of the Astronautics Laboratory, S&E-ASTN. The modifications to the shroud and the fabrication of the PSS/EM will be the responsibility of the Product Engineering and Process Technology Laboratory, S&E-PT. The work may be accomplished by in-house personnel or by subcontract to a local firm. Reliability and quality assurance activity will be the responsibility of the Quality and Reliability Assurance Laboratory, S&E-QUAL. R&QA tasks, such as design review, test and inspection, and checkout, will be accomplished in accordance with accepted policies and operating procedures. Existing resources and facilities will be utilized.

The design development and fabrication of the flight satellite, the dummy satellite, the retroreflectors, and the qualification test sector will be the responsibility of SAO. Fabrication of depleted uranium parts will be contracted to a firm which has an AEC license for handling uranium materials. Fabrication of the retroreflectors will be contracted to a firm qualified in optical glass technology. Reliability and quality assurance activity will be the responsibility of Quality and Reliability Assurance Laboratory, S&E-QUAL. R&QA authority will be delegated to a cognizant government agency (DOD or DCAS) where possible. Quality assurance support will be provided in the documentation, qualification, testing, and acceptance functions. Quality assurance control of material composition and packaging and handling of both the depleted uranium satellite and the retroreflectors are particular concerns. Acceptance testing will be monitored by SAO technical representatives with support from NASA/MSFC quality assurance personnel. A portable temporary clean room will be required at SAO.

The design of the assembly and handling equipment will be the responsibility of NASA/MSFC. The design will be made available to SAO and satellite manufacturer as required. Fabrication will be done by local subcontractors. NASA/MSFC will develop design specifications, qualification, test and checkout procedures. Surveillance of the MSFC in-house and local subcontractor operations will be

the responsibility of Quality and Reliability Assurance Laboratory, S&E-QUAL. R&QA authority will be delegated to a cognizant government agency (DOD or DCAS) where possible at SAO and at the handling equipment contractor facility.

### 6.3.3 R&QA ELEMENTS

The applicable R&QA program elements will be selected from NHB 5300.4 (1A) and NHB 5300.4 (1B). The more significant elements are outlined below. The tasks will be accomplished in accordance with existing agreements between Program Management Directorate and Science and Engineering Directorate. Responsibility is assigned to Quality and Reliability Assurance Laboratory, S&E-QUAL.

R&QA engineering consists of a number of interrelated tasks and is considered an integral part of the project activity. NASA/MSFC, SAO, and the contractors shall generate technical documents, perform design reviews, failure mode analyses, and parts and materials review and selection as required. Material composition and packaging and handling procedures are particular concerns. Technical documents will include CEI specifications; test, inspection, and handling procedures; drawings; fabrication controls; and other planning documents. R&QA personnel will participate in design reviews to insure acceptability of design requirements (environments, test, producibility, inspectibility) and completeness of documentation.

Fabrication controls, including handling, assembly, and operations, shall be developed. Controls shall be established to ensure that only conforming materials and articles are used in fabrication. The fabrication, assembly, inspection, and test shall be controlled in accordance with cleanliness requirements for environments, work surfaces, tools, fixtures, handling, storage and shipping containers, and test and inspection equipment to prevent contamination. Process controls and procedures and equipment certification shall be required where necessary.

An inspection and test program to demonstrate that contract, drawing, and specification requirements are met shall be implemented. In process and end item tests and checkouts shall be incorporated. Test specifications shall include test objectives, test parameters and tolerances, and acceptance and rejection criteria. Written test procedures shall be utilized. Test and environmental

conditions shall be controlled where necessary to prevent contamination of critical parts and materials. Test equipment shall be controlled, maintained, and calibrated as specified in procedures for each equipment. Test data and records on critical materials and test parameters shall be supplied with the test item. Quality assurance personnel will verify that all test and inspection documentation is sufficient and accurate, and will monitor all tests involving critical materials and parameters.

The qualification testing and verification will be performed as a minimum cost program. Only those tests necessary to prove new hardware will be implemented. Hardware that has prior flight history will be qualified by similarity or analysis. The qualification testing program will be conducted as detailed in Test Program Plan for Smithsonian Earth Physics Satellite (as outlined in Section 5 of the report). Testing levels will be in accordance with those experienced on prior Saturn IB flights. Written test requirements and procedures will be used, and all documentation will be reviewed by reliability and quality assurance personnel to insure compliance with all R&QA program requirements.

## SECTION 7. FACILITIES UTILIZATION PLAN

### 7.1 PURPOSE AND SCOPE

This plan identifies and establishes those government and contractor owned facilities necessary to support the development, manufacture, test, and launch of the Smithsonian Earth Physics Satellite. The plan covers the facilities requirements for program activity at the Marshall Space Flight Center (MSFC), the Smithsonian Astrophysical Observatory (SAO), Kennedy Space Center (KSC) and the contractors and suppliers. The following is developed on the assumption that the launch vehicle will be a SATURN IB.

### 7.2 FACILITIES REQUIREMENTS

The facilities requirements are developed under the guidelines that the launch vehicle will consist of existing hardware with minimum modifications and that the payload and related hardware (except the shroud) will be new hardware.

#### 7.2.1 MANUFACTURING FACILITIES

##### 7.2.1.1 LAUNCH VEHICLE

The modifications to the launch vehicle will be accomplished under existing SATURN contracts and in the facilities of the stage contractors. The facilities presently exist and are judged adequate for accomplishing the required activity.

##### 7.2.1.2 PAYLOAD

The payload consists of the satellite proper, the payload support structure and ejection mechanism (PSS/EM), and the shroud. The satellite and the PSS/EM are new hardware.

##### 7.2.1.2.1 DEPLETED URANIUM SATELLITE

The satellite will be fabricated in the facilities of a contractor who has an AEC license for handling depleted uranium materials. The assembled satellite will weigh approximately 3620 kg (8000 lbm) and a suitable crane facility will be required. A second requirement concerns the control of the depleted uranium dust and

particles during the machining operations. Two AEC licensed commercial firms have been contacted, and either one has the capability and facilities to accomplish the task. There is no anticipated requirement for new resources or facilities at the contractor manufacturing site. The depleted uranium assembly will be shipped to SAO for the installation of the retroreflectors and the final balance tests. A portable type hoist capable of lifting the 3620 kg (8000 lbm) satellite and a portable type clean room, rated to class 100,000, will be required at SAO. The clean room cost should not exceed \$15,000.

#### 7.2.1.2.2 RETROREFLECTORS

The retroreflector fabrication will be by a contractor qualified in optical glass technology. The standard procedures presently used in commercial practice for material selection, contamination control, and measurement of optical parameters are sufficient to meet the satellite requirements. Existing resources and facilities appear to be adequate.

#### 7.2.1.2.3 SHROUD

The shroud, consisting of the SLA and the nose cone, are available and will require some modification to adapt to the satellite and the payload support structure. Existing facilities and resources in the Product Engineering and Process Technology Laboratory, and the Quality and Reliability Assurance Laboratory will be used.

#### 7.2.1.2.4 PAYLOAD SUPPORT STRUCTURE AND EJECTION MECHANISM

The payload support structure and ejection mechanism (PSS/EM) will be fabricated either in-house by the Product Engineering and Process Technology Laboratory or by a local contractor. Existing resources and facilities will be utilized.

#### 7.2.1.3 ASSEMBLY AND HANDLING EQUIPMENT

The assembly and handling equipment is used to assemble the satellite, to perform checkout and balance tests, to ship the satellite, and to install the satellite into the launch vehicle. The fabrication will be performed in the facilities of a local contractor to NASA/MSFC.



## 7.2.2 TESTING FACILITIES

### 7.2.2.1 LAUNCH VEHICLE

The launch vehicle will undergo quality assurance testing during the manufacturing cycle. No additional environmental qualification tests will be required. The facilities presently exist at the contractor's plant and are judged adequate for accomplishing the required activity.

### 7.2.2.2 PAYLOAD

The payload assembly will be subjected to environmental qualification testing to insure compatibility with the launch vehicle and to qualify the new hardware.

#### 7.2.2.2.1 ASSEMBLY, TEST AND CHECKOUT

The depleted uranium satellite assembly will be shipped to SAO for the installation of the retroreflectors and for the checkout and balance of the complete assembly. The satellite must be assembled and contained in a contamination-free environment, and a portable-type clean room installation will be required at SAO.

#### 7.2.2.2.2 ENVIRONMENTAL QUALIFICATION TESTING

Environmental qualification tests will be performed on the complete payload assembly and on a special satellite test sector.

The payload assembly, consisting of the shroud, support structure and ejection mechanism, and the dummy satellite will be subjected to static load tests, structural and acoustical vibration, and operation of the ejection mechanism. Existing facilities and equipment will be used at NASA/MSFC, and no new facilities appear to be needed.

The satellite test sector is primarily a fixture used to qualify the retroreflectors mounted in the satellite assembly. The test sector will have a mass of approximately 56.75 kg (125 lbm). The test will include vibration, shock, thermal vacuum, and radiation. The required equipment is relatively small and is available at NASA/MSFC. No new facilities or equipment appear to be needed.

### 7.2.3 LAUNCH SITE FACILITIES

The proposed launch site is Kennedy Space Center (KSC). The only capability for launching a SATURN IB in this time period will exist on Pad LC-39B, as modified, with a pedestal to adapt the SATURN IB to the SATURN V tower. The pedestal and other provisions will be available from other programs, and only minor modifications will be needed to adapt to the Earth Physics Program satellite configuration.

The use of the Vertical Assembly Building (VAB) and other supporting facilities will be required. A clean room, rated to 100,000, will be required for assembly of the satellite and payload structure. Ground support equipment peculiar to the SATURN IB presently exists at KSC.

Tracking and range safety coverage is required only to final orbit insertion and ephemeris determination. The tracking capability existing during the time period of this launch will be acceptable and used.

In summary, the existing facilities at KSC appear adequate, and no new facilities or equipment seem to be needed.

## SECTION 8. SCHEDULE

### 8.1 GENERAL

The proposed schedule, Figure 8-1, indicates a start of the project in January 1972. This will allow sufficient time for all design, development, and production requirements, leading to a launch date of April 1974. In this schedule the SEPS project follows the Skylab project immediately to take full advantage of the momentum of the Skylab project, especially in the KSC launch and operations area. Pad 39B and the KSC launch GSE, previously used for Skylab, are available to SEPS project with only slight additional modifications. A most important item is that the launch crew at KSC can be retained for SEPS with minimum cost to the project.

### 8.2 PAYLOAD

The development of the depleted uranium satellite is the pacing item, and establishes the project duration. The design phase for the satellite and the support and handling equipment should begin immediately following project authorization. The support and handling equipment and the support structure and ejection mechanism in the SLA are required to support the satellite development, and are scheduled to become available when required by the satellite development.

### 8.3 LAUNCH VEHICLE

The Saturn launch vehicle selected for this project consists of the S-IB-212 first stage, the S-IVB-513 second stage, and the S-IU-212 Instrument Unit. All elements are presently in storage and are available when needed. The S-IVB stage is the pacing item for the launch vehicle.

Lead times for the design and modifications to the stages range from approximately 18 months for the S-IVB stage to 12 months for the S-IU instrument unit. The modifications to the launch vehicle GSE will require about six months. The KSC operations will require about five months leading to a launch readiness date of April 1974.

## DISTRIBUTION

### INTERNAL

DIR  
Dr. Rees

DEP-T  
Dr. Lucas

AD-S  
Dr. Stuhlinger

PD-DIR  
Mr. Murphy  
Mr. Downey  
Dr. Mrazek

PD-MP-DIR  
Mr. Gierow

PD-MP-P  
Mr. Dudley  
Mr. Spencer (12)

PD-PP-DIR  
Mr. Sneed (2)

PD-PP-E  
Mr. Rutledge/Mr. Wood (4)

PD-PP-R  
Mr. Wallace (2)  
Mr. Trexler (2)

PD-DO-DIR  
Mr. Goerner (2)  
Mrs. Andrews

PD-DO-S  
Mr. Marshall

PD-DO-SA  
Mr. Denton (6)

PD-DO-E  
Mr. Digesu

PD-PS-DIR  
Mr. Goodrum (2)

PD-PS-T  
Mr. McFolin (2)

PM-DIR  
Mr. Shepherd

PM-SAT-MGR  
Mr. Smith

PM-SAT-E  
Mr. Bell (2)  
Mr. Beaman (12)

S&E-DIR  
Dr. Weidner

S&E-AERO-DIR  
Dr. Geissler (2)

S&E-ASTR-DIR  
Mr. Moore (2)

S&E-ASTR-RP  
Dr. Randall (2)

S&E-ASTN-DIR  
Mr. Heimburg (2)

DISTRIBUTION (Continued)

INTERNAL (Concluded)

S&E-CSE-DIR  
Dr. Haeussermann (2)

S&E-CSE-L  
Mr. May

S&E-CSE-LA  
Mr. McKay (12)  
Mr. Price ( 2)

S&E-COMP-DIR  
Dr. Hoelzer (2)

S&E-PR-DIR  
Mr. Daniel (2)

S&E-PT-DIR  
Dr. Siebel (2)

S&E-PT-T  
Mr. Crumpton (2)

S&E-PT-TAC  
Mr. Ehl (2)

S&E-P-DIR  
Mr. Kroeger (2)  
Mr. Wiley (2)

S&E-QUAL-DIR  
Mr. Grau (2)

S&E-QUAL-E  
Mr. E. Smith (2)

S&E-SSL-DIR  
Mr. Heller (2)

PM-PR-M  
Mr. Stevens

A&TS-MS-H  
Mr. Akens

A&TS-MS-I  
Mr. Remer

A&TS-MS-IP  
Mr. Ziak (2)

A&TS-MS-IL  
Miss Robertson (8)

A&TS-MS-D  
Mr. Garrett

A&TS-PAT  
Mr. Wofford

A&TS-TU  
Mr. Wiggins (6)

EXTERNAL

NASA Headquarters  
Code MT/Mr. Culbertson  
Code MTL /Mr. Armstrong (6)  
Code OA /Dr. DeNoyer  
Code OA /Dr. Swetnick (12)  
Code OA /Mr. Hubbard

DISTRIBUTION (Concluded)

EXTERNAL (Concluded)

Smithsonian Astrophysical Observatory  
Cambridge, Massachusetts 02138

•Attn: Mr. John Gregory (12)

Scientific and Technical Information Facility  
College Park Maryland 20740

Attn: NASA Representative (S-AK/RKT) (25)